An Assessment of the Role of Transient Flow on the Dispersion of Non-Reactive Solutes in Porous Media: A Numerical Study

by

David Anthony Farrell

A Thesis
Submitted to the Faculty of Graduate Studies
in Partial Fulfillment of the Requirements of the Degree of

Doctor of Philosophy in Geophysics.

Department of Geological Sciences
University of Manitoba
Winnipeg, Manitoba

THE UNIVERSITY OF MANITOBA

FACULTY OF GRADUATE STUDIES

COPYRIGHT PERMISSION

An Assessment of the Role of Transient Flow on the Dispersion of Non-Reactive Solutes in Porous Media: A Numerical Study

by

David Anthony Farrell

A Thesis submitted to the Faculty of Graduate Studies of the University of Manitoba in partial fulfillment of the requirements of the degree of

Doctor of Philosophy

Preamble

This thesis consists of three independently researched chapters (Chapters 2, 3 and 4). Each chapter is completely self-contained with its own in-depth introduction and literature review, methodology, results, discussion and conclusions, and bibliography. This format is considered advantageous since it facilitates publication of the findings of the overall research effort. The three research chapters are preceded by an in-depth literature review which concludes with a statement of the overall research problem (Chapter 1), and followed by a fifth chapter in which the primary focus is to (i) provide a general summary of the research findings, (ii) put the various aspects of the research into focus and (iii) point out areas of future research which have evolved as a natural consequence of this study.

Abstract

It is generally assumed that solute migration and dispersion in hydrogeological environments are controlled solely by the material properties of the porous medium (i.e., the spatial distribution of hydraulic conductivity, porosity and reaction parameters). The inability of stochastic methodologies based solely on this premise to completely account for the field scale dispersion observed during the Stanford-Waterloo field tracer experiment (conducted at the Borden site) is well documented and discussed in the literature. As a result, researchers have focussed on other mechanisms, including flow transients, as possible contributors to the phenomenon of field scale dispersion. Several stochastic analytical formulations have attempted to quantify the impact of flow transients on the dispersion process [Rehfeldt and Gelhar, 1992; Dagan et al., 1996]. Due to limitations in the quantity and quality of data collected during past field tracer experiments, proper validation of these analytical solutions is difficult.

The current study utilized a numerical simulation experiment involving the finite element modelling of the groundwater flow and mass transport equations to examine the impact of flow transients on solute dispersion processes in hydrogeologic environments, with emphasis on dispersion processes observed at the Borden tracer test site. The numerical approach utilized a limited Monte Carlo simulation in which the flow boundary conditions were treated as temporal but deterministic whereas the hydraulic conductivity was treated as a heterogeneous, second order stationary, randomly correlated process. The parameters characterizing these properties were based on data collected at the Borden tracer test site.

Analysis of the results for the individual simulations showed that plume evolution is affected by the temporal nature of the flow field. In particular, the transverse spreading of the individual plumes was commonly enhanced under transient flow conditions compared to steady-state flow conditions. However, the magnitude of the enhancement varied within and across realizations thus making prediction difficult. In the longitudinal direction enhanced spreading is sometimes observed; however, this was not consistent across all of the realizations. Comparison of the ensemble average results to available stochastic analytic theories produced mixed results. In general it was found that although the model of Dagan et al. [1996] reproduced the trends in the ensemble second moment data quite well, it nonetheless over-predicted the observed data. The asymptotic model of Rehfeldt and Gelhar [1992] tended to over-predict the late time transverse spreading present in the ensemble data. However, the enhanced longitudinal dispersion predicted by the model showed some agreement with that observed from the simulations.

As part of this study, matrix methods for solving the system of equations which result from the finite element discretization of the mass transport equation were also investigated. In this aspect of the study emphasis was focussed on the performance of the Arnoldi modal reduction method (AMRM) relative to the Laplace Transform Galerkin (LTG) method. The performance was measured in terms of the accuracy and efficiency with which the methods could solve numerically challenging one and two-dimensional mass transport problems. Again the results were inconsistent in that for some classes of problems the AMRM greatly out performed the LTG method, whereas in other cases the results were reversed. However, for the more realistic case of steady-state flow and mass transport in heterogeneous second order

stationary randomly correlated hydraulic conductivity fields, it was found that the AMRM greatly out-performed the LTG method.

Based on these results a "shift" version of the AMRM was implemented and evaluated. The purpose of the shift was to improve the approximation of the eigenvalues of the problem and thus increase the convergence rate of the method. The results showed that shifting could be a "double edged sword", in that some shifts could improve the convergence of the AMRM, whereas other shifts could degrade the convergence. Estimation of an "optimal" shift was shown to be a difficult (and perhaps an inefficient) task since the optimal shift varies with the number of Arnoldi vectors considered, the material properties of the problem, the discretization of the domain, and the solution time considered. However, when utilized, the optimal shift was shown to improve convergence especially when only a few Arnoldi vectors were utilized.

Acknowledgments

This thesis has been the product of several years of research. During this period many individuals have made significant contributions towards its completion. Therefore it is only fitting that I use this opportunity to thank as many of these individuals as space allows. Foremost amongst these individuals is my thesis advisor Dr. Allan Woodbury, who in addition to funding and directing this study has shown unwavering enthusiasm and support for my work over the years. The many discussions we have had concerning this research and other issues were always enlightening and thought provoking. In addition I would like to thank Dr. Woodbury for providing the computational facilities and some components of the computer software used in this study. Along this same vein I would like to thank Dr. Edward Sudicky (Waterloo Centre for Groundwater Research, University of Waterloo) for his advice over the years and for openly sharing various aspects of his research with me; in particular the waterlevel data for the Borden site and the computer codes for de Hoog algorithm and the ORTHOMIN procedure. I would also like to thank the members of the Departments of Civil and Geological Engineering, and Geological Sciences for their help over the course of this study. Special thanks are extended to Dr. Emery Lajtai for all of the help and support he has given me over the years and for providing me with unlimited access to the computer facilities of the Rock Mechanics Group; and to Dr. Ian Ferguson for the many impromptu discussions which we have had regarding this research. I would also like to thank Dr. Leslie Smith and Dr. Scott Dunbar for reviewing this work and for their suggestions regarding its improvement. In addition I would like to extend special thanks to Ingrid Trestrail and

Elizabeth Ross for putting up with my many questions and for being valuable sources of information regarding university regulations and funding. As well I would like to thank Ingrid for being a good listener during time of stress. I also wish to thank all of the students of Rm. 312C for the advice, laughs and support which they provided.

Special thanks are extended to Danya Lougheide (who endured not only many broken promises but also many of my ups and downs over the last three years), my parents (Lionel and Audrey Farrell), my brothers (Kevin and Robert), my grand-parents (Henry Farrell and Clarice Clarke), my uncles and aunts, and my friends (Victor, Dayle, Alexis, Ray, Andrew, Aceita, Joan, Tarquin and Vera to name a few) all of whom provided me with the emotional support required to complete this task.

Finally, I would like to dedicate this work to my parents and grand-parents who never had many of the opportunities in life with which they have provided me. Your unselfishness is greatly appreciated.

Table of Contents

List of Figures

List of Tables

Chapter 1

Introduction

1.1 Background

The primary focus of hydrogeology during most of the 20th century has been on locating and evaluating groundwater resources. In response to mounting public concerns regarding public health, environmental protection and sustainable development, much of the focus in recent years has shifted from groundwater location and development to resource protection and remediation. As a consequence much attention has been focussed on groundwater contamination by hazardous industrial wastes, by leachate from landfills, by agricultural activities such as the use of fertilizers, pesticides, and herbicides and by radioactive waste repositories located in deep geological formations [Bear and Verruijt, 1987]. In an attempt to reduce the potential of groundwater contamination various policies have been implemented by governments and agencies worldwide. In many instances these policies seek not only to regulate the nature and disposal of waste but also to regulate land use. The regulation of land use and waste disposal practices requires that the interaction between potential contaminants and the environment be understood from both physical and chemical perspectives. Achievement of this goal requires a thorough knowledge of hydrogeological and geochemical processes.

Perhaps all groundwater contamination can be rectified through the use of appropriate remediation schemes; however due to financial and practical constraints remediation is not feasible at all sites. In those instances where remediation is considered feasible, the design of

adequate yet cost effective, clean-up strategies generally involves some aspect of mathematical and probabilistic modelling. For the modelling process to be successful, two conditions must be met. The first condition requires that the model be based on a good understanding of the physics and chemistry governing the migration of the particular contaminants in the subsurface, while the second condition requires that parameters utilized adequately represent the real system.

The fundamental processes governing mass transport continue to be the source of much debate. One aspect of the debate has focussed on how best to pass from the macroscopic continuum level of a Representative Elementary Volume (REV) to some "effective" field-scale value which when incorporated into a mathematical model, reproduces results which are analogous to those observed in the actual medium. Informative discussions and analyses which addressed the issues associated with the use of "effective" field-scale values have been provided by Neuman [1982], Rubin and Gómez-Hernández [1990], Indelman and Dagan [1993a and 1993b], Beckie et al. [1994], and Sanchez-Villa et al. [1995] among others. Among the issues raised by Neuman [1982], was whether a universal approach could be defined which would allow averaged parameters to be defined over a region without the use of limiting assumptions (i.e., for the most general case can an equivalent porous medium be defined which behaves in a similar manner to that of the actual medium), and whether field based spatial variability can be incorporated into models using such a definition. Neuman [1982] conjectured that "if the concept of average parameters is invalid under certain conditions, or if these averages cannot be determined in a satisfactory manner from available data, what utility, if any can the hydrologist hope to derive from the number of sophisticated

computer models that are presently at his disposal?" Since questionable estimates of field-scale parameters are of limited practical use to hydrogeologists, alternate approaches have been sought.

One alternate approach for determining hydrogeological parameters for use in numerical models is based on a statistical framework. This statistical framework is in turn based on a stochastic methodology, in which the variables of interest (e.g. hydraulic conductivity, porosity and sorption parameters, etc.) are assumed to be random and correlated in space. This spatial correlation is necessitated by the fact that in nature geologic deposits tend to exhibit definite spatial arrangements [Neuman, 1982]. The probabilistic approach differs from the deterministic approach described earlier in that since some of the input variables are uncertain, the model output also needs to be described in a probabilistic framework [Neuman, 1982]. Note that in the stochastic framework material properties are most often assumed to be statistically homogeneous (constant mean) with fixed and finite correlation scales. Evidence supporting the possible stochastic representation of hydrogeologic properties are found in the works of Sudicky et al. [1986] and Hess [1992].

The general assumption of statistical homogeneity of hydrogeological parameters is an issue which has been the focus of much discussion in recent years. Sposito et al. [1986] pointed out that stochastic models based on the assumption that hydraulic heterogeneities are statistically homogeneous on a scale much smaller than the region being studied are unable to account for the growth of the dispersivity parameter as a function of scale; the "scale effect". In order to explain the "scale effect" some researchers have adopted a framework for solute transport based on a fractal representation [Wheatcraft and Tyler, 1988; Wheatcraft

and Cushman, 1991]. Evidence supporting possible fractal scaling relationships for some hydrogeological properties such as hydraulic conductivity and porosity are found in the works of Muller and McCauley [1992], Kemblowski and Chang [1993], Molz and Boman [1993], and Desbarats and Bachu [1994] among others.

Mass transport models based on these porous media concepts must be able to reproduce field observed behaviours using physically based parameters if these models are to be of any practical value. One aspect of solute migration under field conditions which has challenged researchers for a comprehensive explanation is the phenomenon of *hydrodynamic dispersion*. This phenomenon refers to the spreading of solutes beyond the region predicted by pure advection and was originally thought to be the result of two process operating at the pore level. At this level, the more dominant of the two processes is mechanical mixing which results from a combination of velocity variations across pore throats and the shape and inter-connectivity of the pore structure of the medium, whereas the less dominant effect is molecular diffusion. Due to its importance in redistributing solutes, the phenomenon of hydrodynamic dispersion has been extensively studied over the last few decades by numerous researchers using a variety of approaches, which range from field and laboratory investigations to numerical, mathematical and statistical studies. In the ensuing discussion a summary of the findings of these analyses is provided.

The mechanical component of dispersion is classically quantified using a parameter termed the *dispersivity*. Bear [1972], described dispersivity as being a characteristic single-valued property of a porous medium. This concept of dispersivity has been the subject of much debate in light of recent results from field experiments and mathematical studies. These

results suggest that in heterogeneous hydraulic conductivity fields dispersivity displays a scale dependence.

1.2 Scale Dependence of Dispersion

The discussion in this section summarizes the current findings regarding solute dispersion in porous media. Note that in an effort to control the length of this manuscript only the most notable studies on this subject which are of relevance to this thesis are discussed in the sequel.

1.2.1 Laboratory Studies

Laboratory studies provide fast and inexpensive ways to study dispersion in porous media at a small scale. Such experiments in which the longitudinal dispersivity of granular porous media were measured yielded values in the range of 10^{-4} m to 10^{-2} m [Bear, 1961b; Shamir and Harleman, 1966; Lawson and Elrick, 1972; Reynolds, 1978; Robbins, 1989]. Transverse dispersivity values for these experiments were usually found to be between 5 and 23 times less than the reported longitudinal values [Shamir and Harleman, 1966; Lawson and Elrick, 1972; Robbins, 1989].

Some laboratory studies have demonstrated scale dependent dispersion. Martin [1971] performed a series of laboratory experiments on different lengths of Fontainebleau sandstone and observed that the spreading pattern reached an asymptotic state after the injected tracer had travelled a large distance compared to the scale of the heterogeneity. Silliman and Simpson [1987] using depth averaged break-through curves showed that scale effects can be

demonstrated under laboratory conditions for several types of heterogeneities. They concluded that the scale effect becomes negligible as the scale of transport becomes large in relation to the scale of the heterogeneity.

1.2.2 Field Studies

As mentioned above, the results of field studies conducted over the last 30 years have indicated that dispersion in heterogeneous porous media displays a scale dependence. Evidence supporting this assertion can be found in works as early as Fried [1972]. On the basis of studies at several field sites, Fried [1972] reported longitudinal dispersivities which ranged from 0.1 m to 0.6 m for the local scale (aquifer stratum), 5.0 m to 11.0 m for the global scale (aquifer thickness) and 12.2 m for the regional scale (several km). The transverse dispersivity observed in this study showed no scale dependence.

Oakes and Edworthy [1977] performed a series of two-well pulse and radial injection experiments in a sandstone aquifer. An analysis of the experimental data revealed that the dispersivity value for a fully penetrating well was 2 to 4 times the values for discrete layers. Pickens et al. [1978] performed a two-well injection test in a sandy aquifer. Analysis of the data collected from a fully penetrating well was found to give a longitudinal dispersivity of 0.5 m, whereas data collected by means of a network of multi-level point samplers from the plane of highest velocity yielded a much smaller dispersivity. Pickens et al [1978] suggested that this difference may be due to vertical averaging performed by the fully penetrating well of concentrations that were observed with depth.

On the basis of a number of field tests, Sauty [1980] concluded that dispersivity

initially increased with distance and then remained constant after a characteristic value (related to travel distance) had been reached. Sauty [1980] suggested that irregularities seen in the plume shape at travel distances less than 1.0 m were due to the influence of heterogeneities in the porous media. At later times the plumes were observed to become much smoother [Sauty, 1980]. The work of Dieulin [1980] supported the findings of Sauty [1980]. Based on the analysis of break through curves obtained from a tracer experiment conducted in a heterogeneous alluvial aquifer, Dieulin [1980] concluded that dispersivity increased with travel distance.

Sudicky et al. [1983] reported the results of a tracer experiment performed in a sandy aquifer at Canadian Forces Base, Borden, Ontario. Attempts to simulate the experimental results at each sample time by means of analytical solutions to the three-dimensional advection-dispersion equation provided poor fits to the observed data when a constant dispersivity was used. Instead, Sudicky et al. [1983] found that by increasing the dispersivity with the residence time of the tracer a better fit between the simulated and observed data could be achieved. The calculated dispersivity estimates showed that the dispersivity eventually attained an asymptotic value. Farrell et al. [1994] re-analysed the field data for this experiment using the method of spatial moments. Their results confirmed the earlier conclusions of Sudicky et al. [1983] that scale dependent dispersion processes were active in the aquifer. Further evidence supporting the presence of a scale dependent dispersivity in the Borden aquifer has been provided by Freyberg [1986] who performed a spatial moment analysis of the Stanford-Waterloo tracer experiment data. Based on his analysis, Freyberg [1986] found that during the course of the experiment (about 3 years) the longitudinal

dispersivity increased from 0.06 m to its asymptotic value of 0.43 m.

Garabedian et al. [1991] presented the results of a spatial moment analysis performed on solute concentration data collected from a field tracer experiment conducted in a sand and gravel aquifer at a site in Cape Cod, Massachusetts. Their results showed the presence of a non-linear trend in the longitudinal variance of the solute concentration during the first 26 m travelled by the centre of mass. This early time non-linear behaviour was shown to produce an increase in the apparent dispersivity.

A critical review of data on field-scale dispersion (macrodispersion) in aquifers was performed by Gelhar et al. [1992] (see Figure 1). Their work examined 59 field sites at which the following information was available: aquifer type, hydraulic properties, flow configuration, type of monitoring network, tracer, method data interpretation, overall scale of observation, and longitudinal, horizontal transverse and vertical transverse dispersivities. The data were then used to evaluate the reliability of the reported dispersivity information. Based on the criteria outlined by Gelhar et al. [1992], only two of the above field experiments were considered to produce dispersivity estimates which were of high reliability, the Stanford-Waterloo and Cape Cod experiments. The others produced results which were considered to be of either intermediate or low reliability. Even if the reliable data alone is accepted, then it appears that field-scale dispersion is a scale dependent process.

1.2.3 Stochastic Analytic Analyses

Stochastic models of dispersion have traditionally assumed that dispersivity is influenced solely by the material properties of the porous medium through which solute transport takes place. Indeed, the majority of these models assume that the dispersivity estimated from field experiments results exclusively from the spatial distribution of hydraulic conductivities. Whether this assumption is entirely valid will be addressed in later sections of this chapter and in later chapters of this thesis.

If the structure of a medium can be determined exactly (i.e. deterministically) and the hydraulic conductivity variation is known, it is possible to estimate the dispersivity of the medium by using indirect theoretical methods [Schwartz, 1977]. However, this approach is unrealistic since a detailed description of a porous medium, as required for such an analysis, would require an unprecedented amount of data. To circumvent this problem, a number of researchers within the last decade have used a geostatistical description of say log-hydraulic conductivity *[Y=Ln(K)]*, specifically its mean, variance and integral scale, to characterize hydrogeologic properties of aquifers. When these geostatistical parameters are incorporated into modern stochastic theories, they provide an indirect means of obtaining estimates of the macrodispersivity. Several stochastic theories have been proposed which attempt to quantify macrodispersivity using this approach.

Using stochastic analytic methodologies based on a geostatistical description of *Ln(K)*, Gelhar and Axness [1983], and Neuman et al. [1987] presented in-depth analyses of macrodispersivity in heterogeneous porous media, for the case where a solute plume has reached a constant (or asymptotic) rate of spreading. The results of the analyses differ in

several important ways. For example, Neuman et al. [1987] showed that when the mean velocity is at an angle to the principal axis of statistical anisotropy, the asymptotic macrodispersivity tensor reduces to a single non-zero principal component. Gelhar and Axness [1983] demonstrated that under such flow conditions more than one non-zero component will exist. Neuman et al. [1987] also showed that the principal axis of the plume will be offset in a direction opposite to that suggested by Gelhar and Axness [1983]. Neuman et al. [1987] suggested that the reason for these discrepancies is that their approach is a consistent first-order analysis whereas the analysis of Gelhar and Axness [1983] combines both first and second order approximations.

Using ensemble averages, Dagan [1988] proposed a transient theory for the evolution of the macrodispersivity in a heterogeneous statistically anisotropic porous medium. This work showed that the longitudinal macrodispersivity grows with travel time to an asymptotic value which is independent of the anisotropy ratio. In the transverse direction, the theory predicts that the spatial moments will tend to a constant value which is dependent on the anisotropy ratio. A further result of this work is that the orientation of the principal component is along the direction of mean flow in accordance with the theory of Neuman et al. [1987].

Neuman and Zhang [1990], and Zhang and Neuman [1990] also examined time-dependent dispersion. Their analysis involved the use of an extended quasi-linear theory describing the evolution of the dispersion process from early to late time in statistically isotropic and anisotropic media. One of the main advantages of their work is that fluctuations in the log-hydraulic conductivity are not required to be small. This requirement is necessary

in other theories so that non-linear terms in the governing equations can be disregarded. When the variance in the log-hydraulic conductivity is less than one ($\sigma_Y^2 < 1$), all existing theories show that the asymptotic longitudinal macrodispersivity is proportional to the product of σ_Y^2 and the correlation length of the log-hydraulic conductivity in the direction of flow [Neuman and Zhang, 1990]. For anisotropic media, the effect of non-linearities in the solution procedure can be pronounced even for $\sigma_Y^2 \ll 1$. A short-coming with this proposed theory is that it predicts stronger vertical transverse dispersion than horizontal transverse dispersion [Sudicky and Huyakorn, 1991]. This prediction is inconsistent with the results of field experiments.

Naff [1990] also examined the dispersion process using a stochastic methodology which showed certain similarities to the approach employed earlier by Gelhar and Axness [1983]; however unlike previous models his considered the effects of local dispersion. Naff's examination of the dispersive flux in saturated heterogeneous porous media yielded several interesting results. In particular, it was shown that (i) when the medium is well stratified the local transverse dispersivity can become an effective means by which tracer mass can be transferred laterally, (ii) local dispersion cannot always be used to explain the transverse dispersion observed during field tracer experiments, and (iii) the "global" dispersive flux takes the form of a convolution integral which introduces non-Fickian[1] effects into the flux and non-Gaussian effects into the tracer cloud which will persist for a travel time of approximately 20 length scales.

---

[1] Under the "Fickian" assumption it is assumed that the dispersive mass flux is proportional to the solute concentration gradient.

The works described in the above paragraphs are based on the concept of an ensemble average concentration field which may be equated to the motion of a "single tracer particle" [see Dagan, 1990, and 1991; Rajaram and Gelhar, 1993*a*, and *b*]. In a recent series of publications Dagan [1990 and 1991] and Rajaram and Gelhar [1993a, and b] have shown that analyses based on ensemble average concentration can overestimate the dispersivity associated with a plume of finite source size. Using methodologies which relate the ensemble average second moment to the separation of two particles (the "two particle approach") these authors independently derived stochastic analytic expressions which describe the dispersion of a plume with finite source dimensions. The dispersion described by these models is generally found to be in better agreement with results of field simulations and numerical simulation studies.

The applicability of dispersivities estimated from stochastic models to real world situations is a concern. Dagan [1990] showed that the tendency towards an agreement between an "actual effective" dispersion coefficient determined from a field test and that predicted by stochastic theory can be very slow, and that this tendency also depends on the initial dimensions of the real solute plume. Graham and McLaughlin [1989] pointed out that while macrodispersivities describing the spread of an ensemble mean concentration solute plume are in reasonable agreement with those predicted by stochastic-analytic theory, plume concentrations and dispersivity values for individual realizations can be markedly different.

1.2.4 Fractal Analyses

The fractal concept provides another possible way to describe large-scale hydrogeologic structures. Under this concept it is postulated that for hydrogeologic materials there is a self-similarity or self-affinity (at least in the statistical sense) in the variation of the process over many different scales [Gelhar 1993]. Unlike the volume averaging approach, the fractal concept does not define one characteristic scale. A concise mathematical definition of such self-affine processes in hydrogeology has been summarized by a number of researchers including Gelhar [1993], and Molz and Boman [1993] and is reproduced here for the benefit of the reader. A self-similar random process such as the hydraulic conductivity of a formation essentially satisfies the following conditions:

$$E[m(t+\xi)-m(t)]=0$$
$$\gamma=\frac{1}{2}E[(m(t+\xi)-m(t))^2]=\beta|\xi|^{2H} \qquad (1.1)$$

where $E[\ ]$ represents the mean or expected value, γ represents the variogram of the process, $m(t)$ is a single valued continuous function in time or space, ξ represents a separation distance or time, β is a constant and H which represents the Hurst coefficient lies in the range $0 < H < 1$. Thus the variogram is a function of the power of the separation distance or time. In addition, if t and m are scaled according to $t'=t/r$ and $m'=m/(r^H)$ it can be shown that the variogram of the process scales by r^{2H} [Molz and Boman, 1983].

Fractal scaling concepts have been used to represent various physical properties of porous media. For example, Katz and Thompson [1985] reported on studies in sandstones, in which the porosities displayed fractal characteristics; Burrough [1983a, b] studied the

fractal properties of soils; Muller and McCauley [1992] demonstrated how a simple fractal model can give an understanding of the fluid flow and hydraulic conductivity properties of a porous medium in terms of empirical relations such as the known Carman-Kozeny and Archie laws; Barton and Larson [1985], and Ross [1986] showed how fracture networks may be characterized by fractal scaling relationships; Kemblowski and Chang [1993], Molz and Boman [1993], and Desbarats and Bachu [1994] all showed that the hydraulic conductivity at some sites may scale according to a fractal relationship; Chang et al. [1994] showed how the use of fractal relationship to represent surface tension in soils can possibly explain fingering in soils.

Other studies have shown that some observed scale dependent processes in porous media may be adequately described using fractal concepts. For example, Ayra et al. [1985], Hewett [1986], and Wheatcraft and Tyler [1988] examined scale-dependent dispersion processes in oil reservoirs and heterogeneous aquifers using fractal concepts. On the basis of their work, Wheatcraft and Tyler [1988] tentatively concluded that a fractal model is able to explain dispersivities from field experiments better than available stochastic theories. Using a theoretical approach, Kemblowski and Wen [1993] investigated how the fractal character of permeability distribution influences spreading and mixing in porous media. In their work, the porous media was perfectly stratified with fractal scaling of hydraulic conductivity in the vertical direction. The results of this analysis showed that the asymptotic macrodispersivity depended strongly on the fractal dimension of the hydraulic conductivity; the higher the fractal dimension the lower the macrodispersivity.

None of the works previously described examined both flow and associated mass

transport in a fractal porous media using numerical simulation methodologies. The work of Wheatcraft et al. [1990] did examine this issue. As a part of this work, Wheatcraft et al. [1990] designed a number of hydraulic conductivity fields based on a Sierpinski carpet[2] (see Figure 2.2), each sharing the same fractal dimension, but where the length scales varied for each design. They then solved for the steady-state flow field within the domain for a specified set of boundary conditions. The method of characteristics was then used to solve the specified transport problem. Several important features are revealed in their work:

1. As the complexity of the fractal pattern is increased, the particle paths through the domain become more tortuous;
2. Dispersion increases with the fractal scale with the observed rate of dispersion being greater than that predicted by other models;

Wheatcraft et al. [1990] suggested that fractal scales present in hydrogeologic media can only be determined by developing new field sampling techniques; standard techniques currently employed are inappropriate since observed properties (e.g., hydraulic conductivity) and their variances are dependent on the scale of measurement. Cushman and Ginn [1993] also echo similar sentiments. They point out that new theories are needed to describe transport in porous media displaying fractal scaling relationships since averaging volume concepts on which current models of mass transport are based are invalid when no one characteristic scale can be defined. Current research into new theories describing mass transport and solute dispersion in porous media in which the hydraulic conductivity scales according to a fractal

---

[2] For a detailed explanation outlining the construction of the Sierpinski carpet the reader is referred to Turcotte [1992, p. 9].

law are found in the works of Cushman [1991], Cushman and Ginn [1993] and Neuman [1995] among others.

Up to this point, the discussion in this section has focussed on site and case specific scenarios in which fractal scaling relationships were identified or assumed for the property under study (e.g., hydraulic conductivity, porosity, dispersivity, etc.). The subsequent discussion examines the case of universal scaling relationships based on fractal concepts. In particular the widely discussed "universal scaling" concept of Neuman [1990] is considered. Using apparent longitudinal dispersivity data collected from various sources for various sites, Neuman [1990] postulated a universal scaling relationship between dispersivity and the scale of the study. The postulated relationship which was based on "unconditional stochastic theory"[3] was shown to be fractal in form. It is important to note that Neuman [1991] explicitly stated that his model does not assume self-similarity in the log-hydraulic conductivity field at the local scale but on the global scale self-similarity appears to be evident. Neuman [1991] further points out that the proposed scaling rule should only be used to predict local conditions at a site if site specific information is lacking. Application of the relationship under such conditions will produce results which are highly uncertain.

The scaling relationship proposed by Neuman [1990] has been the focus of much discussion. Anderson [1991] addressed the implications of the scaling relationship from a geological perspective and pointed out that such a model was incapable of representing local

---

[3] The "unconditional stochastic theory" utilized by Neuman [1990] assumed the hydraulic conductivity possessed a uniform mean, and accounted for spatial variability through the macrodispersivity parameter. Thus dispersivities derived from models which deterministically accounted for spatial variability of hydraulic conductivity were not considered in the analysis.

peculiarities such as channelling of flow which results from the presence of connected units of high hydraulic conductivity. For such cases Anderson [1991] suggested that effective parameters such as dispersivities were unsuitable for describing contaminant transport. At the regional scale, Anderson [1991] suggested that fractal relationships such as that proposed by Neuman [1990] may apply within geological facies assemblages and possibly within a set of assemblages. However under such circumstances the hierarchy of scales will extend only up to the scale of the depositional system.

The model proposed by Neuman [1990] has also been discussed by Gelhar et al. [1992 and 1993]. The focus of these discussions centred on several issues, the most important of which involved the reliability of the data utilized by Neuman [1990]. As pointed out by Gelhar et al. [1993], the data utilized Neuman [1990] were taken from several secondary sources and were determined using a number of different procedures. Along these lines Gelhar et al. [1993] further argued that the data discrimination procedure and the interpretation procedure utilized in the study were inconsistent, since some form of conditioning is implicit in the determination of dispersivities from field data. Gelhar et al. [1993] further argued that a fundamental problem with the proposed model is that it does not recognize the essential role of plume size in determining the degree of dispersion in scaleless heterogeneous media.

1.2.5 Other Physical Factors Influencing Dispersion

Stochastic models which consider dispersion to be strictly controlled by variations in hydraulic conductivity [e.g., Gelhar and Axness, 1983; Dagan, 1988; Zhang and Neuman, 1990] have been unable to predict the observed horizontal transverse dispersion observed

during the Stanford-Waterloo tracer experiment [cf, Woodbury and Sudicky, 1991]. This disagreement between theory and observation has prompted several researchers to investigate other potential causes of field scale dispersion. On the basis of studies conducted on a solute plume emanating from an abandoned landfill at the Borden site, Sykes et al. [1982] conjectured that the observed enhanced transverse dispersion was perhaps caused by flow transients which were known to exist at the site. Later, Sudicky [1986] used a similar argument to explain the enhanced horizontal transverse dispersion reported by Freyberg [1986] for the Stanford-Waterloo tracer experiment.

The potential impact of flow transients on the dispersion process has been examined in several theoretical studies. The first such analysis was performed by Kinzelbach and Ackerer [1986] who considered the case of unsteady flow in a homogeneous aquifer. From their work, deterministic expressions for the apparent transverse and longitudinal dispersivities due to unsteady flow, α_{Ta} and α_{La} respectively, were developed based on the time averaged groundwater velocities and the assumed true dispersivities associated with steady-state flow [cf, Goode and Konikow, 1990]. These apparent dispersivities were later incorporated into steady-state models to predict plume migration and evolution under transient conditions. An interesting aspect of the relationships proposed in that work was that the sum of the apparent dispersivities were approximately equal to the sum of the true dispersivities *(i.e.* $\alpha_L + \alpha_T = \alpha_{La} + \alpha_{Ta}$*)*, where α_L and α_T are the assumed true longitudinal and transverse dispersivities respectively. Note that this result essentially implies a "conservation of dispersivity". In other words, the dispersivity of a hydrogeologic system is a fixed quantity. This relationship has been challenged by Goode and Konikow [1990] who also developed a set of deterministic

relationships for a similar problem. Contrary to Kinzelbach and Ackerer [1986] their results showed that the sum of the apparent dispersivities exceeded the sum of the assumed true dispersivities observed under steady-state conditions *(i.e.* $\alpha_L + \alpha_T < \alpha_{La} + \alpha_{Ta}$*)*. The study further demonstrated that increases in the apparent transverse dispersivity occurred because longitudinal dispersion acted in a direction which was not parallel to the mean flow direction and that the increase in the apparent dispersivity was controlled by the magnitude of the flow angle variation and the ratio of the longitudinal to transverse dispersivity.

Naff et al. [1988 and 1989] postulated that small-scale velocity fluctuations could be responsible for large-scale transverse solute spreading. This was illustrated using a simple formulation in which time-dependent frequency components were added to the mean velocity field thereby creating a transient flow field [Naff et al., 1989]. Using this formulation it was shown that in theory a significant increase in the transverse variance of the concentration field could be obtained [Naff et al., 1989].

Rehfeldt and Gelhar [1992] extended the earlier proposed stochastic methodology of Gelhar and Axness [1983] in an attempt to evaluate the asymptotic values of macrodispersivity due to an unsteady flow field. Their approach considered the aquifer hydraulic conductivity to be stationary and the mean hydraulic head gradient to be uniform in space but fluctuating in time about a constant mean. Further, these fluctuations are assumed to be random and small. Their formulation showed that for statistically ergodic[4] plumes migrating under such conditions, enhancement in both the asymptotic longitudinal and

[4] The ergodic hypothesis assumes that time or space averages associated with a single realization can be used in place of ensemble averages [Gelhar, 1993].

horizontal transverse dispersivity relative to those observed under steady-state conditions can be expected. The formulation further suggested that after an extensive travel time the dispersion induced by the gradient fluctuations can be treated independently from that induced from velocity fluctuations associated with the natural heterogeneity of the hydraulic conductivity field.

Farrell et al. [1994], utilizing waterlevel data collected at the Borden site during the period from July 1989 to January 1991 in conjunction with stationarity assumptions, attempted to use the Stanford-Waterloo tracer data to validate the proposed formulation of Naff et al. [1989] and Rehfelft and Gelhar [1992]. Their findings suggested that whereas the formulation of Naff et al. [1989] provided a poor fit to the observed second moment data, the proposed formulation of Rehfeldt and Gelhar [1992] provided a plausible explanation for the observed enhanced transverse dispersivity. Here it is stressed that the results were plausible, in light of the fact that the stationarity of the waterlevel data could not be verified due to the short length of the time series in relation to the assumed annual periodicity present at the site.

Recently, Zhang and Neuman [1996], and Dagan et al. [1996] cited several perceived difficulties in the formulation of Rehfeldt and Gelhar [1992]. These difficulties revolved around:

1. The independent treatment of the dispersion process at late times;
2. The apparent Fickian horizontal transverse dispersion predicted by the model under uniform mean flow conditions conflicts with the zero transverse dispersion generally observed at late time for steady-state flow in heterogeneous formations;
3. In the absence of local dispersive processes, the solute plume should simply

translate and rotate without spreading, hence the dispersion predicted by the model reflects uncertainty associated with the random nature of the gradient fluctuations;

4. The fact that temporal periodicity in the hydraulic gradient field is not expected to have an impact on the macrodispersivity.

The models proposed by Zhang and Neuman [1996], and Dagan et al. [1996] are similar, with both revolving around the Lagrangian formulation found in the works of Dagan and co-workers [Dagan, 1984 and 1989; and Rubin, 1990]. In both cases time dependent integral functions were derived which characterized the longitudinal and transverse variances. It is noteworthy to mention that in both formulations separate treatments of the processes contributing to solute dispersion were not required. Finally, the hydraulic gradient utilized in both models was assumed to be deterministic, which is contrary to the model of Rehfeldt and Gelhar [1992] which treated the hydraulic gradient as being part of a stochastic process. Both models showed that changes in the direction of the hydraulic gradient enhanced the transverse dispersivity, while at the same time having minimal impact on the longitudinal spreading of the solute plume.

1.2.6 Numerical Simulations: Scale- and Time-Dependent Dispersion

Numerous numerical simulations of mass transport have been reported in literature; however, very few have been reported which (i) examine various aspects of the dispersion process and (ii) have been used to validate proposed stochastic analytic solutions. The following presents a limited discussion of the results of these simulation experiments.

Early use of numerical methods in the study of macroscopic dispersion is found in the

work of Smith and Schwartz [1980]. In this work, Monte-Carlo simulations of two-dimensional mass transport in steady-state velocity fields were used to assess the impact of spatial heterogeneity in hydraulic conductivity on the dispersion of nonreactive solutes. The important findings of this work were that (i) macrodispersion results from large-scale spatial variations in hydraulic conductivity, (ii) microscopic (laboratory scale) dispersion theories cannot be scaled up to field-scale situations without a proper analysis of the hydraulic conductivity field, (iii) asymptotic macrodispersivity occurs after an unknown travel distance which depends on the spatial structure of the porous medium, and (iv) modelling techniques based on the advection-dispersion equation with large values of dispersivity do not reflect the physical process fer which predictions are being made.

Quinodoz and Valocchi [1990] used detailed two-dimensional single realization numerical simulations to examine the practical conditions under which the ergodic hypothesis can be invoked. The reader should recall that most stochastic analytic solutions are based on ensemble averaging schemes, whereas the moment results from field tracer experiments are based on spatial averaging of one realization. In their analysis, the heterogeneous hydraulic conductivity field was randomly correlated and second order stationary. In addition, fluid flow within the medium was assumed to be at steady-state. By varying the source dimensions for each simulation considered in the study, and calculating the second moments of the evolving plumes the authors were able to show (through a comparison with the solution of Dagan [1982]) that for ergodic conditions to be invoked at all times the source dimensions of the plume must incorporate several integral scales of log-hydraulic conductivity. Other two-dimensional simulations studies have been performed in an attempt to examine the limitations

of stochastic theories, notably Schellenberg [1987]. In that work single realization numerical experiments were performed and the resulting spatial moments were compared to existing stochastic theories with some degree of success.

Burr et al. [1994] suggested that two-dimensional simulation studies of field observed mass transport phenomena may in *some cases* be of restricted value, since the factors which influence mass transport in hydrogeologic media are three-dimensional in nature. Instead, they suggested that a fully three-dimensional modelling approach incorporating heterogeneous porous media is needed when attempting to either confirm the validity of stochastic transport theories and or gauge the relative importance of various hypothesized transport mechanisms. Although this is true, three-dimensional simulation studies of mass transport are rarely utilized due to the excessive computational resources required. This is especially the case for regional scale studies (on the order of 100's of metres) where the areal dimensions of the formation under investigation are significantly greater than its depth. For such studies two dimensional models which incorporate depth averaged parameters are commonly utilized. This view is reinforced by Shapiro and Cvetkovic [1990] who pointed out that for many practical problems it is more convenient and consistent with measuring techniques (e.g., the determination of transmissivity as opposed to hydraulic conductivity in some pump tests) to consider flow and transport as an areal, two dimensional phenomenon. Although this does not fully justify the use of two-dimensional models it nonetheless shows that an in-depth understanding of the mechanisms influencing mass transport within such models is essential, especially when regional systems are being evaluated. In addition, the work of Quinodoz and Valocchi [1990] discussed above demonstrates to some degree the usefulness of two-

dimensional simulation studies. In the following paragraphs, a chronology of the most recent three-dimensional mass transport simulation studies is presented.

Tompson and Gelhar [1990] examined the migration of nonreactive solutes in a high resolution three-dimensional heterogeneous (second order stationary and randomly correlated in space) hydraulic conductivity field in which steady-state flow conditions are enforced. In this work the mass transport was simulated using a particle tracking methodology. The authors reported that the trajectory and longitudinal spreading of the solute plumes in hydraulic conductivity fields displaying low variability compared favourably with the spectral predictions of Gelhar and Axness [1983] at late times, with nonergodic effects being observed at early times. In the more variable fields the simulations results over-estimated the predicted values of Gelhar and Axness [1983].

Robin [1991] modelled reactive and non-reactive mass transport in a statistically anisotropic randomly correlated second order stationary hydraulic conductivity field. As in the above study mass transport was simulated in a steady-state flow environment, however contrary to that study flow and transport were both modelled using the finite element (FE) method. Results from the nonreactive simulations showed that in the longitudinal direction, the theoretical dispersivities of Gelhar and Axness [1983] and Dagan [1984] were two to four times larger than those obtained from the simulation experiment. Robin [1991] concluded that this disagreement may be reflective of nonergodic conditions which were known to be present in the simulation experiment.

Chin and Wang [1992] combined a three-dimensional numerical simulation analysis with a Monte Carlo analysis to (i) investigate the accuracy of approximations that are implicit

in first-order stochastic dispersion theories and (ii) to identify the accuracy limits of first-order dispersion theories in isotropic porous media. As in the previous simulation studies, the mass transport occurs in steady-state flow fields, with the transport being simulated by a particle tracking methodology. However, this study differed from the earlier studies in that local dispersive effects were ignored and the source dimensions extended over several integral scales of hydraulic conductivity, thus satisfying the ergodic criterion. The authors found that their longitudinal results agreed well with the longitudinal dispersivity given by Dagan [1984], whereas the overall approach of Gelhar and Axness [1983] was shown to underestimate the longitudinal Fickian dispersivity.

Burr et al. [1994] also used a numerical simulation approach coupled with a Monte Carlo analysis to investigate reactive and non-reactive solute evolution under steady-state flow conditions. Note that their simulation approach is similar in principle to that performed by Robin [1991]. Their findings for non-reactive transport showed that with regard to the macrodispersion the first-order stochastic analytic solutions of Gelhar and Axness [1983], Dagan [1988] and Naff [1990] tended to over-predict the simulated temporal spreading behaviour and the estimated asymptotic longitudinal macrodispersivity.

Naff et al. [1996], using a simulation methodology similar to that utilized by Burr et al. [1994], simulated the transport of a nonreactive solute under a range of variances in log-hydraulic conductivity ($\sigma_f^2 \leq 0.9$, where σ_f^2 represents the variance in the log-hydraulic conductivity). Stochastic models which corrected for the effects of local transverse dispersion and which incorporated a second order correction appeared to best explain the simulated corrected longitudinal dispersivities. Again, due to the source dimensions nonergodic effects

were generally observed.

The simulation experiments described above generally produced differing results which are influenced by the assumptions inherent in the models and the solution methods. However, despite these differences they all demonstrate a scale dependence of the longitudinal dispersivity which appears to mimic that observed in field tracer experiments. This confirms that to some degree the scale dependence of the longitudinal dispersivity observed in field tracer experiments is controlled by the heterogeneity present in the hydraulic conductivity field. However, the simulations described above are based on the simplifying assumption of steady-state flow. As pointed out by Dagan et al. [1996] this assumption is usually only appropriate for transport of a relatively short duration. Nonetheless, the experiments illustrate how practical methodologies may be developed to evaluate proposed theoretical hypotheses.

The effect of flow transients on the dispersion process has been partially examined with the aid of finite element numerical models by Goode and Konikow [1990]. Unlike the models discussed above, the model considered by Goode and Konikow [1990] utilized a homogeneous hydraulic conductivity field. Their results showed that flow transients affected the evolution of solute plumes and enhanced the transverse dispersion process, due to the fact that longitudinal dispersion acted in a direction which was not parallel to the mean flow direction. Further, Goode and Konikow [1990] point out that in aquifers having large storativity, a high frequency of hydraulic head boundary condition changes would reduce the apparent dispersion effect because the boundary stresses would not propagate far into the aquifer in a short period of time.

The fact that few high resolution simulations have been performed under steady-state conditions and none under transient conditions is more than likely due to the prohibitive computational costs involved with solving the large system of equations at each time step. Note that for the transient simulations both the flow and mass transport equations must be solved at each time step. In the following, methods aimed at efficiently solving the systems of equations which result from the mass transport formulation are discussed.

1.2.6.1 Finite Element Solution of the Advection-Dispersion Equation

Application of the finite element method to the governing mass transport equation subject to initial and boundary conditions results in a matrix differential equation of the form

$$\boldsymbol{M}\frac{d\boldsymbol{c}}{dt}+\boldsymbol{K}\boldsymbol{c}=\boldsymbol{f} \tag{1.2}$$

where $\boldsymbol{c}$ is a vector of unknowns at the nodes of the finite element mesh used to discretize the domain Ω, $\boldsymbol{K}$ is the "stiffness" or "conductivity" matrix, $\boldsymbol{M}$ is the "mass" or "capacity" matrix and $\boldsymbol{f}$ is a vector which contains the effects of the boundary conditions as well as source/sink terms. Both $\boldsymbol{M}$ and $\boldsymbol{K}$ are $n \times n$ matrices, with being $\boldsymbol{K}$ unsymmetric, and $\boldsymbol{M}$ being symmetric and positive-definite. Here n represents the number of nodes in the finite element grid. It is important to note that the matrix $\boldsymbol{K}$ is composed of advective and dispersive terms.

The traditional approach to solving the above matrix differential equation is to apply a finite difference approximation to the time derivative followed by a time-stepping routine such as the Crank-Nicolson routine (see for example Pinder and Huyakorn, 1983). Applying the Crank-Nicolson routine to (1.2) gives

$$\left(M+\frac{\Delta t}{2}K\right)c^{s+1}=\left(M-\frac{\Delta t}{2}K\right)c^{s}+(\Delta t)f^{s+\frac{1}{2}} \tag{1.3}$$

where Δt is the time-step between evaluation periods and s is the current time step. If the time-step remains constant during the simulation, the solution of (1.3) is obtained by applying an LU decomposition to the LHS, followed by matrix-vector multiplications of the RHS and repeated back-solves.

It is apparent that the cost of solving the above expression will be a function of the size of the matrices $\boldsymbol{K}$ and $\boldsymbol{M}$, as well as the number of time-steps required to reach the desired time. In addition, for simulations involving transient flow conditions or non-constant dispersivities, the matrix $\boldsymbol{K}$ must be reformed and the LHS of the system in (1.3) decomposed at each time step. Thus for large systems requiring many time steps and numerous decompositions the described approach is computationally expensive. The enormous cost associated with the described solution scheme is further demonstrated when data storage costs are taken into account. Assuming that the bandwidths of $\boldsymbol{M}$ and $\boldsymbol{K}$ are stored in double precision the storage requirements in bytes for each matrix may be approximated by, $n*[2*(R+1)]*8$, where R is the difference between the maximum and minimum node numbers for an element. For large three-dimensional simulations n and R can be extremely large, thus leading to overwhelming storage requirements.

The desire to mathematically model complex hydrological systems realistically has prompted researchers to examine various alternate approaches for solving (1.2). The following summarizes some of these methodologies.

1.2.6.2 Iterative Matrix Solvers

An alternate approach for solving (1.3) is through the use of iterative techniques. Iterative methods start with a guess for the solution vector, which is then refined in successive stages of the iteration procedure until a desired level of accuracy is attained. Depending on the level of accuracy required, solution times using iterative methods can be very short. Angeleri et al. [1989] pointed out that in iterative schemes the matrix is preserved in its original form so that there are no fill-in elements encountered in the factorization. For very sparse matrices with large bandwidths, this can lead to significant savings in storage over factorization methods. Despite these advantages iterative methods suffer from the disadvantage that convergence can only be proved for symmetric positive definite matrices.

Several iterative schemes are currently employed in the solution of flow and mass transport problems in the field of hydrogeology. Of these methods, Sudicky and Huyakorn [1990] described the Preconditioned Conjugate Gradient (PCG) method as the most promising for handling sparse three-dimensional numerical solutions. In addition, through the use of various extensions, the PCG method can be applied to problems involving asymmetry. One such extension is the ORTHOMIN formulation [Behie and Forsyth, 1984] which has been applied increasingly in subsurface contaminant transport and variably saturated flow simulations [cf, Sudicky, 1990]. Other iterative methodologies which have been employed to solve flow and transport problems in variably saturated porous media include the generalized minimal residual (GMRES; see Saad and Schultz, 1986, and Vanderkwaak et al., 1995) and the conjugate gradient stabilization scheme (CGSTAB; see van der Vorst, 1992, Chin and Forsyth, 1993, and Vanderkwaak et al., 1995).

1.2.6.3 Laplace Transform Galerkin Method

The Laplace Transform Galerkin (LTG) method has been applied to the solution of the mass transport problems by Sudicky [1989] and Sudicky and MacFarlane [1990]. Under the LTG formulation a Laplace transform is applied to the governing mass transport equation, and the initial and boundary conditions. This procedure eliminates the temporal derivative and results in a matrix equation of the form

$$(\boldsymbol{K}+p\boldsymbol{M})\bar{c}=\bar{f} \tag{1.4}$$

where $\bar{c}$ is the Laplace transformed vector of nodal concentrations, $\bar{f}$ is the Laplace transformed vector containing the effects of the boundary conditions as well as source and sink terms, and p is the Laplace transform variable. Equation (1.4) is then solved using either direct methods or iterative methods. Sudicky [1990], Robin [1991], Burr et al. [1994] and Naff et al. [1996] all report using the ORTHOMIN method to solve this system of equations. The solution obtained in Laplace space is then inverted back to original space using suitable numerical inversion schemes. The advantages of the LTG method are [Sudicky, 1989]:

1. The method provides a highly accurate and robust solution for grid Peclet numbers[5] (Pe_i) which are in excess of 30;
2. The method allows time-continuous solutions to be obtained;
3. The method is well suited for high speed execution on parallel processing computers;

---

[5] The grid Peclet number is defined as $Pe_i = (v_i * \Delta x_i)/D_{ii}$ $(i=1, 2, 3)$ where v_i represents the groundwater velocity in the i^{th} direction, Δx_i is the maximum grid spacing in the i^{th} direction, and D_{ii} is the ii component of the hydrodynamic tensor [see Bear, 1972].

4. The method is well suited for handling convolution integrals which describe rock-fluid interactions in dual porosity formulations.

Sudicky [1989] has shown that for reasonably simple mass transport problems involving steady-state groundwater flow and constant dispersivity, the LTG method out performs the standard finite element approach.

1.2.6.4 The Arnoldi Modal Reduction Method

The Arnoldi modal reduction method is based on the recursive Arnoldi algorithm. Using this algorithm a matrix differential equation such as (1.2) is transformed into a smaller system of equations, the size of which is dependent on the number of modes (Arnoldi vectors) chosen. The reduced system is then solved using an appropriate numerical procedure in-conjunction with a time-stepping scheme such as the Crank-Nicolson approach. The solution in the original space is then obtained from the reduced space using matrix vector multiplications.

Nour-Omid et al. [1991] and Woodbury et al. [1990] have shown that application of the Arnoldi modal reduction method to (1.2) results in a matrix differential equation of the form

$$H\dot{w}+w=Q_m^T MK^{-1}f \qquad (1.5)$$

where H is an $m \times m$ upper Hessenberg matrix, Q_m is a matrix of Arnoldi vectors and w is a vector of length m which is chosen such that

$$c \approx \hat{c} = Q_m w \qquad (1.6)$$

It is important to note that in general $m \ll n$. Equation (1.5) may be solved using the traditional time-stepping method previously described. The solution in the original space is easily obtained from the reduced space through the use of matrix vector multiplications.

Woodbury et al. [1990] have shown that for reasonably simple mass transport problems involving steady-state groundwater flow and constant dispersivity, the Arnoldi modal reduction method is much faster than the standard finite element approach.

1.3 Summary

Dispersion phenomenon in porous media has been examined using a variety of approaches. Several detailed field tracer experiments designed to examine field-scale dispersion processes have been conducted in mildly heterogeneous sand deposits. The results of these experiments have shown that both the longitudinal and horizontal transverse dispersivities initially grow with travel distance before reaching asymptotic values. Some researchers have argued that hydrogeologic conditions observed at a site can be considered as one realization of a stochastic process. Using ergodic assumptions, various stochastic-analytic theories have been proposed to explain field observed behaviours. To date no single stochastic theory proposed can explain the whole spectrum of observed behaviours. Depending on the assumptions made, only certain aspects can be explained. Further, due to the design of the conducted field tests, data necessary to validate other aspects of proposed stochastic theories are unavailable. Therefore, it is evident that refinement of available

stochastic theories is required, as well as additional data from better designed field tracer experiments.

Other researchers have shown that in some cases hydrogeologic media may be best represented by fractal scaling relationships. The study of dispersion in heterogeneous media represented by fractal scaling concepts is a new area of research and as a result has been the focus of very few studies. However, limited theoretical and simplistic numerical studies have shown that in such environments dispersion is influenced by the fractal dimension and the fractal scaling length. Detailed field studies of dispersion in media displaying fractal scaling relationships are currently unavailable. One of the main reasons for this is that methods for obtaining detailed fractal scaling relationships from field data are unavailable. As a result, proposed theories of dispersion in fractal media still require validation.

Mass transport formulations derived from volume averaging approaches are commonly used due to their easy numerical implementation, and the fact that in some cases closed form analytic solutions are available. The main disadvantage of this approach is that variables such as dispersivity and hydraulic conductivity are valid only at the level of the averaging volume used. For hydrogeologic environments which contain several length scales the choice of the appropriate averaging volume poses a problem; a poor choice of averaging volume can in some cases result in scale dependent dispersivities which although appearing plausible misrepresent the true physical situation. The scale dependence observed in such cases usually results in dispersivities which are orders of magnitude greater than those obtained from detailed tracer experiments and stochastic theory. Although the use of these scale dependent dispersivities can produce acceptable solutions when calibrated against field

observed plumes, the approach is not justified from a theoretical perspective.

Several recent research efforts have shown that numerical simulation techniques combined with Monte Carlo analysis can be used to investigate various aspects of solute dispersion in heterogeneous hydrogeologic media. In these simulations, some field observed and theoretically predicted behaviours have been displayed. Although the simulations reported are based on the simplifying assumption of steady-state flow, they nonetheless appear to be reasonably successful at reproducing some field observed and theoretically predicted behaviours. As observed by Burr et al. (1994), simulations based on steady-state flow will produce significant longitudinal dispersion values and negligible horizontal transverse dispersion. Note that current field evidence does not necessarily support the latter observation. Several researchers have concluded that much of the transverse dispersion observed at field tracer test site may be attributed to the presence of flow transients [Farrell et al., 1994]. If numerical simulation techniques are to aid in our knowledge of dispersion processes in hydrogeologic media, then it is necessary for these models to account for such features as transient flow. Based on the success of studies conducted to date it appears that numerical simulation techniques have the potential to play a vital role in validating new theories associated with mass transport as well as aid in the design of future field-scale tracer experiments. However, in order to achieve this goal more field based phenomena (e.g. the dynamic behaviour of flow systems, the spatial distribution of reactive parameters and the interactions of geochemical processes among others) must be incorporated into the numerical simulation procedure. Accounting for such processes in the simulation procedure requires more field and laboratory data as well as faster and more efficient matrix solution techniques.

1.4 Research Objectives

An understanding of the dispersion process in hydrogeologic media has been gained primarily through the use of field tracer experiments, laboratory experiments and mathematical studies. Although tracer experiments provide valuable information they are time consuming and prohibitively expensive to perform. Whereas in most cases laboratory studies of dispersion are convenient and generally inexpensive to perform, they generally fail to give information regarding large scale processes which are commonly seen at the aquifer level. Mathematical studies provide informative insights into the dispersion phenomena. However, due to the simplifying assumptions required to achieve tractable solutions, these studies in most cases over-simplify the real physical situation and as a result are only applicable to the simplest of cases. Numerical simulations provide a relatively inexpensive means of obtaining some information about mass transport processes in the subsurface as well as allowing mathematical theories to be evaluated. In addition, these simulations can act as valuable predictive tools and so aid in the design of cost effective remediation or experimental strategies.

The primary aim of this study is to investigate the effects of groundwater flow transients on the evolution of nonreactive or inert solutes. In order to evaluate these impacts a numerical simulation procedure will be employed. As a result, part of this work will focus on the construction of a numerical simulator which is capable of efficiently solving the coupled groundwater flow and mass transport equations. The simulator will then be utilized in limited Monte-Carlo simulations involving solute transport in second order stationary heterogeneous hydraulic conductivity fields under both steady state and transient flow

conditions. The results of the simulations under steady-state and transient conditions will then be compared to determine the importance of unsteady flow on solute migration. The simulation data will also be used in an attempt to validate analytical models which predict solute migration and dispersion under transient flow conditions. It is noteworthy to point out that the advantage of the Monte Carlo approach as applied in this analysis is that it does not introduce any assumptions regarding the small variations in the hydraulic conductivity field [Gelhar, 1993]. However, the disadvantages of the approach are that (i) a large number of simulations are required in order to accurately estimate the statistical moments and (ii) changes in the value of the random parameter from element to element must be small if a high degree of accuracy is to be maintained. It is clear that satisfying the latter two conditions can result in a computationally intensive system.

As discussed earlier, simulations of this nature are limited by the efficient and accuracy of available matrix solvers. In response to these limitations, part of this work focuses on evaluating the performance of the Arnoldi modal reduction matrix (AMRM) solver relative to other solvers for various classes of problems encountered by the practising computational hydrogeologist. The goal being to identify the classes of problems for which the Arnoldi modal reduction method is best suited. As well, some effort will be spent examining methods designed to improve the performance of the method.

In particular the following will be examined

1. Whether many of the features observed in field tracer experiments can be simulated using realistic hydrogeologic environments (i.e., unsteady flow and stochastically generated hydraulic conductivity fields) along with local-scale

dispersivity values;

2. The conditions under which the equations for predicting asymptotic macrodispersivity, such as those proposed by Rehfeldt and Gelhar [1992], are applicable;
3. The applicability and performance of the Arnoldi modal reduction method for solving various classes of problems associated with mass transport in hydrogeological environments.

1.5 Scope

In order to achieve the objectives of this work and to reduce the computational cost of the proposed approach the following will be considered:

* The competitiveness of the Arnoldi method compared to other new solution methods such as the Laplace Transform Galerkin method [Sudicky, 1989] will be examined for various numerically difficult hydrogeologic problems [e.g., highly advective systems and high grid Peclet number problems]. The focus here will be on accuracy and computational efficiency.
* Examination of possible improvements to the Arnoldi algorithm which increase the rate of convergence so reducing the computational cost and yet maintain the accuracy of the solution. The focus here will be on a 'shift' variant of the Arnoldi algorithm. Shifting is known to increase the rate of convergence while reducing the number of Arnoldi vectors required to achieve a desired level of accuracy.
* Efficient methods for incorporating observed time-dependent hydraulic heads into

the simulation procedure.

* Efficient methods for simulating coupled flow and mass transport in high resolution simulation experiments.

References

Anderson, M. P., Comment on "Universal upscaling of hydraulic conductivities and dispersivities in geologic media" by S. P. Neuman, Water Resour. Res., 27(6), 1381-1382, 1991.

Angeleri, F., V. Sonnad, K.-J. Bathe, Studies of finite element procedures. An evaluation of preconditioned iterative solvers, Computers and Structures, Vol. 32, No. 3/4, p. 671-677, 1989.

Ayra, A., T. A. Hewett, R. Larson, and L. W. Lake, Dispersion and reservoir heterogeneity, Paper SPE 14364 presented at the 6th Annual Technical Conference, Society of Petroleum Engineers, Las Vegas, Nevada, 22-25 September, 1985.

Barton, C. C., and E. Larson, Fractal geometry of two-dimensional fracture networks at Yucca Mountain, Southwest Nevada. Paper presented at the International Symposium on Fundamentals of Rock Joints, Swedish National Group of the International Society of Rock Mechanics, Bjorkliden, Sweden, 15-20 September, 1985.

Bear, J., Some experiments in dispersion, J. Geophys. Res., 66, p. 2455-2467, 1961b.

Bear, J., Dynamics of Fluids in Porous Media, American Elsevier Environmental Series, 1972.

Bear, J., and Y. Bachmat, Introduction to Modeling of Transport Phenomena in Porous Media, Kluwer Academic Publishers, 1990.

Bear, J., and A. Verruijt, Modeling Groundwater Flow and Pollution, D. Reidel Publishing Company, 1987.

Beckie, R., A. A. Aldama, and E. F. Wood, The universal structure of the groundwater flow equations, Water Resour. Res., 30(5), 1407-1419, 1994.

Behie, A., and P. A. Forsyth, Incomplete factorization methods for fully implicit simulation of enhanced oil recovery, SIAM J. Stat. Comput., 5(3), p. 543-561, 1984.

Burr, D. T., E. A. Sudicky, and R. L. Naff, Nonreactive and reactive solute transport in three-dimensional heterogeneous porous media: Mean displacement, plume spreading, and uncertainty, Water Resour. Res., 30(3), p. 791-815, 1994.

Burrough, P. A., Multiscale sources of spatial variationin soil. I: The application of fractal concepts to nested levels of soil variation, J. Soil Sci., 34, p. 577-597, 1983a.

Burrough, P. A., Multiscale sources of spatial variation ins soil. II: A non-Brownian fractal model and its application on soil surveys, J. Soil Sci., 34, p. 599-620 , 1983b.

Chang, W.-L., J. W. Biggar, and D. R. Nielsen, Fractal description of wetting front instability in layered soils, Water Resour. Res., 30(1), 125-132, 1994.

Chin, D. A., and T. Wang, An investigation of the validity of first-order stochastic dispersion theories in isotropic porous media, Water Resour. Res., 28(6), p. 1531-1542, 1992.

Cushman, J. H., On diffusion in fractal porous media, Water Resour. Res., 27(4), 643-644, 1991.

Cushman, J. H., and T. R. Ginn, On dispersion in fractal porous media, Water Resour. Res., 29(10), 3513-3515, 1993.

Dagan, G., Stochastic modeling of groundwater flow by unconditional and conditional probabilities, 2, The solute transport, Water Resour. Res., 18(4), p. 835-848, 1982.

Dagan, G. , Solute transport in heterogeneous porous formations, J. Fluid Mech., 145, 151-177, 1984.

Dagan, G, Time-dependent macrodispersion for solute transport in anisotropic heterogeneous aquifers, Water Resour. Res., 24(9), p. 1491-1500, 1988.

Dagan, G., Transport in heterogeneous porous formations: Spatial moments, ergodicity and effective dispersion, Water Resour. Res., 26(6), p. 1281-1290, 1990.

Dagan, G., Dispersion of a passive solute in non-ergodic transport by ateady velocity fields in heterogeneous formations, J. Fluid Mech., 233, 197-210, 1991.

Dagan, G., A. Bellin, and Y. Rubin, Lagrangian analysis of transport in heterogeneous formations under transient flow conditions, Water Resour. Res., 32(4), 891-899, 1996.

Desbarats, A. J., and S. Bachu, Geostatistical analysis of aquifer heterogeneity from the core scale to the basin scale: A case study, 30(3), 673-684, 1994.

Dieulin, A., Propagation de pollution dans un aquifère alluvial: l'effet de parcours, D. Ing. Thesis, University of Sciences and Medicine of Grenoble, Grenoble, 1980.

Farrell, D. A, A. D. Woodbury, E. A. Sudicky, and M. O. Rivett, Stochastic and deterministic analysis of dispersion in unsteady flow at the Borden tracer-test site, Journal of Contaminant Hydrology, 15, p. 159-185, 1994.

Farrell, D. A., A. D. Woodbury, and E. A. Sudicky, The 1978 Borden tracer experiment: Analysis of the spatial moments, Water Resour. Res. 30(11), p. 3213-3223, 1994.

Freyberg, D. L., A natural gradient experiment on solute transport in a sand aquifer, 2, Spatial moments and the advection and dispersion of nonreactive tracers, Water Resour. Res., 22(13), p. 2031-2046, 1986.

Fried, J. J., Miscible pollution of groundwater: A study of methodology, in Preceedings of International Symposium on modelling Techniques in Water Resources systems, Vol. 2, edited by A. K. Biswas, p. 362-371, Environment Canada, Ottawa, Ont., 1972.

Fried, J. J., Groundwater Pollution, 330 p., Elsevier, New York, 1975.

Garabedian, S. P., D. R. LeBlanc, L. W. Gelhar, and M. A. Celia, Large-scale natural-gradient test in sand and gravel, Cape Cod, Massachusetts, 2, Analysis of spatial moments for a non-reactive tracer, Water Resour. Res., 27(5), p. 911-924, 1991.

Gelhar, L. W., Stochastic Subsurface Hydrology, Prentice Hall, Englewood Cliffs, New Jersey, USA, 1993.

Gelhar, L. W., and C. L. Axness, Three-dimensional stochastic analysis of macrodispersion in aquifers, Water Resour. Res., 19(1), p. 161-180, 1983.

Gelhar, L. W., C. Welty, and K. R. Rehfeldt, A critical review of data on field-scale dispersion in aquifers, Water Resour. Res., 28(7), p. 1955-1974, 1992.

Gelhar, L. W., C. Welty, and K. R. Rehfeldt, Reply, Water Resour. Res., 29(6), 1867-1869, 1993.

Goode, D. J., and L. F. Konikow, Apparent dispersion in transient groundwater flow, Water Resour. Res., 26(10), p. 2339-2351, 1990.

Graham, W., and D. McLaughlin, Stochastic analysis of non-stationary subsurface solute transport, 1, Unconditional moments, Water Resour. Res., 25(2), p. 215-232, 1989.

Graham, W., and D. McLaughlin, Stochastic analysis of non-stationary subsurface solute transport, 2, Conditional moments, Water Resour. Res., 25(11), p. 2331-2355, 1989.

Hess, K., S. H. Wolf, and M. A. Celia, Large-scale natural gradient tracer test in sand and gravel, Cape Cod Massachusetts, 3, Hydraulic conductivity variability and calculated macrodispersivities, Water Resour. Res., 28(8), 2011-2020, 1992.

Hewett, T. A., Fractal distributions of reservoir heterogeneity and their influence on fluid transport, Paper SPE 15386 presented at the 61th Annual Technical Conference, Society of Petroleum Engineers, New Orleans, LA, 5-8 October, 1986.

Huyakorn, S. P., and G. F. Pinder, Computational Methods in Subsurface Flow, Academic Press, Inc. (London) LTD., 473 pp., 1983.

Indelman, P., and G. Dagan, Upscaling of permeability of anisotropic heterogeneous formations, 1, The general framework, Water Resour. Res., 29(4), 917-923, 1993.

Indelman, P., and G. Dagan, Upscaling of permeability of anisotropic heterogeneous formations, 2, General structure and small perturbation analysis, Water Resour. Res., 29(4), 925-933, 1993a.

Indelman, P., and G. Dagan, Upscaling of permeability of anisotropic heterogeneous formations, 3, Applications, Water Resour. Res., 29(4), 935-943, 1993b.

Katz, A. J., and A. H. Thompson, Fractal sandstone pores: Implications for conductivity and pore formation, Phys. Rev. Let. 54, p. 1325-1328, 1985.

Kemblowski, M. W., and C.-M. Chang, Infiltration in soils with fractal permeability distribution, Ground Water, 31(2), 187-192, 1993.

Kemblowski, M. W., and J.-C. Wen, Contaminant spreading in stratified soils with fractal permeability distribution, Water Resour. Res., 419-425, 1993.

Kinzelbach, W., and P. Ackerer, Modelisation de la propagation d'un champ d'écoulement transitoire, Hydrogeologie, 2, p. 197-206, 1986.

Lawson, D. E., and D. E. Elrick, A new method for determining and predicting dispersion coefficients in porous media, Proc. of 2nd Symposium on Fundamentals of Transport Phenomena in Porous Media, University of Guelph, Guelph, Ont., p. 753-777, 1972.

Martin, J. M., Displacements miscilbles dans des milieux naturels de grande extension, Rev. Inst. Fr. Pèt., 26, p. 1065-1075, 1971.

Molz, F. J., and G. K. Boman, A fractal-based stochastic interpolation scheme in subsurface hydrology, Water Resour. Res., 29(11), 3769-3774, 1993.

Naff, R. L., On the nature of the dispersive flux in saturated heterogeneous porous media, Water Resour. Res., 26(5), 1013-1026, 1990.

Naff, R. L., D. F. Haley, and E. A. Sudicky, High-resolution Monte-Carlo simulation of flow and conservative transport in heterogeneous porous media: 2, Transport results, [draft manuscript], 1996.

Naff, R. L., T.-C. Yeh, and M. W. Kemblowski, A note on the recent natural gradient tracer test at the Borden site, Water Resour. Res., 24(12), 2099-2103, 1988.

Naff, R. L., T.-C. Yeh, and M. W. Kemblowski, Reply, Water Resour. Res., 25(12), p. 2523-2525, 1989.

Neuman, S. P., Statistical characterization of aquifer heterogeneities: An overview, Geological Society of America, Special Paper 189, 1982.

Neuman, S. P., Universal upscaling of hydraulic conductivities and dispersivities in geologic media, Water Resour. Res., 26(8), 1749-1758, 1990.

Neuman, S. P., Reply, Water Resour. Res., 27(6), 1383-1384, 1991.

Neuman, S. P., On advective transport in fractal permeability and velocity fields, Water Resour. Res., 31(6), 1455-1460, 1995.

Neuman, S. P., C. L. Winter, and C. M. Newman, Stochastic theory of field-scale Fickian dispersion in anisotropic porous media, Water Resour. Res., 23(3), p. 453-466, 1987.

Neuman, S. P., and Y.-K. Zhang, A quasi-linear theory of non-Fickian and Fickian subsurface dispersion, 1, Theoretical analysis with application to isotropic media, Water Resour. Res., 26(5), p. 887-902, 1990.

Nour-Omid, B., W. S. Dunbar, and A. D. Woodbury, Lanczos and Arnoldi methods for the solution of convection-diffusion equations, Comput. Methods in Appl. Mech. and Eng., 88, p. 75-95, 1991.

Oakes, D. B., and D. J. Edworthy, Field measurements of dispersion coefficients in the United Kingdom, Groundwater Quality, Measurement, Prediction and Protection, p. 327-340, Water Resources Centre, Reading, England, 1977.

Pickens, J. F., J. A. Cherry, R. W. Gillham, and W. F. Merritt, Field studies of dispersion in a shallow sandy aquifer, Proc. Invitational Well-Testing Symposium, Berkeley, Calif., p. 55-62, 1978.

Quinodoz, H. A. M., and A. J. Valocchi, Macrodispersion in heterogeneous aquifers: Numerical experiments, Paper presented at International Conference and Workshop on Transport and Mass Exchange Processes in Sand and Gravel Aquifers: Field Modeling Studies, AGU, Ottawa, Ont., Canada, 1-4 October, 1990.

Rajaram, H., and L. W. Gelhar, Plume scale-dependent dispersion in heterogeneous aquifers, 1., Lagrangian analysis in a stratified aquifer, 29(9), 3249-3260, 1993.

Rajaram, H., and L. W. Gelhar, Plume scale-dependent dispersion in heterogeneous aquifers, 2., Eulerian analysis and three-dimensional aquifers, 29(9), 3249-3260, 1993.

Rehfeldt, K. R., and L. W. Gelhar, Stochastic analysis of dispersion in unsteady flow in heterogeneous aquifers, Water Resour. Res., 28(8), p. 2085-2099, 1992.

Reynolds, W. D., Column studies of strontium and cesium transport through granular geologic porous medium, M. Sc. Thesis, Dept. of Earth Sci., Univ. of Waterloo, Waterloo, Ont., Canada, 1978.

Robbins, G. A., Methods for determining transverse dispersion coefficients of porous media in laboratory column experiments, Water Resour. Res., 25(6), 1249-1258, 1989.

Robin, M. J. L., Migration of reactive solutes in three-dimensional heterogeneous porous media, Ph. D. Thesis, Dept. of Earth Sci., Univ. of Waterloo, Waterloo, Ont., Canada, 1991.

Ross, B., Dispersion in fractured fractal networks, Water Resour. Res., 22, p. 823-827, 1986.

Rubin, Y., and J. J. Gómez-Hernández, A stochastic approach to the problem of upscaling of conductivity in disordered media: Theory and unconditional numerical simulations, Water Resour. Res., 26(4), 691-701, 1990.

Sánchez-Villa, X., J. P. Girardi, and J. Carrera, A synthesis of approaches to upscaling of hydraulic conductivities, Water Resour. Res., 31(4), 867-882, 1995.

Sauty, J. P., An analysis of hydrodispersive transfer in aquifers, Water Resour. Res., 16, p. 145-158 , 1980.

Schellenberg, S. L., Groundwater flow and nonreactive tracer motion in heterogeneous statistically anisotropic porous media, M. Sc. Thesis, Dept. of Earth Sci., Univ. of Waterloo, Waterloo, Ont., Canada, 1987.

Schwartz, F. W., Macroscopic dispersion in porous media: The controlling factors, Water Resour. Res., 13(4), p. 743-752, 1977.

Shamir, U. Y., and D. R. E. Harleman, Numerical and analytical solutions of dispersion problems in heterogeneous and layered aquifers, Mass. Inst. Technol., Cambridge, Mass., Hydrodyn. Lab. Rep. 89, 1966.

Shapiro, A., and V. D. Cvetkovic, A comparison of two- and three-dimensional stochastic models of regional solute movement, Transport in Porous Media, 5, 1-25, 1990.

Silliman, S. E., and E. S. Simpson, Laboratory evidence of scale effect in dispersion of solutes in porous media, Water Resour. Res., 23(8), p. 1667-1673, 1987.

Smith, L., and F. W. Schwartz, Mass transport, 1, A stochastic analysis of macrodispersion, Water Resour. Res., 16(2), p. 303-313, 1980.

Sudicky, E. A., A natural gradient experiment on solute transport in a sand aquifer: Spatial variability of hydraulic conductivity and its role in the dispersion process, Water Resour. Res., 22(13), p. 2069-2082, 1986.

Sudicky, E. A., The Laplace transform Galerkin technique: A time-continuous finite element theory and application to mass transport in groundwater, Water Resour. Res., 25(8), p. 1833-1846, 1989.

Sudicky, E. A., The Laplace transform Galerkin technique for efficient time-continuous solution of solute transport in double-porosity media, Geoderma, 46, p. 543-561, 1990.

Sudicky, E. A., J. A. Cherry, and E. O. Frind, Migration of contaminants in groundwater at a landfill: A case study, 4, A natural-gradient dispersion test, J. of Hydrol., 63, p. 81-108, 1983.

Sykes, J. F., S. B. Pahwa, R. B. Lantz and D. S. Ward, Numerical simulation of flow and contaminant migration at an extensively monitored landfill, Water Resour. Res., 18(6), p. 1687-1704, 1982.

Tompson, A. F. B., and L. W. Gelhar, Numerical simulation of solute transport in three dimensional, randomly heterogeneous porous media, Water Resour. Res., 26(10), p. 2541-2562, 1990.

Turcotte, D. L., Fractals and Chaos in Geology and Geophysics, Cambridge University Press, 1992.

Wheatcraft, S. W., G. A. Sharp, and S. W. Tyler, Fluid flow and solute transport in fractal heterogeneous porous media, Chapter XI, Dynamics of Fluids in Hierarchial Porous Media, ed. J. H. Cushman, Academic Press, p. 305-326, 1990.

Wheatcraft, S. W., and S. W. Tyler, An explanation of scale-dependent dispersivity in heterogeneous aquifers using concepts of fractal geometry, Water Resour. Res., 24, p. 566-578, 1988.

Woodbury, A. D., W. S. Dunbar, and B. Nour-Omid, Application of the Arnoldi algorithm to the solution of the advection-dispersion equation, Water Resour. Res., 26, p. 2579-2590, 1990.

Woodbury, A. D., and E. A. Sudicky, A reexamination of the geostatistical characteristics of the Borden aquifer, Water Resour. Res., 27(4), p. 533-546, 1991.

Yeh, T.-C. J., Comment on "Modeling of scale-dependent dispersion in hydrogeologic systems" by J. F. Pickens and G. E. Grisak, Water Resour. Res., 23(3), p. 522, 1987.

Zhang, Y.-K., and S. P. Neuman, A quasi-linear theory of non-Fickian and Fickian subsurface dispersion, 2, Application to anisotropic media and the Borden site, Water Resour. Res., 26(5), p. 903-913, 1990.

Zhang, D., and S. P. Neuman, Head and velocity covariances under quasi-steady state flow and their effects on advective transport, Water Resour. Res., 32(1), 77-83, 1996.

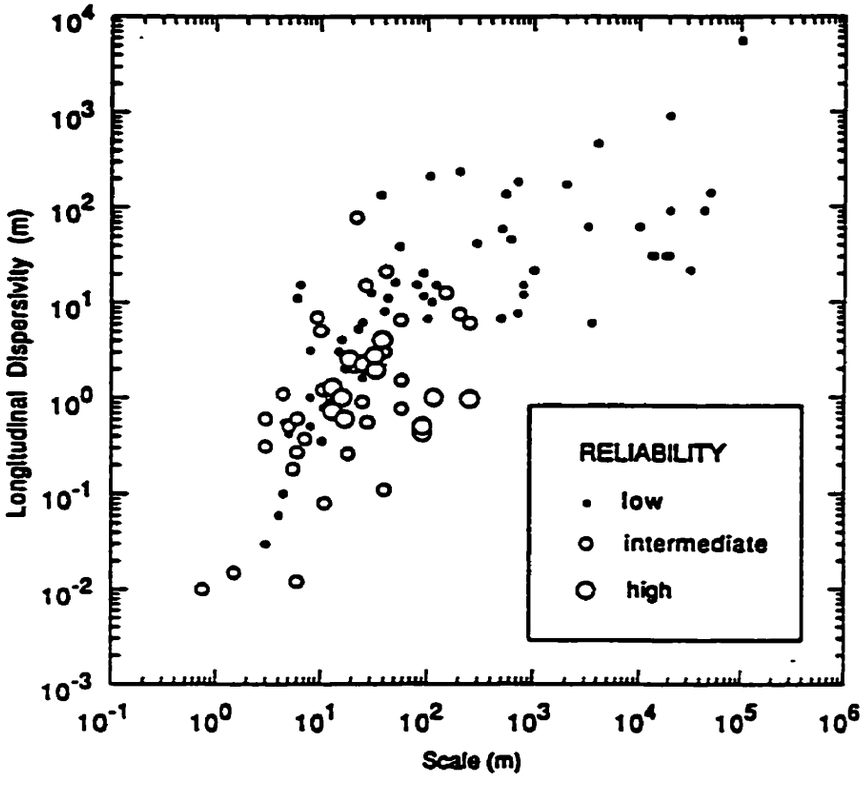

Figure 1.1: Field longitudinal dispersivity data classified according to reliability (from Gelhar et al., 1992).

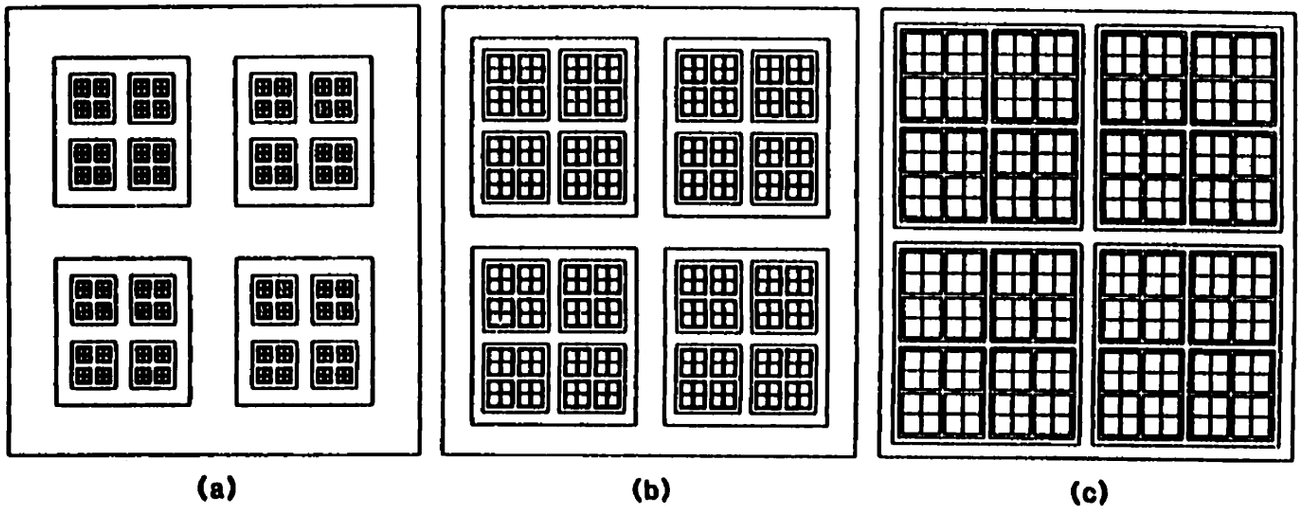

Figure 1.2: Schematic of a Sierpinski carpet showing the impact of varying fractal dimension, D: (a) D = 1.25; (b) D = 1.5; (c) D = 1.75 [from Wheatcraft et al., 1990].

Chapter 2

Numerical Modelling of Mass Transport in Hydrogeologic Environments: Performance Comparison of the Laplace Transform Galerkin and Arnoldi Modal Reduction Schemes

2.1 Introduction

The advection-dispersion equation (ADE) is commonly used to model solute transport in hydrogeologic environments. Hydrogeologic environments typically consist of irregular domains, heterogeneous material properties and complex boundary conditions. Due to these factors closed form analytical expressions describing solute transport in such environments are impossible. An alternate approach to solving the ADE over such domains involves the use of numerical formulations. Of the numerical formulations proposed, the finite element (FE) and finite difference (FD) methods are by far the most utilized. In both methods, spatial discretization of the ADE is performed. Depending on the approach being utilized, temporal discretization of the ADE may be performed, and an appropriate time marching scheme employed to yield a solution at the desired time.

Numerical modelling of the advection-dispersion equation using either of the above approaches requires that certain criteria be met in order to obtain a stable and accurate solution. For the FE formulation employing linear basis functions these criteria can be mathematically stated as [Huyakorn and Pinder, 1983; Daus et al., 1983; Celia and Gray, 1992]:

$$Pe_i = \frac{(v_i \Delta x_i)}{D_{ii}} \leq 2 \tag{2.1}$$

$$Cn_i = \frac{(v_i \Delta t)}{\Delta x_i} \leq 1 \tag{2.2}$$

where Pe_i represents the grid Peclet number in the i^{th} direction, Cn_i represents the Courant number, v_i represents the groundwater velocity in the i^{th} direction, D_{ii} is the i^{th} diagonal component of the hydrodynamic tensor, Δx_i is the maximum local grid spacing in the i^{th} direction and Δt is the time step. In cases where the advective displacement overwhelms the dispersive advance, such that the solute front is relatively sharp, an exceedingly fine spatial and temporal discretization is required to ensure an accurate solution [Sudicky, 1989]. The need for proper grid design and time step selection is further necessitated by the fact that in natural geologic environments the groundwater velocity may vary considerably in magnitude and direction throughout the domain.

Additional constraints are commonly placed on the mesh discretization when simulating fluid and mass transport in correlated hydraulic conductivity fields. For such simulations it is acknowledged that the mesh discretization must be smaller than the correlation scale of the process. However, there appears to be no unanimous agreement on the ratio of the mesh discretization to the correlation scale. This general lack of agreement is illustrated in [Tompson and Gelhar, 1990; Chin and Wang, 1992; Ababou et al., 1989]. In these works, the discretizations ranged from one-half to one-fifth of the correlation scale of the hydraulic conductivity field. Chin and Wang [1992] suggested that a discretization on the order of one-half the correlation scale of hydraulic conductivity may be too large to accurately

determine the velocity flow field. It is therefore apparent that for many realistic problems, in particular those involving small correlation scales, a fine mesh discretization may be required. Depending on the size of the domain, the use of a fine discretization can result in grids which contain several hundred thousand nodes and elements. Application of the FE method to such problems typically requires large amounts of data storage and CPU time. For problems requiring small time steps, the computational costs can be prohibitive.

Several numerical approaches have been developed which attempt to efficiently solve the system of equations which result from the spatial discretization of the advection-dispersion equation using the finite element approach. These approaches include the use of iterative solution algorithms, matrix exponentials, numerical Laplace transforms, Rayleigh-Ritz reduction and symmetrized matrix algorithms. A summary of these methods is provided by Woodbury et al. [1990] and the reader is therefore referred to this article for further information.

In this work, the focus is on comparing the accuracy and efficiency of the continuous in time Laplace Transform Galerkin (LTG) method [Sudicky, 1989] and a subspace method based on the Arnoldi modal reduction strategy [Woodbury et al., 1990; Nour-Omid et al., 1991], hereafter referred to as the Arnoldi modal reduction method (AMRM). In addition, the class of problems for which each method is best suited is determined. To accomplish these goals, one- and two-dimensional solute transport simulations are performed in both homogeneous and heterogeneous media utilizing a variety of boundary conditions. Emphasis is placed on the performance of the solvers for problems involving heterogeneity since heterogeneity of material properties is typical of hydrogeologic environments and is known

to influence field-scale mass transport.

At this point it is important to impress upon the reader that the AMRM described in this work should not be confused with Arnoldi like iterative solvers such as generalized minimal residual (GMRES [Saad and Schultz, 1986]). The difference between these will be made obvious later in this work.

2.2 Theory

2.2.1 The Mass Transport Equation

Solute transport is governed by the following differential equation, boundary and initial conditions [Bear, 1972]:

$$\nabla\cdot(\boldsymbol{D}\cdot\nabla c)-\boldsymbol{v}\cdot\nabla c+f=\frac{\partial c}{\partial t} \qquad in\ \Omega \tag{2.3a}$$

$$c(t=0)=c_0 \qquad in\ \Omega \tag{2.3b}$$

$$c=c_b \qquad on\ \Gamma \tag{2.3c}$$

$$\boldsymbol{D}\cdot\nabla c\cdot\boldsymbol{n}=q_b \qquad on\ \Gamma \tag{2.3d}$$

where c is the solute mass concentration, q_b is a specified mass flux, f is a source/sink term, $\boldsymbol{D}$ is a tensor of dispersion coefficients, $\boldsymbol{v}$ is the transport velocity which depends on the spatial coordinates, $\boldsymbol{n}$ is the unit-outward normal, and t is time. Ω denotes the interior of the domain under consideration whose boundary is Γ. The components of $\boldsymbol{D}$ for an isotropic medium are given by [Bear, 1972]:

$$D_{ij}=\alpha_T|v|\delta_{ij}+(\alpha_L-\alpha_T)\frac{v_i v_j}{|v|}+D^* \tag{2.4}$$

where D^* is the coefficient of molecular diffusion in the porous medium, and α_L and α_T are the longitudinal and transverse dispersivities respectively.

2.2.2 Traditional Solution of the Finite Element Formulation

Application of the finite element method to the governing mass transport equation subject to initial and boundary conditions results in a matrix differential equation of the form:

$$M\dot{c}+Kc=b \tag{2.5}$$

where c is a vector of unknowns at the nodes of the finite element mesh used to discretize the domain Ω, K is the "stiffness" or "conductivity" matrix and M is the "mass" or "capacity" matrix. For the mass transport equation K is unsymmetric while M is symmetric and positive-definite. Finally, b is a vector which contains the effects of the boundary conditions as well as source/sink terms.

The traditional approach to solving (2.5) involves applying a finite difference approximation to the time derivative. This is then followed by the application of a time stepping scheme such as the Crank-Nicolson scheme. Application of the Crank-Nicolson scheme to (2.5) yields:

$$\left(M+\frac{\Delta t}{2}K\right)c^{s+1}=\left(M-\frac{\Delta t}{2}K\right)c^{s}+b^{s+\frac{1}{2}}(\Delta t) \tag{2.6}$$

where Δt is the time-step. Equation (2.6) is then solved using direct solvers such as the LU decomposition scheme. If the time-step and flow parameters remain constant during the simulation, the solution of (2.6) can be obtained using an LU decomposition of the left hand side, followed by matrix-vector multiplications of the RHS and repeated back-solves. Utilizing this approach, the cost of solving (2.6) is dependent on the size $\boldsymbol{K}$ and $\boldsymbol{M}$ matrices as well as the number of time-steps required to reach the designated time. Therefore, for large problems requiring many back-solves a high computational cost can be incurred.

2.2.3 Laplace Transform Galerkin Method

Sudicky [1989] provided a comprehensive development of the theory of the LTG method, hence the interested reader is referred to this work for background information. The method essentially involves applying a Laplace transformation to the ADE and boundary conditions, thus eliminating the temporal derivative. The solute concentrations at nodes in the transformed space (p-space) are then solved for using a Galerkin formulation. The matrix differential equation resulting from the Galerkin formulation is given by[Sudicky, 1989]:

$$(\boldsymbol{K}+p\boldsymbol{M})\bar{\boldsymbol{c}}=\bar{\boldsymbol{b}} \tag{2.7}$$

Here $\bar{\boldsymbol{c}}$ is the transformed vector of nodal concentrations, p is the Laplace transform variable and $\bar{\boldsymbol{b}}$ is the transformed vector containing the effects of the boundary conditions as well as source and sink terms. The mass matrix $\boldsymbol{M}$ in (2.7) is computed using a consistent formulation as opposed to lumped since it has been shown to be superior for reducing numerical dispersion in time marching solutions to linear problems [Sudicky, 1989 and Daus et al.,

1985]. Note that this is not unique to the LTG method but is also the case for the traditional approach previously described. Due to the unsymmetric nature of M the coefficient matrix in (2.7) is also unsymmetric. A solution to (2.7) therefore requires the use of either preconditioned iterative solvers such as the preconditioned ORTHOMIN solver [Behie and Forsyth, 1984; Mendoza, 1991], or direct matrix solvers such as LU decomposition.

The inversion of the solution in Laplace space is performed numerically. For the benefit of the reader, a brief discussion of the inversion procedure used is presented. Inversion algorithms generally require knowledge of the value of the transformed variable for different values of $p=p_k$, $k=0, 1, 2,...2K$ [Sudicky and McLaren, 1992]; here K is a user specified variable. As a result, (2.7) must be solved anew for each p_k [Sudicky and McLaren, 1992]. The inversion approach used is based on the algorithm of de Hoog et al. [1982; Sudicky and McLaren, 1992]:

$$c_j(t)=\frac{1}{T}\exp(p_0 t)\left[\frac{1}{2}\bar{c}_j(p_0)+\sum_{k=1}^{2K} Re\left(\bar{c}_j(p_0+\frac{k\pi i}{T})\exp\frac{k\pi t i}{T}\right)\right]+E \qquad (2.8)$$

Here $c_j(t)$ is the time domain concentration, $2T$ is the period of the Fourier series approximating the inverse on the interval $[0, 2T]$, Re denotes the real part of $\bar{c}_j$, $i^2=-1$, E is an error term, $p_0=\mu-[(\ln E)/2T]$, $p_k=p_0+k\pi i/T$ and μ is the order of $c_j(t)$ [assumed exponential such that $|cj(t)| \leq \xi exp(\mu t)$, ξ constant]. Sudicky [1989] suggests that $\mu = 0$ and $E = 10^{-6}$ are adequate for general cases. Equation (2.8) indicates that the inversion process must be repeated for each solution time. The advantage of (2.8) over the Crump [1976] algorithm initially used by Sudicky [1989] is seen in the form of a more efficient convergence [Sudicky and McLaren, 1992].

Several advantages of the LTG methodology have been reported in various works. These may be summarized as follows:

1. The method provides a high degree of accuracy and robustness for Pe » 2 [Sudicky, 1989];
2. The method is independent of Courant constraints and allows for the generation of time continuous solutions [Sudicky, 1989; Sudicky and McLaren, 1992; Xu and Brusseau, 1995];
3. The solutions in p-space are independent [Sudicky, 1989; Xu and Brusseau, 1995], therefore the method is adaptable for parallel processing;
4. The method is well suited for handling convolution integrals which describe rock fluid iterations in dual-porosity formulations [Sudicky, 1989].

A potential short-coming of the LTG formulation was recently addressed by Xu and Brusseau [1995]. In this work they showed that the negative dispersion which is inherent in the Galerkin finite element scheme can be potentially problematic when the LTG method is applied to highly advective problems under high grid Peclet number conditions. In addition to this short-coming, the LTG approach is known to be limited to problems involving linear mass transport in steady flow fields.

2.2.4 The Arnoldi Modal Reduction Method (AMRM)

The AMRM may be appropriately described as a subspace method. The mathematical development of this method and its application to the solution of the generalized transport equation is described by Nour-Omid et al. [1991]. Further work by Woodbury et al. [1990]

explored the applicability and feasibility of the method for reducing the computational cost associated with modelling two-dimensional mass transport problems.

At this point it is prudent to present a summary of the derivation of the AMRM as applied in this work so as to draw the distinction between it and iterative methods based on the Arnoldi process. Although this derivation is documented in Woodbury et al. [1990] a summary is nevertheless provided in an attempt to avoid needless confusion on the part of the reader.

The application of the AMRM to the mass transport problem is initiated by multiplying (2.5) by K^{-1} to produce:

$$K^{-1}M\dot{c}+c=K^{-1}b \tag{2.9}$$

At this point the aim is to reduce (2.9) to a smaller system of equations which can be solved accurately and efficiently. Application of m steps of the recursive Arnoldi algorithm [Woodbury et al., 1990] to the matrix $K^{-1}M$, results in the following system of equations:

$$K^{-1}MQ_m=Q_mH+r_me_m^T \tag{2.10}$$

where e_m is the last column of the $m \times m$ identity, H is an $m \times m$ upper Hessenberg matrix, Q_m is an $n \times m$ $(n \gg m)$ matrix of Arnoldi vectors and r_m is a residual vector. Both Q_m and r_m satisfy the following orthogonality conditions

$$Q_m^TMQ_m=I_m \tag{2.11a}$$

$$r_m^TMQ_m=0 \tag{2.11b}$$

The Rayleigh-Ritz reduction procedure requires that an approximate solution be defined as the linear combination of Arnoldi vectors, i.e.

$$c \approx \hat{c} = Q_m w \tag{2.12}$$

Since $\hat{c}$ is an approximation to the true solution, substitution of (2.12) into (2.9) produces a residual vector p_m:

$$p_m = K^{-1} M Q_m \dot{w} + Q w - K^{-1} b \tag{2.13}$$

The vector w is computed such that p_m is M orthogonal to the set of Arnoldi vectors Q_m. Therefore premultiplying (2.13) by $Q_m^T M$ gives:

$$Q_m M K^{-1} M Q_m \dot{w} + Q_m^T M Q_m w = Q_m^T M K^{-1} b \tag{2.14}$$

Using (2.11a), (2.11b) and (2.10), (2.14) reduces to:

$$H\dot{w} + w = g \tag{2.15}$$

where

$$g = Q_m^T M K^{-1} b \tag{2.16}$$

The reduced system of equations, (2.15), is then solved using a suitable time stepping procedure such as the Crank-Nicolson method. Woodbury et al. [1990] indicated that the time required for the time stepping procedure is not significant if $n \gg m$. However, this is only the case if the number of time-steps required is not excessive. The reader should further note

that due to the form of (2.12), inversion of the subspace solution is computationally inexpensive and contributes little to the overall computational cost. At this point it should be stated that the reduction procedure described [Woodbury et al., 1990] can be implemented using either direct or iterative solvers.

Compared to more conventional methods, the main advantage of the AMRM is its efficiency. This efficiency can be further enhanced due to the fact that as a result of the Arnoldi modal reduction the nodal spacing has effectively been increased so that in theory a larger time step can be employed without violating the Courant constraint. The efficiency to be gained from the implementation of the AMRM is currently only available for problems involving steady groundwater flow. For problems involving transient flow, the $\boldsymbol{K}$ matrix must be reformulated and the reduction process repeated each time the velocity field changes. This process is computationally expensive and severely reduces the efficiency of the AMRM.

2.3 Numerical Simulations

In this work, the performance of the LTG and Arnoldi modal reduction approaches were tested using one- and two-dimensional problems for which analytical solutions were available. In particular, the test problems were designed to examine solute transport under highly advective conditions (i.e. negligible dispersion) as well as for grid Peclet numbers, greater than two $(Pe_i > 2)$. As stated earlier, the criteria used in evaluating the performances of the numerical solvers are efficiency and accuracy.

The efficiency of numerical algorithms can be measured in terms of the number of floating point operations (FLOPS) performed. Woodbury et al. [1990] utilized this

methodology in their analysis of the efficiency of the AMRM. In their work, the modal reductions were performed with the aid of a band matrix solver based on the LU decomposition. A count of the number of FLOPS involved in the LTG approach has not been performed. However, the version of the LTG algorithm implemented in this work requires the LU decomposition and back-solve of a banded system of complex valued equations for each value of p_r. In addition, a de Hoog inversion of the Laplace transformed concentrations is performed at each desired time. Since the solution time increases as the number of FLOPS increase it is used as an indirect means of evaluating the efficiency of the numerical algorithms.

The solution accuracy was estimated by computing the root-mean-square error (RMSE) between the computed solution and the analytical solution for the posed problem:

$$RMSE = \sqrt{\frac{1}{n-1}\|e\|^2}$$

Here $e = c^N - c^A$, where c^N is the solution computed using the numerical method, c^A is the solution computed using the analytical method and n represents the number of nodes used in the discretization. Although the RMSE was the primary error estimate reported in this work other error estimates such as the absolute error, the standard deviation of the error and the average residual error, were also recorded and used to evaluate the accuracy of the generated solutions. The spatial distribution of errors was not often assessed. However, experience does indicate that spatially, the largest errors will occur in regions where large concentration gradients are present. Such areas would include the near source region and regions in which

large contrasts in material properties are observed. Thus some attention was paid to the solutions in such areas.

The dilemma faced in this work is that while solution accuracy for the various schemes is known to improve with an increase in the number of p-space variables and Arnoldi vectors used, the computational cost also increases. This trade-off between improved accuracy and reduced efficiency will be addressed later.

Implementation of the AMRM and the LTG method involves the solution of matrix equations of the form $\boldsymbol{Ax}=\boldsymbol{b}$. The solution of this system can be accomplished using either iterative or direct matrix solvers. Iterative solvers are generally found to be more efficient than direct solvers for problems involving large bandwidths, such as those associated with three-dimensional FE meshes. However, for most two-dimensional problems reordering techniques can be employed to improve the efficiency of direct matrix solution methods. In addition, iterative solvers have generally been shown to be best suited to problems involving symmetric positive semi-definite matrices. For unsymmetric systems such as those associated with mass transport, preconditioning based on incomplete decomposition techniques is generally required before iterative solution techniques can be applied. The nature and degree of the preconditioning utilized adds over-heads to the solution procedure and is generally problem dependent and subjective. By contrast direct solvers can be applied to both symmetric and unsymmetric systems without the need for preconditioning, hence minimizing any potential subjective bias associated with preconditioning. As a result, a direct solver based on the LU decomposition technique was utilized in both the AMRM and the LTG method.

The use of direct solvers based on the LU decomposition technique raises other

questions regarding the fairness of the analysis being conducted. For example, use of the LU decomposition technique with the LTG method requires that a costly factorization and backsolve of (2.7) be performed in the complex domain for each p-space variable; whereas for the Arnoldi reduction procedure only one factorization of the $\boldsymbol{K}$ matrix (for $\boldsymbol{r_j=K^{-1}p}$ see Woodbury et al., 1990) followed by m (where m represents the number of Arnoldi vectors) backsolves is required. If iterative solvers are utilized then the systems $\boldsymbol{r_j=K^{-1}p}$ and (2.7) must be solved for each Arnoldi vector and p-space variable respectively. The effect of iterative solvers on the comparison is an issue which will be addressed later in this work.

The numerical simulations were performed on a SUN SPARC 1^+ work station running version 4.1.3 of the Sun operating system and version 1.3 of the SUN Fortran77 compiler. The computer code used for the simulations consisted of three modules (see Figure 1); the *pre-processor*, the *processor* and the *post-processor*. The *pre-processor* served two purposes, (i) it read the data required for the simulation, and initialized all essential variables; and (ii) it built the global mass and stiffness matrices. The *processor* was used to build and solve the system of equations required for the simulation. Within this module, the LTG method and AMRM were implemented. It is noteworthy to mention that the matrix solvers implemented in these approaches utilized the factorization subroutines DGBFA and ZGBFA, and the backsolve subroutines DGBSL and ZGBSL contained in the LINPACK package [Dongarra, 1979]. In order to minimize any potential bias all timing routines were placed within the processor module of the code (see Figure 2.1). The timing subroutines utilized are the DTIME and ETIME subroutines contained in version 1.3 of the Sun Fortran77 library. The function of the *post-processor* is to write the results of the simulations to output files for later

analysis.

2.3.1 One-Dimensional Simulations

One-dimensional simulations are generally not representative of field-scale hydrogeological phenomena. However, to illustrate various aspects of the numerical schemes under consideration the results from such problems will be examined in this section. It is important to note that the parameters used in the one-dimensional models were homogeneous and uniformly distributed. The initial and boundary conditions for the models were

$$c(x>0,t=0)=0.0 \tag{2.17a}$$

$$c(x=0,t>0)=1.0 \tag{2.17b}$$

$$c(x=\infty,t>0)=0.0 \tag{2.17c}$$

The analytical solution for this general problem was given by Ogata [1970; Freeze and Cherry, 1979].

$$c(x,t)=\frac{c_0}{2}\left[erfc\left(\frac{x+vt}{\sqrt{4D_x t}}\right)+\exp\left(\frac{vx}{D_x}\right)erfc\left(\frac{x-vt}{\sqrt{4D_x t}}\right)\right] \tag{2.18}$$

2.3.1.1 High Grid Peclet Number Analysis

The following describes the model parameters used for this portion of the analysis. The system was of length, $L = 50\ m$, with groundwater velocity, $v = v_x = 0.1\ m/day$ and Dirichlet boundary conditions imposed on both the up-stream and down-stream ends of the

domain (see (2.17)). The longitudinal dispersivity of the system, α_L, was *0.05 m* and the coefficient of molecular diffusion, D^*, was $4.3x10^{-5}$ m^2/day. It was assumed that the source had been in place for *250 days*. The solute concentration profile for this problem 250 days after emplacement of the source was obtained using (2.18).

The numerical simulations performed in this analysis involved the use of three nodal spacings, $\Delta x = 0.0625$ *m*, *0.125 m*, and *1.0 m*. These produced mesh discretizations of *800*, *400* and *50* elements and grid Peclet number values of *1.3*, *2.5*, and *19.8*, respectively. The value of Courant number for each simulation was kept fixed at *1.0*. These parameters are summarized in Table 2.1. At each nodal spacing, numerical solutions were generated for various numbers of p-space variables [$nP_k = 2K + 1$; (see page 58)] and Arnoldi vectors. Using the analytical solution, RMSE values were estimated for each numerical solution. In addition, RMSEs were computed based on the numerical solutions generated by the traditional FE approach. Figure 2.2 shows plots of the RMSE versus the number of p-space variables and Arnoldi vectors utilized.

The results show a general decline in the RMSE associated with each scheme as the numbers of p-space variables or Arnoldi vectors are increased. It is also evident that the degree of accuracy achieved by the numerical schemes increases with reduced grid Peclet number. For example, use of the Arnoldi method on the *800*, *400* and *50* element mesh discretizations resulted in RMSE values at convergence of approximately $5x10^{-5}$, $1.0x10^{-3}$ and $3x10^{-2}$ respectively; whereas use of the LTG method on identical mesh discretizations resulted in RMSE values at convergence of approximately 10^{-5}, $3x10^{-5}$ and $4x10^{-3}$ respectively. The RMSE value of approximately 10^{-5} associated with the *800* element LTG simulation is

dubious and essentially reflects the influence of the user supplied relative error ($E = 1x10^{-5}$). Nevertheless, the LTG results appear to support Sudicky's [1989] assertion that the LTG scheme maintains a high level of accuracy at relatively high grid Peclet numbers. Figure 2.2 also shows that at convergence the RMSE values associated with the AMRM approximate those obtained using the traditional FE approach. This is to be expected since as the number of Arnoldi vectors increases, the AMRM approximates the traditional FE method.

The simulation results allow the level of accuracy attained by the two methods to be compared. As a starting point, compare the accuracy of the two schemes on similar mesh discretizations. For this comparison, the LTG method shows better convergence than the AMRM. This tendency is best exemplified by comparing the results of the *400* and *50* elements simulations shown in Figure 2.2. Further compare, the level of accuracy achieved on a coarse mesh by the LTG method can be compared to that achieved on a refined mesh by the AMRM. Again the LTG method shows better convergence than the AMRM despite a 200% increase in the grid Peclet number. This is illustrated by comparing the RMSE values at convergence for the LTG method (approximately $3x10^{-5}$) to the RMSE values at convergence for the AMRM (approximately $5x10^{-4}$). A comparison of the results for the *400* and *50* element simulations, indicates that for this problem the superior accuracy of the LTG method (over the AMRM) extends up to grid Peclet number increases of approximately 600% to 700%. Hence for this test problem, the LTG method outperforms the AMRM with respect to accuracy. In the following discussion the efficiency of both numerical methods is examined.

As mentioned earlier, computational time can be used as a measure of the efficiency associated with various aspects of the numerical schemes. For the AMRM three components

of the solution time were recorded: (i) the time associated with the total solution (T_A); (ii) the time required to performing the time-stepping or re-solution procedure (T_{A2}); and (iii) the time required for the numerical inversion of the solution in reduced space (T_{A3}). The reader should note that execution time for the Arnoldi modal reduction (T_{A1}) is simply $T_A - (T_{A2} + T_{A3})$. Three components of the solution time were also recorded for the LTG solution: (i) the total LTG solution time (T_L); (ii) the time required to perform the de Hoog inversion (T_{L1}); and (iii) the time required to solve the nP_k complex matrix equations which result from the LTG formulation (T_{L2}). The recorded times show that time-stepping, re-solution and inversion procedures accounted for less than half of the AMRM's total solution time. The majority of the remaining time involved executing the recursive Arnoldi algorithm. Note that as the number of time-steps increases, the re-solution time will increase; however its contribution to the overall solution time will grow slowly due to the low cost associated with solving the small system of equations [Woodbury et al, 1990]. For the LTG method, solution of the nP_k matrix equations occupied the majority of the solution time with the De Hoog inversion process requiring little computational effort. The fact that both methods required very little overall time to solve the system of matrix equations is not surprising in light of the small bandwidth associated with one-dimensional FE formulations.

The trade-off between the efficiency and accuracy for the two methods is examined by considering plots of the RMSE versus the total solution time (see Figure 2.3). The figure shows that for similar discretization the LTG method converges to a desired level of accuracy faster than the AMRM. To illustrate this consider a desired level of accuracy of 10^{-3}. For the 800 element mesh, the AMRM attained this level of accuracy in approximately 13 seconds

whereas the LTG method attained it in approximately 2 seconds. On the 400 element mesh, the AMRM converged to the desired level of accuracy after approximately 8 seconds while the LTG method attained this level of accuracy after approximately 1 second. Therefore, it appears that the LTG method is computationally more accurate and efficient than the AMRM for homogeneous one-dimensional problems involving moderate amounts of dispersion.

2.3.1.2 Sharp Front Analysis

In this section, the accuracy and efficiency of the LTG method and AMRM are investigated for the solution of sharp front problems. Sharp fronts are characterized by little mixing beyond the advective front. Such fronts occur where the dispersive transport processes are negligible compared to the advective process. Due to the negligible dispersion, these zones are commonly characterized by steep concentration gradients. In order to accurately reproduce these gradients as well as satisfy the grid Peclet criterion, a small spatial discretization is commonly required. The use of a small spatial discretization may necessitate the use of a small time-step in order to meet the Courant criterion. As a result, application of the traditional FE approach to the solution of sharp front problems can be expensive with respect to computational time and data storage.

The efficiency of the LTG method for solving such problems was alluded to by Sudicky [1989] who suggested that as the grid Peclet number increases no significant increase in the number of p-space variables is required to generate an accurate numerical solution. If this is indeed the case, this property, coupled with no time stepping, suggests that the LTG method may be suitable for the solution of such problems. In light of the work performed by

Xu and Brusseau [1995], it should be pointed out that for highly advective systems, upwind methods [Huyakorn and Pinder, 1983] should be coupled with the LTG method and the AMRM to minimize spatial discretization.

The simulations in this section utilized two models which differed only with respect to the magnitude of the longitudinal dispersivity. The first model represents a hydrogeologic environment in which a moderate longitudinal dispersivity of 0.02 m is present whereas in the second model the longitudinal dispersivity was assumed to be negligible, thus producing a sharp front.

The simulated system was of length, $L = 0.9\ m$ with initial and boundary conditions for the mass transport problem being identical to those previously given in (2.17). The groundwater flow was $v = v_x = 0.1\ m/day$ and the coefficient of molecular diffusion, D^*, was $4.3x10^{-5}\ m^2/day$. A spatial discretization, $\Delta x = 1.0x10^{-4}\ m$, which yielded 9000 elements was applied to the domain. This discretization which resulted in grid Peclet numbers of approximately 0.005 and 0.23 for $\alpha_L = 0.02\ m$ *and* $0.0\ m$, allowed the grid Peclet criterion to be satisfied for both simulations. The value of Courant number for this analysis was maintained at 0.1 for both dispersivity values. A summary of these parameters is provided in Table 2.2. Using the outlined parameters solute concentrations were estimated for time, $t = 4.0\ days$ after emplacement of the source. The RMSE was again used to evaluate the accuracy of the numerical solution.

Figure 2.4 shows plots of the RMSE versus the number of p-space variables and Arnoldi vectors utilized, whereas Figure 2.5 shows plots of the RMSE versus the total solution time. The plots shown mimic those described in the previous section and as a result

a limited discussion is presented. For both models the plots show the LTG method to be more efficient than the AMRM. This is exemplified by the 67 seconds required by the AMRM to attained an RMSE of $7x10^{-5}$ compared to the 33 seconds required by the LTG method to attain a similar level of accuracy. It is important to note that the AMRM utilized 15 Arnoldi vectors in achieving this level of accuracy whereas 11 p-space variables were required by the LTG method (see Figure 2.4).

In terms of accuracy, the results for the case $\alpha_L = 0\ m$ show that 11 p-space variables were again required by the LTG method to attain a level of accuracy similar to that observed for the case $\alpha_L = 0.02\ m$. The computational time required to generate this solution was approximately 42 seconds; a marginal increase from the computational time reported for the previous model. For this model, the AMRM required 75 Arnoldi vectors to attain a RMSE of approximately 10^{-4}. The computational time required for this solution was approximately 811 seconds, with about half of this time being spent performing a re-solution at each of the 40000 time-steps required. This represents a significant increase in computational time compared to the previous model. These results show that for problems requiring many time steps, the LTG method can be significantly more efficient than the AMRM.

It is important to note that in terms of accuracy, the LTG results (i) are consistent with Sudicky's [1989] assertion; and (ii) demonstrate the robustness of the method. The results for the AMRM suggest that as the smoothness of the solution deteriorates, increasing numbers of Arnoldi vectors corresponding to the small wavelengths (larger eigenvalues) contained in the analytical solution are required to maintain accuracy. This leads to increased storage and computational requirements.

2.3.1.3 Two-Dimensional Simulations: Homogeneous Medium

Mass transport in hydrogeologic systems is commonly modelled using two- and three-dimensional forms of the ADE. This necessitates that the performance of any proposed numerical scheme intended for practical use be evaluated in at least two-dimensional space. The use of two-dimensional models to investigate various aspects of proposed numerical schemes in hydrogeology is not new [Huyakorn et al., 1984; Frind and Hokkanen, 1987; Beljin, 1988; Sudicky, 1989; Woodbury et al., 1990]. In this section, the accuracy and efficiency of the AMRM and the LTG method are examined for two-dimensional problems for which analytical solutions are available.

The problem domain (see Figure 2.6) utilized was similar to that used by Sudicky [1989, Figure 1]. The domain was rectangular with length, $L_x = 30\ m$ and width, $L_z = 2\ m$. On the upstream boundary Dirichlet conditions were imposed such that $c = c_o = 1$ for $0 \leq z \leq 0.5\ m$ and $c = 0$ for $z > 0.5\ m$. On all other boundaries zero flux conditions were imposed. The initial condition utilized was $c(x, z, t = 0) = 0$. A uniform groundwater flow was specified with the magnitude of the flow being $v = v_x = 0.1\ m/day$. The longitudinal and transverse dispersivities as well as the coefficient of molecular diffusion were specified to be $\alpha_L = 0.05\ m$, $\alpha_T = 0.005\ m$ and $D^* = 4.3x10^{-5}\ m^2/day$ respectively. It should be noted that since the longitudinal dispersivity parallels the mean flow direction, off diagonal terms in the dispersion tensor can be ignored. Two discretizations of the domain were considered; (i) $\Delta x = \Delta z = 0.1\ m$ and (ii) $\Delta x = 1.0\ m$ and $\Delta z = 0.1\ m$. These discretizations, result in 12000 (refined mesh; 6321 nodes) and 1200 (coarse mesh; 651 nodes) triangular elements, and produce grid Peclet numbers of $Pe_x = 1.98$ and 19.8 respectively. The Courant number for the simulations was

maintained at approximately 1.0. A summary of these model parameters is given in Table 2.3. Using the two models solute concentrations were generated with the AMRM and the LTG method for times $t_1 = 50\ days$ and $t_2 = 150\ days$. The exact analytical solution for this line source problem was derived by Sudicky [unpublished report, 1985]. The results of the simulations performed are discussed in the following paragraphs.

Plots of the RMSE versus the number of p-space variables and Arnoldi vectors (see Figures 2.7 and 2.8) are similar in form to those reported earlier. The figures show that on the refined mesh the level of convergence achieved by the two methods at solution times t_1 and t_2, was approximately 0.003. This contrasts with the results obtained earlier for the one-dimensional analysis, where in terms of accuracy, the LTG method consistently outperformed the AMRM. On the coarse mesh, the results are more reflective of the previously reported results. For this mesh, the convergence of the AMRM was approximately 0.014 at both times, whereas the LTG method converged to approximately 0.007 and 0.004 at solution times t_1 and t_2 respectively. The reader should note that the similar levels of convergence attained by the LTG method on both mesh reflects the robustness of the method.

In terms of accuracy, the one- and two-dimensional simulations complement each other, since they show that (i) the LTG method maintains a high degree of accuracy despite large changes in the mesh discretization and (ii) the accuracy of the AMRM is sensitive to changes in the mesh discretization. As in the previous sections, the former warrants that the LTG solution on the coarse mesh be compared to the Arnoldi modal reduction solution on a refined mesh. This comparison will be performed later in this section.

The influence of mesh discretization on the number of p-space variables and Arnoldi

vectors required for convergence was addressed in the one-dimensional analysis. For the two-dimensional analysis results similar to those reported earlier are again observed. Again, changes in the mesh diccretization had minimal influence on the number of p-space variables required by the LTG method for convergence, whereas for the AMRM the ratio of the number of modes utilized to the maximum number of modes available increased as the mesh discretization was reduced. The simulation results also indicate that as the transport time increases, fewer numbers of Arnoldi vectors were required for convergence. For example, on the refined mesh the AMRM required 40 vectors to achieve convergence for the *50* day simulation and 30 vectors for the 150 day simulation. This result reaffirms the conclusion drawn earlier in which it was stated that the number of Arnoldi vectors required to achieve an accurate solution was influenced by the smoothness of the solution.

As in the case of the one-dimensional analysis, the efficiency of the two methods warrants a comparison. Figures 2.9 and 2.10 show plots of the RMSE versus solution time for the two methods. In order to perform meaningful comparisons of the solution times, RMSE values greater than some $RMSE_{min}$ must be considered. For the purposes of this analysis and due to its poorer convergence, the value of $RMSE_{min}$ is chosen to be the value to which the AMRM converges. For RMSE values greater than $RMSE_{min}$, Figures 2.9 and 2.10 show the AMRM to be computationally more efficient than the LTG method.

As pointed out earlier, the efficiency of the LTG method on the coarse mesh can be compared to that of the AMRM on the refined mesh. As a starting point in this comparison, consider the results of the 50 day simulation. A comparison of Figures 2.7 and 2.9 indicates the best choice for the value of $RMSE_{min}$ to be 0.007, the RMSE associated with the LTG

solution at convergence. Figure 2.9 shows that on the coarse mesh the LTG method attained this level of convergence after approximately 40 seconds whereas the on the refined mesh the AMRM attained it after approximately 100 seconds. For the 150 day simulation the value of $RMSE_{min}$ is approximately 0.004, the RMSE associated with the LTG method at convergence (compare Figures 2.8 and 2.10). On the coarse mesh, this level of convergence was attained by the LTG method after approximately 42 seconds, whereas on the refined mesh the AMRM attained this convergence after approximately 110 seconds (see Figures 2.10). Hence, at both simulation times and for similar levels of accuracy, the LTG method applied to the coarse mesh is more efficient than the AMRM on the refined mesh.

The analysis in this section is concluded by examining the components of the solution times. For the AMRM analysis, the components of the solution time are similar to those observed for the one-dimensional simulations; i.e., the modal reduction process requires over half of the total execution, with the re-solution and inversion processes requiring relatively little time. The results of the LTG analysis show that the time needed to solve the nP_k complex matrix equations again forms a significant component of the total solution time, with the De Hoog inversion process requiring very little time. These results are therefore quite similar to those reported for the one-dimensional simulations and thus appear to be insensitive to changes in dimensionality.

2.3.1.4 Two-Dimensional Simulation: Heterogeneous Medium

Homogeneous hydrogeologic properties are rarely encountered in nature. Instead hydrogeologic properties tend to vary spatially and in some cases spatially. As a result, any

numerical scheme intended for modelling "real" hydrogeologic environments must be evaluated under such conditions. In this section the relative performances of the AMRM and the LTG methods are evaluated for problems involving heterogeneous hydraulic conductivity values.

The solution of the mass transport equation in a heterogeneous hydraulic conductivity domain requires a definition of the velocity field within the domain. Fluid flow in a rigid saturated porous medium involves solving the following differential equation

$$\frac{\partial}{\partial x_i}\left(K(x)\frac{\partial H}{\partial x_i}\right) = S_s \frac{\partial H}{\partial t} \tag{2.19}$$

where H represents the hydraulic head, $K(x)$ represents the hydraulic conductivity as a function of space and S_s represents the specific storage of the medium. Note that under a finite element formulation the hydraulic conductivity $K(x)$ becomes an element property. Using (2.19), the velocity field, $v_i(x)$, needed to solve the mass transport equation is approximated by

$$v_i(x) = -\frac{K(x)}{\theta}\frac{\partial H}{\partial x_i} \tag{2.20}$$

where θ represents the porosity.

Hydraulic conductivity values observed in several aquifers which have been studied in great detail appear to be correlated and log-normally distributed [Freeze, 1975; Sudicky, 1986]. Based on this evidence, the synthetic hydraulic conductivity field used in this analysis

conforms to such a distribution. Synthetic hydraulic conductivity fields displaying such properties are commonly generated using random correlated field generators. Note that hydraulic conductivity fields generated in this manner will represent reality only to the extent that the statistical model on which they are based does [Robin et al., 1993]. Several methods, each having various advantages and disadvantages, exist for generating spatially correlated fields in two- and three-dimensions. These include the spectral method [Meija and Rodriguez-Iturbe, 1974; Robin et al., 1993; Ruan and McLaughlin, 1995], the matrix decomposition method [Clifton and Neuman, 1982] and the turning bands method [Delhomme, 1979; Mantoglou and Wilson, 1982; Mantoglou, 1987; Tompson et al., 1989]. Of these, the easiest to implement is the matrix decomposition method. For small systems involving several hundred elements, the computational costs associated with this method are generally not excessive. As a result this method was used to generate the desired hydraulic conductivity field.

The problem domain utilized was rectangular in shape with dimensions $L_x = 9.6\ m$ and $L_z = 4.8\ m$ (see Figure 2.11). For the simulations two mesh designs were considered $\Delta x = \Delta z = 0.2\ m$ *and* $0.4\ m$. These discretizations produced 2304 and 576 triangular elements, or 1152 and 325 nodes respectively within the domain. Flow in the domain was assumed to be at steady-state with the mean flow parallel to the x-axis. In addition, the porosity of the system was specified to be 30 %. The synthetic hydraulic conductivity field described a silty sand with a mean hydraulic conductivity, $\overline{K} = 0.0501\ m/day\ (\log_{10}\overline{K} = -1.3)$; an integral scale, $\lambda_K = 2.8\ m$; and a standard deviation, $\sigma_K = 0.40\ m/day$. Figure 2.11 shows the hydraulic conductivity field utilized in the simulations. Note that on the refined and coarse meshes 14

and 7 elements respectively were contained within an integral scale. Realistic local dispersivity values based on laboratory and field experiments were used in the mass transport simulations; $0.05\ m < \alpha_L < 1.0\ m$ and $0.005\ m < \alpha_T < 0.1\ m$. The boundary conditions required to solve the flow equation across the domain were (see Figure 2.12):

$$H(x=0,z)=41.0\ m \tag{2.21a}$$

$$H(x=9.6,z)=40.0\ m \tag{2.21 b}$$

$$\frac{\partial H(x,z=0)}{\partial z}=\frac{\partial H(x,z=4.8)}{\partial z}=0 \tag{2.21 c}$$

while boundary conditions for the mass transport problem were (see Figure 2.12):

$$c(x,z,t=0)=0.0 \tag{2.22 a}$$

$$c(x=9.6,z,t)=c(x=0,0\le z<2.0,t)=c(x=0,2.8<z\le 4.8,t)=0.0 \tag{2.22 b}$$

$$c(x=0,2.0\le z\le 2.8,t)=1.0 \tag{2.22 c}$$

$$\frac{\partial c(x,z=0,t)}{\partial z}=\frac{\partial c(x,z=4.8,t)}{\partial z}=0.0 \tag{2.22 d}$$

Using the boundary conditions defined in (2.21), and the synthetic hydraulic conductivity field the steady-state form of (2.19) was solved for the unknown hydraulic heads. The computed hydraulic head field was then used along with (2.20) to estimate the velocity field across each element. Application of the element velocity field along with the initial and boundary conditions specified in (2.22) allowed the mass transport equation to be solved using the AMRM and the LTG method. For the purposes of this study solute concentrations were estimated after 350 and 600 days of solute transport.

Since analytic solutions were not available for this problem, convergence was determined using a two-step approach. In the first step, the solutions generated using m_1 and m_2 ($m_1 > m_2$) p-space variables or Arnoldi vectors were compared using the RMSE. If the computed RMSE was less than some prescribed tolerance, in this case approximately 10^{-5}, it was assumed that convergence had been achieved. In the second step the accuracy of the solutions was further examined by comparing the converged LTG and AMRM solutions to ascertain whether the computed RMSE was within a specified tolerance, in this case 10^{-4}. In general, plots of the computed solutions were irregular in shape. This is to be expected based on field tracer experiments [Sudicky et al., 1983; Freyberg, 1986] where such irregularities are commonly attributed to local variations in the flow field which result from variations in the hydraulic conductivity field.

A summary of the efficiency analysis is presented in Table 2.4. In accordance with the results of the previous sections the AMRM again appears to be considerably more efficient than the LTG method on an identical mesh when several hundred time-steps are required. For these simulations the AMRM is approximately 4.5 times more efficient than the LTG method. A breakdown of the solution times reveals trends similar to those previously presented in the discussion of the homogeneous two-dimensional results. Hence no further discussion is presented.

As pointed out earlier, two mesh discretizations were considered. A comparison of the coarse and fine mesh shows that one element of the coarse mesh contains four elements of the fine mesh. The element hydraulic conductivity values required to solve the continuity equation (2.19) on this new mesh were obtained by averaging the element hydraulic

conductivity values of the fine mesh (see Figure 2.13). Gelhar [1993] showed that for two-dimensional steady-state flow in a statistically isotropic medium the geometric mean is the most appropriate averaging scheme. In addition to the geometric mean, the arithmetic mean was also computed for illustrative purposes. The hydraulic conductivity fields generated using the geometric and arithmetic means visually displayed all of the major spatial characteristics of the original field (Figure 2.12). Semi-variograms of these fields showed that although the computed integral scales approximated that of the original field, some smoothing occurred resulting in a 50% reduction of the variance.

The boundary conditions needed to solve the flow and mass transport equations across the new mesh were identical to those previously given (see (2.21) and (2.22)). Using the procedures outlined earlier the coupled flow and mass transport equations were solved on the new mesh. Note that both the AMRM and LTG methods were again used to solve the mass transport problem. Procedures similar to those previously described were again used to evaluate the accuracy of the solutions.

Comparison of the solutions on the coarse and refined mesh show differences in the dimensions of the plumes. These differences can be illustrated by taking longitudinal and transverse profiles across the plumes (Figure 2.14). The figure shows that in both directions the solution on the coarse mesh overpredicts its counterpart on the refined mesh, with the overprediction being most significant when the arithmetic mean was used. It is also noteworthy to point out that although not shown in Figure 2.14, the concentrations in the near-source region of the coarse mesh exhibited some enhanced transverse spreading relative to those observed on the refined mesh.

The cause of these overpredictions has been investigated using additional simulations which incorporated the AMRM and the LTG method. These simulations utilized several mesh discretizations, $\Delta x = 0.4\ m$ *and* $0.6\ m$, and $\Delta y = 0.2\ m$. For each discretization the geometric mean was again used as the averaging procedure. Both solution methods yielded similar results. These results show that in the transverse direction the overprediction with respect to the solution on the refined mesh was minimal; hence no enhanced spreading occurred in this direction. However, in the longitudinal direction the overprediction was more significant, being most noticeable for the case $\Delta x = 0.6\ m$. Note that for the two-dimensional simulations involving homogeneous material properties, no overpredictions were observed when Δx was increased from 0.1 m to 1.0 m. This suggests that some of the overprediction observed may be a consequence of the averaging procedure. These results suggest that mesh discretization and associated averaging of the material properties contributed to the enhancement of the plume dimensions.

As in the previous cases, solution times for the simulations performed were recorded in order to examine the efficiency of the two methods (see Table 2.4). As expected, these solution times are significantly smaller than those associated with the refined mesh. The AMRM is again appears be more efficient than the LTG method. However, the factor of 4.5 efficiency previously reported from the use of the AMRM as opposed to the LTG method decreased to 2.5. The decreased efficiency of the AMRM relative to the LTG method results mainly from the reduced bandwidth and the smaller system of equations which the LTG method was required to solve in Laplace space.

2.3.1.5 The Impact of Iterative Solvers on the Comparative Analysis

This section addresses whether the choice of matrix solver biassed the simulation results. To address this issue the ORTHOFEM package [Mendoza, 1991], which utilizes the ORTHOMIN iterative solver, was implemented into both the LTG scheme and the AMRM. This implementation required that the systems $\boldsymbol{r_j=K^{-1}p}$ and (2.7) be solved iteratively at each recursive step in the Arnoldi reduction process and for each p-space variable respectively. For the simulations performed an absolute convergence criterion of 10^{-6} was deemed satisfactory. Figures 2.15 and 2.16 display the results of the comparison based on these implementations for the 50 days simulation on the two-dimensional refined mesh (refer to section 2.3.1.3).

The results show that use of the iterative solver results in a marginal increase in the number of Arnoldi vectors required for convergence, whereas for the LTG method no such increase in the number of p-space variables is apparent. With regards to efficiency, the solution times reveal that implementation of the iterative solver enhances the efficiency of the LTG method by between 30% to 50% when compared to previous results generated using the direct solver. Unlike the LTG method, implementation of the iterative solver into the AMRM results in an approximately 500 % decrease in efficiency when compared to previous results. The net result of these changes in efficiency is that the most efficient implementation of the LTG method is as efficient as the most efficient implementation of the AMRM. It is noteworthy to mention that as the convergence criteria used in ORTHOMIN becomes stricter, increases in the solution times for the AMRM and the LTG method will occur.

The reduced solution times obtained for the LTG method suggest that complete factorization of (2.7) for each p-space variable is a computationally inefficient process. For

the AMRM, the ORTHOMIN procedure is inferior to the LU decomposition approach since the complete system has to be solved for each r_j in the recursive Arnoldi algorithm. This analysis thus shows that there is some degree of bias in the matrix methods applied. It should be pointed out that the gains to be expected from the efficient implementation of the AMRM will be controlled by the size and matrix bandwidth of the problem being solved and as a result the performance differential between the most efficient implementations of the AMRM and the LTG method may vary.

2.4 Discussion and Conclusions

This work examined the relative performance of two techniques, the AMRM and the LTG method, used to solve the system of equations which result from the application of the finite element approach to the ADE. The problems utilized in the evaluation were representative of problems experienced in computational hydrogeology. They included (i) mass transport in homogeneous and heterogeneous flow fields, (ii) mass transport under highly advective conditions and (iii) mass transport under high and low grid Peclet numbers. In general, the results showed that in terms of accuracy, both methods were stable and robust, and in many cases either out-perform or were as reliable as the traditional method described earlier. This result agrees well with the results reported by Sudicky [1989] and Woodbury et al. [1990]. In terms of efficiency, the results showed that both schemes greatly out-perform the traditional time-marching approach. Again, this result is supported by the earlier works of Sudicky [1989] and Woodbury et al. [1990].

Several conclusions may be drawn from the comparison performed in this work. One

important conclusion is that the choice of matrix solver utilized in both the AMRM and the LTG method plays an important role in the efficiency of the methods. As discussed and demonstrated earlier, the efficiency of the AMRM was greatest when direct solvers were utilized, whereas the efficiency of the LTG method was greatest when iterative solvers were utilized. This indicates that for accurate evaluation of numerical algorithms a thorough understanding of the structure of the algorithm being used is important. With this in mind, a summary and discussion of the results of this work is presented. As a starting point the results of the comparison preformed using direct solvers in both the AMRM and the LTG methods is presented.

The simulation results obtained from the use of direct solvers in both the AMRM and LTG methods allow several conclusion to be drawn. One obvious conclusion is that the relative efficiency of the solution schemes appears to be influenced by the nature and dimensionality of the problem being modelled. For example, when one-dimensional transport in a homogeneous medium was modelled it was found that the LTG method was more efficient and accurate than the AMRM for the two classes of problems considered [simulating mass transport (1) under high grid Peclet numbers and (2) in highly advective systems]. For the two-dimensional problems considered the converse was generally observed with respect to efficiency, i.e, the AMRM was generally found to be more efficient than the LTG method on identical mesh and at similar levels of accuracy. For the more realistic case of mass transport in a heterogeneous hydraulic conductivity field, the simulation results (using the direct solver) showed that both the AMRM and the LTG method maintained similar levels of accuracy but differed with respect to efficiency. In this case the AMRM was found to be

superior to the LTG method with respect to efficiency. When iterative solvers were implemented in both solution schemes the simulation results show that this result can be reversed, such that the most efficient implementation of the LTG method compares favourably with the most efficient implementation of the AMRM.

Further, this work showed that under homogeneous conditions the LTG method could accommodate large charges in the grid Peclet number, through reduced mesh discretization, with out sacrificing accuracy. In this way the efficiency of the method could be enhanced. However, under heterogeneous conditions this work showed that the efficiency gained in this manner can be at the expense of accuracy, particularly in the near-source region. This observation has important implications. It suggests that simulations for which a high degree of accuracy is essential (e.g., the validation of hypotheses or the simulation of the migration of an extremely toxic substance) attempts to improve the efficiency of the LTG method relative to other available methods or to take advantage of features observed in homogeneous simulations, may have an adverse impact. For example, in the near-source region and particularly in the transverse direction, increasing the mesh discretization can enhance the dimensions of the simulated plume and thus affect the applicability of the near-source mass and dispersivity calculations.

Finally, it should be pointed out that although the applicability of the methods to three-dimensional problems was not directly addressed in this work, the methods are applicable to such problems. Indeed the works of Robin [1991], Therrien [1993] and Burr [1994] showed that by using iterative solvers the LTG method can be utilized in the solution of mass transport problems in three-dimensions. As shown in this work, iterative solvers can

also be implemented in the AMRM, however, no studies have been reported regarding the performance of this solution scheme for mass transport problems in three-dimensions.

References

Ababou, R., D. McLaughlin, L. W. Gelhar, and A. F. B. Tompson, Numerical simulation of three dimensional saturated flow in randomly heterogeneous porous media, Transport in Porous Media, 4, 549 - 565, 1989.

Bear, J., Dynamics of Fluids in Porous Media, Elsevier, New York, 1972.

Behie, G. A., and P. A. Forsyth, Incomplete factorization methods for fully implicit simulation of enhanced oil recovery, SIAM J. Sci. Stat. Comput., 5(3), 543 - 561, 1984.

Beljin, M., Testing and validation of models for simulating solute transport in groundwater: Code intercomparison and evaluation of validation methodology, I.G.W.M.C., GWMI 88 - 11, 1988.

Burr, D. T., E. A. Sudicky and R. L. Naff, Nonreactive and reactive solute transport in three-dimensional heterogeneous porous media: Mean displacement, plume spreading , and uncertainty, Water Resour. Res., 30(3), 791-815, 1994.

Celia, M. A., and W. G. Gray, Numerical Methods for Differential Equations: Fundamental Concepts for Scientific and Engineering Applications, Prentice Hall, Englewood cliffs, New Jersey, 436 pp., 1992.

Chin, D. A., and T. Wang, An investigation of the validity of first-order stochastic dispersion theories in isotropic porous media, Water Resour. Res., 28(6), 1531 - 1542, 1992.

Clifton, P. M., and S. P. Neuman, Effects of kriging and inverse modelling on conditional simulation of the Avra Valley Aquifer in Southern Arizona, Water Resour. Res., 18(4), 1215 - 1234, 1982.

Crump, K. S., Numerical inversion of Laplace transforms using a Fourier Series approximation, J. Assoc. Comput. Mach., 23(1), 89 - 96, 1976.

Daus, A. D., E. O. Frind, and E. A. Sudicky, Comparative error analysis in finite element formulations of the advection-dispersion equation, Adv. Water Resour., 8, 86 - 95, 1983.

de Hoog, F. R., J. H. Knight, and A. N. Stokes, An improved method for numerical inversion of Laplace transform, SIAM J. Sci. Stat. Comput., 3(3), 357 - 366, 1982.

Delhomme, J. P., Spatial variability and uncertainty in groundwater flow parameters: A geostatistical approach, Water Resour. Res., 15(2), 269 - 280, 1979.

Dongarra, J. J., Linpack: User's Guide, Philidelphia: Society for Industrial and Applied Mathematics, 320 pp, 1979.

Freeze, R. A., A stochastic-conceptual analysis of one-dimensional groundwater flow in nonuniform homogeneous media, Water Resour. Res., 11(5), 725 - 741, 1975.

Freeze, R. A., and J. A. Cherry, Groundwater, Prentice Hall, Englewood Cliffs, New Jersey, U.S.A., 1979.

Freyberg, D. L., A natural gradient experiment on solute transport in a sand aquifer; 2. Spatial moments and the advection and dispersion of nonreactice tracers, Water Resour. Res., 22(13), 2031 - 2046, 1986.

Frind, E. O., and G. E. Hokkanen, Simulation of the Borden plume using the Alternating Direction Galerkin technique, Water Resour. Res., 23(5), 918 - 930, 1987.

Gelhar, L. W., Stochastic Subsurface Hydrology, Prentice Hall, Englewood Cliffs, New Jersey, U.S.A., 1993.

Huyakorn, P. S., A. G. Kretschek, R. W. Broome, J. W. Mercer, and B. H. Lester, Testing and validation of models for simulating solute transport in groundwater, HRI Rep. 35, Holcomb Res. Inst., Indianapolis, Ind., 1984.

Huyakorn, P. S., and G. F. Pinder, Computational Methods in Subsurface Flow, Academic Press, Inc. (London) LTD., 473 pp., 1983.

Mantoglou, A., Digital simulation of multivariate two- and three-dimensional stochastic processes with a spectral turning bands method, Math. Geol., 19(2), 129 - 149, 1987.

Mantoglou, A., and J. L. Wilson, The turning bands method for the simulation of random fields using line generation by a spectral method, Water Resour. Res., 10(4), 1379 - 1394, 1982.

Meija, J., and I. Rodriguez-Iturbe, On the synthesis of random fields from the spectrum: An application to the generation of hydrologic spatial processes, Water Resour. Res., 10(4), 705 - 711, 1974.

Mendoza, C. A., ORTHOFEM User's Guide Version 1.02, Waterloo Centre for Groundwater Research, University of Waterloo, Waterloo, Ontario, Canada, N2L 3G1.

Nour-Omid, B., W. S. Dunbar, and A. D. Woodbury, Lanczos and Arnoldi methods for solution of convection-diffusion equations, Comput. Methods Appl. Mech. Eng., 88, 75 - 95, 1991.

Ogata, A., Theory of dispersion in a granular medium, U. S. Geol. Surv. Prof. Paper 411 - I.

Robin, M. J. L., Migration of reactive solutes in three-dimensional heterogeneous porous media, Ph. D. thesis, 124 pp., Dept. of Earth Sci., Univ. of Waterloo, Waterloo, Ont., Canada, 1991.

Robin, M. J. L., A. L. Gutjahr, E A. Sudicky, and J. L. Wilson, Cross-correlated random field generator with direct Fourier transform method, Water Resour. Res., 29(7), 2385 - 2397, 1993.

Ruan, F., and D. McLaughlin, An efficient multivariate random field generator using the Fast Fourier Transform, Eos Trans. AGU, 76(17), Spring Meeting Suppl., S57, 1995.

Saad, Y., and M. H. Schultz, GMRES: A generalized minimal residual algorithm for solving nonsymmetric linear systems, SIAM J. Sci. Stat. Comput., 7, 856-869, 1986.

Sudicky, E. A., The Laplace Transform Galerkin technique: A time-continuous finite element theory and application to mass transport in groundwater, Water Resour. Res., 25(8), 1833 - 1846, 1989.

Sudicky, E. A., A natural gradient experiment on solute transport in a sand aquifer: Spatial variability of hydraulic conductivity and its role in the dispersion process, Water Resour. Res., 22(13), 2069 - 2082, 1986.

Sudicky, E. A., J. A. Cherry, and E. O. Frind, Migration of contaminants in groundwater at a landfill: A case study; 4. A natural gradient dispersion test, Jour. of Hydrol., 63, 81 - 108, 1983.

Sudicky, E. A., and R. G. McLaren, The Laplace Transform Galerkin technique for large-scale simulation of mass transport is discretely fracured porous formations, Water Resour. Res., 28(2), 499 - 514, 1992.

Therrien, R., Three-dimensional analysis of variably-saturated flow and solute transport in discretely-fractured porous media, Ph. D. thesis, 116 pp., Dept. of Earth Sci., Univ. of Waterloo, Waterloo, Ont., Canada, 1992.

Tompson, A. F. B., R. Ababou, and L. W. Gelhar, Implementation of the three-dimensional turning bands random field generator, Water Resour. Res., 25(10), 2227 - 2243, 1989.

Tompson, A. F. B., and L. W. Gelhar, Numerical simulation of solute transport in three dimensional, randomly heterogeneous porous media, Water Resour. Res., 26(10), 2541 - 2562, 1990.

Woodbury, A. D., W. S. Dunbar, and B. Nour-Omid, Application of the Arnoldi algorithm to the solution of the advection-dispersion equation, Water Resour. Res., 26(10), 2579 - 2590, 1990.

Xu, L., and M. L. Brusseau, A combined Laplace transform and streamline upwind approach for nonideal transport of solutes in porous media, Water Resour. Res., 31(10), 2483 - 2489, 1995.

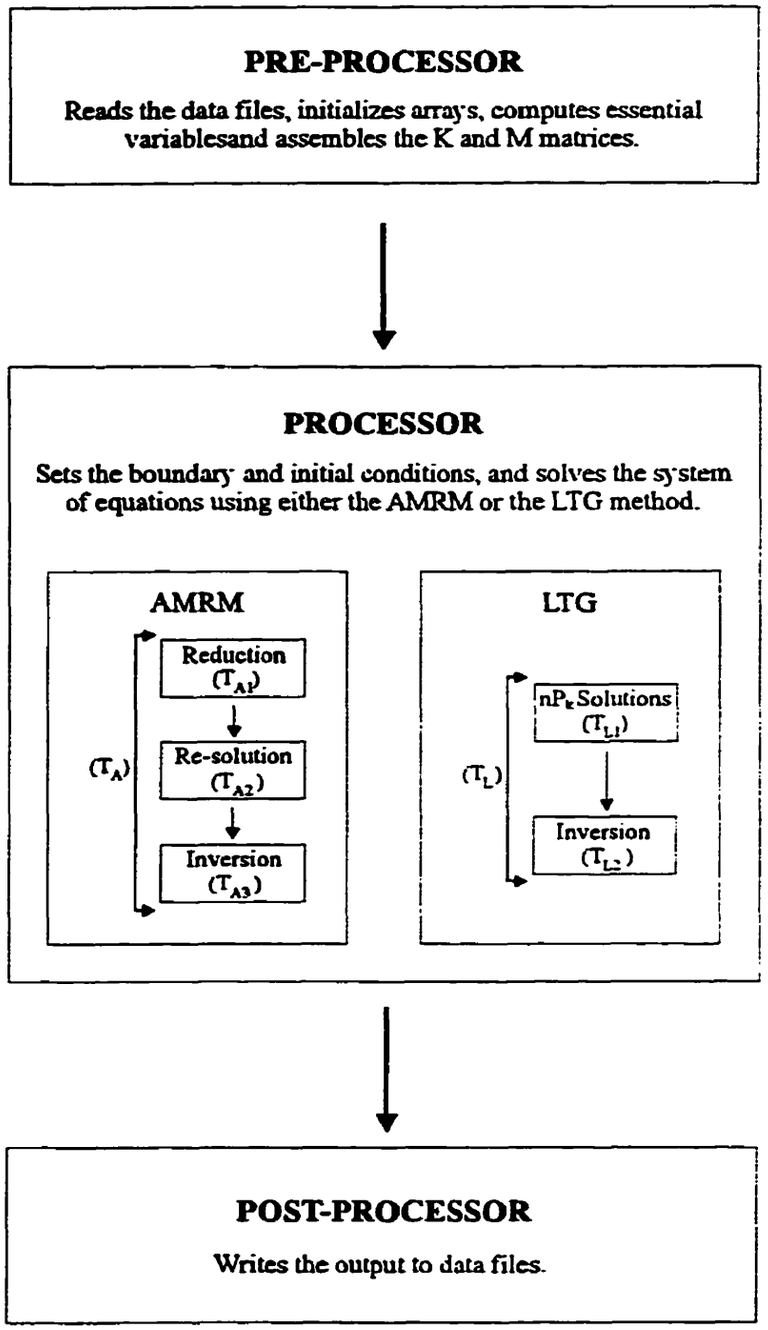

Figure 2.1:Flow chart of computer code.

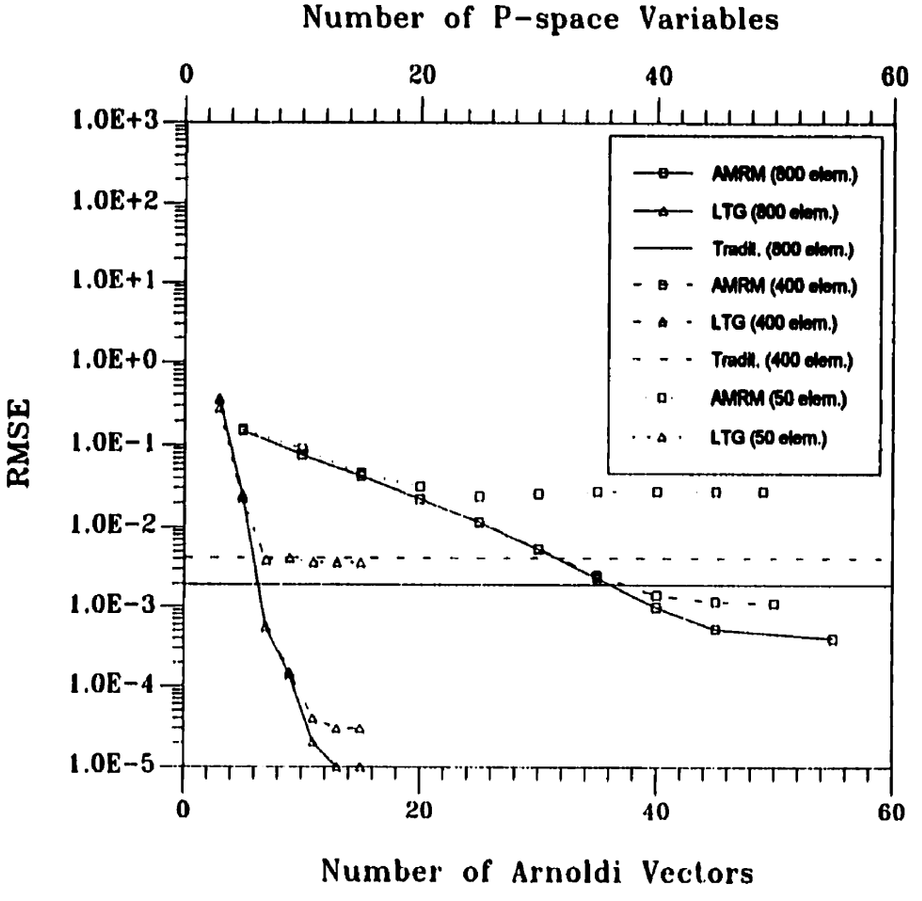

Figure 2.2: RMSE as function of the number of Arnoldi vectors and p-space variables for the high grid Peclet number analysis.

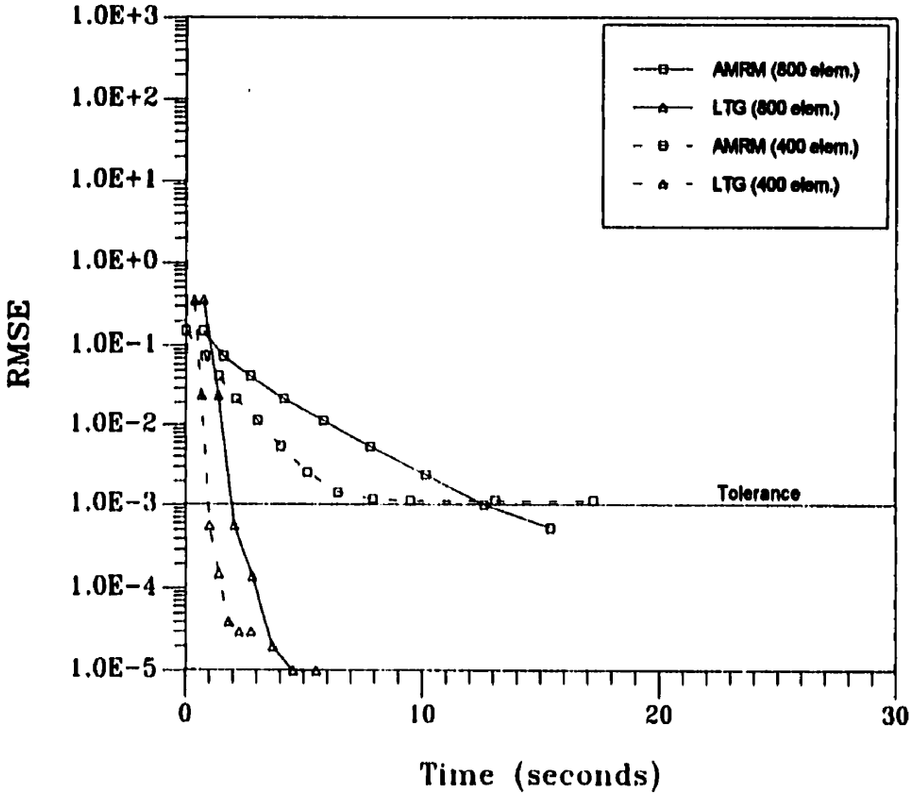

Figure 2.3: Solution times for the high grid Peclet number analysis.

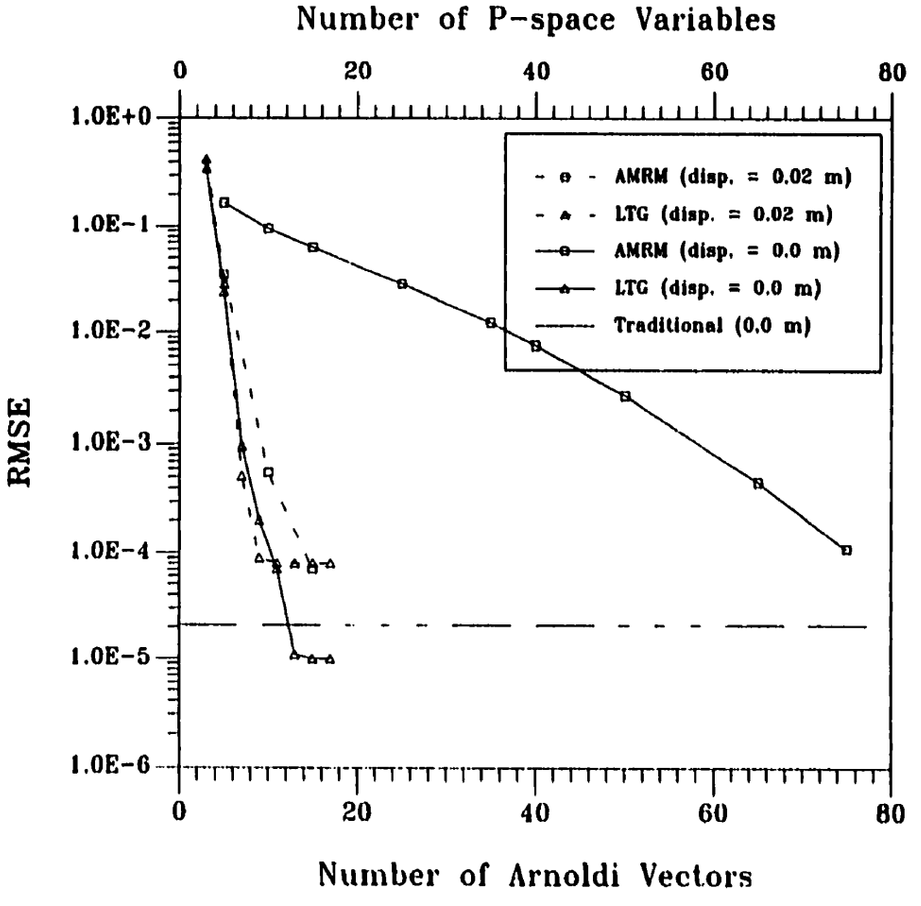

Figure 2.4: RMSE as a function of the number of Arnoldi vectors and p-space variables for the sharp front analysis.

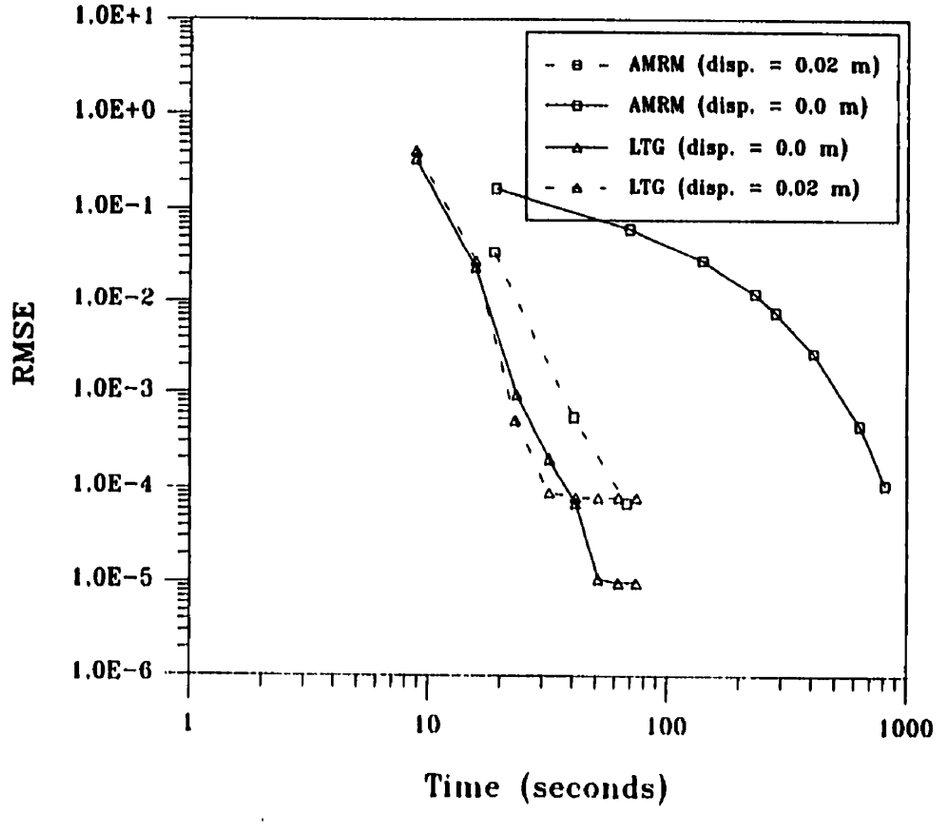

Figure 2.5: Solution times for the sharp front analysis.

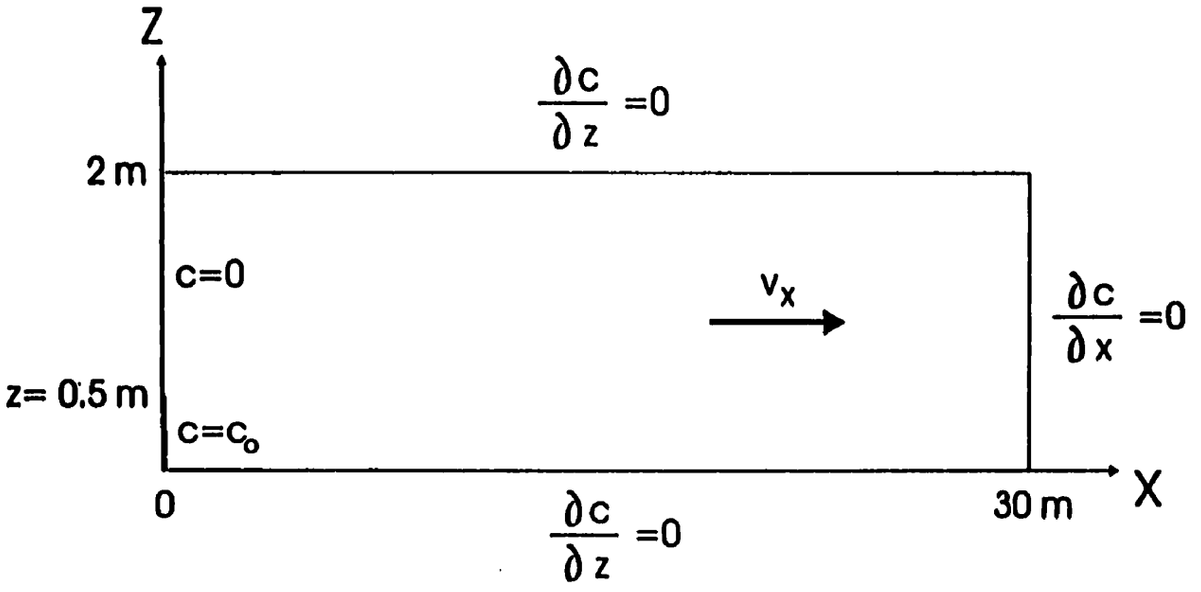

Figure 2.6: Schematic of the two-dimensional problem domain used in the simulations involving homogeneous material properties.

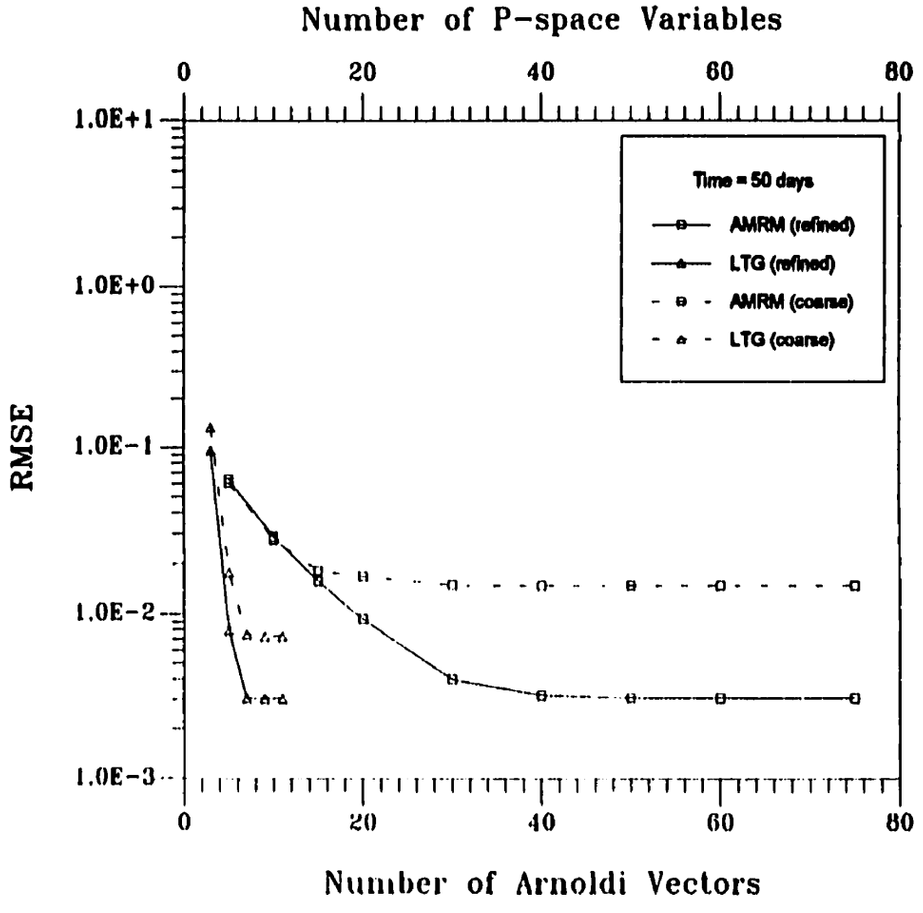

Figure 2.7: RMSE as a function of the number of Arnoldi vectors and p-space variables; 50 day simulation.

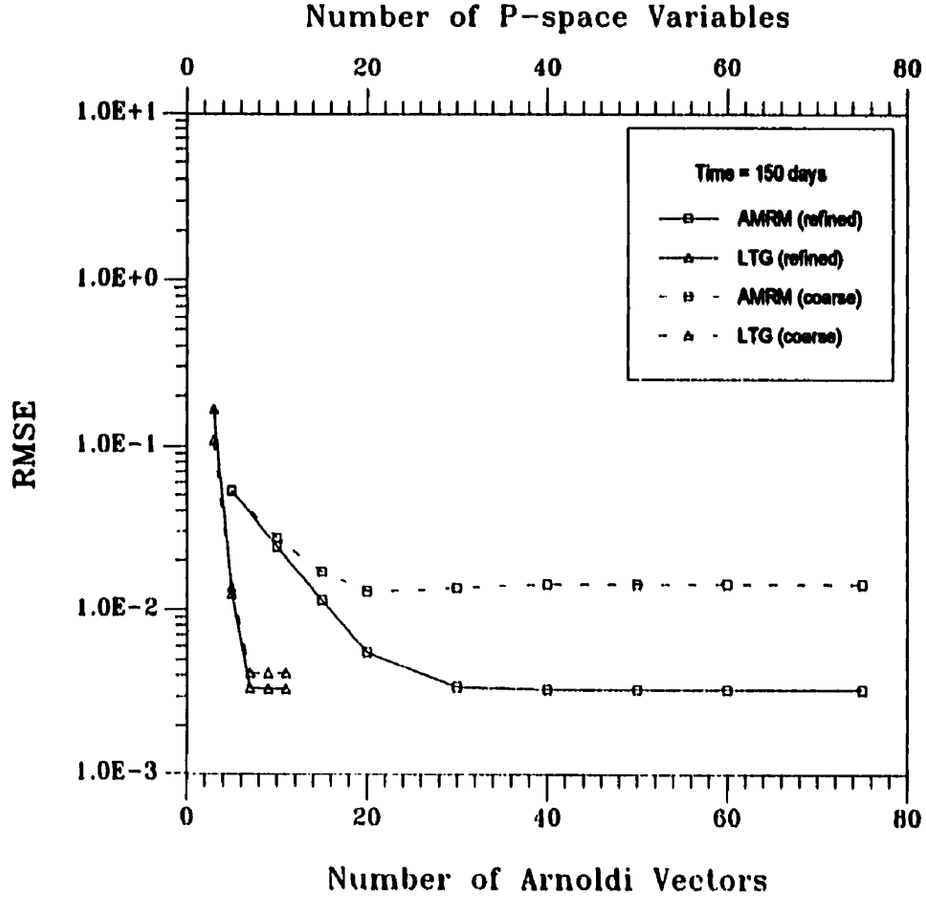

Figure 2.8: RMSE as a function of the number of Arnoldi vectors and p-space variables; 150 day simulation.

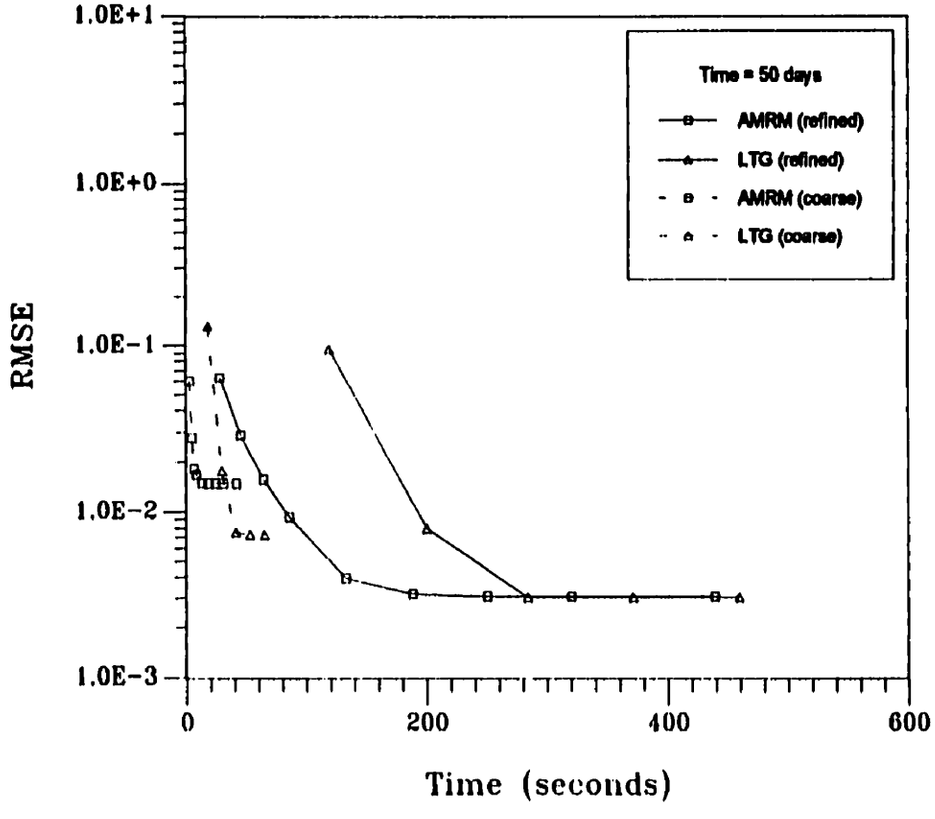

Figure 2.9: Solution times for the 50 day simulations.

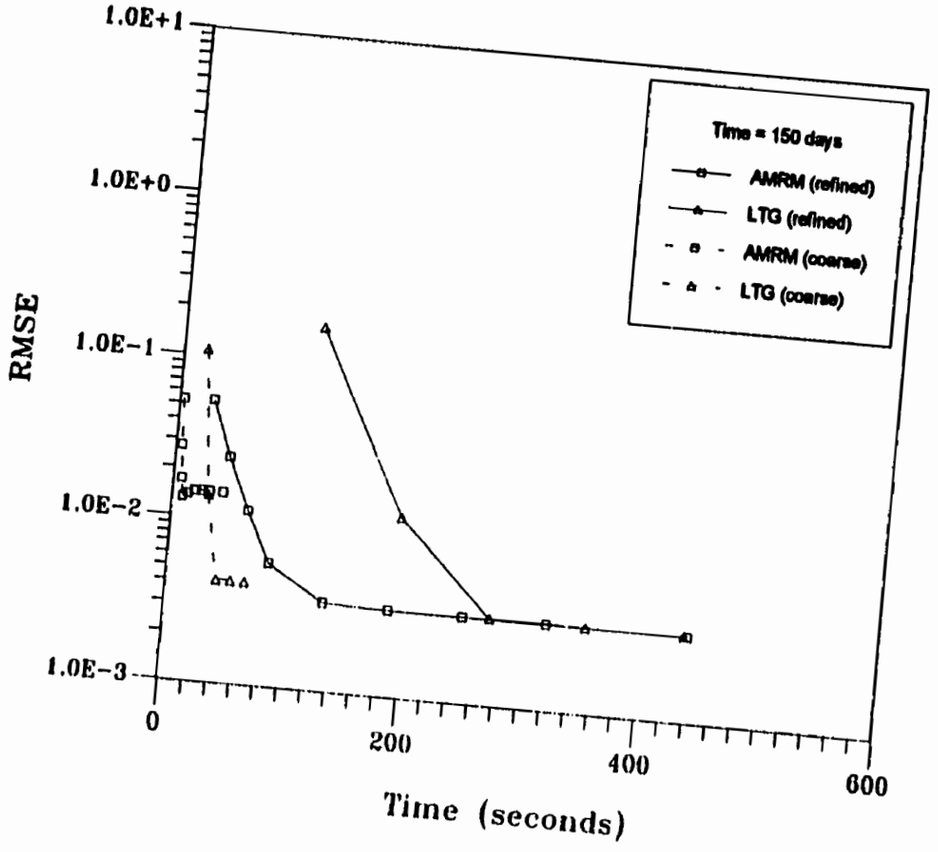

Figure 2.10: Solution times for the 150 day simulations.

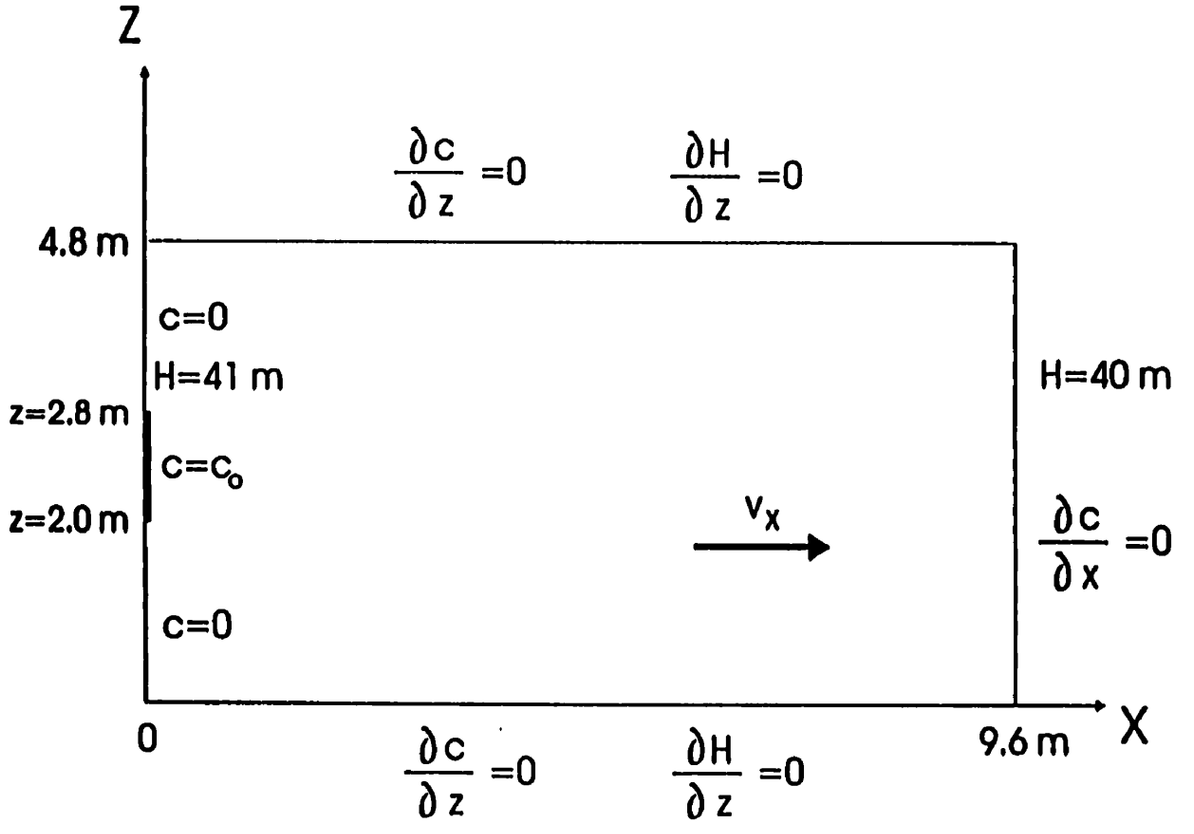

Figure 2.11: Schematic of the two-dimensional problem domain used in the simulations involving heterogeneous material properties.

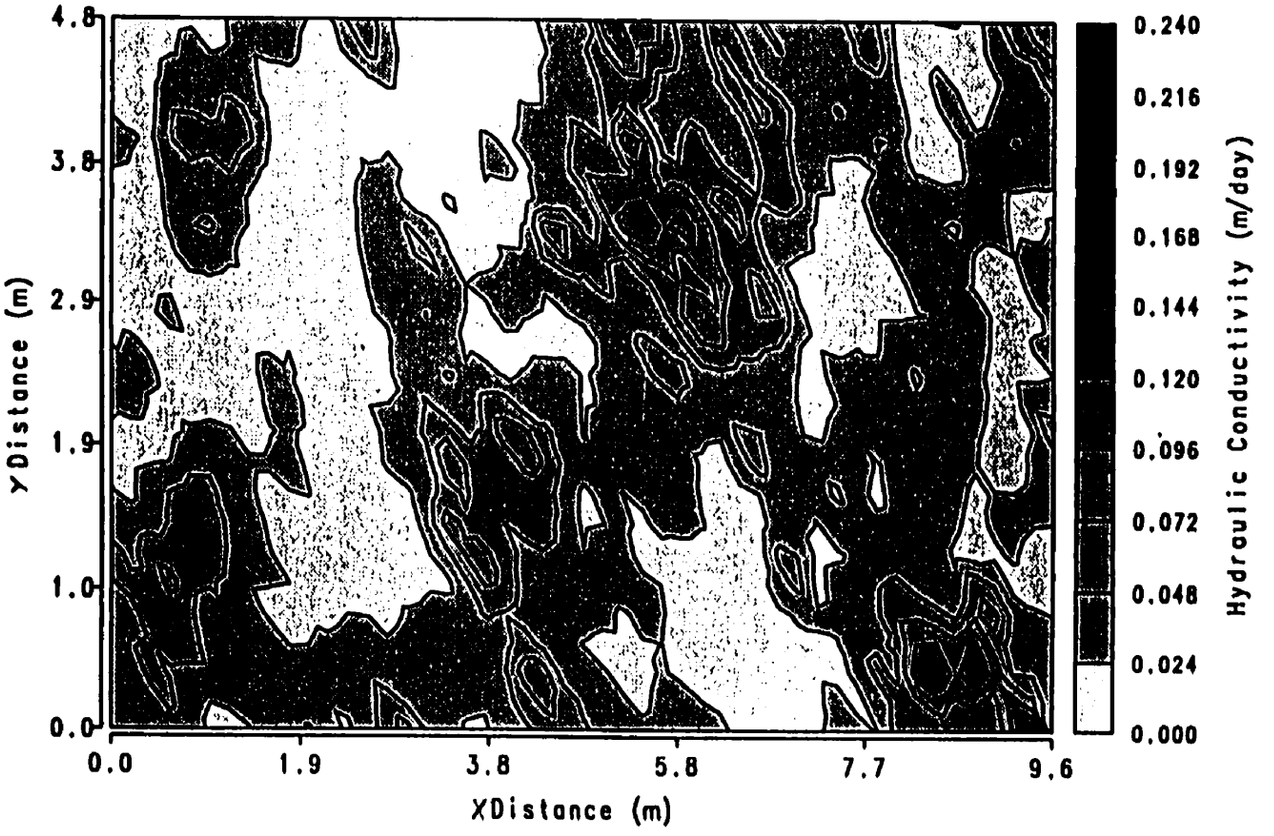

Figure 2.12: Contour map of the hydraulic conductivity field on the refined mesh.

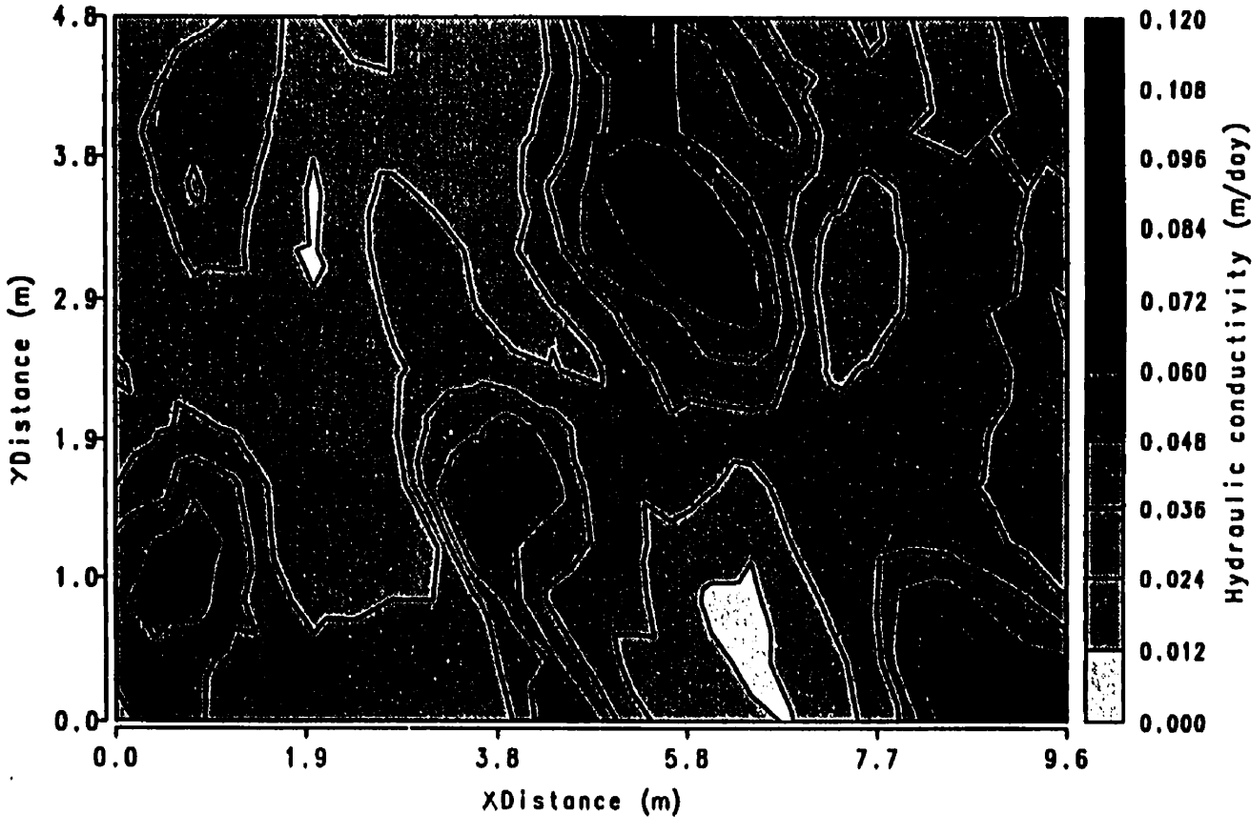

Figure 2.13: Contour map of the hydraulic conductivity field on the coarse mesh computed using the geometric mean.

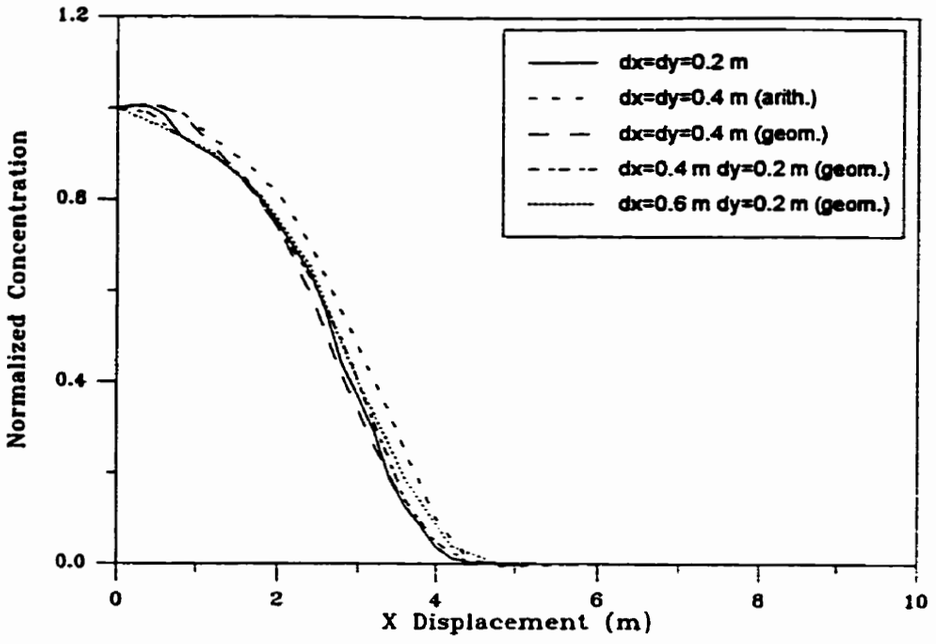

(a)

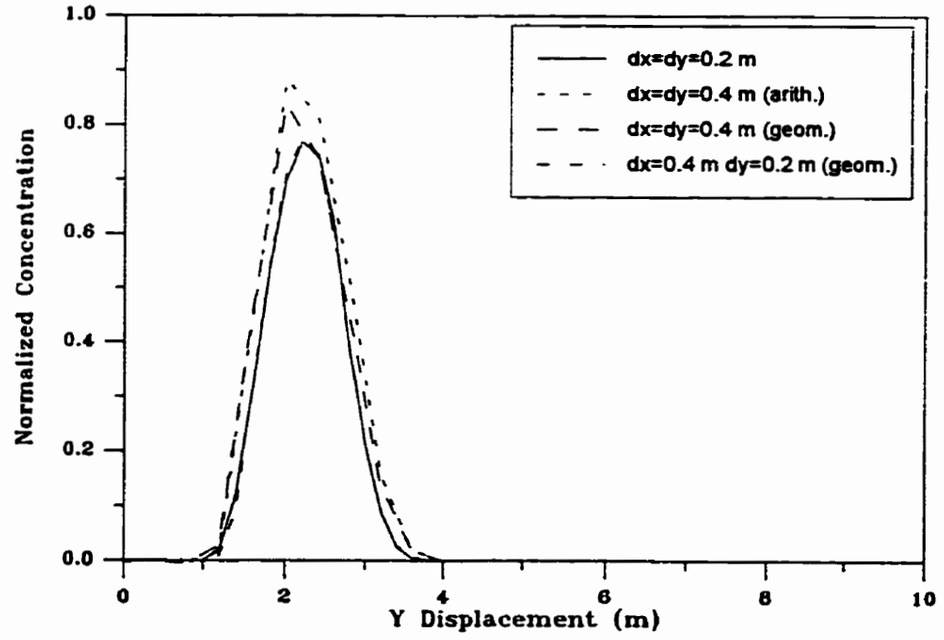

(b)

Figure 2.14: Profiles of the computed solute concentration; (a) longitudinal and (b) transverse.

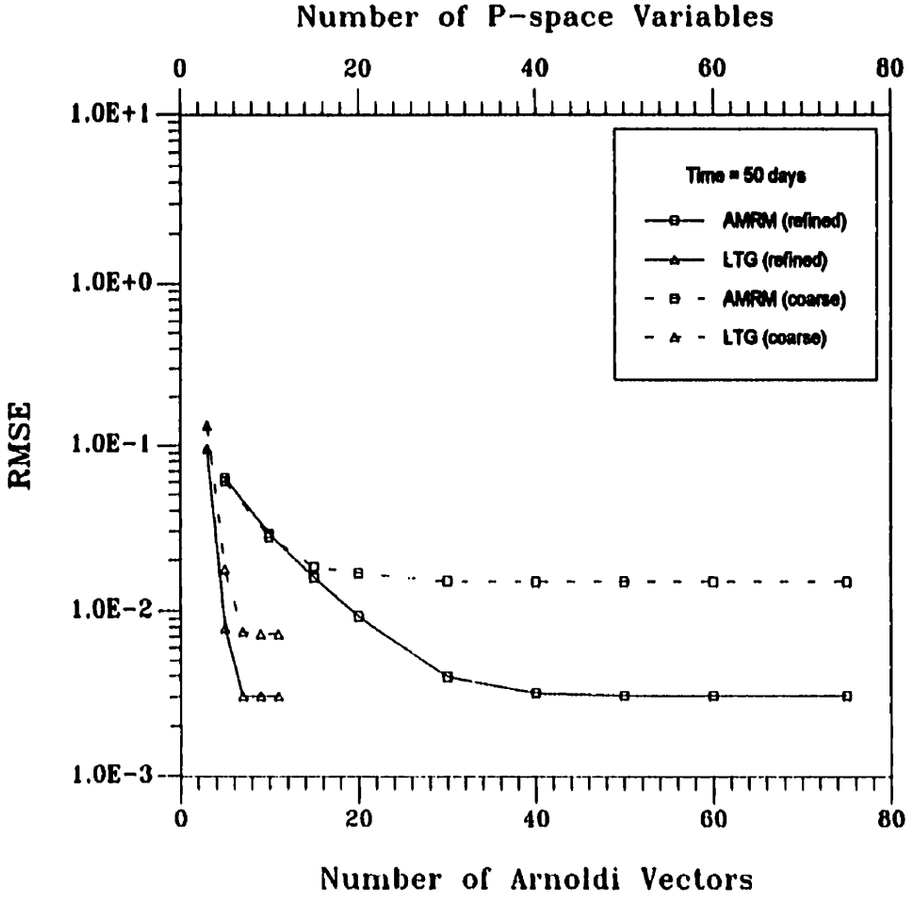

Figure 2.15: RMSE as a function of the number of Arnoldi vectors and p-space variables for the 50 day simulation; comparison of direct and iterative solutions.

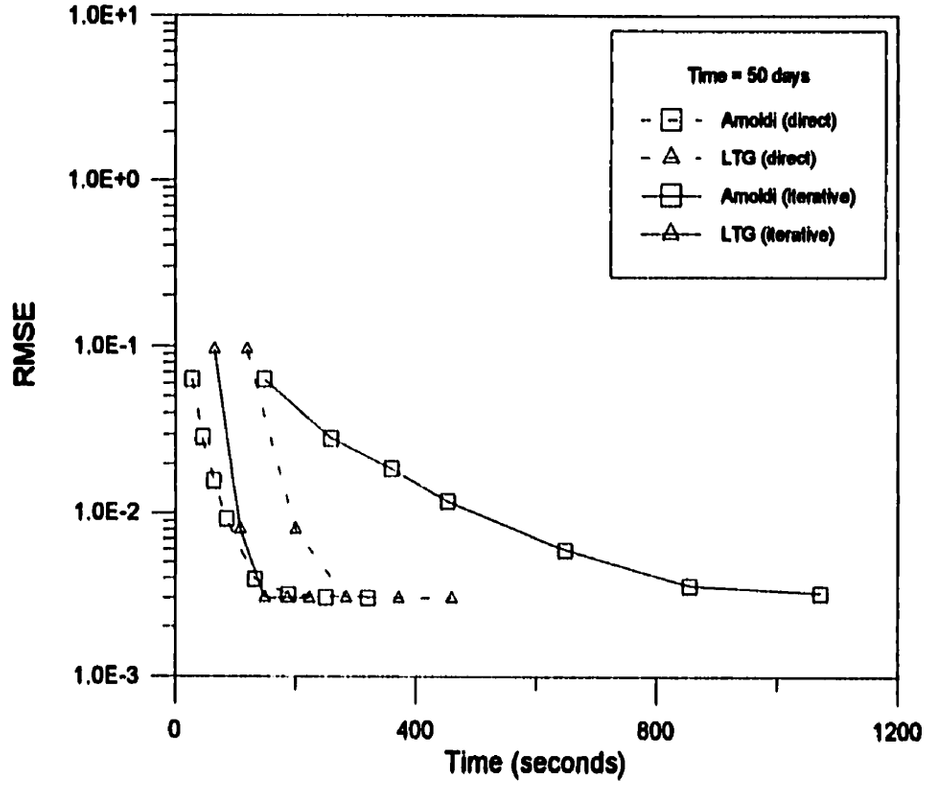

Figure 2.16: Comparison of the direct and iterative solution times for the 50 day simulations.

Table 2.1
Model Parameters for One-Dimensional Model:
High Grid Peclet Number Analysis

L (m)	50
$v = v_x$ (m/day)	0.1
α_L (m)	0.05
D^* (m^2/day)	4.3×10^{-5}
Δx (m)	0.0625, 9.125, 1.0
Elements	800, 400, 50
Grid Peclet Number	1.3, 2,5, 19,8
Courant Number	1.0

Table 2.2
Model Parameters for One-Dimensional Model: Sharp Front Analysis

L (m)	0.9
$v = v_x$ (m/day)	0.1
α_L (m)	0.02, 0
D^* (m^2/day)	4.3×10^{-5}
Δx (m)	1.0×10^{-4}
Elements	9000
Grid Peclet Number	0.005, 0.23
Courant Number	0.1

Table 2.3
Model Parameters for Two-Dimensional Model: Homogeneous Medium

Lx, Ly (m)	30, 2
$v = v_x$ (m/day)	0.1
α_L, α_T (m)	0.05, 0.005
D^* (m^2/day)	4.3×10^{-5}
[1] Δx, Δz (m)	0.1, 0.1
[2] Δx, Δz (m)	1.0, 0.1
Elements	12000, 1200
Nodes	6321, 651
Grid Peclet Number	1.98, 19.8
Courant Number	1.0, 1.0

Table 2.4
Solution Times for Simulations in Heterogeneous Medium

	SOLUTION TIMES (seconds)			
	350 Day Simulation		**600 Day Simulation**	
	AMRM	LTG	AMRM	LTG
Coarse Mesh	5.2	34.3	5.5	33.6
Refined Mesh	27	290	28	270

Chapter 3

Numerical Solution of the Advection-Dispersion Equation: The "Shift" Arnoldi Modal Reduction Method

3.1 Introduction

Recent developments in computer technology and stochastic theories have resulted in considerable emphasis being placed on the use of numerical models as predictive tools in assessing the fate of contaminants in complex subsurface environments. The accuracy of these predictions is dependent on how well the physical, chemical and biological processes governing the transport are expressed, as well as the accuracy of the solution technique used. As a consequence, these requirements may result in large numerical systems which are computationally expensive to solve using traditional finite difference (FD) and finite element (FE) techniques. The demand for accurate and efficient numerical techniques has lead to the development of such methods as: the method of characteristics [Konikow and Bredohoeft, 1974, 1978], random walk particle models [Prickett et al., 1981; Tompson and Gelhar, 1990; Hunter et al., 1993], the boundary element method [Brebbia and Skerit, 1984], multigrid methods [McCormick, 1989] and local adaptive grid methods [Neuman, 1984; Cady and Neuman, 1987; Yeh, 1990; Bhuiyan et al., 1990; Wolfsberg and Freyberg, 1994].

In spite of the various methods available, variants of the FE method still form the core of modelling packages commonly used by practising hydrogeologist. This is in part due to the method's ability to handle irregular domains and complex boundary conditions. Application of the finite element approach for two- and three-dimensional problems commonly results in

sparse matrices. The dimensions of these matrices are dependent on the degree of spatial discretization employed, which is in turn controlled by the grid Peclet criterion [cf. Daus et al., 1983; Huyakorn and Pinder, 1983; Celia and Gray, 1992]. The estimation of solute concentrations at any time on the spatially discretized domain generally dictates that a time integration be performed. The temporal discretization used to perform this integration is controlled by the Courant criterion [cf. Daus et al., 1983; Huyakorn and Pinder, 1983; Celia and Gray, 1992]. In a FE formulation such as described, the spatially discretized system of equations must be solved at each time step. Depending on the dimensions of matrices involved and the number of time steps required to attain the desired solution, this process can be computationally expensive. As alluded to earlier, several variants of the FE method exist for modelling mass transport in the subsurface. Included in these are Laplace transform methods [Yu et al., 1987; Sudicky, 1989], modal reduction schemes [Woodbury et al., 1990; Nour-Omid et al., 1991], matrix exponential methods [Loaiciga and Marino, 1987], semi-analytic methods [Kuiper, 1973; Sahuquillo, 1983; Hwang et al., 1984; Umari and Gorelick, 1986] and iterative methods [Schmid and Braess, 1988]. Of these the approach which is of relevance to this chapter is the modal reduction method based on the recursive Arnoldi algorithm [Woodbury et al., 1990; Nour-Omid et al., 1991], and hereafter referred to as the Arnoldi modal reduction method (AMRM).

The AMRM essentially transforms a system of equations from an initial space to a much smaller space, the size of which is determined by the number of Arnoldi vectors considered. The reduced system is then solved using an appropriate numerical method and then inverted by a linear transformation back into the original. The works of Woodbury et al.

[1990] and Farrell et al. [1997; cf. Chapter 2] illustrated how the method can be successfully applied to mass transport problems in hydrogeology. In both works it was shown that the considerable time savings observed when compared to the conventional FE solution approach, were due to the reduced time needed to solve the smaller system of equations at each time step.

The focus of this paper is to introduce and investigate the properties of a 'shift' variant of the Arnoldi algorithm. The investigation to be performed will focus on the practical aspects of the method for solving mass transport problems commonly encountered in hydrogeology.

3.2 Theory

3.2.1 The Mass Transport Equation

Solute transport in an incompressible fluid is governed by the following differential equation, boundary and initial conditions [Bear, 1972, p. 613-617]:

$$\nabla\cdot(\boldsymbol{D}\cdot\nabla c)-\boldsymbol{v}\cdot\nabla c+f=\frac{\partial c}{\partial t} \qquad in\ \Omega \tag{3.1a}$$

$$c(t=0)=c_0 \qquad in\ \Omega \tag{3.1b}$$

$$c=c_b \qquad on\ \Gamma \tag{3.1c}$$

$$\boldsymbol{D}\cdot\nabla c\cdot\boldsymbol{n}=q_b \qquad on\ \Gamma \tag{3.1d}$$

where c is the solute mass concentration, q_b is a specified mass flux, f is a source/sink term, $\boldsymbol{D}$ is a tensor of dispersion coefficients, v is the transport velocity which depends on the spatial coordinates, n is the unit-outward normal, and t is time. Ω denotes the interior of the domain under consideration whose boundary is Γ. The components of $\boldsymbol{D}$ for an isotropic medium are given by [Bear, 1972]:

$$D_{ij}=\alpha_T|v|\delta_{ij}+(\alpha_L-\alpha_T)\frac{v_i v_j}{|v|}+D^* \tag{3.2}$$

where D^* is the coefficient of molecular diffusion in the porous medium, and α_L and α_T are the longitudinal and transverse dispersivities respectively.

Application of the finite element method to the governing mass transport equation subject to initial and boundary conditions results in a matrix differential equation of the form:

$$\boldsymbol{M}\dot{\boldsymbol{c}}+\boldsymbol{K}\boldsymbol{c}=\boldsymbol{b} \tag{3.3}$$

where c is a vector of unknowns at the nodes of the finite element mesh used to discretize the domain Ω, $\boldsymbol{K}$ is the "stiffness" or "conductivity" matrix and $\boldsymbol{M}$ is the "mass" or "capacity" matrix. For the mass transport equation $\boldsymbol{K}$ is unsymmetric while $\boldsymbol{M}$ is symmetric and positive-definite. Finally, $\boldsymbol{b}$ is a vector which contains the effects of the boundary conditions as well as source/sink terms.

3.2.2 The Shifted Arnoldi Approach

A discussion of the application of the standard AMRM to the solution of the mass transport problem has been given by Woodbury et al. [1990], Nour-Omid et al. [1991] and

Farrell et al., [1997; cf. Chapter 2]. As a result the theory outlining this approach will not be reproduced here, instead, the focus of this section will be on the development of the shift-AMRM method.

The generalized eigenvalue problem which arises from the application of the finite element formulation to the ADE is of the form:

$$\boldsymbol{K}\boldsymbol{z}_j=\lambda_j\boldsymbol{M}\boldsymbol{z}_j \qquad j=1,\ldots,n \tag{3.4}$$

where z_j and λ_j represent the eigenvectors and associated eigenvalues of $\boldsymbol{M}^{-1}\boldsymbol{K}$. Nayar and Ortega [1993] have shown that application of the Arnoldi algorithm to this system results in the formation of an upper Hessenberg matrix $\boldsymbol{L}$, the eigenvalues of which approximate those of the matrix $\boldsymbol{M}^{-1}\boldsymbol{K}$, especially those in the outer part of the spectrum (i.e. the largest eigenvalues). Note that the solution of the ADE is controlled by the smallest eigenvalues of $\boldsymbol{M}^{-1}\boldsymbol{K}$ which form the largest eigenvalues of $\boldsymbol{K}^{-1}\boldsymbol{M}$. Thus an efficient way of estimating the smallest eigenvalues of $\boldsymbol{M}^{-1}\boldsymbol{K}$ is to first use the Arnoldi algorithm to generate the largest eigenvalues for the system $\boldsymbol{K}^{-1}\boldsymbol{M}$ and later invert these values using what is commonly termed a *"shift and invert"* strategy [Ericsson and Ruhe, 1980; Nayar and Ortega, 1993]. These relationships are expressed mathematically as:

$$(\boldsymbol{K}-\sigma\boldsymbol{M})^{-1}\boldsymbol{M}\boldsymbol{z}_j=\mu_j\boldsymbol{z}_j \tag{3.5a}$$

$$\mu_j=\frac{1}{\lambda_j-\sigma} \tag{3.5b}$$

where σ represents a shift in the eigenvalue spectrum. Here the eigenvalues of $\boldsymbol{M}^{-1}\boldsymbol{K}$ close to

σ correspond to eigenvalues of μ with the largest absolute value as determined by an application of the Arnoldi algorithm to (3.5a).

The modal reduction process which forms the basis of this work is initiated by adding $-\sigma Mc$ to both sides of (3.3) to give:

$$M\dot{c}+K_\sigma c=b-\sigma Mc \tag{3.6}$$

where $K_\sigma=(K-\sigma M)$. Multiplying both sides by K_σ^{-1} gives:

$$K_\sigma^{-1}M\dot{c}+\left(I+\sigma K_\sigma^{-1}M\right)c=K_\sigma^{-1}b \tag{3.7}$$

After m Arnoldi steps, the recursion results in the following system of equations [cf. Woodbury et al., 1990]:

$$K_\sigma^{-1}MQ_m=Q_mH+r_me_m^T \tag{3.8}$$

where e_m is the last column of the $m \times m$ identity matrix, H which has been previously defined is an $m \times m$ matrix, Q_m is an $n \times m$ $(n \gg m)$ matrix of Arnoldi vectors and r_m is a residual vector. Both Q_m and r_m satisfy the following orthogonality conditions:

$$Q_m^TMQ_m=I_m \tag{3.9a}$$

$$r_m^TMQ_m=0 \tag{3.9b}$$

The Rayleigh-Ritz reduction procedure requires that an approximate solution to (3.7) be defined as the linear combination of Arnoldi vectors. That is:

$$c \approx \hat{c} = Q_m w \tag{3.10}$$

Since $\hat{c}$ is an approximation to the true solution substitution of (3.10) into (3.7) produces a residual vector p_m:

$$p_m = K_\sigma^{-1} M Q_m \dot{w} + \left(I + \sigma K_\sigma^{-1} M\right) Q_m w - K_\sigma^{-1} b \tag{3.11}$$

Multiplying (3.11) by $Q_m^T M$ to take advantage of the orthogonality relationships gives:

$$Q_m^T M p_m = Q_m^T M K_\sigma^{-1} M Q_m \dot{w} + Q_m^T M \left(I + \sigma K_\sigma^{-1} M\right) Q_m w - Q_m^T M K_\sigma^{-1} b \tag{3.12}$$

After manipulation (3.12) reduces to:

$$Q_m^T M K_\sigma^{-1} M Q_m \dot{w} + \left(I + \sigma Q_m^T M K_\sigma^{-1} M Q_m\right) w = Q_m^T M K_\sigma^{-1} b \tag{3.13}$$

Equation (3.13) can be further simplified by multiplying (3.8) by $Q_m^T M$ and recognizing that:

$$Q_m^T M K_\sigma^{-1} M Q_m = H \tag{3.14}$$

As a result, (3.13) reduces to:

$$H\dot{w} + (I + \sigma H) w = g \tag{3.15a}$$

$$g = Q_m^T M K_\sigma^{-1} b \tag{3.15b}$$

The reduced system is then solved for w using a suitable time stepping procedure such as Crank-Nicolson [Woodbury et al., 1990; Farrell et al., 1997, cf. Chapter 2]. The solution is then inverted back to the original space using the linear transform (3.10) which has been

shown to be computationally inexpensive [Woodbury et al., 1990; Farrell et al., 1997; cf. Chapter 2].

An operations count comparison between the standard LU decomposition approach and the AMRM was performed by Woodbury et al. [1990, Table 1]. The results of a similar analysis performed on the 'shift' Arnoldi approach are presented in Table 3.1. It is important to note that in this analysis the operations count associated with calculating $\boldsymbol{K}_{\sigma}$, has not been taken into account, since this step occurs prior to the initiation of the Arnoldi process. However for the sake of completeness the operations count associated with this step is given here as nn_b . The results show that implementation of the shift-AMRM does not produce a significant increase in the operations count compared to the AMRM.

3.3 Numerical Simulations

In this work, the performance of the shift-AMRM approach is first examined for both one- and two-dimensional mass transport problems for which analytical solutions are available. The problems, which are similar to those presented in Farrell et al. [1997; cf. Chapter 2], are designed to examine the accuracy and stability of the approach at high and low grid Peclet numbers. The solution accuracy is estimated by computing the root-mean-square error (RMSE) between the computed solution and the analytical solution for the problem posed:

$$RMSE=\sqrt{\frac{1}{n-1}\|\boldsymbol{e}\|^2} \tag{3.16}$$

Here $e = c^N - c^A$, where c^N is the solution computed using the numerical method, c^A is the solution based on the analytical method and n represents the number of nodes used in the discretization. As in Chapter 2, the RMSE was the primary error estimate used in the analysis although other estimates were computed.

The grid Peclet number, *Pe*, is defined as [cf., Daus et al., 1983; Huyakorn and Pinder, 1983; Celia and Gray, 1992]:

$$Pe_i = \frac{v_i \Delta x_i}{D_{ii}} \tag{3.17}$$

where v_i represents the groundwater velocity in the ith direction, D_{ii} is the i^{th} diagonal of the hydrodynamic tensor and Δx_i maximum local grid spacing in the ith direction. It is important to note that in order to maintain numerical accuracy and stability a grid Peclet number less than two $(Pe_i < 2)$ is commonly used [cf., Daus et al., 1983; Huyakorn and Pinder, 1983; Celia and Gray, 1992]. A further criterion used to ensure numerical accuracy and stability is the Courant criterion *(Cn)* [cf., Dauss et al., 1983; Huyakorn and Pinder, 1983; Celia and Gray, 1992]:

$$Cn = \frac{v_i \Delta t}{\Delta x_i} \leq 1 \tag{3.18}$$

where Δt is the time step used in the time integration.

The numerical simulations were performed on a SUN SPARC 1+ work station running version 4.1.3 of the SUN operating system and version 1.3 of the SUN Fortran77

compiler. The computer code utilized in this study was similar in structure to that utilized in [Farrell et al., 1997; cf. Chapter 2] and as a result a limited description is presented here. The solution scheme utilized a banded matrix data storage scheme and a direct matrix solver which was based on the factorization subroutine DGBFA and the backsolve subroutine DGBSL contained in the LINPACK package [Dongarra, 1979].

In the analyses performed only real values of the shift were considered. The eigenvalues associated with mass transport problems are generally found to be distributed symmetrically about the positive real axis. As a result, real values of the shift are obtained by averaging the eigenvalues of the problem with an averaging "volume" centred along the real axis. Not all shifts are desirable; some shifts result in improved solutions while others produce degraded solutions. Therefore, an "optimal" shift is desirable. The optimal shift is considered to be that value of shift which results in the most improved solution for the problem using a given number of Arnoldi vectors. A priori knowledge of the optimal shift is generally not available for most realistic problems. Approaches based on averaging the eigenvalues have been proposed to approximate the optimal shift [Ericsson and Ruhe, 1980]; however these methods have been found to produce values which are less than optimal. One approach to determining the optimal shift involves the use of an iterative procedure in which N shifts are systematically chosen and evaluated to see which produces the minimum root-mean-square error (RMSE). Although this approach is inefficient, it never-the-less provides additional information regarding the behaviour of the solution over a large range of shifts.

Finally, from a computer programming stand point, the implementation of a real shift requires little modification of the code used for the AMRM analysis.

3.3.1 One-Dimensional Simulations

As part of this analysis a series of one-dimensional simulations were used to evaluate the convergence which results from the implementation of a shift. Although one-dimensional simulations are not in most cases representative of field-scale hydrogeological phenomena. However, such simulations can be important for evaluating various aspects of a proposed numerical formulation.

The parameters used in the one-dimensional model are assumed to be homogeneous. As a result a constant velocity across the domain can be assumed. The initial and boundary conditions being considered are:

$$c(x,t=0)=0.0$$
$$c(x=0,t>0)=1.0$$
$$c(x=L,t>0)=0.0$$

where L represents the length of the system. Similar boundary conditions were also utilized by Farrell et al. [1997; cf. Chapter 2] in their comparison of the LTG method and the AMRM. The analytical solution for this one-dimensional problem was given by Ogata [1970; c.f., Freeze and Cherry, 1979, p. 391, equation 9.5]:

$$c(x,t)=\frac{c_0}{2}\left[erfc\left(\frac{x+vt}{\sqrt{4D_x t}}\right)+\exp\left(\frac{vx}{D_x}\right)erfc\left(\frac{x-vt}{\sqrt{4D_x t}}\right)\right] \qquad (3.19)$$

Using (3.16) an estimate of the accuracy of the numerical solution can be determined.

For this analysis two one-dimensional models were considered. The models were designed to examine the improvements in the solution to be gained from shifting under high (model #1) and low (model #2) grid Peclet numbers. The parameters for these models are listed in Tables 3.2a and 3.2b.

In model #1, the grid Peclet number was adjusted by varying the domain discretization, Δx, while in model #2 the grid Peclet number was adjusted by varying the value of the dispersivity, α_L. These models allowed a systematic evaluation of the effects of dispersivity and discretization on the optimal shift to be studied. In these simulations, RMSEs were generated for over 1000 shifts.

3.3.1.1 Model #1

The purpose of this model was to investigate the behaviour of the optimal shift as the domain discretization varied. An understanding of this behaviour is essential from a numerical modelling perspective since in most cases the domain discretization is varied in order to improve the accuracy of the numerical solution during the calibration. The discretizations considered and their associated grid Peclet numbers are summarized in Table 3.3. Note that in the simulations the Courant number is maintained at 1.0. Plots of the RMSE vs shift over the interval $0 \leq \sigma \leq -1$ for several numbers of Arnoldi vectors (20, 35 and 50) are shown in Figure 3.1.

The plots in Figures 3.1 are composed of two sections, which correlate with small and large values of shift. The plots show that at large shifts the RMSE displays exponentially decreasing growth with the magnitude of the growth being controlled by the number of

Arnoldi vectors utilized (see Figure 3.1). At small shifts plots of the RMSE also appear to be influenced by the number of Arnoldi vectors utilized. For example, when large numbers of Arnoldi vectors are employed an apparent linear relationship appears to exist between the RMSE and the shift (see Figure 3.1). The slope of this linear relationship is negative and appears to be independent of the number of Arnoldi vectors utilized (provided enough Arnoldi vectors were considered). This is illustrated by the 1600 element simulation which shows the linear relationship for 35 and 50 Arnoldi vectors to be identical. When smaller numbers of Arnoldi vectors are utilized the apparent linear relationship deteriorates into a small amplitude, small wavelength oscillation. This suggests that the apparent linear behaviour described may actually represent a long wavelength low amplitude oscillation. This oscillation may be related to eigenvalues captured in the numerical solution. The value of shift to which the apparent linearity persists depends on the number of Arnoldi vectors utilized; the greater the number of Arnoldi vectors utilized, the further the linear persistence. To illustrate this consider the plots for 50 and 35 Arnoldi vectors in Figure 3.1d. The plots show that for 35 Arnoldi vectors the linear behaviour persists up to a shift of approximately -0.20 whereas for 50 Arnoldi vectors the linear behaviour persists up to a shift of approximately -0.45.

To investigate the possible significance of the observed linearity, ordinary least squares (OLS) lines were fitted to the small shift regions of the plots. Figure 3.2 provides a plot of the computed slopes of the OLS fits versus the grid Peclet number. The figure shows an inverse relationship between the grid Peclet number and the slope. This indicates that as the mesh discretization increases, the effects of shifting on the RMSE are reduced (i.e., the RMSE becomes insensitive to shift).

To this point the existence of an optimal shift has been neither addressed nor demonstrated. Figure 3.3 shows plots of the RMSE versus shift (based on 35 Arnoldi vectors), over the range $-0.01 \leq \sigma \leq 0$, for the four discretizations being considered. The plots show that the RMSE attains a minimum value at some value of shift, which is assumed to be the optimal shift. The figure also shows that the optimal shift is not constant, but varies with grid discretization. In fact for the problem under consideration the optimal shift decreases as the grid discretization increases; i.e. as the grid Peclet number decreases. It is worth noting that for the 1600 element simulation presented in Figure 3.3, the optimal shift does not appear within the range shown. However, within this range the 1600 element simulation does appear to attain a minimum value, thus supporting the contention that the small shift behaviour is dominated by long wavelength small amplitude oscillations.

An investigation of the influence of the number of Arnoldi vectors utilized, on the optimal shift was performed. Table 3.4 lists some of the results of this investigation. The table demonstrates that prior to convergence the optimal shift varies with the number of Arnoldi vectors utilized. An examination of Table 3.4 and Figure 3.4 shows that for small numbers of Arnoldi vectors the optimal shift appears to be large and erratic; however as the number of Arnoldi vectors increases the optimal shift appears to converge. Recall that as the number of Arnoldi vectors utilized increases, the numerical solution converges, i.e. the RMSE tends to its minimum value. Therefore, the results in Figure 3.4 suggest that as the numerical solution converges, the optimal shift also convergences with the convergence value for the model under consideration being zero. Whether or not this result can be generalized requires further investigation.

Figure 3.5 illustrates the impact of the optimal shift on the numerical solution. Note that the figure compares RMSEs computed under both the optimal and zero shift. The graphs show a significant deviation between $RMSE_{opt}$ and $RMSE_0$ when few Arnoldi vectors are utilized. One approach to quantifying this deviation is through the use of a "percentage improvement", where the percentage improvement is calculated using the expression shown at the bottom of Table 3.4. The table shows that under optimal shifting significant improvements in the numerical solution can be achieved, particularly when the convergence of the solution is initially poor. For example, applying the optimal shift (-0.077) to the simulation involving 20 Arnoldi vectors produces a 29% improvement in the numerical solution. In contrast to this, application of the optimal shift (-0.002) to the simulation involving 50 Arnoldi vectors produced only a 2% improvement in the numerical solution. Figure 3.6 shows that this phenomenon is also observed for the other discretizations. The reader should recall that for the posed problem 20 Arnoldi vectors yielded poor convergence, whereas 50 Arnoldi vectors yielded a much improved convergence.

3.3.1.2 Model #2

As earlier stated, the purpose of this model was to investigate the behaviour of the optimal shift as the model dispersivity varied. An understanding of this behaviour is essential from a numerical modelling perspective since in most cases the dispersivity is one of the parameters commonly varied in the calibration procedure. In this analysis, dispersivity values of $\alpha_L = 0.01$, 0.015 and 0.02 m were considered (Table 3.2b). The domain which was 0.9 m long (Table 3.2b) was discretized using a nodal spacing of 1.0×10^{-3} m, which resulted in 9000

elements. The grid Peclet numbers associated with these dispersivities are listed in Table 3.5. The Courant number for the simulations was maintained at 1, and the numerical solution sought was for solute transport after 3 days. Plots of the RMSE versus shift for various Arnoldi vectors (5, 10, 15, and 20) are shown in Figure 3.7.

The plots in Figure 3.7 are similar in form to those previously presented. As in the previous analysis, the slope of the apparently linear section of the RMSE versus shift plots was examined. The results of this analysis are presented in Table 3.5. The slopes appear to be positive and small, approximately 10^{-7} (see Table 3.5). On the basis of the data presented in Table 3.5 a proportional relationship between the grid Peclet number and the magnitude of the slope is again plausible, since as Pe increases the magnitude of the slope also increases. Since the increase in the grid Peclet number results from a decrease in the dispersivity, it may be inferred that the slope is inversely proportional to the dispersivity. Thus, as dispersivity decreases, the sensitivity of the RMSE to small changes in shift can be expected to increase. Note however that the small slopes in the RMSE versus shift plot (for small shifts) indicate that for small grid Peclet numbers such as those associated with this problem the sensitivity of this relationship is quite small. This tendency is also apparent in model #1. Finally, the reader should note that the apparent linear relationship between the grid Peclet number and the slope of the linear portion of the plots is similar to the results presented in the previous section; however, the positive gradient contradicts that determined earlier. This apparent contradiction is influenced by the location of the optimal shift within the small shift region. For example in the problem previously considered the optimal shift was located close to zero (see Figure 3.1) whereas for the current problem under consideration the optimal shift is

located close to the transition point between the small shift and large shift regions of the graphs (see Figure 3.7). Note that if the absolute value of the slope is considered then there does appear to be some consistency. In this case the smallest slopes correlate to the smallest grid Peclet numbers and the largest slopes correlate with the largest grid Peclet numbers.

Using the methodology outlined earlier the optimal shift associated with various numbers of Arnoldi vectors was determined. Plots of the optimal shift versus the number of Arnoldi vectors utilized are presented in Figure 3.8. The figure shows that for small numbers of Arnoldi vectors the optimal shift is located close to zero; however, as the number of Arnoldi vectors utilized increases, the optimal shift moves away from zero. This tendency differs from that described in the previous section (recall that the optimal shift decreased as the number of Arnoldi vectors were increased) and illustrates the difficulties associated with predicting the behaviour of the optimal shift.

Whether there was a significant predictable change in the optimal shift due to a modification of the model dispersivity may be addressed using the information contained in Figure 3.8. The figure shows that when large numbers of Arnoldi vectors ($\geq$ 20) are utilized the optimal shift decreases as dispersivity increases. In this case the change in the optimal shift (i.e., at each set of Arnoldi vectors, the optimal shift for $\alpha_L = 0.01\ m$ minus the optimal shift for $\alpha_L = 0.02\ m$) ranged from approximately 4.0 at 20 Arnoldi vectors to approximately 4.7 at 30 Arnoldi vectors. Beyond 30 Arnoldi vectors, the maximum change increases significantly, due to the apparent convergence of the optimal shift associated with the $\alpha_L = 0.01$ m model. When less than 20 Arnoldi vectors are utilized no patterns can be discerned since only minor changes occur in the optimal shift as the model dispersivity varies. For

example, when 5 Arnoldi vectors are utilized no change in the optimal shift is observed and little change (approximately 1.2) is observed when 15 Arnoldi vectors are utilized. Whether this behaviour can be generalized cannot be determined due to the limited number of simulations performed.

The effect of the optimal shift on the numerical solution is illustrated in Figure 3.9 which shows plots of the $RMSE_{opt}$ and $RMSE_0$ versus the number of Arnoldi vectors utilized. As seen in the previous section, the use of the optimal shift results in significant improvements in the numerical solution, with the greatest gains occurring when small number of Arnoldi vectors are utilized. Table 3.6, summarizes the results for the case $\alpha_L = 0.01$ m. The table shows that for small numbers of Arnoldi vectors (less than 15) the accuracy of the numerical solution can be improved by over 64 %. At convergence when larger numbers of Arnoldi vectors are utilized, improvements in the numerical solution of approximately 30 % are possible. It should be noted that Figure 3.9 shows that as the dispersivity increases a general decline in the improvement in the solution obtained from the use of the optimal shift occurs.

3.3.1.3 Two-Dimensional Model

For most practical problems involving mass transport in hydrogeologic systems two- or three-dimensional forms of the ADE are commonly applied. As a result, any numerical scheme intended for practical use should be evaluated in two-dimensional space. Evaluation of numerical methodologies in two-dimensional space has been performed by several researchers [Huyakorn et al., 1984; Frind and Hokkanen, 1987; Belgin, 1988; Sudicky, 1989; Woodbury et al., 1990; Farrell et al., 1997; cf. Chapter 2]. Following these examples, two-

dimensional models were used to evaluate the improved performance gained from the use of the optimal shift.

The problem domain (see Figure 3.10) was similar to that used by Sudicky [1989, Figure 1] and Farrell et al. [1997, Figure 6; cf. Chapter 2, Figure 2.6]. The domain was rectangular with length, $L_x = 30\ m$ and width, $L_z = 2\ m$. On the upstream boundary a Dirichlet boundary condition was imposed for the solute concentration such that $c = c_o$ for $0 \leq z \leq 0.5\ m$ and $c = 0$ for $z > 0.5\ m$, while on all other boundaries zero flux boundaries were imposed. The initial condition imposed was $c(x, z, t = 0) = 0$. The hydraulic conductivity of the domain is treated as deterministic and homogeneous, and groundwater flow was restricted to a direction parallel to the x-axis. The magnitude of the groundwater velocity was $v = v_x = 0.1\ m/day$. The longitudinal and transverse dispersivities as well as the coefficient of molecular diffusion were specified to be $\alpha_L = 0.05\ m$, $\alpha_T = 0.005\ m$ and $D^* = 4.3x10^{-5}\ m^2/day$ respectively. A summary of these parameters is provided in Table 2.3 of Chapter 2. Note that since the longitudinal dispersivity parallels the mean flow direction, off diagonal terms in the dispersion tensor were ignored.

For this analysis, two discretizations of the domain were considered. One discretization consisted of $\Delta x = \Delta z = 0.1\ m$, while for the other $\Delta x = 1.0\ m$ and $\Delta z = 0.1\ m$. These discretizations resulted in 12000 (refined mesh; 6321 nodes) and 1200 (coarse mesh; 651 nodes) triangular elements and produce Pe_x values of 1.98 and 19.8 respectively. In these simulations the Courant number was maintained at one. Again the reader is referred to Table 2.3 of Chapter 2 for a summary of these parameters. The simulations considered involved generating numerical solutions to the posed boundary value problem at early (t_1 = 50 days)

and later time (t_2 = 150 days). Of particular interest were the optimal shift and $RMSE_{opt}$ associated with various numbers of Arnoldi vectors and the improvement in the numerical solution. Since the solution at two times was sought, a time dependence of the optimal shift was investigated.

Plots of the RMSE versus shift for the coarse and refined meshes at 50 and 150 days are shown in Figure 3.11 for the interval $-1 \leq \sigma \leq 0$. Figure 3.11b shows that within this interval, the 150 day simulation on the refined mesh displays all of the features previously described in the analyses of models #1 and #2. Over the same interval, a similar plot for the 50 day simulation on the refined mesh (Figure 3.11a) is dominated by small shift behaviours, i.e. linearity over the interval. A more in-depth analysis shows that the slopes of the linear sections of the plots differ, with the magnitude of the slope appearing to increase with increasing simulation time. This is exemplified by the -0.03 slope computed for the 50 day simulation and the -0.05 slope computed for the 150 days simulation (see Table 3.7). This indicates a possible time dependence of the RMSE versus shift relationship. Plots of the RMSE versus shift for the simulations on the coarse mesh (Figures 3.11c and 3.11d) also appear to be dominated by small shift behaviours over the interval $-1 \leq \sigma \leq 0$. Estimates of the slopes of the linear sections of these plots are -0.53 for the 50 day simulation and -0.88 for the 150 day simulation (see Table 3.7). These appear to support the assertion of a time dependence of the RMSE versus shift relationship. It is also noteworthy to point out, that as in the analysis of model #1, an increase in the mesh discretization results in a reduction of the magnitude of the slope of the linear section of the RMSE versus shift relationship (see Table 3.7), i.e. the RMSE became less sensitive to changes in the shift.

Plots of the optimal shift versus the number of Arnoldi vectors utilized are shown in Figure 3.12. The plots reiterate the point that when few Arnoldi vectors are utilized the optimal shift tends to be both highly variable and unpredictable (see also Table 3.8). However, as the number of Arnoldi vectors increase, the optimal shift tends toward convergence. Table 3.8 illustrates this tendency for the 50 days simulation on the refined mesh.

Other comparisons can be made based on Figure 3.12. The figure shows that as the grid discretization increases (i.e, the grid spacing reduced), the optimal shift associated with given numbers of Arnoldi vectors decreases. Further, as the simulation time increases, the magnitude of the optimal shift for a given number of Arnoldi vectors appears to converge. This tendency is further illustrated in Figure 3.13 which shows a plot of the optimal shift versus simulation time for 20 Arnoldi vectors. The reader should recall that as the simulation time increases the concentration gradients at the solute front are reduced. As a result, fewer numbers of Arnoldi vectors are required for convergence of the numerical solution. Hence, the optimal shift associated with a given number of Arnoldi vectors should also converge.

The improvement in the numerical solution gained from the use of the optimal shift is presented in Figure 3.14. In general, the figure reiterates the earlier findings which showed that the most substantial improvements in the numerical solution occur when few Arnoldi vectors are utilized. A comparison of the results reveals that as the simulation time increases, the percentage improvement in the numerical solution gained from the use of the optimal shift decreases. To demonstrate this consider the solution on the refined mesh. When 5 Arnoldi vectors are used the improvement in the solution from the use of the optimal shift is -71 % at 50 days and -23 % at 150 days. Similar results were also obtained at all other numbers of

Arnoldi vectors considered. This general result is independent of the number of Arnoldi vectors utilized and the mesh discretization considered. It therefore suggests that for practical problems involving transport over long periods of time, determination and use of the optimal shift may not always be required.

3.4 Eigenvalue Analysis

In the previous sections the accuracy of the shift-AMRM method was examined for various one- and two-dimensional problems. The analysis produced several observations which required further explanation. The discussion in this section attempts to these observations through an eigenvalue analysis. This approach is chosen since the solution of the problem is controlled by the eigenvalues of the system. The more accurate the approximation of these eigenvalues (particularly the smaller eigenvalues) the more accurate the solution to the problem. Since the eigenvalues associated with the upper Hessenberg matrix, $\boldsymbol{H}$, approximate those contained in the outer spectrum of the $\boldsymbol{K}_e^{-1}\boldsymbol{M}$, this analysis focuses on $\boldsymbol{H}$. Note that the *"shift and invert"* strategy described by (3.5b) is employed in order to obtain the eigenvalues of the generalized eigenvalue problem, $\boldsymbol{M}^{-1}\boldsymbol{K}$. The eigenvalues associated with $\boldsymbol{H}$ are computed using the QR algorithm [Press et al.,1989].

As a starting point in this analysis, the solutions on the 1600 element mesh described in model #1 are considered. Figure 3.15a shows the inverse of the eigenvalues estimated directly from $\boldsymbol{H}$ (i.e., $1/\mu_j=\lambda_j-\sigma$), whereas Figure 3.15b shows the eigenvalues for the posed problem (i.e., those associated with $\boldsymbol{M}^{-1}\boldsymbol{K}$). Due to the advection present in the system the eigenvalues for this problem are complex valued and distributed symmetrically about the

positive real axis (see Figure 3.15b). Note that for purely diffusive mass transport problems the eigenvalues are distributed along the real axis (i.e, the imaginary components are zero). In addition, the magnitudes of the computed eigenvalues are generally found to be less than one. Further, it should be noted that as the number of Arnoldi vectors utilized increases the gap between the largest and smallest eigenvalues also increases (see Figure 3.15b). Within the eigenvalue spectrum an intense clustering of the eigenvalues generally occurs at the low end of the spectrum resulting in a non-uniform distribution. Figure 3.15b also ahows that under optimal shifting the eigenvalues estimated based on the various numbers of Arnoldi vectors converge. These observations are reiterated by Figure 3.15c which shows plots of the magnitude of the eigenvalues versus the positive phase angle for the various simulations.

The impact of shifting on the computed eigenvalues is illustrated in Figure 3.16. The inverse of the eigenvalues estimated directly from $\boldsymbol{H}$ are presented (Figure 3.16a), as well as the eigenvalues associated with $\boldsymbol{M}^{-1}\boldsymbol{K}$ (Figure 3.16b). In the figures the estimates displayed are based on shifts of $\sigma = 0$, optimal, -0.1, -0.2, -0.3 and -0.4; note that 35 Arnoldi vectors are used to solve the posed problem. Recall from Figure 3.1d, that the -0.1 and -0.2 values of shift correlate to the small shift behaviour, the -0.3 value correlates to the transition between the small and large shift behaviours, and the -0.4 value correlates to the large shift behaviour. Assuming that the eigenvalues associated with the optimal shift provide the best representation of the eigenvalues which control the system, then it is apparent that the eigenvalues estimated by shifts less than -0.3 are those which exert minimal control on the solution (i.e., the larger eigenvalues). This is bourne out by the poor results obtained when a shift of -0.4 is applied.

In the following sequel the impacts of the reduced resolution are examined. The magnitude and phase of the complex eigenvalues are related according to

$$|Z| = \sqrt{a^2 + b^2} \tag{3.20a}$$

$$\tan\varphi = \frac{b}{a} \tag{3.20b}$$

where $Z=a+ib$, and φ represents the phase of the eigenvalues. Plot of these quantities for the various shifts considered are shown in Figure 3.16c. The figure shows that for shifts between -0.2 and 0 (i.e., the linear portion of Figure 3.1d) only changes in the magnitude of the eigenvalues are apparent. Thus the small shift behaviour appears to be due to small changes in the magnitude of the eigenvalues. At shifts in the range -0.3 to -0.4 significant changes in both the magnitude and phase of the eigenvalues are observed. These changes indicate that the larger eigenvalues are dominating the solution. The impacts of these changes on the numerical solution are shown in Figure 3.17. The solution shows that when the larger eigenvalues in the solution are resolved at the expense of the smaller eigenvalues large oscillations are produced in the numerical solutions. These large oscillations render the numerical solution meaningless for modelling purposes.

3.5 Discussion and Conclusions

In this work, a 'shift' variant of the Arnoldi algorithm is introduced and its performance analyzed. Here the primary objective of shifting is to improve the approximation of the eigenvalues of the system and hence improve the convergence of the numerical solution. The shift Arnoldi algorithm is similar to the standard Arnoldi algorithm which

reduces the finite element matrix differential equation of size n to a much smaller system of size m by means of orthogonal matrix transformations. The smaller system consists of a new capacity matrix H which is upper Hessenberg in form, and a conductivity matrix $(I-\sigma H)$. Note that when $\sigma = 0$, the eigenvalues of H approximate those of the original problem. The smaller system of equations is then solved using a suitable time stepping procedure such as the Crank-Nicolson algorithm. The solution at the desired time is then inverted back into the original space using a linear transform. An operations count performed on the algorithm shows that it is as computationally efficient as the standard Arnoldi algorithm. This implies that significant cost saving can be achieved by using this method in place of more traditional methods [Farrell et al., 1997; cf. Chapter 2].

The primary focus of this work, was an evaluation of the performance of the shift AMRM approach for solving the system of equations which result from the FE method was evaluated. The evaluation problems consisted of simple one- and two-dimensional models for which analytic solutions were available. Since a priori information regarding the effects of shifting on the numerical solution of the selected problems was not available, numerous shifts were considered. The consideration of many shifts resulted in several interesting conclusions. However, the most general conclusion obtained was that some shifts improved the numerical solution while others produced degraded solutions. Hence, the choice of shift is extremely important.

Of the many shifts considered, the most important shift is the optimal shift. This is defined as the shift which minimized the RMSE. This minimization occurs since the optimal shift effectively provides the best estimation of the true eigenvalues of the system. In general,

use of the optimal shift was found to both improve the absolute convergence of the numerical solution as well as increase the rate of convergence. However, efficient estimation of the optimal shift is a difficult task and forms the basis of current and future research.

The causes of degraded solutions in the numerical procedure were investigated as part of this work. On the basis of an eigenvalue analysis, it was concluded that degradation occurred when shifting resulted in poor approximation of the eigenvalues of the system. Two aspects of the degradation process were identified; that due to magnitude effects and that due to phase effects. In general, small real shifts away from the optimal shift were found to increase the magnitudes of the eigenvalues without significantly increasing their phases. By contrast, in addition to increasing the magnitude of the eigenvalues, large real shifts also resulted in phase increases. As a result, knowledge of the effects of shifting on the numerical solution is important.

The ultimate aim of this work was to examine whether the shift-AMRM approach can be applied to problems commonly modelled in hydrogeology. As a result, the impact of several, common and potential, model calibration procedures on the optimal shift were investigated. These included, choice of the number of Arnoldi vectors, mesh refinement, dispersivity uncertainty and simulation time. The results showed that each of these impacts influenced the optimal shift in ways which were not always predictable. As a result, for each new calibration run a new optimal shift must be estimated. Therefore, unless efficiently automated, the estimation process can be computationally expensive and time consuming, thus making the approach inefficient for practical use.

References

Bear, J., Dynamics of Fluids in Porous Media, Elsevier, New York, 1992.

Beljin, M., Testing and validation of models for simulating solute transport in groundwater: Code intercomparison and evaluation of validation methodology, I.G.W.M.C., GWMI 88 - 11, 1988.

Bhuiyan, M. A., R. I. Allayla, T. Hussain, A. M. Ishaq, and M. F. N. Mohsen, Solutions of the transport equation by collocation method in conjunction with the adaptive hermite element family, Water Resour. Res., 26(11), 2661 - 2677, 1990.

Brebbia, C. A., and P. Skerit, Convection problems using boundary elements, in Proceedings of the 5th International Conference on Finite Elements in Water Resources, edited by J. P. Laible, C. A. Brebbia, W. Gray, and G. Pinder, pp. 747 - 768, Springer-Verlag, New York, 1984.

Cady, R., and S. P. Neuman, Advection-dispersion with adaptive Eulerian-Lagrangian finite elements, in Advances in Transport Phenomena in Porous Media, edited by J. Bear and M. Y. Corupcioglu, pp. 923 - 951, North-Holland, New York, 1987.

Celia, M. A., and W. G. Gray, Numerical Methods for Differential Equations: Fundamental Concepts for Scientific and Engineering Applications, Prentice Hall, Englewood Cliffs, New Jersey, 436 pp., 1992.

Daus, A. D., E. O. Frind, and E. A. Sudicky, Comparative error analysis in finite element formulations of the advection-dispersion equation, Adv. Water Resour., 8, 86 - 95, 1983.

Ericsson, T., and A. Ruhe, The spectral transformation Lanczos method for the numerical solution of large sparse generalized eigenvalue problems, Math. Comput., 35(152), 1251-1268, 1980.

Farrell, D. A., A. D. Woodbury, and E. A. Sudicky, Numerical modelling of mass transport in hydrogeologic environments: Performance comparison of the LTG and Arnoldi solution schemes, in submission of to Advances in Water Resources, July, 1995.

Frind, E. O., and G. E. Hokkanen, Simulation of the Borden plume using the alternating direction Galerkin technique, Water Resour. Res., 23(5), 918 - 930, 1987.

Freeze, R. A., and J. A. Cherry, Groundwater, Prentice Hall, Englewood Cliffs, New Jersey, U.S.A., 1979.

Frind, E. O., and G. E. Hokkanen, Simulation of the Borden plume using the Alternating Direction Galerkin technique, Water Resour. Res., 23(5), 918 - 930, 1987.

Hunter, J. R., P. D. Craig, and H. E. Phillips, On the use of random walk models with spatially variable diffusivity, Jour. Comput. Phys., 106, 366 - 379, 1993.

Huyakorn, P. S., A. G. Kretschek, R. W. Broome, J. W. Mercer, and B. H. Lester, Testing and validation of models for simulating solute transport in groundwater, HRI Rep. 35, Holcomb Res. Inst., Indianapolis, Ind., 1984.

Huyakorn, P. S., and G. F. Pinder, Computational Methods in Subsurface Flow, Academic Press, Inc. (London) LTD., 473 pp., 1983.

Hwang, J. C., W. C. Cho, and G. T. Yeh, An eigenvalue solution continuous in time to the spatially discretized solute transport equation in steady groundwater flow, Water Resour. Res., 20, 1725 - 1732, 1984.

Konikow, L. F., and J. D. Bredehoeft, modelling flow and chemical quality changes in an irrigated stream aquifer system, Water Resour. Res., 10, 546 - 562, 1974.

Konikow, L. F., and J. D. Bredehoeft, Computer model of 2-dimensional solute transport and dispersion in groundwater, in USGS TEchniques of Water Resources Investigations, book 7, chap. C2, U.S. Geological Survey, Reston, Va., 1978.

Kuiper, L. K., Analytical solution of spatially discretized groundwater flow equations, Water Resour. Res., 9(4), 1094 - 1097, 1973.

Loaiciga, H., and M. Marino, The inverse problem for confined aquifer flow: Identification and estimations with extensions, Water Resour. Res., 23, 92 -104, 1987.

McCormick, S. T., Multigrid methods, in Frontiers in Applied Mathematics, vol. 3, pp. 15 - 25, Society of Industrial and Applied Mathematics, Philadelphia, Pa., 1989.

Nayar, N., and J. Ortega, Computation of selected eigenvalues of generalized eigenvalue problems, J. Comput. Phys., 108, 8 - 14, 1993.

Neuman, S. P., Adaptive Eulerian-Lagrangian finite element method for advection-dispersion, Inst. J. Numer. Methods Eng., 20, 309 - 323, 1984.

Nour-Omid, B., W. S. Dunbar, and A. D. Woodbury, Lnaczos and Arnoldi methods for solution of convection-diffusion equations, Comput. Methods Appl. Mech. Eng., 88, 75 - 91, 1991.

Ogata, A., Theory of dispersion in a granular medium, U. S. Geol. Surv. Prof. Paper 411 - I, 1970.

Press, W. H., B. P. Flannery, S. A. Teukolsky, W. T. Vetterling, Numerical Recipes in Fortran, The Art of Scientific Computing, Cambridge University Press, 1986

Prickett, T. A., T. A. Naymik, and C. G. Lonnquist, A random-walk solute transport model for selected water quality evaluations, bulletin, Ill. State Water Surv., Champaign, 1981.

Sahuquillo, A., An eigenvalue numerical technique for solving unsteady linear groundwater models continuously in time, Water Resour. Res., 19(1), 87 - 93, 1983.

Schmid, G., and D. Braess, Comparison of fast solvers for ground-water flow problems, in Groundwater Flow and Quality Modeling, edited by E. Custodio et al., pp. 173 - 188, D. Reidel, Hingham, Mass., 1988.

Sudicky, E. A., The Laplace Transform Galerkin technique: A time-continuous finite element theory and application to mass transport in groundwater, Water Resour. Res., 25(8), 1833 - 1846, 1989.

Tompson, A. F. B., and L. W. Gelhar, Numerical simulation of solute transport in three-dimensional, randomly heterogeneous porous media, Water Resour. Res., 26(10), 2541 - 2562, 1990.

Umari, A. M. J., and S. M. Gorelick, The problem of complex eigensystems in the semianalytical solution for the advancement of time in solute transport simulations: A new method using rea arithmetic, Water Resour. Res., 22(7), 1149 - 1154, 1986.

Wolfsberg, A. V., and D. L. Freyberg, Efficient simulation of single species and multispecies transport in groundwater with local adaptive grid refinement, Water Resour. Res., 30(11), 2979 - 2991, 1994.

Woodbury, A. D., W. S. Dunbar, and B. Nour-Omid, Application of the Arnoldi algorithm to the solution of the advection-dispersion equation, Water Resour. Res., 26(10), 2579 - 2590, 1990.

Yeh, G. T., A Lagrangian-Eulerian method with zoomable hidden fine-mesh approach to solving advection-dispersion equations, Water Resour. Res., 26(6), 1133 - 1144, 1990.

Yu, Y. S., M. Heidari, and W. T. Wang, A semi-analytical method for solving unsteady flow equations, paper presented at Proceedings ASCE National Conference on Hydraulic Eng., Am. Soc. Civ. Eng., Williamsburg, Va., Aug. 3 - 7, 1987.

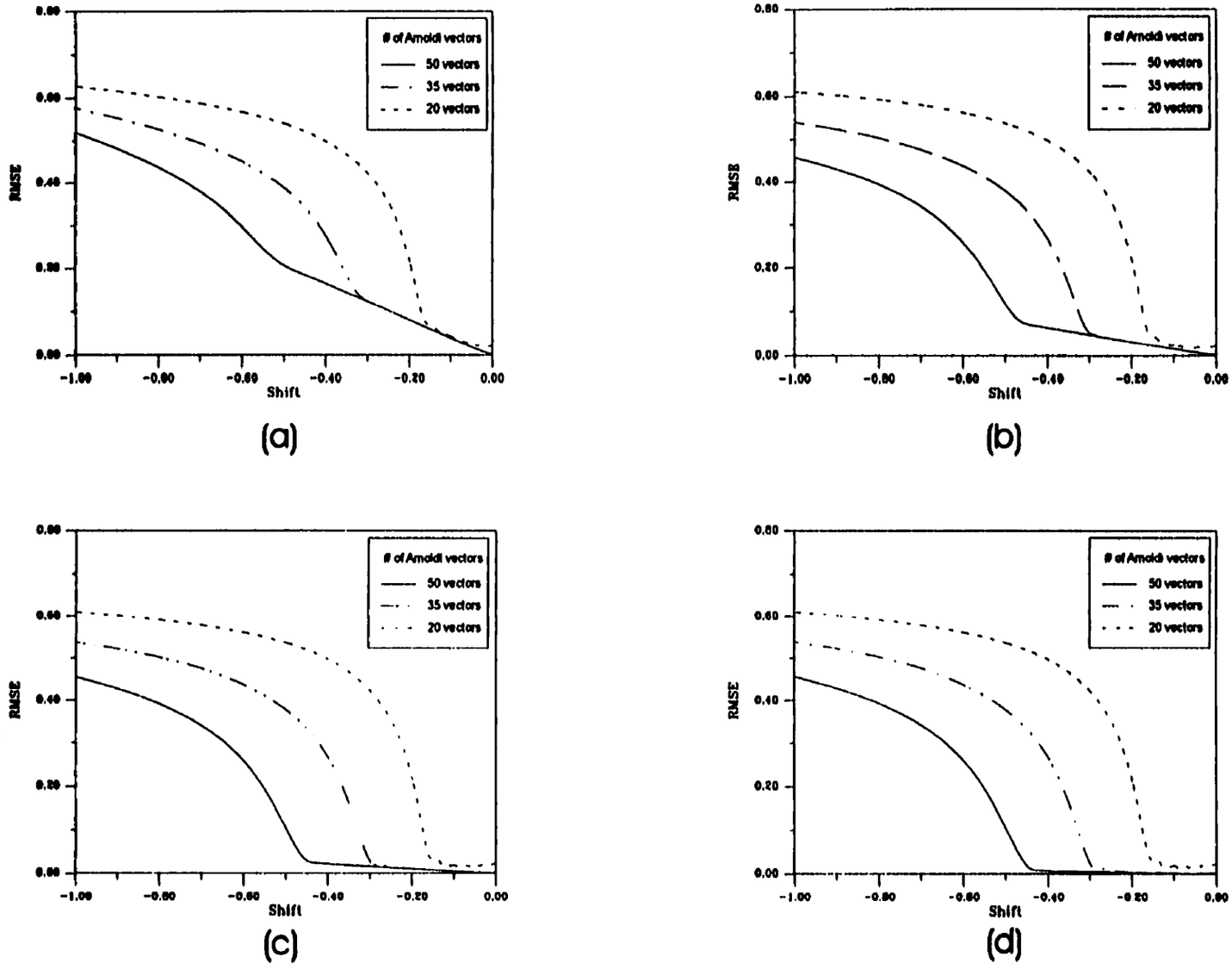

Figure 3.1: Simulation results for model #1: RMSE versus shift (a) 200 elements; (b) 400 elements; (c) 800 elements; and (d) 1600 elements.

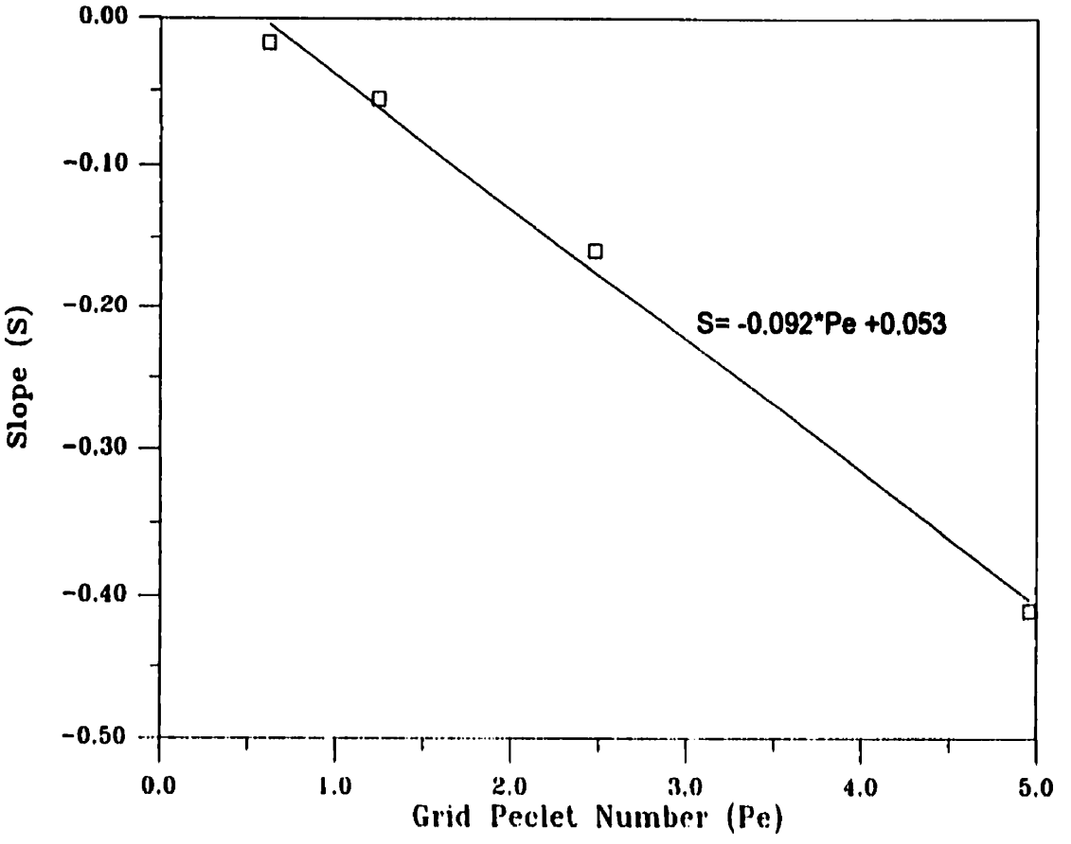

Figure 3.2: Simulation results for model #1: Slope *(of linear part of RMSE versus shift plot)* versus grid Peclet number.

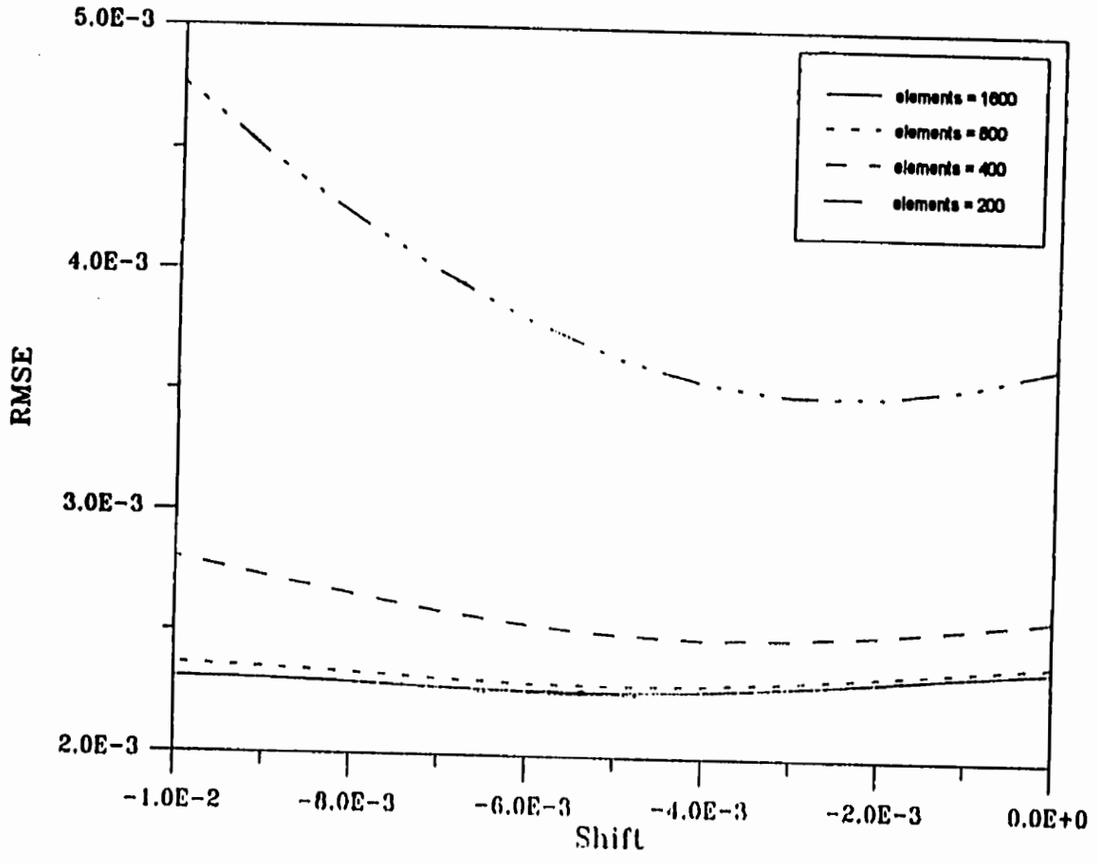

Figure 3.3: Simulation results for model #1: RMSE versus shift over the interval $-1.0\times10^{-2} \le \sigma \le 0$ for the various mesh discretizations when 35 Arnoldi vectors are utilized.

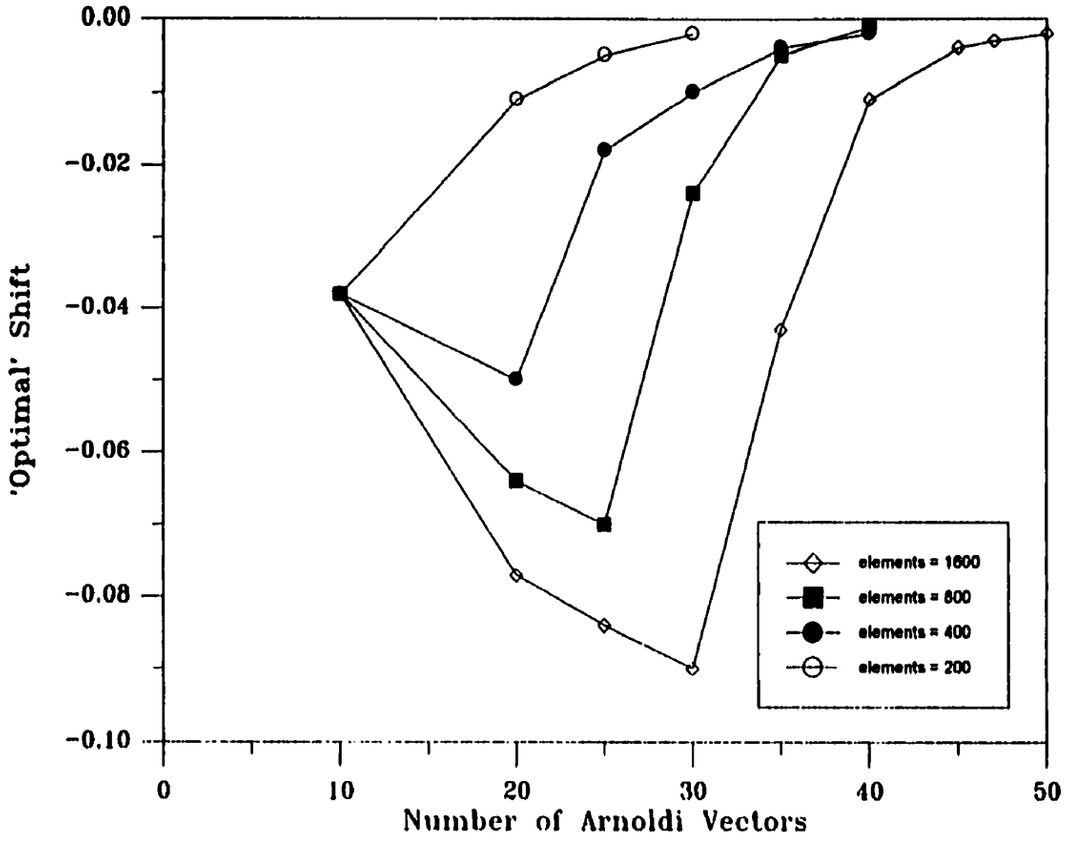

Figure 3.4: Simulation results for model #1: Optimal shift versus the number of Arnoldi vectors utilized for the various mesh discretizations.

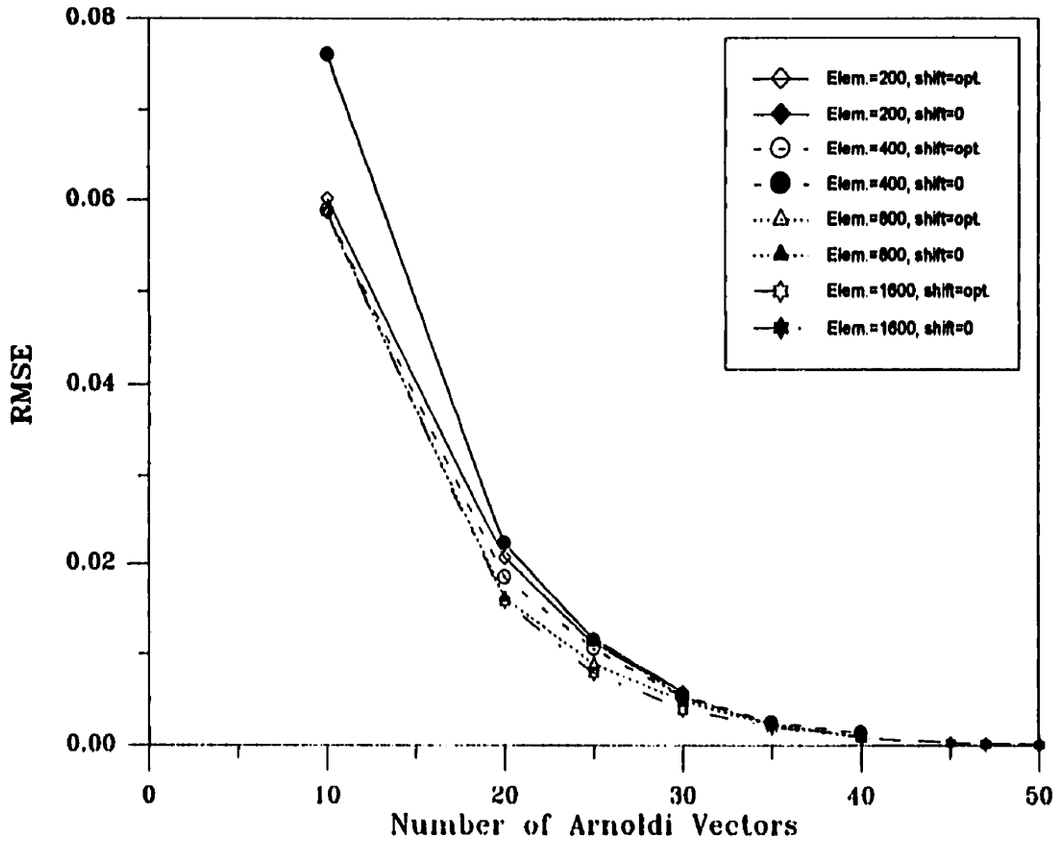

Figure 3.5: Simulation results for model #1: Comparison of the RMSE versus the number of Arnoldi vectors for the cases $\sigma = 0$ and $\sigma =$ optimum.

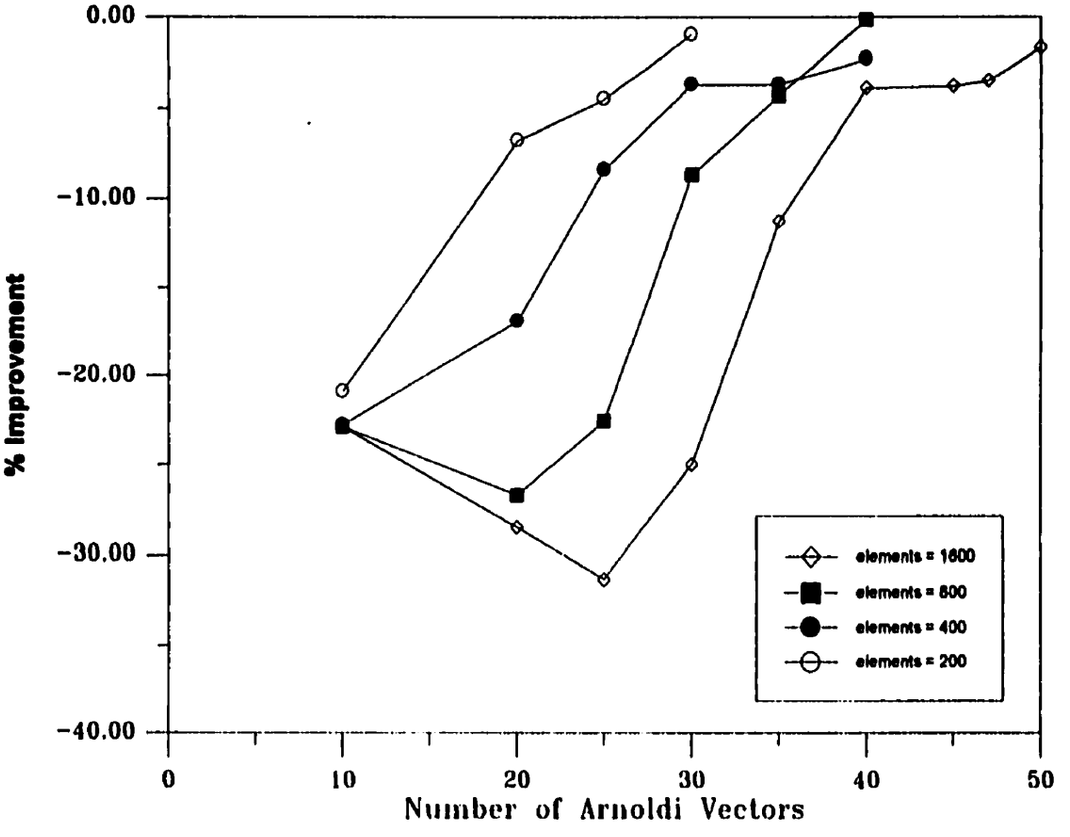

Figure 3.6: Simulation results for model #1: Comparison of the percentage improvements in the numerical solution under various discretizations due to the optimal shift versus the number of Arnoldi vectors utilized.

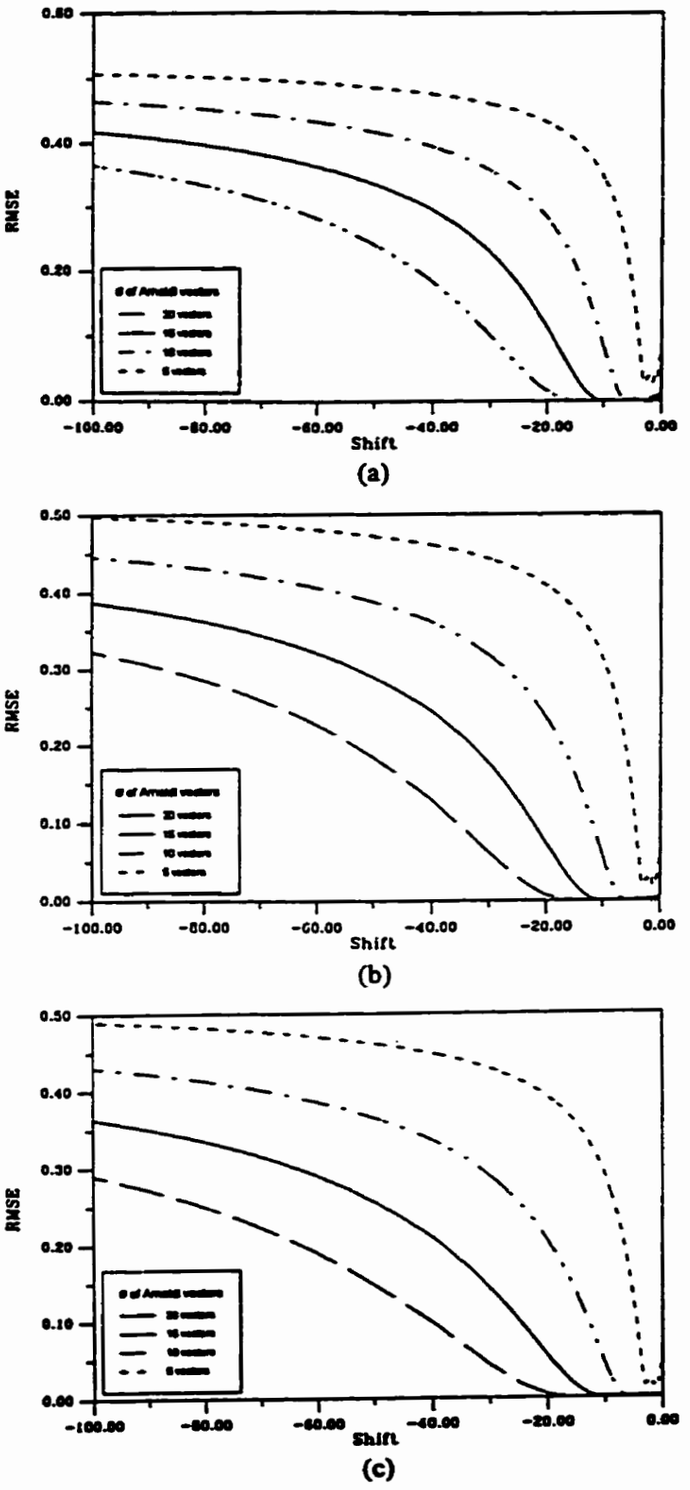

Figure 3.7: Simulation results for model #2: RMSE versus shift (a) $\alpha_L = 0.010$ m; (b)$\alpha_L = 0.015$ m; (c) $\alpha_L = 0.020$ m.

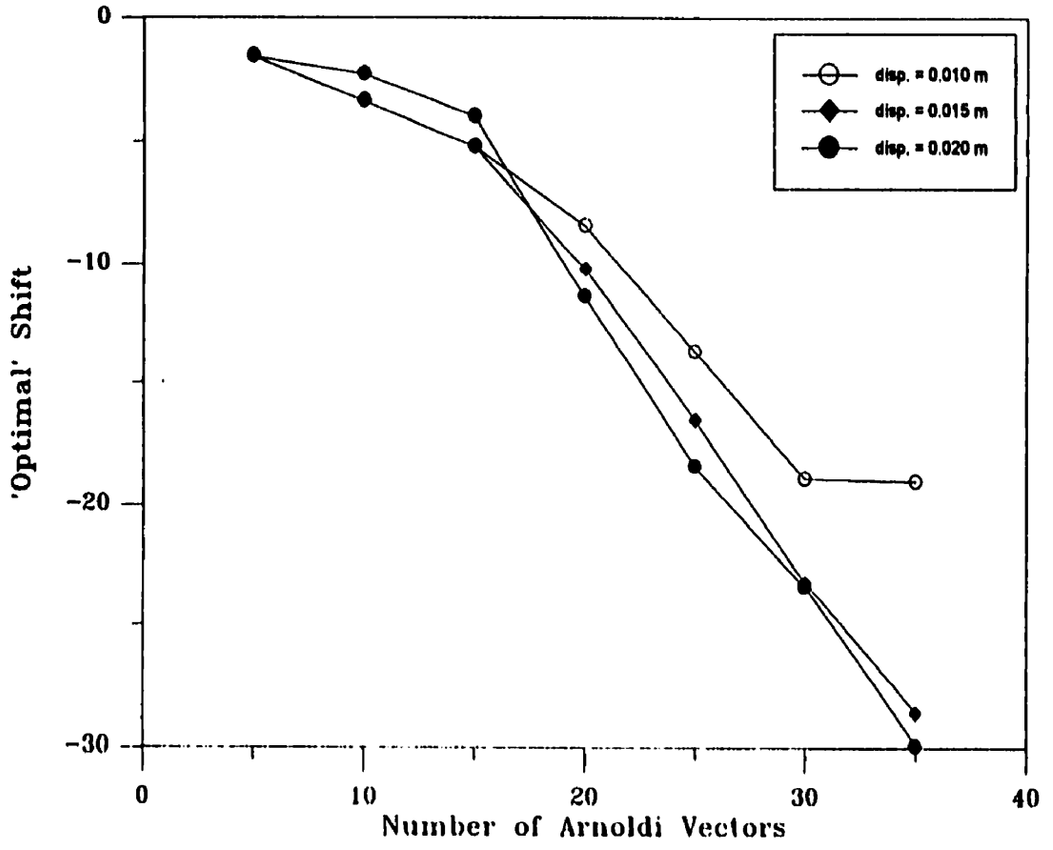

Figure 3.8: Simulation results for model #2: Optimal shift versus the number of Arnoldi vectors utilized for the various dispersivities considered.

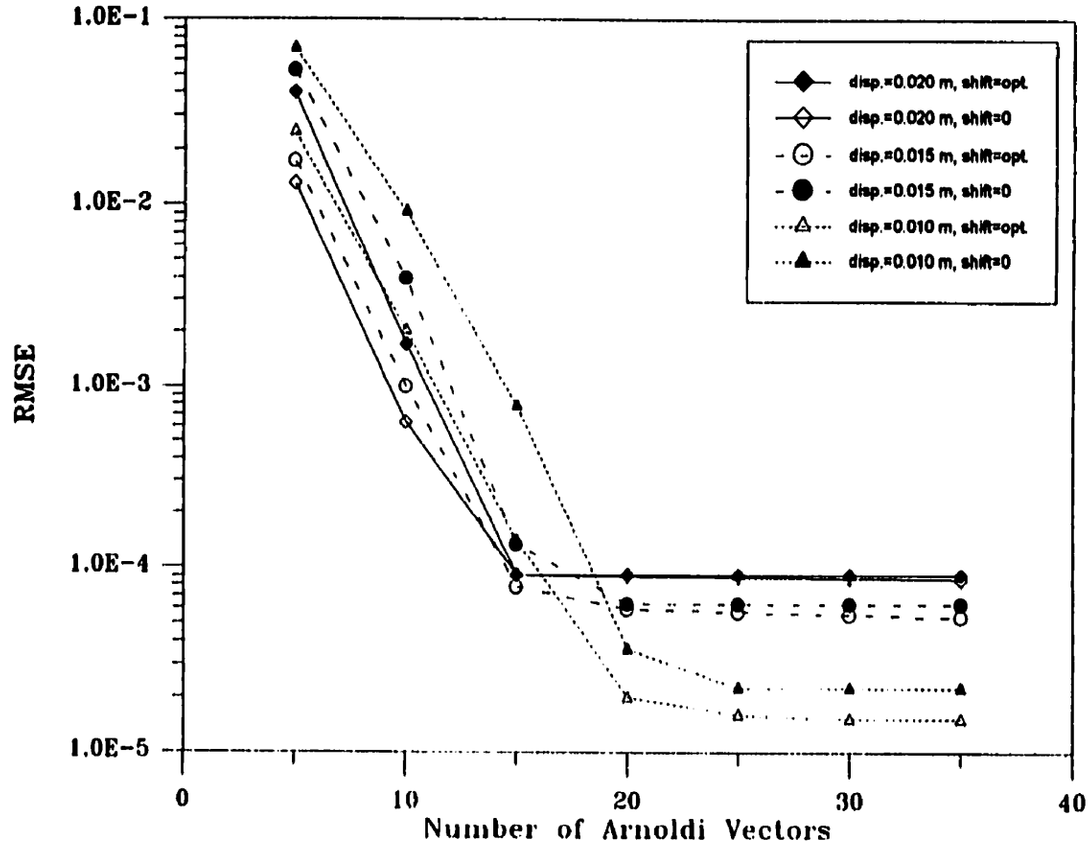

Figure 3.9: Simulation results for model #2: Comparison of the RMSE versus the number of Arnoldi vectors for the cases $\sigma = 0$ and σ = optimum.

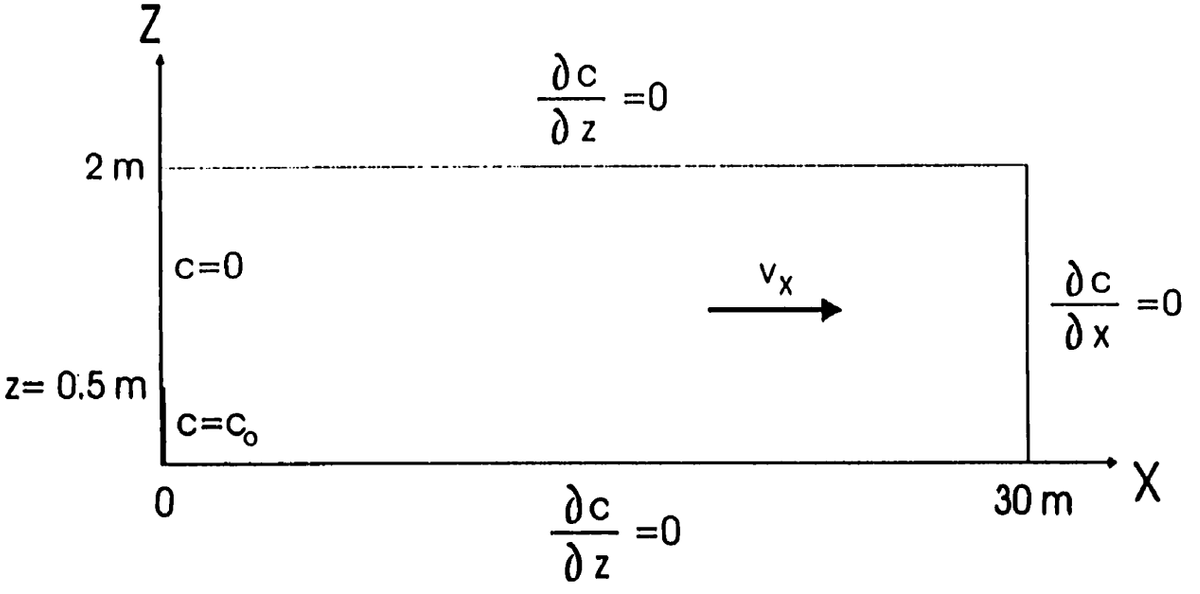

Figure 3.10: Schematic of two-dimensional domain.

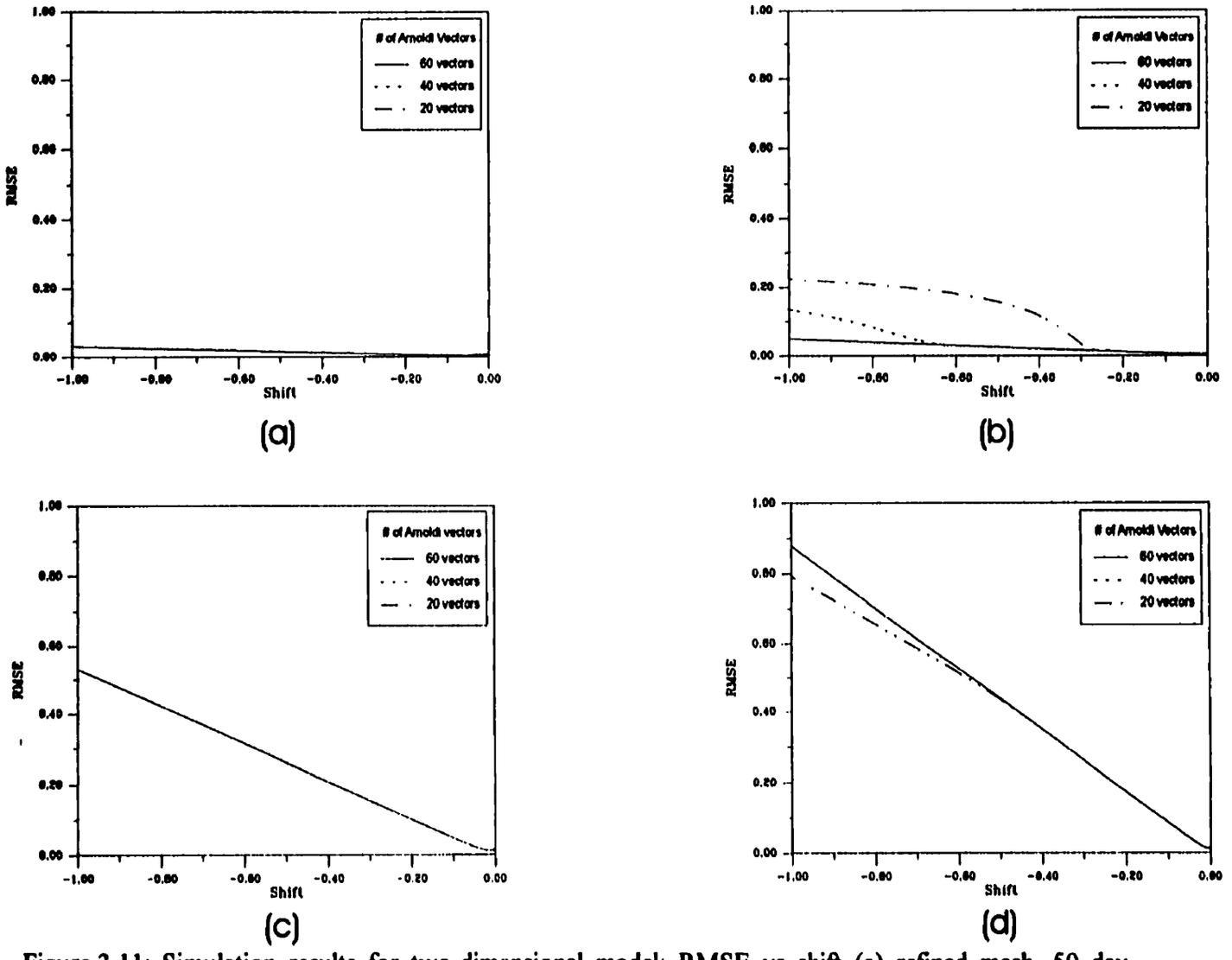

Figure 3.11: Simulation results for two-dimensional model: RMSE vs shift (a) refined mesh, 50 day simulation; (b) refined mesh, 150 day simulation; (c) coarse mesh, 50 day simulation; (d) coarse mesh, 150 day simulation.

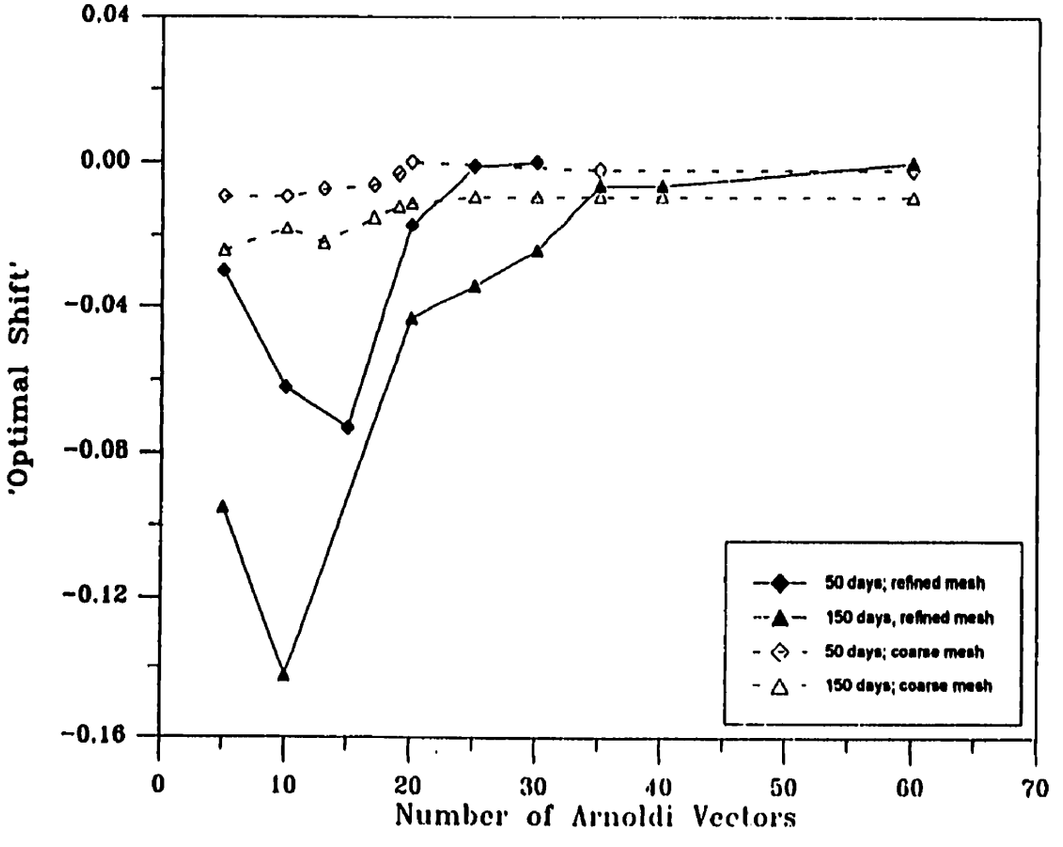

Figure 3.12: Simulation results for two-dimensional model: Optimal shift versus the number of Arnoldi vectors for the simulations performed.

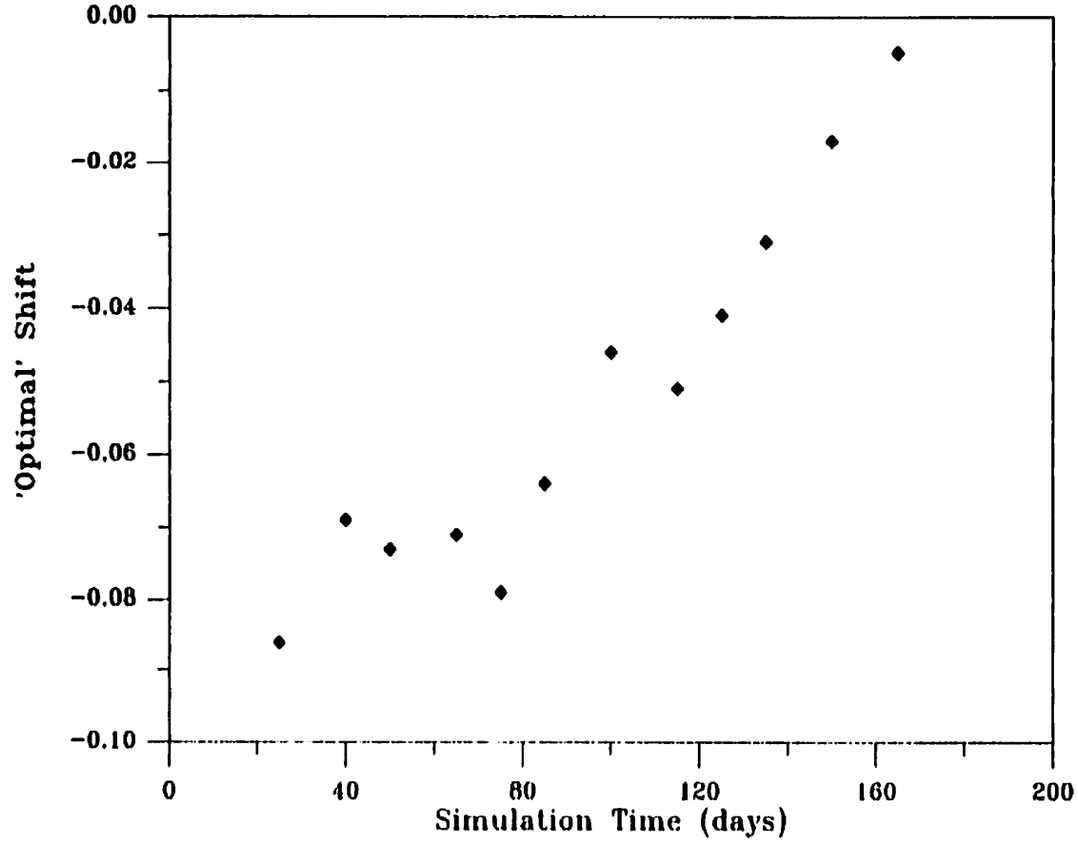

Figure 3.13: Simulation results for two-dimensional model: Optimal shift versus simulation time for the 50 day simulation on the refined mesh (20 Arnoldi vectors utilized).

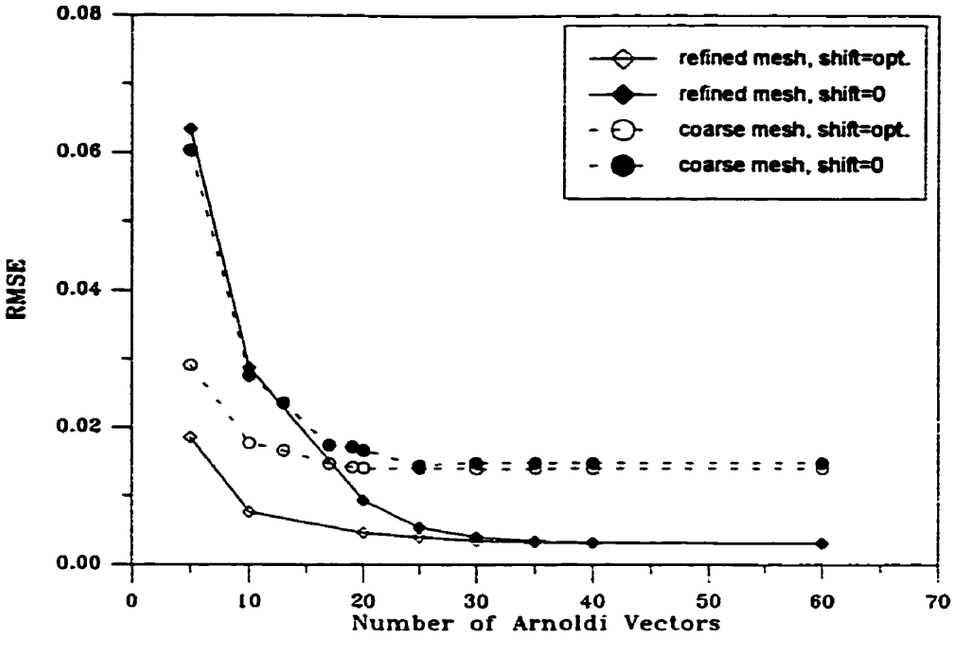

(a)

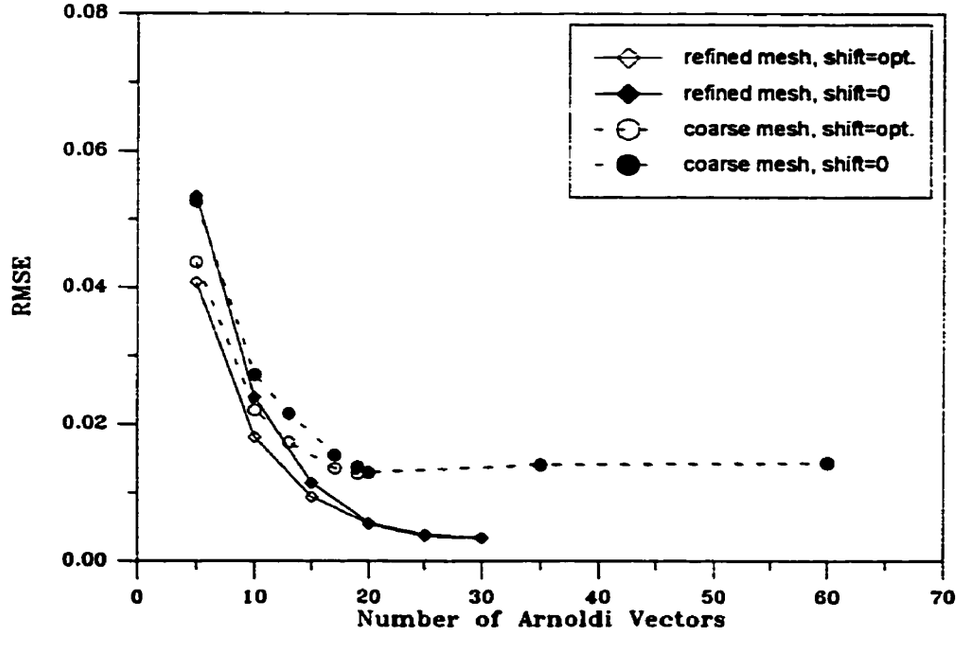

(b)

Figure 3.14: Simulation results for two-dimensional model: Comparison of the RMSE versus the number of Arnoldi vectors for the cases $\sigma = 0$ and $\sigma =$ optimum (a) 50 days; (b) 150 days.

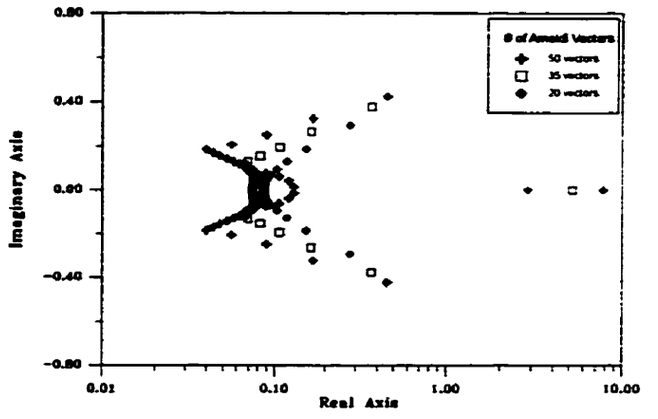

(a)

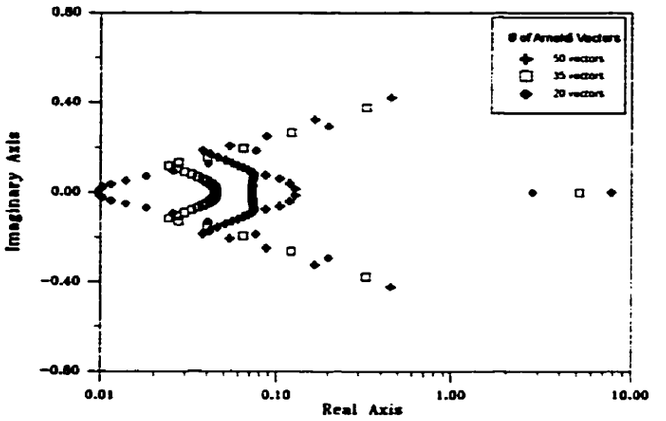

(b)

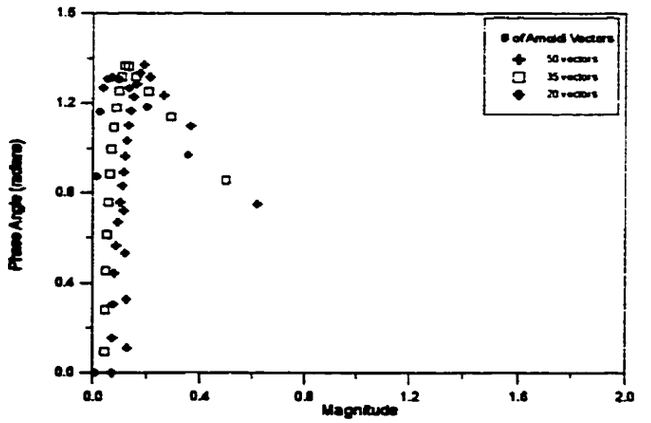

(c)

Figure 3.15: Distribution of the eigenvalues at the optimal shift for the 1600 element problem (a) Inverse of eigenvalues estimated directly from H; (b) Eigenvalues for posed problem ($M^{-1}K$); (c) Phase angle vs magnitude relationship for eigenvalues.

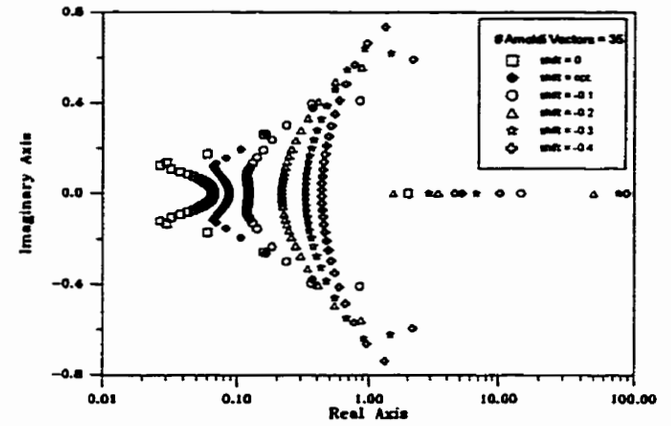

(a)

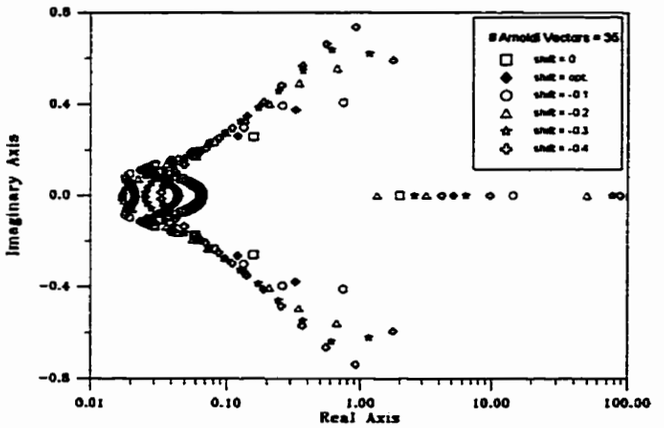

(b)

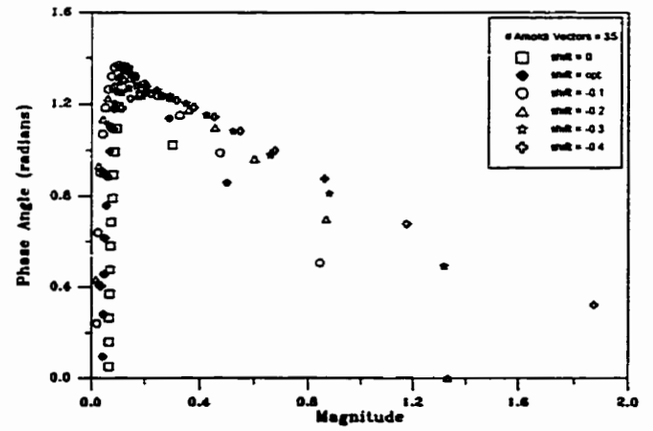

(c)

Figure 3.16: Eigenvalues computed under varying shifts for the 1600 element problem; (a) Inverse of eigenvalues estimated directly from H; (b) Eigenvalues for posed problem ($M^{-1}K$); (c) Phase angle vs magnitude relationship for eigenvalues.

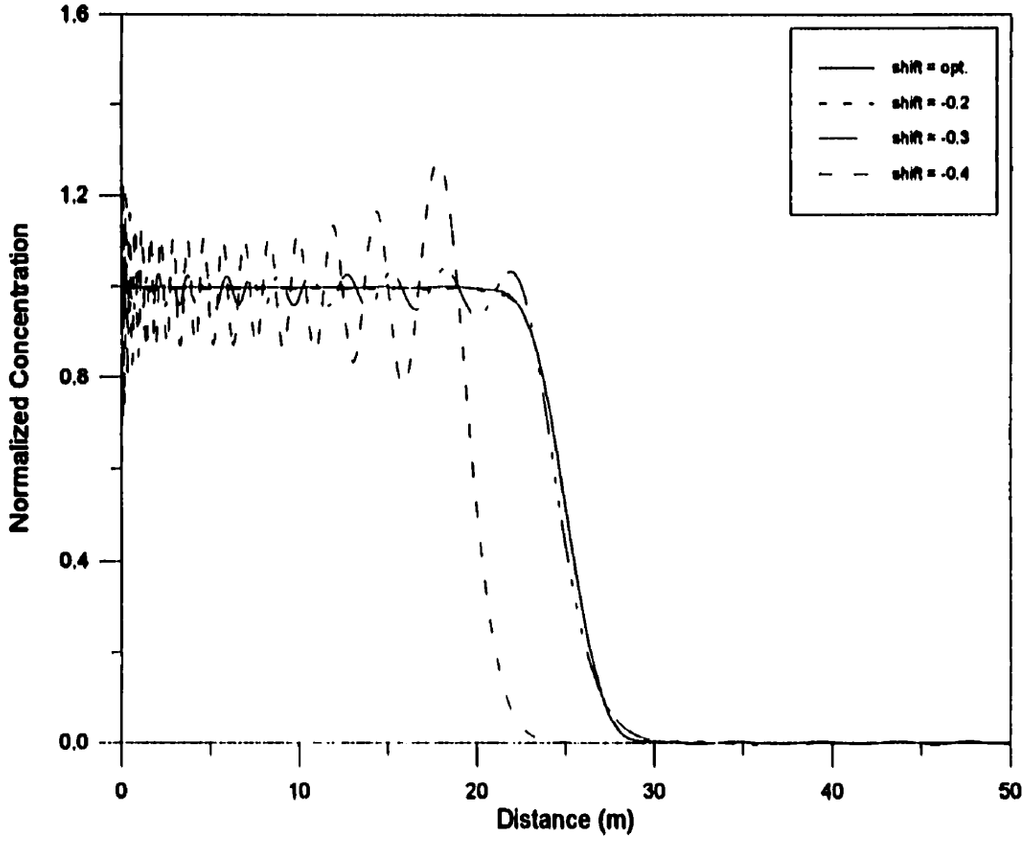

Figure 3.17: Concentration profiles computed for differing shifts for 1600 element model (35 Arnoldi vectors utilized).

Table 3.1
Operations Count for Shift-AMRM

Operation	Floating Point Operations	Totals
For every Arnoldi vector		
Re-solution	$2nn_b$	
Matrix vector multiplication	nn_b	
Inner or scalar-vector products	$5n$	
	$= n(2n_b + 5)$	
For m Arnoldi vectors		$mn(2n_b + 5)$
Solution of reduced system		
Decomposition of upper Hessenberg matrix		m
Matrix vector multiplication	m^2	
Scalar multiply and addition	$3m$	
Re-solution	m^2	
	$m(2m+3)$	
For NT time steps		$m(2m +3)NT +m$
Total		$mn(2n_b +5) +m(2m +3)NT +m$

Table 3.2a
Parameters Defining the Physical System for One-Dimensional Models
(Model #1)

System Length, L (m)	50
Groundwater Velocity, v (m/day)	0.1
Solution Time, t (days)	250
Longitudinal Dispersivity, α_L (m)	0.05
Molecular Diffusion Coefficient D^* (m^2/day)	4.3×10^{-5}

Table 3.2b
Parameters Defining the Physical System for One-Dimensional Models
(Model #2)

System Length, L (m)	0.9
Groundwater Velocity, v (m/day)	0.1
Solution Time, t (days)	3
Longitudinal Dispersivity, α_L (m)	0.01, 0.015, 0.02
Molecular Diffusion Coefficient D^* (m^2/day)	4.3×10^{-5}

Table 3.3
Summary of Domain Discretizations for Model #1

Mesh Discretization Δx (m)	Number of Elements	Grid Peclet Number
0.25000	200	4.94
0.12500	400	2.48
0.06250	800	1.24
0.03125	1600	0.62

Table 3.4
Results of Optimal Shift Analysis for Model #1
(number of elements = 1600)

Number of Arnoldi Vectors	Optimal Shift	Root Mean Square Error		Percentage Improvement
		Shift = optimal	Shift = 0.0	
10	-0.038	0.058624	0.076022	-22.9
20	-0.077	0.015925	0.022272	-28.5
25	-0.084	0.007955	0.011583	-31.3
30	-0.090	0.004028	0.005369	-25.0
35	-0.043	0.002102	0.002369	-11.3
40	-0.011	0.000907	0.000944	-3.9
45	-0.004	0.000356	0.000370	-3.8
47	-0.003	0.000251	0.000260	-3.5
50	-0.002	0.000169	0.000172	-1.7

% Improvement = $100*(RMSE_{optimal} - RMSE_0)/RMSE_0$

Table 3.5
Dispersivity-Slope Data for Model #2

Dispersivity (m)	Grid Peclet Number	Slope (RMSE vs Shift)
0.01	9.6×10^{-3}	4.9×10^{-7}
0.015	6.5×10^{-3}	3.3×10^{-7}
0.020	4.9×10^{-3}	1.9×10^{-7}

Table 3.6
Results of the Optimal Shift Analysis for Model #2
($\alpha_L = 0.01$ m)

Number of Arnoldi Vectors	Optimal Shift	RMSE		Percentage Improvement
		Shift = opt.	Shift = 0	
5	-1.6	0.0245740	0.0688399	-64.3
10	-3.4	0.0020354	0.0090952	-77.6
15	-5.2	0.0001394	0.0007766	-82.0
20	-8.4	0.0000200	0.0000364	-45.0
25	-13.7	0.0000161	0.0000225	-28.5
30	-18.9	0.0000154	0.0000225	-31.7
35	-19.0	0.0000153	0.0000225	-31.8

Table 3.7
Small-Shift Results for Two-Dimensional Simulation Models

Mesh	Simulation Time (days)	Slope
refined	50	-0.03
refined	150	-0.05
coarse	50	-0.53
coarse	150	-0.88

Table 3.8
Two-Dimension Simulation Results
(refined mesh; 50 days)

Number of Arnoldi Vectors	optimal Shift	Root Mean Square Error		% Improvement
		Shift = optimal	Shift = 0.0	
5	-0.095	0.01853	0.06343	-70.8
10	-0.142	0.00763	0.02874	-73.4
20	-0.073	0.00463	0.00930	-50.2
25	-0.034	0.00395	0.00538	-26.7
30	-0.024	0.00343	0.00395	-13.1
35	-0.006	0.00324	0.00338	-4.1
40	-0.006	0.00313	0.00316	-0.6
60	0.000	0.00305	0.00305	0.0

Chapter 4

Dispersion Under Transient Flow Conditions: A Numerical Simulation Analysis.

4.1 Introduction

Early approaches to the study of solute migration in subsurface environments considered large-scale spatial heterogeneity of natural formations as the primary factor influencing dispersion [Dagan, 1988]. This view was reinforced by early field experiments (for reviews see Gelhar et al., 1992) which collectively showed that spreading increased with the scale of the experiment. To date, much theoretical work has been focussed on relating the evolution of solute plumes to spatial variability of aquifer properties such as hydraulic conductivity. In most of these studies the flow field is assumed to be steady and recharge is generally assumed to be spatially uniform. However, the assumption of steady-state is only appropriate for transport of a relatively short duration [Dagan et al., 1996].

The inability of stochastic approaches based on steady flow and spatially variable hydraulic conductivity to fully account for the horizontal transverse dispersion observed during the Stanford-Waterloo tracer experiment is well documented [Naff et al., 1988 and 1989; Zhang and Neuman, 1990; and Woodbury and Sudicky, 1991]. This disagreement between theory and observation lead Sudicky [1986] to conjecture that the enhanced dispersion observed during the experiment may have been caused by groundwater flow transients known to be present at the site but not taken into account. The possible influence of flow transients on the dispersion process at the site had earlier been addressed by Sykes

et al. [1982] who suggested that this phenomenon may be partially responsible for the enhanced dispersion observed in a leachate plume migrating from a landfill at the site. Though plausible, these conjectures were not substantiated by their proponents.

The potential impact of flow transients on the dispersion process has been examined in a limited number of theoretical studies. The first significant investigation along these lines was performed by Kinzelbach and Ackerer [1986] for the case of unsteady groundwater flow in homogeneous hydraulic conductivity fields. As part of their work, deterministic relationships were developed which utilized components of the deterministic time-averaged groundwater velocity and the assumed true dispersivities to approximate the apparent dispersivities observed under transient flow conditions. These apparent dispersivities were later incorporated into steady-state models to predict solute migration. The relationships developed in that work indicated that for the case of temporal variability in the direction of flow the sum of the apparent dispersivities was equal to the sum of the true dispersivities. The validity of these proposed relationships was questioned by Goode and Konikow [1990] following their studies of the effects of temporal velocity fluctuations on calibrated dispersivities and the conditions under which transverse spreading of a plume is enhanced by transient changes in velocity. Contrary to Kinzelbach and Ackerer [1986], Goode and Konikow [1990] found that the sum of the apparent dispersivities exceeded the sum of the true dispersivities. As well, their study demonstrated that increases in the apparent transverse dispersivity occurred because longitudinal dispersion acted in a direction which was not parallel to the assumed flow direction. This increase in the apparent dispersivity was shown to be controlled by the magnitude of the flow angle variation and the ratio of the longitudinal

to transverse dispersivity.

Prior to the work of Goode and Konikow [1990], Naff et al. [1988] had postulated that the enhanced transverse spreading observed during the Stanford-Waterloo experiment may have been due to small temporal directional changes in the flow field relative to the mean flow direction. In a follow up study [Naff et al., 1989], the plausibility of this hypothesis was illustrated using a deterministic time-dependent model along with hydraulic conductivity and tracer data obtained from the Stanford-Waterloo tracer experiment. However, due to the lack of adequate hydraulic gradient data for the Borden site, Naff et al. [1989] were unable to validate their proposed model.

The impact of flow transients on the dispersion process has also been studied using stochastic formulations. In the first such study, Rehfeldt and Gelhar [1992] extended the earlier work of Gelhar and Axness [1983] and showed that for ergodic plumes, transients in the flow field can enhance the transverse asymptotic macro-dispersivity without significantly affecting the asymptotic macro-dispersivity in the longitudinal direction. In their approach, the temporal fluctuations in the hydraulic head were assumed to be random and small. Their approach further assumed that after an extensive travel time the dispersion induced by the fluctuating hydraulic gradient can be treated independently from the dispersion induced by the velocity fluctuations associated with the natural heterogeneity of the hydraulic conductivity field [cf. Dagan et al., 1996].

In a recent study, Farrell et al. [1994] used waterlevel data collected at the Borden site during the period July, 1989 to January, 1991 along with stationarity assumptions, to determine whether the proposed formulations of Naff et al. [1989], and Rehfeldt and Gelhar

[1992] could possibly account for the horizontal transverse dispersion observed during the Stanford-Waterloo experiment. Farrell et al. [1994] showed that whereas the deterministic approach of Naff et al. [1989] failed to adequately account for the observed transverse dispersion, the stochastic approach of Rehfeldt and Gelhar [1992] provided a reasonable estimate of the observed asymptotic transverse macro-dispersivity.

Zhang and Neuman [1996], and Dagan et al [1996] recently expressed several reservations regarding the approach utilized by Rehfeldt and Gelhar [1992]. Of particular concern to these authors were (i) the independent treatments of the dispersion processes, (ii) the fact that periodic fluctuations in the hydraulic gradient were not expected to affect the macrodispersivity and (iii) the non-zero transverse dispersion at late time. In contrast to the approach utilized by Rehfeldt and Gelhar [1992], Zhang and Neuman [1996], and Dagan et al. [1996] adopted formulations which (i) did not treat the various processes contributing to the dispersion phenomena separately and (ii) allowed the dispersivity to be calculated at any point along the migration path. In addition, both approaches considered the temporal variation in the hydraulic head gradient to be deterministic and the spatial moments to be independent of time. The latter condition is applicable if the duration of sampling periods for the plume is small compared to the smallest periods present in the hydraulic gradient time series. Both formulations showed that under transient flow conditions transverse dispersion can be enhanced without any significant enhancement of the longitudinal dispersion. At this point it is worth noting that the formulations of Zhang and Neuman [1996], and Dagan et al. [1996] are quite similar with both being extensions of the Lagrangian formulation presented by Dagan and co-workers [Dagan, 1984 and 1989; Rubin, 1990]. Thus, the similarity in the

results of the models is not surprising.

The criticisms presented by Zhang and Neuman [1996], and Dagan et al. [1996] emphasize the need to develop methodologies to systematically evaluate proposed hypotheses regarding solute migration and evolution in hydrogeologic environments. Numerical approaches such as utilized by Goode and Konikow [1990], though enlightening, cast the mass transport problem in a framework which over-simplifies the relevant hydrogeologic parameter; in particular the assumption of uniform hydraulic conductivity is an unrealistic simplification. In recent years, several numerical simulation experiments have been performed to evaluate proposed hypotheses related to spreading in heterogeneous environments [Tompson and Gelhar, 1990; Chin and Wang, 1992; Robin et al., 1992; Burr et al., 1994]. However, in all of these experiments a fundamental simplifying assumption has been steady-state flow. Although from a computational perspective steady-state models are advantageous, they do not necessarily represent natural hydrogeologic phenomena.

The present work focuses on the use of two-dimensional simulations to evaluate the effect of unsteady flow on the migration of non-reactive plumes. The proposed approach utilizes a limited Monte Carlo analysis involving twenty detailed fluid flow and mass transport simulations for nonreactive solutes migrating in heterogeneous statistically isotropic hydraulic conductivity fields. It is important to note that for the simulations both the statistics of the hydraulic conductivity field and the temporal dependence of the hydraulic gradient are representative of the Borden tracer test-site. In order to determine whether spreading is enhanced under transient flow conditions, the results of the simulations are compared to similar simulations performed under steady-state flow conditions. In addition, the simulated

results are also compared to similar simulations performed in homogeneous hydraulic conductivity fields. Note that wherever possible, the results of the simulations will be compared to reported analytical solutions. At this point, it is important to mention that in this work the analytic solutions of Dagan et al. [1996] (as opposed to Zhang and Neuman [1996]) are utilized in the subsequent dispersion analysis. The choice of the Dagan et al.[1996] model is based primarily on the fact that their formulations are more explicit than those of Zhang and Neuman [1996] and that the former have been applied in the analysis of field-scale dispersion [see Bellin et al., 1996].

4.2 Simulation Methodology

The methodology applied in the simulation part of this study is similar in concept to that previously reported by Tompson and Gelhar [1990], Robin et al. [1991], Chin and Wang [1992] and Burr et al. [1994]. In these studies, large-domain numerical simulations of local-scale contaminant migration were used to characterize the field-scale behaviour of solute plumes [Burr et al., 1994]. In this study, the solute under consideration is non-reactive and as a result its migration is expected to be controlled by local velocity fluctuations. Hence an understanding of the factors influencing the local velocity field is important.

The approach considered in this work utilizes the simplified case of two-dimensional flow in a saturated confined aquifer. As in previous simulation studies, the hydraulic conductivity of the aquifer is assumed to be scalar at the local level [Burr et al., 1994]. However, at the scale of the domain the bulk hydraulic conductivity is statistically isotropic. This is consistent with the findings of Sudicky [1986] and later Woodbury and Sudicky

[1991] for the horizontal component of the hydraulic conductivity structure of the Borden aquifer. The variability within the hydraulic conductivity structure is represented by:

$$F=\ln[K(x)]=\overline{F}+f(x) \tag{4.1}$$

where $\overline{F}$ is the mean such that $K_G = exp(\overline{F})$ is the geometric mean and $f(x)$ is a second-order stationary spatially-correlated random field characterized by a zero mean and variance σ_f^2.

Contrary to previous high resolution studies, flow within the simulation domain is treated as unsteady. The conventional approach for modelling unsteadiness in the flow field is to perform a complete transient analysis in which temporal and spatial variations in boundary conditions, recharge rates, pumping and injection rates are prescribed. For the waterlevel monitoring period (July, 1989 to January, 1991) insufficient information is available for these variables. Even if available, incorporating such information into a mathematical model for the site could prove to be problematic (with regards to the size of the model) since the primary source of the groundwater flow transiency is located some distance from the tracer experiment and waterlevel monitoring sites. To overcome this potential problem while at the same time reproducing a hydraulic gradient field which replicates that observed at the Borden site during the waterlevel monitoring period, a quasi steady-state modelling approach is adopted [c.f. Goode and Konikow, 1990; and Rehfeldt and Gelhar, 1992] in which unsteadiness in the flow field is intoduced into the model domain through the flow boundary conditions. The approach essentially requires that at each time step a steady-state solution to prevailing boundary conditions be sought. Thus in order to reproduce the field observed hydraulic gradients the periodicity present in the waterlevel data as reported

by Farrell et al. [1994] must be incorporated into the flow boundary conditions. It is important to note that the quasi steady-state approach is applicable only if the source of the unsteadiness is located outside of the model domain and is advantageous for relatively small "simple" domains. It is important to recognize that this approach proposed implies that the aquifer storage in the model is negligible, so that boundary stresses propagate instantaneously through the domain. Although this assumption is physically unrealistic, it nonetheless allows flow fields (and hydraulic gradients) representative of the those observed during the waterlevel monitoring period to be reproduced [Rehfeldt and Gelhar, 1992]. Having defined the difference between full transient flow models and the quasi steady-state flow model used in this work, the reader's attention is drawn to the fact that in the rest of this work the term "transient" will often be use in reference to the quasi steady-state flow model. This decision is taken in order to avoid possible confusion with the steady-state flow model used in this work.

As stated earlier, the simulations in this study are performed in a two-dimensional domain. The choice of a two-dimensional domain as opposed to a three-dimensional domain has been influenced by the degree of discretization required, the transient nature of the simulations and the available computational resources. Although the use of two-dimensional models to simulate natural three-dimensional systems is an idealization [Burr et al., 1994], the results from such simulations are useful in understanding the mechanisms controlling solute migration, especially at the regional scale where such models are commonly applied.

4.2.1 Flow Problem

Flow and transport in saturated porous media is a coupled process. For the case of a conservative solute for which density effects can be ignored, the flow aspect of the coupling is independent of the transport. The equation commonly used to model flow in a domain Ω with boundary Γ is given by:

$$\begin{aligned} \nabla\cdot(K\cdot\nabla h) &= S_s\frac{\partial h}{\partial t} \\ h &= h_b(t) \quad on\ \Gamma_u \\ -K\cdot(\nabla h\cdot\eta) &= q_b(t) \quad on\ \Gamma_q \\ h(x,0) &= h^0(x) \quad \in \Omega \end{aligned} \tag{4.2}$$

where K represents the hydraulic conductivity tensor, h is the hydraulic head, S_s is the specific storage of the medium, t is time, h_b is a specified head, q_b is a specified flux and η is a unit outward normal vector to the boundary of the domain.

The spatial structure of the hydraulic conductivity fields considered in this analysis is controlled by a covariance function embedded in $f(x)$. On the basis of field studies at the Borden site, Sudicky [1986], and Woodbury and Sudicky [1991] showed that the horizontal component of this covariance function is exponential and isotropic in form:

$$cov(r) = -\sigma_f^2 \exp\left(-\frac{r}{I_f}\right) \tag{4.3}$$

Here r is a separation vector in two-dimensional space and I_f is the correlation scale of the process. In this study, fields displaying this structure are generated using the spectral method

of Robin et al. [1993]. The input statistics for the generated realizations *[I_f = 5.0 m, σ_f^2 = 0.18 m,* and K_G = *6.18 m/day]* approximate the estimates reported for the site by Woodbury and Sudicky [1991].

The implementation of the unsteadiness into the model requires some discussion. As mentioned earlier, the unsteadiness in the model is generated through time dependent Dirichlet boundary conditions *[$h=h_b(t)$ on Γ_u]* in which the time dependence of the boundary conditions is modelled based on actual waterlevel data collected at the Borden site. On the basis of a trend surface analysis, Farrell at al. [1994] concluded that spatially, the waterlevel data collected at each sampling period was best represented by a first-order polynomial surface. Thus, the transient behaviour of the waterlevel surface can be represented by:

$$h(x,y,t)=s_1(t)x+s_2(t)y+s_3(t) \tag{4.4}$$

Here s_1, s_2, and s_3 are the trend surface coefficients and x and y are Cartesian coordinates. Application of a spectral analysis to the time series representing the various surface coefficients, allows continuous in time expressions for these time series (4.5) to be evaluated.

$$s_j(t)\approx\sum_{i=1}^{n} S_{ji}\ \cos(\omega_{ji}\ t+\varphi_{ji}\ ) \qquad j=1,2,3 \tag{4.5}$$

Here n represents the number of frequencies used, i represents the i^{th} frequency, and ω, S and φ represent the angular frequency, amplitude and phase associated with the ith frequency. Using (4.4) and (4.5), Dirichlet conditions can easily be computed at any coordinate location on the boundary at any desired time.

A comparison of the coefficient time series generated using (4.5) to the coefficient time series estimated directly from the waterlevel data is presented in Figure 4.1. For this comparison, (4.5) was evaluated using the 12 most dominant periods contained within the coefficient time series. These periods reflect seasonal and subseasonal phenomena within the aquifer. Figure 4.1 shows that the proposed model reproduced the essential features contained within the field data.

From the spectral analysis, the mean hydraulic gradients as well as the steady-state flow boundary conditions can be estimated by utilizing the coefficient values associated with zero frequency. Using this approach the estimated mean hydraulic gradient $(\overline{\nabla h})$ is *0.0049* and the associated mean groundwater velocity $(v=-K_G \overline{\nabla h}/n)$ ranges from *0.101 m/day* $(n=0.3)$ to *0.079 m/day* $(n=0.38)$ for the range of porosities, n, commonly reported for the Borden aquifer. These velocity estimates show good agreement with the *0.091 m/day* commonly reported in literature for the groundwater velocity at the Borden site.

In high resolution simulations, (4.2) is commonly solved using either finite element (FE) or the finite difference (FD) methods. For the purposes of this work the FE method is utilized. Application of the FE method to the steady-state form of (4.2), i.e. $S_s = 0$, results in a matrix equation of the form:

$$\boldsymbol{Rh}=\boldsymbol{g} \tag{4.6}$$

where $\boldsymbol{R}$ is the "conductivity" matrix, $\boldsymbol{h}$ is a vector of unknown hydraulic heads and $\boldsymbol{g}$ is a vector which contains boundary conditions as well as source/sink terms. Note that for the flow equation $\boldsymbol{R}$ is symmetric and positive definite. A discussion of the numerical scheme used

to solve (4.6) is reserved for a later section of this work.

4.2.1 Mass Transport Problem

Mass transport is simulated using the standard advection-dispersion equation for a non-reactive, neutrally buoyant species (4.7).

$$\begin{aligned} \nabla\cdot(\boldsymbol{D}\cdot\nabla c)-v\cdot\nabla c+f&=\frac{\partial c}{\partial t} \\ c(x,y,0)&=c_0 \quad \in \Omega \\ c&=c_b \quad on\ \Gamma_b \\ \boldsymbol{D}\cdot\nabla c\cdot\boldsymbol{\eta}&=q_{cb} \quad on\ \Gamma_{cb} \end{aligned} \tag{4.7}$$

Here c is the solute concentration, $\boldsymbol{D}$ is a tensor of local hydrodynamic dispersion coefficients and v is the groundwater velocity which is obtained by applying Darcy's law $(v=-K\nabla h/n)$ to the solution of the flow equation. The coefficients of the local hydrodynamic tensor are computed using the result of Bear [1972]:

$$D_{ij}=\alpha_T|v|\delta_{ij}+(\alpha_L-\alpha_T)\frac{v_i v_j}{|v|}+D^* \tag{4.8}$$

Here D^* is the coefficient of molecular diffusion of the species in the porous medium, and α_L and α_T are the local longitudinal and transverse dispersivities.

For high resolution simulations, (4.7) is commonly solved using either FE methods [Robin et al., 1991; Burr et al., 1994; Naff et al., 1996] or particle tracking methods [Tompson and Gelhar, 1990; Chin and Wang, 1992]. The method of choice usually depends

on the available computational resources and the number of simulations to be performed. Each method has its strengths and weaknesses. In this study, the FE method is utilized in the simulations.

Application of the FE method to (4.7) results in a matrix differential equation of the form:

$$\boldsymbol{M}\dot{\boldsymbol{c}}+\boldsymbol{K}\boldsymbol{c}=\boldsymbol{b} \tag{4.9}$$

where $\boldsymbol{c}$ is a vector of unknowns at the nodes of the finite element mesh used to discretize the domain Ω, $\boldsymbol{K}$ is the "conductivity" matrix and $\boldsymbol{M}$ is the "capacity" matrix. For the mass transport equation $\boldsymbol{K}$ is unsymmetric whereas $\boldsymbol{M}$ is symmetric and positive definite. Finally, $\boldsymbol{b}$ is a vector which contains the boundary conditions as well as source/sink terms.

To solve (4.7) accurately, two criteria, the grid Peclet number *(Pe)* and Courant number *(Cn)*, must be satisfied [Daus et al., 1983]:

$$\begin{aligned} Pe_i &= \frac{(v_i\ \Delta x_i)}{D_{ii}} \le 2 \\ Cn_i &= \frac{(v_i\ \Delta t)}{\Delta x_i} \le 1 \end{aligned} \tag{4.10}$$

Here Pe_i represents the grid Peclet number in the i^{th} direction, Cn_i represents the Courant number, v_i represents the groundwater velocity in the i^{th} direction, D_{ii} is the ii component of the hydrodynamic tensor, Δx_i is the mesh discretization in the i^{th} direction and Δt is the time step used. It should be noted that optimal choices for Δx_i and Δt are crucial not only from an accuracy perspective but also from the perspective of computational efficiency.

4.2.3 Moment Estimation

Freyberg [1986] (cf. Aris, 1956) defined the ij^{th} moment of a concentration distribution in space as:

$$m_{ij}(t)=\int_{-\infty}^{\infty}\int_{-\infty}^{\infty} n\, x^i y^j\, c(x,y,t)\, dxdy \qquad (4.11)$$

where n again represents the porosity of the porous medium. Equation (4.11) is defined over all space; however, it is clear that the integrand will be zero at points where the plume concentration is zero. Hence, the spatial moment gives an integrated measure of the concentration field over the extent of the plume. Using the zeroth $(i+j=0)$, first $(i+j=1)$ and second $(i+j=2)$ moments, properties such as the plume mass, velocity of centre of mass and dispersivity may be computed.

The zeroth moment provides an estimate of the mass of solute present in solution. Hence for a non-reactive solute, this value should approximate the injected mass at all times. Thus the zeroth moment provides a measure of the reliability of the field sampling procedure. For the numerical simulations in this work, it provides a means of assessing the performance of the numerical method.

Normalization of the first moment with respect to the zeroth moment yields the location of the centre of mass of the plume (x_c, y_c).

$$x_c=\frac{m_{100}}{m_{000}} \qquad y_c=\frac{m_{010}}{m_{000}} \qquad (4.12)$$

Using (4.12) the velocity of the centre of mass of the plume, U, may be calculated.

$$U=\left(\frac{\partial x_c}{\partial t}, \frac{\partial y_c}{\partial t} \right)^T \tag{4.13}$$

Properties characterizing solute spread about the centre of mass (eg. dispersion, skew and kurtosis) are generally estimated using central moments (4.14):

$$\overline{m}_{ij}(t)=\int_{-\infty}^{\infty}\int_{-\infty}^{\infty} n\ (x-x_c)^i(y-y_c)^j\ c(x,y,t)\ dxdy \tag{4.14}$$

Normalizing the second central moments with respect to the plume mass allows the terms of the spatial covariance tensor, σ^2, to computed (4.15):

$$\sigma^2=\begin{bmatrix} \sigma_{xx}^2 & \sigma_{xy}^2 \\ \sigma_{yx}^2 & \sigma_{yy}^2 \end{bmatrix} \tag{4.15}$$

$$\sigma_{xx}^2=\frac{\overline{m}_{200}}{m_{000}} \qquad \sigma_{yy}^2=\frac{\overline{m}_{020}}{m_{000}} \tag{4.16a}$$

$$\sigma_{xy}^2=\sigma_{yx}^2=\frac{\overline{m}_{110}}{m_{000}} \tag{4.16b}$$

From the spatial covariance tensor, the terms of the hydrodynamic dispersion tensor, $\boldsymbol{D}$, and the macrodispersivity tensor, $\boldsymbol{A}$, are commonly computed using:

$$D_{ij}=\frac{1}{2}\frac{d}{dt}\sigma_{ij}^2(t) \tag{4.17a}$$

$$A_{ij}=\frac{1}{2|U|}\frac{d}{dt}\sigma_{ij}^2(t) \tag{4.17b}$$

It is important to note that these expressions are accurate only after the solute concentration has attained a normal distribution [Loaiciga, 1988]. Hence (4.17) should only be applied during the later part of the transport process.

The plume moments are computed numerically using the integration method outlined by Garabedian et al. [1991], in which a piecewise integration is applied to the solute concentrations of a finite element mesh. The method, which utilizes triangular elements, approximates the solute concentration ($\hat{c}_e$) within an element using linear basis functions (4.18).

$$\hat{c}_e(x,y)=\sum_{i=1}^{3} c(x,y)\ \varphi_i(x,y) \tag{4.18}$$

Here $\varphi(x, y)$ is a linear basis function and $c(x, y)$ is the concentration at the nodes of the element. The moment integration is then

$$m_{ij}=\sum_{e=1}^{N_\Delta} \int_{\Omega_\Delta} n\ x^i y^j\ \hat{c}_e(x,y)\ d\Omega_e \tag{4.19}$$

where e is defines the region $y_n \le x \le y_{n+1}$ and $x_n \le x \le x_{n+1}$. Using a similar approach expressions for the second central moments can be calculated.

Two approaches can be applied to compute the ensemble averages based on the results of Monte-Carlo realizations. One approach involves first averaging the plume concentrations over the various realizations and then computing the M_{ij} moments for the averaged concentrations $(\bar{c})$.

$$M_{ij}(t)=\int_{-\infty}^{\infty}\int_{-\infty}^{\infty} n\, x^i y^j\, \bar{c}(x,y,t)\, dxdy \tag{4.20}$$

An alternate approach involves averaging the moments computed for the individual realizations $\langle m_{ij} \rangle$.

$$\langle m_{ij} \rangle = \frac{1}{N_r} \sum_{l=1}^{N_r} m_{ij}(l) \tag{4.21}$$

Here N_r represents the number of realizations. Both approaches generally give similar estimates for the zeroth and first moments; however, significant differences can occur between the estimates for the second moments [Naff et al., 1996]. The relationship between the second moment estimates can be expressed as [Dagan, 1990; Rajaram and Gelhar, 1993; Naff et al., 1996]

$$M_{ij}(t)=\langle m_{ij}(t) \rangle + R_{ij}(t) \quad i+j=2 \tag{4.22}$$

where $R_{ij}(t)$ is a positive definite tensor quantifying the deviation of the centre of mass in a realization from the ensemble mean centre of mass. Since $R_{ij}(t)$ is positive definite, the diagonal components of $M_{ij}(t)$ are greater than $\langle m_{ij}(t) \rangle$ for the case $i+j=2$. Under ergodic

conditions, the concentration field of the ensemble can be represented by the concentration field of a single realization, hence $M_{ij}(t) \approx \langle m_{ij}(t) \rangle$ and $R_{ij} \approx 0$ generally holds. However, when ergodicity cannot be assumed $R_{ij} \neq 0$ so that $M_{ij}(t) \gg \langle m_{ij}(t) \rangle$. In such cases if $M_{ij}(t)$ is used, then significant over-prediction of the "true" dispersivities is possible [Rajaram and Gelhar, 1993]. For most field experiments the assumption of ergodicity may be invalid due to the fact that the source dimensions are on the order of the integral scale of the hydraulic conductivity field [see Rajaram and Gelhar, 1993, Table 1]. Thus, the use of methods involving $M_{ij}(t)$ to interpret the second moment data associated with such experiments is potentially problematic. Hence, in this work, in order to avoid complications associated with the assumption of ergodicity, ensemble averages are estimated using $\langle m_{ij}(t) \rangle$.

4.3 The Model

Although most of the material properties associated with the model have been described, several other aspects of the model still require definition. The physical dimensions of the model domain utilized in this study are $L_{x'} = 80\ m$ and $L_{y'} = 15\ m$, where the primed coordinates axes are rotated from the original x and y coordinate axes (see Figure 4.2) in order to coincide with the migration path of the plume. Though not required, rotation of the coordinate system is advantageous since it reduces the transverse dimensions of the modelling domain, and hence the number of elements and nodes required. After several initial runs, a rotation angle of approximately $-9.5\ ^\circ$ was considered acceptable. This rotation angle closely approximates the $-10.5\ ^\circ$ [i.e. $\tan^{-1}(S_{21}/S_{11})$] expected based on the direction of the mean hydraulic gradient estimated from the zero frequency components of the spectral analysis.

The coefficient of molecular diffusion (D^*) and the longitudinal (α_L) and transverse (α_T) dispersivities utilized in the model were $4.3x10^{-5}$ m^2/day, 0.05 m and 0.005 m respectively. Substituting these values along with the estimates for the mean groundwater velocity (determined using S_{21} and S_{11}) into (4.8) and (4.10) indicated the following were acceptable estimates for the mesh and time step time discretizations; $\Delta x = \Delta y = 0.1$ m and $\Delta t = 0.5$ $days$. This discretization resulted in 120,000 linear quadratic elements and 120,951 nodes throughout the domain. Since the flow boundary conditions have already been discussed, no further discussion of these boundary conditions is presented.

The initial and boundary conditions required to solve the mass transport problem are illustrated in Figure 4.2. Along the external boundaries, zero flux boundary conditions were enforced at all times. Within the domain at time, $t=0$ $days$, the solute concentrations were assumed to be zero except along the 2.5 m long line source located approximately 2.0 m from the up-gradient boundary. For $t > 0$ $days$ it was assumed that all external sources of contamination within the domain were removed, and the evolving plume was allowed to migrate under "natural gradient" conditions.

The numerical solution procedure utilized may be summarized as follows. At each time-step, the hydraulic heads for the flow boundaries are up-dated and (4.2) is solved. Using Darcy's law, the up-dated hydraulic heads are used to up-date the velocity field. Since the impact of the velocity field on the transport process is contained in the $\boldsymbol{K}$ matrix of (4.9), this matrix must also be up-dated and the associated equation, (4.9) solved at each time step.

The solution of (4.9) using the AMRM described in Chapters 2 and 3 is problematic due to the need to up-date $\boldsymbol{K}$. It is apparent from Chapters 2 and 3 that an up-date of $\boldsymbol{K}$

requires that a new subspace reduction be performed and new Arnoldi vectors computed. Woodbury et al. [1990] and Farrell et al. [1997, cf. Chapter 2] have shown that a single Arnoldi reduction can be the most computationally expensive aspect of the AMRM. Thus the need to continuously up-date and reduce the system of equations associated with (4.9) makes the AMRM in its current form grossly inefficient for coupled transient simulations. Hence, for the posed problem an alternate solver must be utilized. In this work, (4.6) and (4.9) are solved using the iterative conjugate gradient stabilization scheme (CGSTAB) implemented in the WATSOLV package by Vanderkwaak et al. [1995]. This implementation, which has been found to be accurate and efficient, allows the storage requirements to be minimized by storing only the non-zero entries of the matrices. On an IBM RS/6000 model 595, the CPU time required to solve the coupled problem was generally on the order of 12 hours when 12 frequency components were used, and 5 hours when only the zero frequency components were used (i.e., under steady-state conditions). It is important to note that in terms of real time on a shared machine, this translated into two to four days in many instances and thus severely limited the analysis by reducing the number of simulations which could be performed within a realistic time frame. In terms of storage, the model required a minimum of approximately 64 MB of RAM, even though dynamic memory storage structures in Fortran90 were utilized. These hardware demands and associated limitations heighten the need for faster and more efficient matrix solvers if hydrogeologists are to model field observed phenomena realistically.

4.4 Analysis of Simulations

4.4.1 Analysis of Hydraulic Conductivity Realizations

The hydraulic conductivity fields utilized in the simulations were produced by truncating hydraulic conductivity fields generated on a larger mesh using the spectral method developed by Robin et al. [1991]. Therefore, prior to performing the mass transport simulations, it is prudent to evaluate the statistical characteristics of the utilized hydraulic conductivity fields to ensure that the statistics of the ensemble approximate the input statistics.

Several approaches may be utilized to estimate the statistical parameters present in the truncated fields. Naff et al. [1996] suggest that for Monte Carlo simulations, the ensemble average of the statistical parameters estimated for the full hydraulic conductivity fields should approximate those of the truncated hydraulic conductivity fields, provided several correlation scales are contained within the truncated fields. Thus, only an analysis of the un-truncated hydraulic conductivity field is required. Using their methodology the integral scale of the process can be easily computed from the spectrum of the process, with the mean and variance being computed using standard statistical approaches. However, if the number of realizations considered is relatively small, the results of this methodology may be suspect.

In the present study, a more traditional approach is utilized to determine the variances and integral scales of the truncated fields. The approach consists of two steps. In the first step variograms of the truncated fields are computed using several estimators; the unbiased classical estimator [Matheron, 1963], the Cressie-Hawkins estimator [1980] which reduces the effects of outliers in the data and the SSAD estimator [Omre, 1984]. In the second step,

a theoretical variogram is fitted to averaged hydraulic conductivity data to determine the average variance and integral scale of the ensemble. Of the three estimators used, the unbiased classical estimator yielded the most accurate estimates of the input field parameters *[I_f = 5.33 m; σ_f^2 = 0.212]*. In addition to these estimates, the geometric mean hydraulic conductivity *(K_G)* for the ensemble is approximately 6.12 m/day. Although not exact, the estimates were considered reasonable in light of the limited number of realizations considered.

At this point it is important to mention that the hydraulic conductivity used to represent the medium in the homogeneous simulation is the value of K_G estimated above.

4.4.2 Flow Field Analysis

This section discusses the flow fields used in the coupled fluid and mass transport simulations. The methodology utilized follows that described by Naff et al. [1996] in which variances are calculated at a number of locations for several parameters which characterize the flow field. In an effort to maintain the focus of this work and avoid unnecessary diversion, the parameters considered here are hydraulic head and groundwater flow (hydraulic gradient) direction.

Longitudinal and transverse hydraulic head profiles for the individual steady-state flow fields taken along the mid-sections of the domain show considerable variability away from the boundaries of the domain. This result is summarized in the variance plots shown in Figure 4.3. From Figure 4.3a, it appears that in the longitudinal direction boundary effects penetrate the domain to a depth of approximately 5 m (i.e., approximately one integral scale, I_f, of the hydraulic conductivity field). The relatively small lateral dimensions of the domain make it

difficult to estimate the depth to which boundary effects penetrate the domain in the transverse direction (Figure 4.3b). However, a penetration distance equivalent to I_f does appear plausible. Due to the quasi steady-state formulation used in this analysis, profiles similar in form (but differing in magnitude) to those shown in Figure 4.3 are also observed at each time step of the transient simulations. The form of the hydraulic head variance for nodes at the centre of the domain is shown in Figure 4.4. The figure shows that temporally the variance in the hydraulic head displays a periodicity which appears to mimic that used to compute the hydraulic head boundary conditions (compare to Figure 4.1).

As mentioned previously, the other parameter of interest in characterizing the flow field is the groundwater flow direction (hydraulic gradient). Although showing variability across realizations, the mean flow angle for the steady-state flow fields approximates the -*10.5* ° (measured relative to the positive *x*-axis) obtained using the zero frequency terms of the spectral analysis. However, the computed flow angle variance initially appears to display a directional dependence (Figures 4.5). For example, in the longitudinal direction significant variances are observed within the interior of the domain, with near zero variances observed at the up-gradient and down-gradient boundaries. In the transverse direction the reverse is observed. As will be shown in the following paragraph, this directional dependence is related to the orientation of the domain with respect to the mean flow direction. The penetration of the boundary effects into the domain may also be estimated from plots of the flow angle variance. From these plots the boundary effects are more evident and appear to penetrate the domain a depth of approximately *5 m* or I_f. Therefore, provided the plumes remain within the central region of the domain the impact of boundary effects on plume evolution should be

minimized. However, this is not the case at early time since the line source is located approximately *2 m* from the up-gradient boundary. Hence, the early migration of the plume needs to be carefully monitored.

Steady-state hydrogeologic phenomena are generally exceptions and not the rule. This is also the case for the flow angle variances at the up-gradient and down-gradient boundaries. The reader should recall from the previous paragraph that at these boundaries the flow angle variances were zero. However, under transient flow conditions these variances varied temporally. Figure 4.6a demonstrates this temporal variability. The cause of this temporal variability may be explained as follows. At times when the mean flow direction is aligned with the orientation of the domain, flow at the up-gradient and down-gradient boundaries is normal to the boundary, i.e. these boundaries act as constant head boundaries. Hence at such times the observed flow angle variance should be zero. However, when the domain and the mean flow direction are not aligned the hydraulic head along the boundary varies spatially. This spatial variation in the hydraulic head along the boundary, coupled with local variations in the hydraulic conductivity field, produces highly variable flow directions locally and thus produces the non-zero flow angle variances observed. Away from the domain boundaries, the observed variance in the local flow direction is non-zero and shows a periodicity which is reflective of the periodicity contained in the s_2 (y component of the hydraulic head gradient) time series of the surface fit (compare Figure 4.6b to Figure 4.1b).

4.4.3 The Zeroth Moment and Plume Mass Estimates

The zeroth moment for the individual realizations is computed using (4.11) for the case $i+j=0$. Since this moment provides an estimate of the mass of solute being transported, it is commonly utilized in field tracer experiments to assess the amount of mass recovered, and hence the reliability of the field data. In field experiments, variability in the recovered mass estimates is a common occurrence [see Freyberg, 1986 and Garabedian et al. 1991]. In most cases this is caused by less than perfectly designed monitoring networks which result in discontinuous and incomplete sampling of the solute concentrations.

In this work, the zeroth moment is used to assess the reliability of the simulation results. Provided no mass enters or leaves the domain and no adverse numerical problems are encountered, the computed mass within the system at anytime is expected to approximate the input mass. For most of the simulations performed in this work, the computed mass although showing some variability, generally approximates the input mass (Figures 4.7). This variability results from approximations inherent in the numerical procedure [Naff et al., 1996] and is commonly encountered in numerical simulations of this nature.

4.4.4 First Moment Analysis: Plume Centre of Mass and Velocity

The coordinates of the plume centre of mass and the velocity of the centre of mass for the individual realizations are computed using (4.11) for the case $i+j=1$, (4.12) and (4.13). As a starting point in this analysis, the results of the individual simulations conducted under steady-state flow conditions are considered. Figure 4.8a shows the total displacement of the centre of mass for the individual simulations as a function of time. Trends present in the

trajectories shown may be divided into three categories: (i) linear, (ii) convex and (iii) concave. The first category indicates that the velocity of the centre of mass remains constant over the migration distance, whereas the second and third categories are indicative of acceleration and deceleration respectively. The observed acceleration and deceleration appears to be related to the spatial distribution of hydraulic conductivity. In high hydraulic conductivity zones plume acceleration is observed whereas in low hydraulic conductivity zones deceleration is evident. Although not obvious from Figure 4.8a, minor deviations from the trend are observed. These result from non-uniform local velocities caused by local variations in the hydraulic conductivity field.

The statistics of the velocity estimates for the simulations in the 20 realizations are contained in Table 4.1. The variability in the velocity of the centre of mass, produces varying migrations distances within the various realizations after *600 days*, with the average migration distance being *58.44 m* and the standard deviation being *6.81 m*. This variability reflects the effect of the hydraulic conductivity variations on plume migration.

The migration of the centre of mass of the individual plumes under transient flow conditions is illustrated in Figure 4.8b, which shows total displacement of the centre of mass as a function of time. The displacement of the trajectories of the centres of mass display characteristics similar to those previously described. However, small amplitude perturbations, which may initially appear to be due to the random nature of the hydraulic conductivity field, are superimposed on the trend. A closer examination of these perturbations reveals periodicities which appear to approximate the longer periods present in the flow boundary conditions. Due to the small amplitude of these perturbations, the manifestation of

unsteadiness in the flow field through the trajectory of the centre of mass can go undetected in most cases. The unsteadiness in the flow field is best displayed in the y-displacement of the centres of mass. In this direction, a strong periodicity is observed to be superimposed on a trend which possesses the characteristics previously described. As in the steady-state analysis, constant mean velocities in the x and y directions are again assumed in order to simplify the subsequent analysis.

The statistics of the mean velocity estimates for the 20 simulations conducted under transient flow conditions were found to approximate those observed under steady-state flow conditions (see Table 4.1). Similarly, the statistics computed based on the mean displacements in the 20 realizations (mean equal *58.07 m*; standard deviation equal *6.81 m*) approximated those determined for the steady-state simulations. This suggests that the temporal nature of the flow field does not significantly impede the migration distance of the plume relative to steady-state conditions.

The simulations emphasize that plume migration is controlled by the combined effects of the flow boundary conditions and the hydraulic conductivity distribution within the medium. This can be illustrated by considering Figure 4.9a which shows plots of the centres of mass computed under steady-state and transient flow conditions for several realizations of the hydraulic conductivity field. Within each realization, the migration paths of the plumes deviate from each other. Although the deviations are generally small, their magnitudes are both variable and unpredictable. This randomness results primarily from the variation in the hydraulic conductivity field. It is important to note that if the time dependence of the flow boundary conditions were solely responsible for this deviation, it would be constant and

predictable for all realizations and would approximate that observed for similar simulations under homogeneous conditions (Figure 4.9b). Finally, the reader may recognize that these deviations may be equated to the *2 °* deviation between the temporal mean hydraulic gradient and the mean plume trajectory reported by Freyberg (1986) in his analysis of the migration of the chloride and bromide solute plumes associated with the Stanford-Waterloo experiment.

Although the results for the individual realizations provide interesting insights into plume dynamics, validation of stochastic theories requires the use of the ensemble averages. The ensemble average centres of mass for the plumes migrating under transient and steady-state flow conditions were computed using (4.21). These are shown in Figures 4.8 and 4.10. In the *x*-direction (Figure 4.10a), the displacements of the ensemble average centres of mass for both flow scenarios are quite similar, with both displaying strong linear trends as functions of time. On the basis of these linear trends, the mean velocities of the centres of mass observed under steady-state and transient flow conditions are v_{xs} = -0.097 m/day and v_{xt} = −0.100 m/day respectively. These estimates are in the middle of the range previously reported for the individual realizations. In the y-direction (Figure 4.10b), the ensemble mean displacements also display linear trends. However, for the case of transient flow this trend is partially masked by the large amplitude, long wavelength periodicities previously described. On the basis of the linear trend, the mean velocities of the centres of mass observed under steady-state and transient flow conditions are $v_{ys} = v_{yt}$ = -0.018 m/day respectively; again falling within the middle of the range previously reported for the individual realizations. Also presented in Figure 4.10 are plots of the centres of mass for the plumes in the homogeneous hydraulic conductivity field. It is important to notice that these plots correlate well with the

ensemble means reported for the simulations performed under transient and steady-state flow conditions. Average centre of mass velocity estimates for the plumes migrating in the homogeneous medium were approximately 0.102 m/day for both the steady-state and transient flow simulations. This value is in agreement with the velocity estimate of 0.1 m/day determined earlier by substituting the zero frequency spectral terms into Darcy's law (see Section 4.2.1).

In the following discussion, the ensemble mean velocity estimates reported above are compared to analytical expressions which predict plume migration under ergodic conditions. Dagan [1984 and 1991] suggested that under ergodic conditions, the first-order expression for the plume centroid is:

$$\langle x_j(t) \rangle = \frac{K_G}{n} \int_0^t J_j(\tau)\, d\tau \qquad (4.23)$$

where J_j, $j = 1 \ldots m$ ($m = 2$ in this case) are the directional components of the mean gradient and K_G is the geometric mean hydraulic conductivity. Since all of the variables in (4.23) are well defined in this work, this expression provides a suitable framework for examining the ensemble centre of mass data. Note that in performing this comparison, the geometric mean hydraulic conductivity for the 20 realizations is utilized *(i.e., $K_G = 6.12$ m/day)* and J_j is assumed to be equivalent to the components of the hydraulic gradient estimated from first-order ordinary least squares surface fits to the waterlevel data [Farrell et al., 1994]. Although the ergodicity of the plumes associated with the Stanford-Waterloo experiment may be questioned, some researchers have nonetheless utilized (4.23) in the evaluation of the

trajectory of the observed plumes [Bellin et al., 1996]. In this work, (4.23) is used solely to evaluate the trajectory of the ensemble.

Plots of the trajectories of the centres of mass based on the (4.23), the ensemble mean estimates and the estimates from the simulations in the homogeneous medium are presented in Figure 4.10. The figure shows that in both the x and y directions, good agreement exists between (4.23) and the ensemble results. However, (4.23) agrees best with the results of the simulations performed in the homogeneous medium. Although not shown, a comparison of (4.23) to the results for the individual simulations shows some deviations. These deviations result because the source dimensions of the individual plumes make it unlikely for the evolving plumes to become ergodic.

The fact that information regarding the character of the hydraulic gradient may be contained within the centre of mass data has prompted a crude re-examination of such data for the non-reactive solute plumes associated with the Stanford-Waterloo tracer experiment. A similar analysis has been described by Bellin et al. [1996] who used estimates of the a_2-gradient time series (i.e., the time series of the gradient component perpendicular to the mean gradient direction) found in Farrell et al. [1994]. On the basis of their analysis, Bellin et al. [1996] concluded that the gradients reported by Farrell et al. [1994] were unable to explain the trajectory of the chloride and bromide plumes associated with Stanford-Waterloo (i.e., the implications of this work suggested that the stationarity assumption utilized by Farrell et al. [1994] is invalid). Undeterred by this conclusion a similar analysis was performed to examine whether the gradient field determined by Farrell et al. [1994] could be used to explain some aspects of the migration paths of the centres of mass of the bromide and chloride plumes

associated with the Stanford-Waterloo tracer experiment. Two integrations were performed using (4.23). The first utilized the actual a_2-gradient time series whereas the second considered only the 12 most dominant frequency components. The integration results are shown in Figure 4.11. The fit of the 12 component model to the transverse centre of mass data for the Stanford-Waterloo experiment is reasonable but imperfect. The imperfect fit might suggest that the stationarity assumption utilized by Farrell et al. [1994] for the hydraulic gradient time series is at least weak. A second possibility is that the integrations performed assume ergodic behaviour, which is not necessarily the case for the plumes associated with the Stanford-Waterloo tracer experiment. Note that the better fit by the 12 component model suggests that the short wavelength periodicities present in the gradient time series have minimal impact on plume migration.

4.4.5 Plume Variance and Dispersivity Analysis

The second moment estimates and the terms of the spatial covariance tensor in the field coordinate system are computed using a combination of (4.14) for the case $i+j=2$, (4.15) and (4.16). The terms of the dispersivity tensor are commonly defined with respect to the longitudinal and transverse directions of traditional advection-dispersion terminology. Since the longitudinal direction parallels the mean horizontal trajectory of the centre of mass of the plume, rotation of the covariance tensor is required [see Freyberg, 1986]. The desired rotation is achieved using

$$\begin{bmatrix} \sigma^2_{x'x'} & \sigma^2_{x'y'} \\ \sigma^2_{y'x'} & \sigma^2_{y'y'} \end{bmatrix} = \Lambda^T \begin{bmatrix} \sigma^2_{xx} & \sigma^2_{xy} \\ \sigma^2_{yx} & \sigma^2_{yy} \end{bmatrix} \Lambda \qquad (4.24)$$

$$\Lambda = \begin{bmatrix} \cos\varsigma & -\sin\varsigma \\ \sin\varsigma & \cos\varsigma \end{bmatrix}$$

where the rotation angle, ς, is assumed to be positive when measured in a counter-clockwise direction. Based on the observed migration paths of the centre of mass in the simulations the average estimate for ς is approximately -9.5°.

As a starting point in this discussion, the covariances associated with mass transport in the homogeneous media are considered. In these simulations it was found that under steady-state flow conditions the longitudinal and transverse covariances increase linearly with migration distance and hence travel time (see Figure 4.12). Utilizing least squares fits to the data along with (4.17b) yields longitudinal and transverse dispersivities of $A_{x'x'} = A_{11} = A_L = 0.049\ m$ and $A_{y'y'} = A_{22} = A_T = 0.007\ m$ respectively. The effect of unsteady flow on the longitudinal and transverse covariances observed in homogeneous media are also considered (Figure 4.12). As in the previous case the longitudinal and transverse covariances show strong linear trends as functions of migration distance, with the values of the computed dispersivities at late time ($A_L = 0.049\ m$ and $A_T = 0.007\ m$). Although these estimates appear identical to those reported for the case of steady-state flow, it appears from the figure that there is a slight enhancement in the covariance. Note that these estimated dispersivities are not identical to the input local dispersivities due to the rotation performed. However, their authenticity may be established using Burr et al. [1994, eqn. 18]:

$$\alpha_i^e = \alpha_t + (\alpha_l - \alpha_t)\frac{\langle v_i \rangle^2}{|\langle v \rangle|^2} + \frac{D^*}{|\langle v \rangle|} \qquad (4.25)$$

where α_i^e, $i = 1, 2$, gives the "effective" local-longitudinal and transverse dispersivity estimates. Using (4.25) along with velocity estimates given in Table 4.1 yields values of $\alpha_1^e = 0.049\ m$ and $\alpha_2^e = 0.007\ m$, which are in perfect agreement with those estimated from Figure 4.12.

In the sequel, the evolution of the longitudinal and transverse covariances in heterogeneous media are analysed under both steady and unsteady flow conditions. As a starting point in this analysis the longitudinal covariances are considered. The computed longitudinal covariances display considerable variability between realizations and temporally within realizations. This can be demonstrated by considering Figure 4.13a which compares the covariances observed under transient and steady-state conditions for several selected realizations. Notice from the figure that the growth in the covariance plots is not monotonic and that the phases and magnitude of the observed growth varies across realizations. Similar variability is also displayed in the simulation results of Tompson and Gelhar [1990], Burr et al. [1994] and Naff et al. [1996] and is therefore commonly observed. Despite this variability, two and in some cases three phases of growth can be identified in the evolution of the longitudinal covariance. The first phase occurs at early time in the near source region and is characterized by small increases in the longitudinal covariance with travel time and migration distance. In contrast to the first phase, the second phase occurs at late time after the plume has migrated over several correlation scales and is characterized by much larger increases in

the longitudinal covariance with travel time and migration distance. The third phase when present occurs at very late time and is characterized by a decrease in the rate of growth of the covariance as a function of migration distance. This phase of growth is not unique to this work but may also be identified in other numerical simulation experiments [Tompson and Gelhar, 1990; Burr et al., 1994; and Naff et al., 1996]. A possible explanation of this behaviour has been provided by Naff et al. [1996] who suggested that the observed reduction in longitudinal variance may be influenced by the distribution of hydraulic conductivities utilized in the realizations. For example, when plumes encounter regions of low hydraulic conductivity, lateral spreading is generally observed [Naff et al., 1996]. In doing so, horizontal transverse growth is enhanced at the expense of longitudinal growth. This is particularly the case for two-dimensional simulations, since in three-dimensional flow systems migration and spreading in the vertical direction may also occur. Whether or not corresponding transverse growth occurs will be discussed later in this section. In addition, an associated reduction in the longitudinal velocity of the plume centre of mass should also occur in response to the low hydraulic conductivity zone. The reader should recall from the previous section that such decelerations in the plume velocity have been identified in some of the individual simulations.

When the longitudinal covariances associated with steady-state and transient flow simulations within identical realizations are compared some differences are observed. However, in terms of the percentage change, these differences are in most cases small. For the exceptional cases, significant deviations generally occurred after considerable migration distance when migration paths for the steady-state and transient flow simulations showed the

greatest deviation. As a result, at such times the plumes may migrate in regions with differing flow characteristics.

In the transverse direction, the computed covariances also displays considerable variability between realizations and temporally within realizations, with considerable growth being observed in some simulations and negligible growth in others (Figure 4.13b). Notice that for case 2 negligible growth is clearly displayed by the simulation conducted under steady-state flow conditions (see Figure 4.13b). Similar to the longitudinal covariance, the transverse covariance generally displays two to three phases of growth which correspond to early and late times. The early time behaviour is again generally characterized by marginal increases in the transverse covariance with occasional short wavelength periodicities superimposed. It is important to recognize that in some of the simulations conducted under transient flow conditions, enhanced transverse spreading occurred at much shorter travel times than for migration under steady-state flow conditions. Generally, the early time short wavelength periodicities observed in the transverse covariance data computed under transient and steady-state flow conditions correlate, and as a result they are more than likely due to similar local dispersive processes; in this case similar local flow environments caused by local variations in the hydraulic conductivity. At intermediate to late times, after the plumes have traversed several correlation scales significant growth in the transverse covariance generally occurred. The third phase is generally characterized by an exponential decrease in the growth of the covariance with migration distance.

On the basis of the simulations performed, it was found that at intermediate to late times the transverse plume variance estimated from simulations performed under transient

flow conditions were enhanced relative to those determined from similar simulation performed under steady-state conditions (see Figure 4.13b). It is important to note that the onset of enhancement is controlled by the direction, magnitude and spatial variability of the local velocity fields encountered by the plume. From the previous section, the reader should recall that for a given realization, plume migration paths and their characteristics can vary under transient and steady-state flow conditions. Finally, for the cases in which significant decreases in the longitudinal variances were observed, corresponding enhancements in the transverse variance were observed. Thus, the explanation proposed by Naff et al. [1996] appears justified. Since only twenty realizations were considered, the possible impact of such behaviours on the ensemble variances warrants that some degree of caution be used in interpreting the ensemble results at very late times.

The focus in the ensuing discussion will be on the ensemble longitudinal and transverse covariances. The ensemble average longitudinal and transverse covariances computed for both the steady-state and transient flow simulations are shown in Figure 4.12. In an effort to maintain consistency, the ensemble average longitudinal covariances are again considered first. Clearly evident in Figure 4.12a are the two phases of growth previously associated with early and late time. Since these phases of growth have already been discussed, only a limited discussion is presented here. During the first phase of growth (0 m to approximately 25 m; or approximately $5I_f$), the ensemble average variances are similar in magnitude and marginally exceed those associated with the homogeneous simulations. In the second phase, both covariances initially show rapid growth with the growth later decreasing at an approximate exponential rate. A growth in the ensemble average longitudinal covariance

is predicted by stochastic theory; however, the decline in the rate of growth observed at late time is not. This decline does appear to suggest that the late time decreases observed in the individual longitudinal plume variances are dominant, with this dominance possibly being influenced by the limited number of simulations performed. The longitudinal dispersivities for the various segments of the variance curves are estimated using (4.17). These are summarized in Table 4.2. Since the normality of solute plumes is questionable at early travel times, dispersivities computed for this time period using (4.17) are considered crude. Note that due to the reduced gradient of the longitudinal variance plots at large displacements (Figure 4.12a), dispersivities are also estimated for the 20 m to 45 m regions of the curve where maximum gradients are observed.

Table 4.2 shows that the observed early time longitudinal dispersivities are not significantly larger than the local longitudinal dispersivities; thus the corrected early time dispersivities which reflect the impact of spreading due to other mechanisms (e.g., unsteady flow and hydraulic conductivity heterogeneity) are quite small. This supports the contention that at early times spreading is dominated by local dispersive processes. Within later phases the maximum corrected longitudinal dispersivities range from approximately 1.75 to 3.4 times the local longitudinal dispersivity, indicating that aquifer heterogeneity and transient flow are the major contributors to plume spreading. The lack of agreement between the longitudinal macrodispersivities is a concern, since it is generally assumed that small variations in the magnitude of the gradient do not produce significant enhancements in the longitudinal dispersivity.

The ensemble average transverse covariances computed for the steady-state and

transient flow simulations (Figure 4.12b) reflect the three phases of growth previously discussed. The plots show that the persistence of the first phase of growth varies from one I_f for the case of transient flow to three to four times I_f for the case of steady-state flow. Notice that the persistence of the latter is consistent with that observed in the longitudinal direction. The second phase, which is characterized by rapid growth in the covariance as a function of displacement, extends over a range of one to two I_f. It is important to note that the magnitude of the growth observed under transient flow conditions considerably exceeds that observed under steady-state flow conditions. Within the third phase, the rate of growth of the covariance decreases significantly and on average marginally exceeds the rate of growth observed under homogeneous conditions (i.e. the observed transverse dispersivity marginally exceeds the local transverse dispersivity). For the case of steady-state flow, this result appears to contradict stochastic theories which suggest that at late times the transverse dispersivity should tend to zero [Gelhar and Axness, 1983; Dagan, 1984 and 1988]. However, this is not the case. The reader should recall that in many theoretical studies the local dispersivity is commonly ignored. Thus it should be expected that at late time the observed transverse dispersivity should approximate the local transverse dispersivity. Table 4.3 list the estimated transverse dispersivities for the various parts of the plot.

The table shows that at early times, local dispersive processes are the primary contributors to plume spreading. Note that the negative dispersivity estimates appear to suggest that on average there is some plume shrinkage. Within the second phase of growth enhancements of the transverse dispersivity are observed under both steady-state and transient flow conditions. For the case of steady-state flow, the corrected transverse dispersivity is

approximately 1.2 times that of the local dispersivity indicating that both the heterogeneity of the aquifer and local dispersive effects are contributing equally to transverse dispersion. However, under transient flow conditions, the corrected transverse dispersivity is approximately 2 times that of the local transverse dispersivity, or 1.7 times that observed under steady-state flow conditions. Thus transient flow appears to be an important factor controlling plume growth during this period. At late times, local transverse dispersivity again appears to be dominant, with aquifer heterogeneity and flow transients contributing minimally to plume spreading.

4.4.6 Comparison of the Simulated Results to Stochastic Analytic Theory

In this section, the results of the simulation analysis are compared to results derived from stochastic analytical theories. The analytical solutions under consideration are those of Rehfeldt and Gelhar [1992] and Dagan et al. [1996]. As a starting point in this analysis, the analytical solution of Dagan et al. [1996; cf. Bellin et al., 1996] is considered.

4.4.6.1 Comparison of the Simulation Results to the Model of Dagan et al. [1996]

The plume spatial covariance model proposed by Dagan et al. [1996] (also referred to as the DBR model [see Bellin et al., 1996]) is mathematically expressed as:

$$X_{ij}(t) = \int_0^t \int_0^t U_\alpha(t') U_\beta(t'') v_{ij,\alpha\beta} [\langle X(t') \rangle - \langle X(t'') \rangle] dt' dt'' \qquad (4.26)$$

Here X_{ij} represents terms of the spatial covariance tensor $(i, j = 1, 2)$, U_α and U_β represent

components of the mean groundwater velocity field ($\alpha, \beta = 1, 2$), $v_{ij,\alpha\beta}$ represents the velocity tensor defined as the covariance between the velocity fluctuations $u_i(x)$ and $u_j(y)$ [see Bellin et al., 1996] and X represents the trajectory of the plume centroid. Note that in (4.26) the integrand represents the velocity covariance. Assumptions implicit in the model are:

1. An exponential covariance form for the log hydraulic conductivity;
2. The piezometric head (h), is composed of a mean ($\overline{h}$), and a fluctuation (h'), with the instantaneous mean gradient being constant in space;
3. The flow and Darcy equations can be adequately represented by first-order approximations in σ_f^2;

Dagan et al. [1996] evaluated (4.26) for a flow which fluctuated periodically around a steady, uniform value (DBR*). Using a three-dimensional formulation of the DBR which accounted for anisotropy in the hydraulic conductivity, Bellin et al. [1996] attempted an explanation of the moments associated with the Stanford-Waterloo tracer experiment. Their analysis considered two models; the first incorporated the waterlevel data reported by Farrell et al. [1994], while the second incorporated data obtained from a regression analysis performed on the transverse component of the plume centre of mass data obtained from the Stanford-Waterloo experiment. In both cases the fit to the transverse variance data (X_{22}) was considered poor. As a result, they concluded that "the large transverse spreading in the field experiment could not be completely explained by the observed unsteadiness of the head gradient".

For this analysis, some aspects of the methodology utilized by both Dagan et al.

[1996] and Bellin et al. [1996] were adopted in order to compare the results of the DBR model to the simulated results presented earlier. Since the simulations were conducted in a two-dimensional domain only the two-dimensional forms of the DBR need to be considered. The methodology utilized by Dagan et al. [1996] and Bellin et al. [1996] expressed the velocity terms as

$$U_1=\overline{U}$$
$$U_2=\frac{\beta\overline{U}}{\lambda}\cos(\frac{t\overline{U}}{\lambda I_Y}) \tag{4.27}$$

where U_1 and U_2 are the velocity components in the longitudinal and transverse directions respectively, $\overline{U}$ is the mean velocity, and β and λ are parameters estimated from a regression analysis performed on the plume centre of mass data. In light of the good agreement between the analytical estimates of the centre of mass and the ensemble results (Figure 4.10), the regression analysis utilized in the aforementioned works is not necessary for comparison with the ensemble X_{22} data. However, note that for comparison with the individual realizations β and λ must be used due to possible nonergodic effects. Hence the velocity and displacement terms may be expressed in the following manner which is consistent with the approach utilized in the simulations.

$$U_\alpha(t) = -\frac{K_G}{n}\sum_{l=1}^{N} S'_{\alpha l}\cos(\omega'_{\alpha l}t+\varphi'_{\alpha l})$$

$$X_\alpha(t) = -\frac{K_G}{n}\left[S'_{\alpha 1}t+\sum_{l=2}^{N}\frac{S'_{\alpha l}}{\omega'_{\alpha l}}\left(\sin(\omega'_{\alpha l}t+\varphi'_{\alpha l})-\sin(\varphi'_{\alpha l})\right)\right] \qquad (4.28)$$

In the above, the primed terms represent spectral terms derived from the hydraulic gradient time series. The reader should note that since $\omega'_1=0$, then $l=1$ simply represents the steady state case. The above expressions provide a suitable framework for evaluating the DBR since all of the input parameters are well defined. In addition, these expressions allow $X_{11}(t)$ and $X_{22}(t)$ for the actual record of the hydraulic gradient, J, to be evaluated. It is noteworthy to mention that the accuracy of the formulation proposed in this section has been validated by its ability to reproduce the results described in Dagan et al. [1996] using appropriate substitutions for ω', K_G, n and $S'_{\alpha l}$.

Equations (4.26) and (4.28) were evaluated for three cases which are of general interest. The first case represented the often discussed steady-state flow scenario (i.e., $l=1$, $S'_{11} \neq 0$, $\omega'_{11} = 0$, and $S'_{21} = 0$, $\omega'_{21} = 0$), whereas the second case considered, coupled a mean hydraulic gradient in the longitudinal direction ($S'_{11} \neq 0$, $\omega'_{11} = 0$) with a periodic gradient in the transverse direction, (S'_{2l}, ω'_{2l}, $l=1,...,12$). Note that although the cumulative effects of the 12 dominant frequency terms in the transverse direction have been considered, this formulation nonetheless is equivalent to the single periodicity model (DBR*) evaluated by Dagan et al. [1996] and Bellin et al. [1996]. For the third case, the actual observed

hydraulic gradient $J(S'_{ij}, \omega'_{ij}\ i = 1,2, j = 1,..,12)$ is considered.

Plots of the non-dimensionalized longitudinal and transverse variances for the three cases are shown in Figure 4.14. In both the longitudinal and transverse directions, the plots show that plume spreading initially increases non-linearly with residence time. However, at late times the growth rates for the two curves appear to tend towards asymptotic values. It is evident from Figure 4.14, that while having minimal impact on the longitudinal variance, periodicity in the transverse component of the hydraulic gradient enhances the transverse variance relative to that observed under steady-state flow conditions. Finally, minor differences are observed between the results for cases 2 and 3, indicating that due to the magnitude of the mean gradient in the longitudinal direction the periodic components in this direction are negligible.

The observed and corrected ensemble average longitudinal and transverse variances computed from the numerical simulations are also shown in Figure 4.14. Agreement between the DBR and the ensemble average transverse variance computed under transient flow conditions is seen in the apparent negligible dispersivities observed at late time. Figure 4.14 also demonstrates areas of disagreement between the theoretical and simulation results. For example, in both the longitudinal and transverse directions the analytical solution over-estimates the numerical solution. Though disappointing, such disagreement between analytical solutions and the results of numerical simulations is not uncommon [see for example Burr et al., 1994]. Some of the reasons for this disagreement will be discussed later in this work. Finally, the enhancement in the transverse variance predicted by the DBR formulation is much less than that observed from the simulation results.

4.4.6.2 Comparison of the Simulation Results to the Model of Rehfeldt and Gelhar [1992]

The model proposed by Rehfeldt and Gelhar [1992] to predict the enhanced dispersivity due to transient groundwater flow, is in essence a generalization of the dispersivity model of Gelhar and Axness [1983] which was based on steady-state fluid flow assumptions. In their formulation, Rehfeldt and Gelhar [1992] demonstrated that the late time macrodispersivity can be decomposed into two independent components, which reflect the impacts of spatial variability within the hydraulic conductivity field (the Gelhar and Axness [1983] solution) and temporal variations within the hydraulic gradient field. For this comparison the latter component is the more important of the two. The general expression describing this component of the macrodispersivity, $A_{ij}^{(t)}$, is of the form [Rehfeldt and Gelhar, 1992]:

$$A_{ij}^{(t)} = \frac{q\ \sigma_{J_iJ_j}^2\ \lambda_{J_iJ_j}}{n\gamma^2 \overline{J}_1^2} \tag{4.29}$$

where q is the specific discharge in the mean flow direction, n is the porosity, $\lambda_{J_iJ_j}$ is the integral scale of the hydraulic gradient fluctuation, $\sigma_{J_iJ_j}^2$ is the covariance of the i^{th} and j^{th} components of the gradient and γ is a flow factor which can be defined for two- and three-dimensional isotropic and anisotropic flow systems. Implicitly the model assumes:

1. The hydraulic gradient is comprised of three components: (i) an ensemble mean component $\overline{J}_i$ (ii) a component which is temporally variable but spatially constant at a scale similar to that of $Ln[K]$, J_i' and (iii) a local-scale component which is variable in both space and time;

2. Storage effects in the aquifer are negligible;
3. The covariance functions for the log hydraulic conductivity and hydraulic gradient are exponential in form;
4. The plume is ergodic.

As part of their analysis, Rehfeldt and Gelhar [1992] showed that for the case of isotropic hydraulic conductivity (such that q and J are aligned) and $\overline{J_3}=J_3'=0$, (4.29) may be broken down into two components which represent the impacts of flow angle variation (4.30a) and gradient magnitude variation (4.30b) on the macrodispersivity.

$$A_{22}^{(t)}=\frac{q\sigma_\theta^2\lambda_\theta}{n\gamma^2} \tag{4.30a}$$

$$A_{11}^{(t)}=\frac{q\sigma_J^2\lambda_{J'}}{n\gamma^2\overline{J}^2} \tag{4.30b}$$

In the above expressions σ_θ^2 is the variance in the hydraulic gradient direction, λ_θ is the integral scale present in the hydraulic gradient direction time series, $\sigma_{J'}^2$ is the variance in the hydraulic gradient magnitude and $\lambda_{J'}$ is the integral scale present in the hydraulic gradient magnitude time series. Generally, $A_{11}^{(t)}$ is enhanced by variations in the gradient magnitude, whereas $A_{22}^{(t)}$ is enhanced by variations in the gradient direction.

Although the derivation of (4.29) was based on flow and transport in a three-dimensional system, it is assumed from its form that it can be applied to two-dimensional flow configurations by simply setting the $\overline{J_3}=J_3'=0$ and using an appropriate expression for γ. The

assumption, $\overline{J_3}=J_3'=0$, simply implies that hydraulic gradient fluctuations are restricted to the horizontal plane of a three-dimensional porous medium. Although this assumption may initially appear to be unrealistic, evidence from several field sites suggest that in some cases it may be a reasonable assumption. For example, at the Cape Cod site, researchers were unable to detect vertical gradients in nested piezometers located at the site [LeBlanc et al., 1991 and Garabedian et al., 1991]. Similar observations were also reported for the Borden site [Mackay et al., 1986; Freyberg, 1986; and Sudicky, 1986]. However, in spite of these observations Mackay et al. [1986] and Freyberg [1986] used available plume migration data at the site to infer the presence of "weak" vertical gradients.

Validation of (4.30a) and (4.30b) using the results of the numerical simulations requires estimation of the variances and integral scales present in both the gradient magnitude time series and the gradient direction time series. As shown in the works of Rehfeldt and Gelhar [1992] and later Farrell et al. [1994], these properties may be estimated using experimental semivariograms. Since the gradient fluctuations in the model were described by continuous functions, two sampling procedures were employed to generate the discrete data required to generate the variograms. In the first procedure, it was assumed that the function was sampled at an interval which was identical to that used in the spectral analysis described earlier *($\Delta t \approx 2$ days)*, sampling proc. #1; whereas in the second case it was assumed that the sampling interval was irregular and identical to that utilized during the waterlevel recording phase at the Borden aquifer [see Farrell et al., 1994], sampling proc. #2. This approach allows the effect of waterlevel sampling on the estimated variances and integral scales contained within the time series to be assessed. Due to the short length of the time series, two cases

were considered for each sampling procedure. For the first case (case #1) the actual flow angle and gradient magnitude time series were analysed, whereas for the second case (case #2) what were assumed to be the mean and the annual periodicity present in these time series were removed. The first case essentially assumes that the actual time series can be treated as part of a much longer random function, whereas the second case assumes that periodicities less than one year are entirely random.

Figure 4.15 shows the flow angle semi-variograms estimated from an application of Jackknifing [Shafer and Varljen, 1990] and the classical variogram estimator [Matheron, 1963]. The Jackknifing procedure is utilized so that confidence intervals can be established for the variograms and the estimated macrodispersivities. The variograms in the figure appear exponential in form with perhaps some hole effects being observed. Although not presented, semi-variograms for the gradient magnitude time series showed similar traits. The variances and integral scales contained within these variograms were estimated using a regression analysis in which the covariance function for the theoretical variogram model was assumed to be exponential in form. The estimated variances and integral scales are shown in Tables 4.4a and 4.4b.

The tables show that when the actual time series is analysed (case #1), the estimated semi-variograms are extremely sensitive to the changes in the sampling rate. If it is assumed that sampling proc. #1 represents the true semi-variograms, then it is clear that "poor" sampling of the time series (proc. #2) results in questionable estimates of the variances and integral scales present in the data. These produce questionable estimates of the horizontal transverse macrodispersivity when (4.31a) and (4.31b) are used. For case #2, the

semivariograms for both sampling procedures yielded reduced variances and integral scales. Note that for the flow angle time series, the parameter estimates obtained under both sampling procedures are consistent, thus indicating that the sampling procedure is not an important factor (i.e., all of the important features of the time-series are captured by both methods). However, this is not the case for the hydraulic gradient magnitude time series where differences between the parameter estimates indicate a sensitivity to the sampling procedure utilized.

The expected enhancements in the horizontal transverse macrodispersivities computed using (4.31a) and (4.31b) as well as their associated 95% confidence limits are listed in Table 4.5. The table shows that case #2 generally produces dispersivities which better approximate those determined from the ensemble average variance (Table 4.3), with case #1 significantly over-predicting the listed dispersivities. Since the simulated results represented the combined effects of dispersion due to heterogeneity and transient flow, some over-prediction of the transverse dispersivity is implied by the enhancements presented for case #2. The over-prediction present in the dispersivities computed using the analytic expressions can be further emphasized if one assumes that these enhanced dispersivities can be directly added to the dispersivities estimated from the ensemble average variances associated with steady-state flow. When this exercise was performed using the expected values, the predicted transverse dispersivities were found to range between 1.9 to 2.5 times the maximum corrected transverse dispersivity determined from the ensemble average of the transient flow simulations. Also note that at late time the ensemble average results indicate the corrected transverse dispersivity to be zero whereas the analytical model suggests a non-zero value.

In the longitudinal direction similar results are also observed. For example, the enhancements in the longitudinal dispersivity determined for case #1 significantly exceed the corrected longitudinal dispersivities determined from the numerical simulations; whereas the results computed for case #2 are more in line with those obtained from the simulation experiment. As before it is assumed that the dispersivities computed from the analytical model can be added to the corrected longitudinal dispersivities determined from the steady-state flow simulations. Table 4.6b shows that when this methodology was employed the resulting longitudinal dispersivity estimates agreed well with the corrected longitudinal dispersivity estimates derived from the transient flow simulations. Thus the model of Rehfeldt and Gelhar [1992] appears to account for the enhancement in the longitudinal dispersivity under transient flow conditions; however, the over-prediction of the transverse dispersivity estimates (Table 4.6a) is significant.

4.5 Summary and Conclusions

This chapter presented the results of a detailed numerical simulation experiment designed primarily to address the impact of unsteady or transient flow on solute migration and dispersion in heterogeneous, statistically isotropic hydrogeologic systems. The statistics characterizing the heterogeneity of the media were based on values previously reported for the Borden site by Woodbury and Sudicky [1991], while the temporal nature of the flow field was based on waterlevel data recorded at the site over a 1.5 year period [Farrell et al., 1994]. It was hoped that by using field based values for the Borden site, certain aspects of the non-reactive plumes associated with the Stanford-Waterloo tracer experiment could be directly

addressed or inferred from the results.

In order to accurately and efficiently perform the detailed numerical simulations several simplifying assumptions were adopted. Chief amongst these was the assumption of fluid flow and mass transport in a two-dimensional domain. In addition, the porosity of the domain was assumed to be constant and uniformly distributed, with all pores being utilized in the advective process. Despite these simplifications the results of this work have provided some insights into the dynamics of plume evolution.

The primary goal of this work was to assess whether transient flow enhanced solute spreading relative to that observed under steady-state flow conditions. In this analysis solute spreading was quantified through the plume spatial variance. Under both transient and steady-state flow conditions the spatial variance of the evolved plumes displayed two to three phases of growth which conformed to those commonly described in literature. These were the early time growth phase during which local dispersive processes dominated the dispersion process; the mid-to-late time phase in which significant increases in dispersion were observed. Within and across realizations the evolution of the plume variance differed. These differences were controlled not only by the distribution of hydraulic conductivities but also by the nature of the flow boundary conditions.

Within most of the realizations transient fluid flow produced an enhancement of the transverse plume variance. In the longitudinal direction enhancement of the plume variance was observed within some realizations; however this enhancement was not consistent across realizations. In both directions enhancement of the variance generally occurred at mid-to-late travel times. The enhancements in the longitudinal and transverse variances observed in the

individual realizations were also captured in the ensemble averages. These averages reiterated that under transient conditions enhancements in the variances primarily occurred during mid to late travel times.

The simulation data was also used to investigate the validity of proposed first-order stochastic formulations which attempt to predict solute dispersion under transient flow conditions. The models considered were those of Rehfeldt and Gelhar [1992] and Dagan et al. [1996]. To summarize, it was found that both models were unable to fully account for the enhanced dispersion observed in the simulations. For example, although the model of Dagan et al. [1996] predicted the general form of the longitudinal and transverse variances, it nevertheless over-predicted these quantities. In addition, the model was unable to reproduce the observed enhancements in the longitudinal and transverse variances observed in the simulation experiments.

The model of Rehfeldt and Gelhar [1992] was used to compute the enhanced macrodispersivities at late time. These enhancements were later used to augment the late time dispersivities determined from the steady-state simulations in order to predict the dispersivities expected under field conditions. Comparison of the augmented longitudinal dispersivity values to those estimated from the simulations showed reasonable agreement; however, in the transverse direction the predicted dispersivities generally overestimated those based on the simulation experiments. Recall that under transient flow conditions the simulation experiments generally produced on average a negligible transverse dispersivity at late time whereas the model of Rehfeldt and Gelhar [1992] generated a non-zero transverse dispersivity at such times.

The lack of uniform agreement between the simulated and theoretical results may be influenced by several factors, with the primary causes being the ergodic assumption inherent in the theoretical analyses and the limited number of simulations used for comparison. The ergodicity assumption poses several problems. As pointed out, (4.22) relates the second moments computed based on averaged solute concentrations, M, to those computed from an average of the individual plume second moments, $\langle m \rangle$. These quantities approximate each other under ergodic conditions when $R_{ij}=0$; however, under non-ergodic conditions $R_{ij} \neg 0$ as $t \rightarrow \infty$. Hence for relatively short travel distances M can significantly exceed $\langle m \rangle$. Thus the use of analytic models based on M (for example the models of Gelhar and Axness [1983], Dagan [1984, 1988], and Naff [1990]) can lead to an over prediction of the second moments under nonergodic conditions such as those inherent in the simulations performed in this work.

The over prediction present in the transverse dispersivity model of Rehfeldt and Gelhar [1992] is not only a consequence of the ergodic assumption but may also result from the fact that the model essentially considers uniform mean flow in the longitudinal direction. Under such assumptions Dagan [1996] agreed that at late time D_{22} should tend toward a constant non-zero "Fickian" limit. Dagan [1990] further argued that this is not equivalent to the case of steady-state flow through a heterogeneous hydraulic conductivity field. If this is indeed the case, then it implies that it may be more appropriate to compare the enhancement predicted by the Rehfeldt and Gelhar [1992] model with that observed for the transient simulations in the homogeneous medium. Such a comparison shows that the transverse dispersivities predicted by the Rehfeldt and Gelhar [1992] model overestimates that determined from the homogeneous model based on transient flow.

Other factors which may contribute to the disagreement between the ensemble results and theory include source geometry (the stochastic theories utilized were based on the assumption of an infinitely small pulse source, whereas the simulations in this analysis were based on a finite pulse source) and the inclusion of local dispersion (the stochastic formulation of Dagan et al. [1996] neglect local dispersive processes whereas such processes were considered in this work). The latter argument has been used by Burr et al. [1994] to explain the relatively good agreement between their simulation results for a highly stratified aquifer and the stochastic solution of Naff [1990] which accounted for local dispersion. In contrast, a less than satisfactory agreement was obtained between their simulation results and the Dagan [1988] model which did not account for local dispersion. Note that for highly stratified aquifers local dispersive phenomena are considered important factors in the redistribution of solutes [Naff, 1990; Burr et al., 1994].

The first moment analyses performed in this work were informative. It was demonstrated that that under non-ergodic conditions, the migration paths associated with the transient and steady-state flow can be highly variable and complex. Further, within any realization the migration of the centres of mass observed under transient and steady-state flow conditions may either diverge or converge in response to the distribution of hydraulic conductivities. The reader may recall that during the Stanford-Waterloo experiment a 2° divergence was observed between the mean gradient direction and the horizontal trajectory of the non-reactive plume. On the basis of the simulation experiments it may be argued that this observed deviation resulted from the combined effects of transient flow and heterogeneity in the hydraulic conductivity field and is not necessarily caused by a misalignment between

the mean hydraulic gradient and the axes of anisotropy in the hydraulic conductivity field. This result suggests that in some cases it may be difficult to determine whether such deviations are due to anisotropy in the hydraulic conductivity field or whether they result from the combination described above. This is particularly the case if the hydraulic gradient field is not carefully monitored.

In spite of the complexity of the migration paths associated with the transient simulations, the long wavelength periodicities contained within the flow boundary conditions are discernable, especially in the y-component of the centre of mass data. The fact that these periodicities can be discerned suggests that for field tracer experiments information regarding the nature of the hydraulic gradient field may be recovered from the centre of mass data. Assuming that such information can be recovered from the centre of mass data, then it can be conjectured that the additional information contained in the time series simply reflects what may be termed an "aquifer response". It may be further conjectured that the information contained within this response function reflects various aspects of aquifer heterogeneity. However, in this work such a decoupling has not been attempted.

In addition to shedding light on issues regarding plume dynamics, this work has illustrated a practical framework which can be used to incorporate field observed hydraulic gradients into numerical simulation models provided that sources influencing these gradients are not located within the domain of interest. The approach, which has been shown to be efficient and relatively easy to implement, allows complex time dependent flow boundaries to be introduced into the model.

Finally, the fact that transient flow has been shown to influence the migration and

dispersion of solutes in hydrogeologic environments suggests that a possible re-analysis of field tracer tests be undertaken, particularly for cases where the assumption of steady-state flow may have severely biased the results of the analysis. This is especially the case where choices have been made between competing models as is the case when modelling the migration and dispersion of reactive solutes. For such cases, an appropriate sorption model must be chosen from a number of competing models with the decision being partially based on the goodness to fit of the modelled data to some field observed data [see Srivastava and Brusseau, 1996]. Further, it is common in contaminant modelling efforts to assume a steady-state groundwater velocity. The results presented in this work suggest that such an approach may not be universally applicable and that variations in the hydraulic conductivity as well as time variations in the hydraulic head must also be taken into account. This has implications in site and risk assessment if perhaps years of prior monitoring at designated sites are required before commissioning.

References

Barry, D. A., and G. Sposito, Three-dimensional statistical moment analysis of the Stanford/Waterloo Borden tracer data, Water Resour. Res., 26(8), 1735-1747, 1990.

Bear, J., Dynamics of fluids in Porous Media, Elsevier, New York, 1972.

Bellin, A., G. Dagan and Y. Rubin, The impact of head gradient transients on transport in heterogeneous formations: Applications to the Borden site, Water Resour. Res., 32(9), 2705-2713, 1996.

Burr, D. T., E. A. Sudicky and R. L. Naff, Nonreactive and reactive transport in three-dimensional heterogeneous porous media: Mean displacement, plume spreading, and uncertainty, Water Resour. Res., 30(3), 791-815, 1994.

Chin, D. A. and T. Wang, An investigation of first order stochastic dispersion theories in isotropic porous media, Water Resour. Res., 28(6), 1531-1542, 1992.

Cressie, N., and D. Hawkins, Robust estimation of the variogram, Math. Geol., 12(2), 115-125, 1980.

Dagan, G., Solute transport in heterogeneous porous formations, J. Fluid Mech., 145, 151-177, 1984.

Dagan, G., Statistical theory of groundwater flow and transport: Pore to laboratory, laboratory to formation, and formation to regional scale, Water Resour. Res., 22(9), 120S-134S, 1986.

Dagan, G., Time-dependent macrodispersion for solute transport in anisotropic heterogeneous aquifers, Water Resour. Res., 24(9), 1491-1500, 1988.

Dagan, G., Flow and Transport in Porous Formations, Springer-Verlag, New York, 1989.

Dagan, G., Transport in heterogeneous porous formations: Spatial moments, ergodicity, and effective dispersion, Water Resour. Res., 26(6), 1281-1290, 1990.

Dagan, G., Dispersion of passive solute in non-ergodic transport by steady velocity fields in heterogeneous formations, J. Fluid Mech., 223, 197-210, 1991.

Dowd, P. A., The variogram and kriging: Robust and resistant estimators, Geostatistics for Natural Resources Characterization, Part 1, NATO ASI Ser., Ser. C, 122, 91-107, 1984.

Einstein, A., On the movement of suspended particles in stationary fluids deduced from molecular-kinetic theory of heat (in German), Ann. Phys., 17, 539-560, 1905.

Farrell, D. A., A. D. Woodbury, E. A. Sudicky and M. O. Rivett, Stochastic and deterministic analysis of dispersion in unsteady flow at the Borden Tracer-test site, Ontario, Canada, J. Contam. Hydrol., 15, 159-185, 1994.

Freyberg, D. L., A natural gradient experiment on solute transport in a sand aquifer, 2, Spatial moments and the advection and dispersion of nonreactive tracers, Water Resour. Res., 22(13), 2031-2046, 1996.

Garabedian, S. P., D. R. LeBlanc, L. W. Gelhar and M. A Celia, Large-scale natural gradient tracer test in sand and gravel, Cape Cod, Massachusetts, 2, Analysis of the spatial moments for a nonreactive tracer, Water Resour. Res., 27(5), 911-924, 1991.

Gelhar, L. W. and C. L. Axness, Three-dimensional stochastic analysis of dispersion in a stratified aquifer, Water Resour. Res., 19(1), 161-180, 1983.

Gelhar, L. W., C. Welty and K. R. Rehfeldt, A critical review of data on field-scale dispersion in aquifers, Water Resour. Res., 28(7), 1955-1974, 1992.

Goode, D. J. and L. F. Konikow, Apparent dispersion in transient groundwater flow, Water Resour. Res., 26(10), 2339-2351, 1990.

Kinzelbach, W. and P. Ackerer, Modélisation de la propagation d' un contaminant dans un champ d' écoulement transitoire, Hydrogéologie, 2, 197-205, 1986.

Loaiciga, H. A., Comment on "A natural gradient experiment on solute transport in a sand aquifer, 2, Spatial moments and the advection dispersion of nonreactive tracers" by D. L. Freyberg, Water Resour. Res., 24(7), 1221-1222, 1988.

Matheron, G., Principles of geostatistics, Econ. Geol., 58, 1246-1266, 1963.

Naff, R. L., D. F. Haley and E. A. Sudicky, High resolution Monte-Carlo simulation of low and conservative transport in heterogeneous porous media: 1, Methodology and flow results, [submitted to Water Resour. Res.]

Naff, R. L., D. F. Haley and E. A. Sudicky, High-resolution Monte-Carlo simulation of flow and conservative transport in heterogeneous porous media: 2, Transport results, [submitted to Water Resour. Res.]

Naff, R. L., J. T. -C. Yeh and M. W. Kemblowski, A note on the recent natural gradient tracer test at the Borden site, Water Resour. Res., 24(12), 2099-2103, 1988.

Naff, R. L., J. T. -C. Yeh and M. W. Kemblowski, Reply to comment on "A note on the recent natural gradient tracer test at the Borden site", by G. Dagan, Water Resour. Res., 25(12), 2523-2525, 1989.

Rajaram, H., and L. W. Gelhar, plume scale-dependent dispersion in heterogeneous aquifers 2. Eulerian analysis and three-dimensional aquifers, Water Resour. Res., 29(9), 3261-3276, 1993.

Rehfeldt, K. R. and L. W. Gelhar, Stochastic analysis of dispersion in unsteady flow in heterogeneous aquifers, Water Resour. Res., 28(8), 2085-2099, 1992.

Robin, M. J. L., A. L. Gutjahr, E. A. Sudicky and J. L. Wilson, Cross correlated random field generator with direct Fourier transform method, Water Resour. Res., 29(7), 2385-2397, 1993.

Rubin, Y., Stochastic modeling of macrodispersion in heterogeneous media, Water Resour. Res., 26(1), 133-142, 1990.

Srivastava, R., and M. L. Brusseau, Nonideal transport of reactive solutes in heterogeneous porous media: -1. Numerical model development and moment analysis, J. Contam. Hydrol., 24(2), 117-144, 1996.

Sudicky, E. A., A natural gradient experiment in solute transport in a sand aquifer - Spatial variability of hydraulic conductivity and its role in the dispersion process, Water Resour. Res., 23(13), 2069-2082, 1986.

Sykes, J. F., S. B. Pahwa, R. B. Lantz and S. D. Ward, Numerical simulation of flow and contaminant migration at an extensively monitored landfill, Water Resour. Res., 18(6), 1687-1704, 1982.

Tompson, A. F. B and L. W. Gelhar, Numerical simulation of solute transport in three-dimensional, randomly heterogeneous porous media, Water Resour. Res., 26(10), 2541-2562, 1990.

Vanderkwaak, J. E., P. A. Forsyth, K. T. B. MacQuarrie and E. A. Sudicky, WATSOLV Sparse Matrix Iterative Solver Package User's Guide Version 1.01, Waterloo Centre for Groundwater Res., University of Waterloo, Ont., Canada, 1995.

Woodbury, A. D. and E. A. Sudicky, The geostatistical characteristics of the Borden aquifer, Water Resour. Res., 27(4), 533-546, 1991.

Zhang, Y, -K. and S. P. Neuman, A quasi-linear theory of non-Fickian and Fickian subsurface dispersion, 2., Application to anisotropic media and the Borden site, Water Resour. Res., 26(5), 903-913, 1990.

Zhang, D., and S. P. Neuman, Head and velocity covariances under quasi-steady flow and their effects on advective transport, Water Resour. Res., 32(1), 77-83, 1996.

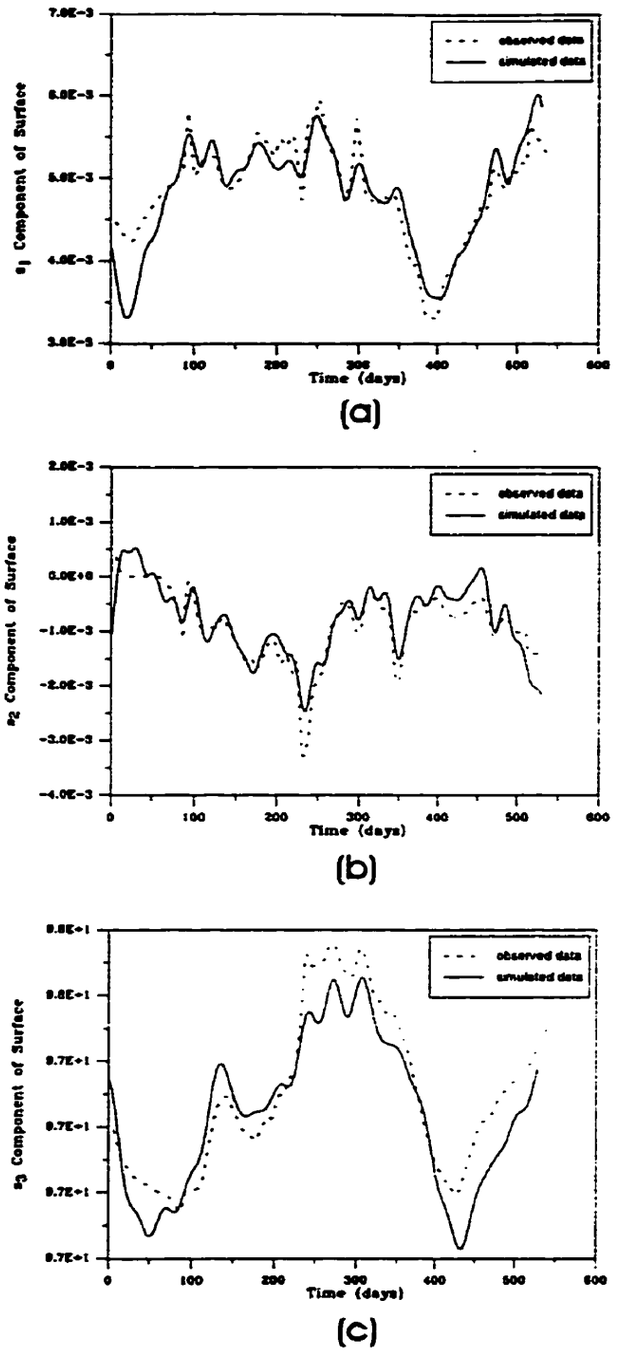

Figure 4.1: Comparison of the modelled coefficient time series to those determined directly from first-order fits to the Borden waterlevel data: (a) s_1 component; (b) s_2 component; (c) s_3 component.

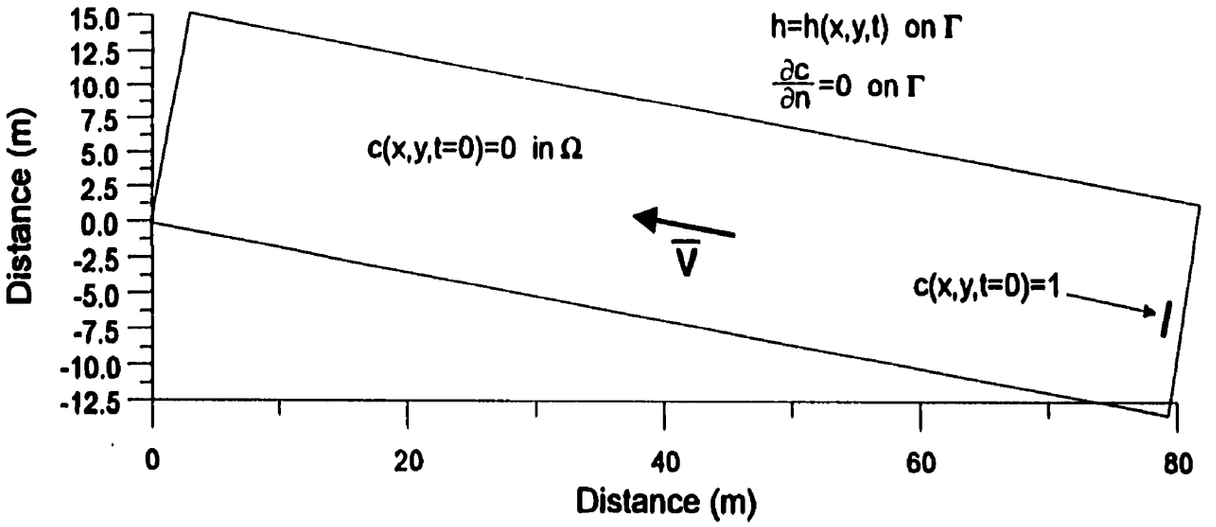

Figure 4.2: Schematic of the simulation domain.

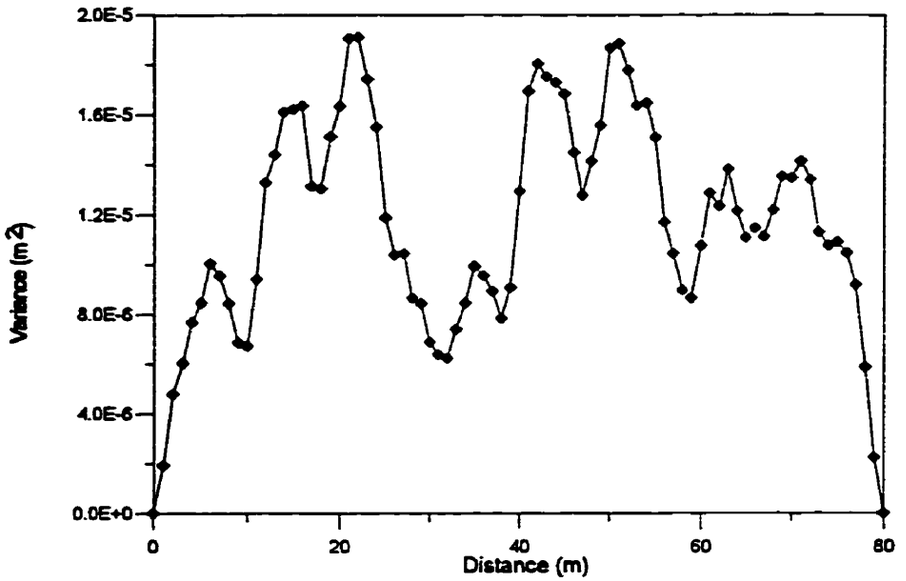

(a)

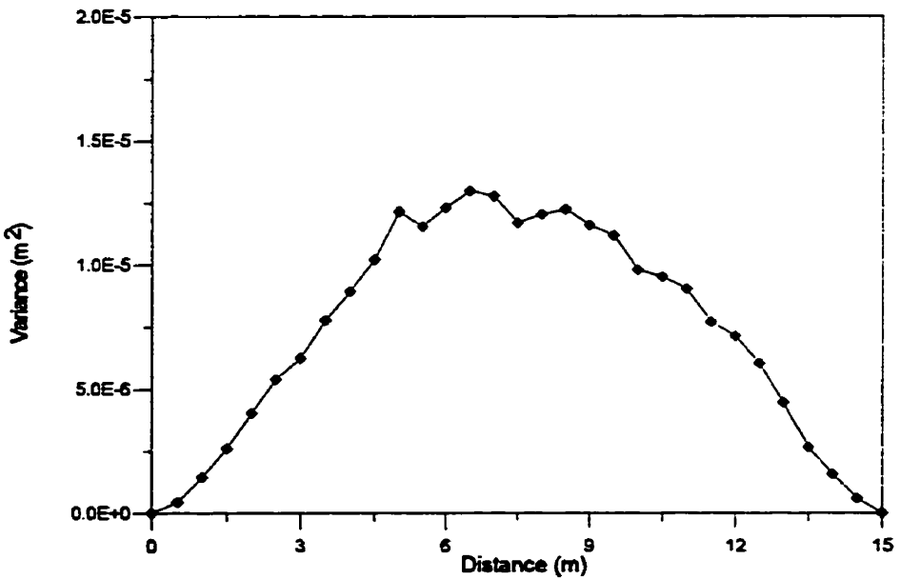

(b)

Figure 4.3: Computed spatial hydraulic head variance for the case of steady-state flow; (a) longitudinal direction; (b) transverse direction.

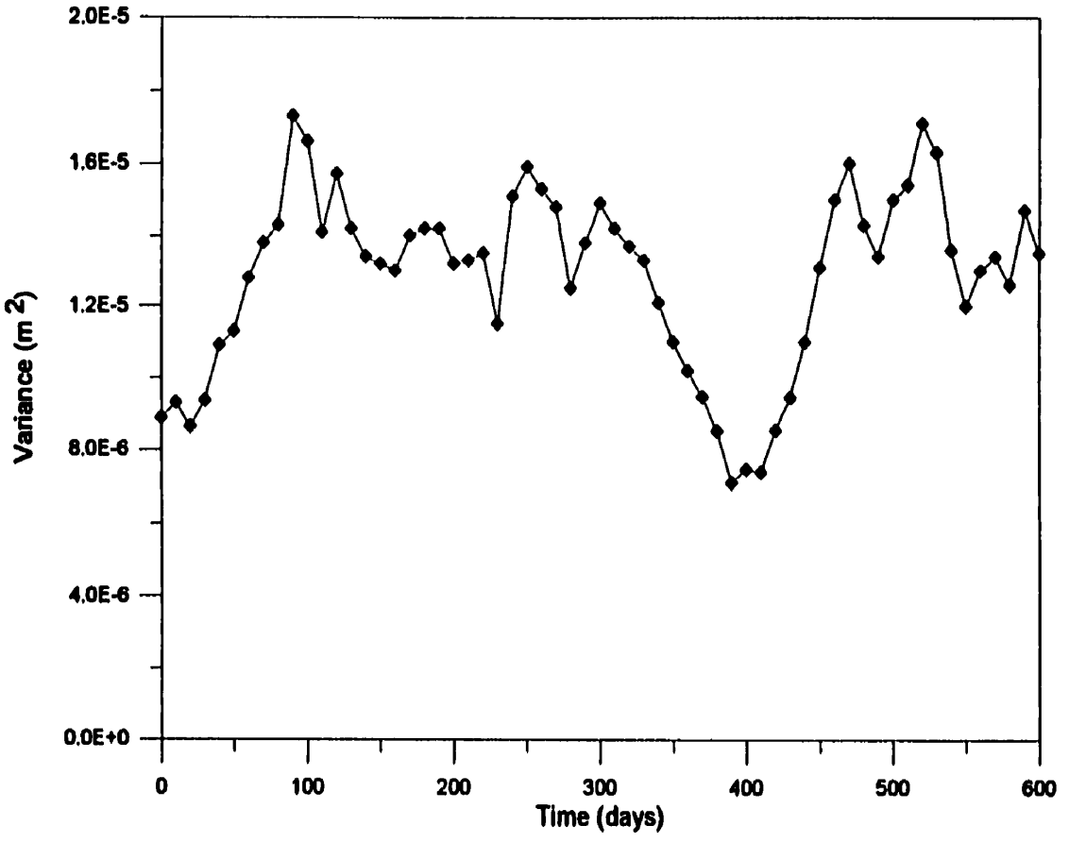

Figure 4.4: Temporal variation of the hydraulic head variance at the centre of the domain.

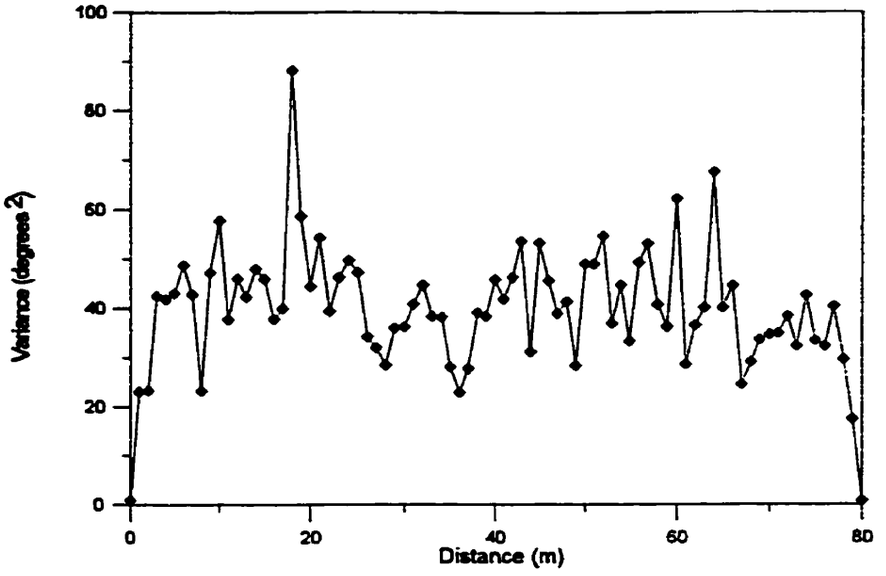

(a)

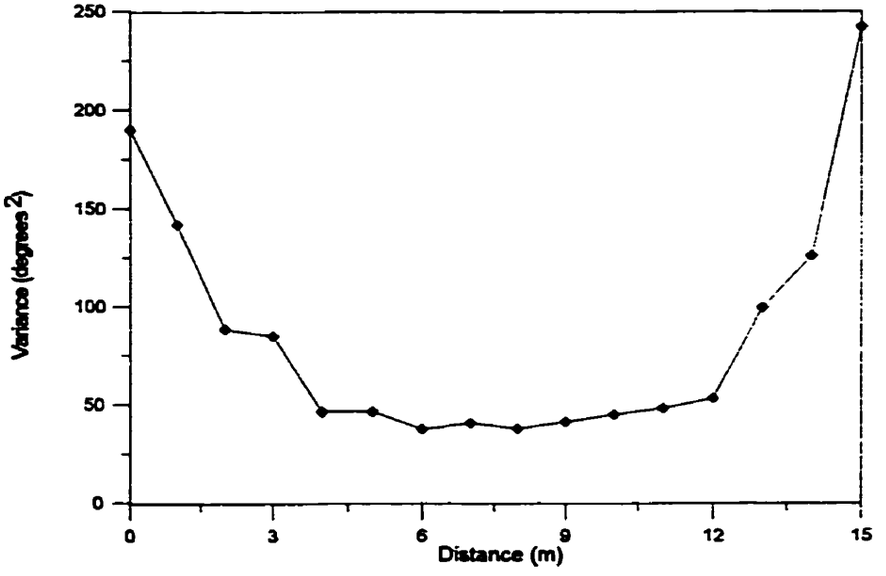

(b)

Figure 4.5: Computed spatial flow angle (hydraulic gradient) variance for the case of steady-state flow; (a) longitudinal direction; (b) transverse direction.

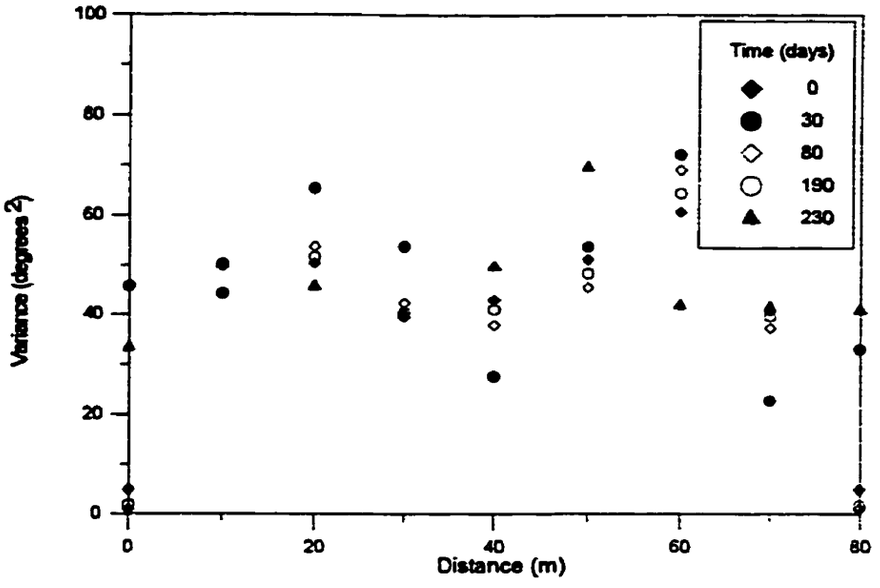

(a)

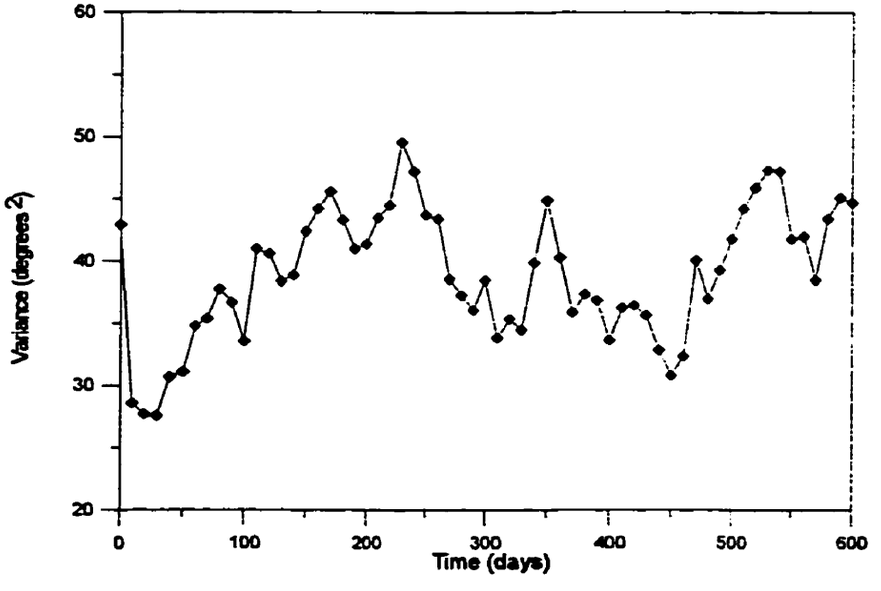

(b)

Figure 4.6: Temporal variation of the flow angle variances (a) in the longitudinal direction and (b) at the centre of the mesh.

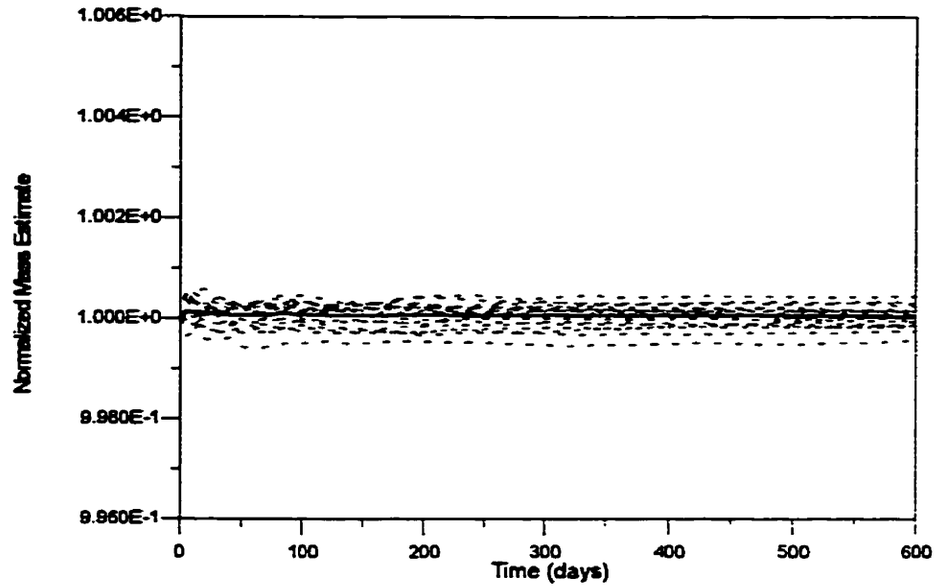

(a)

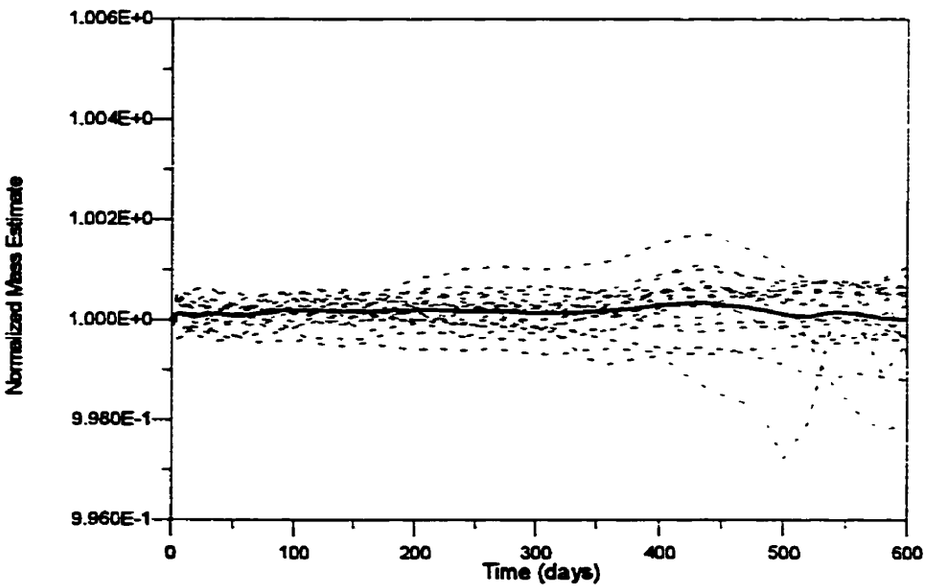

(b)

Figure 4.7: Computed mass estimates for individual simulations under (a) steady-state flow; (b) transient flow. Note that the thin dashed lines represent the results for the individual simulations and the thick dashed line represents the ensemble average for the simulations.

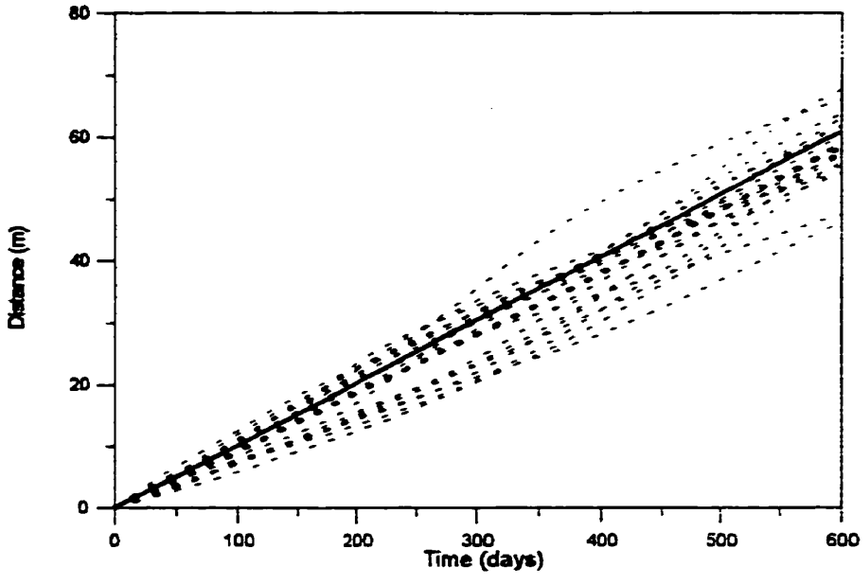

(a)

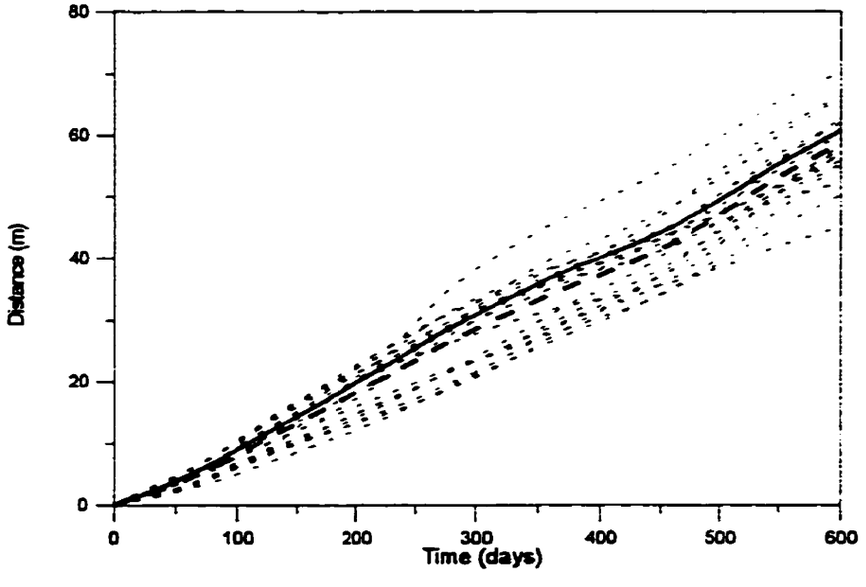

(b)

Figure 4.8: Displacement of the centre of mass for the individual simulations under (a) steady-state flow; (b) transient flow. Note that the thin dashed lines represent the results for the individual simulations, the thick dashed line represents the ensemble average values for the simulations and the thick solid line represents the simulation results in the homogeneous medium.

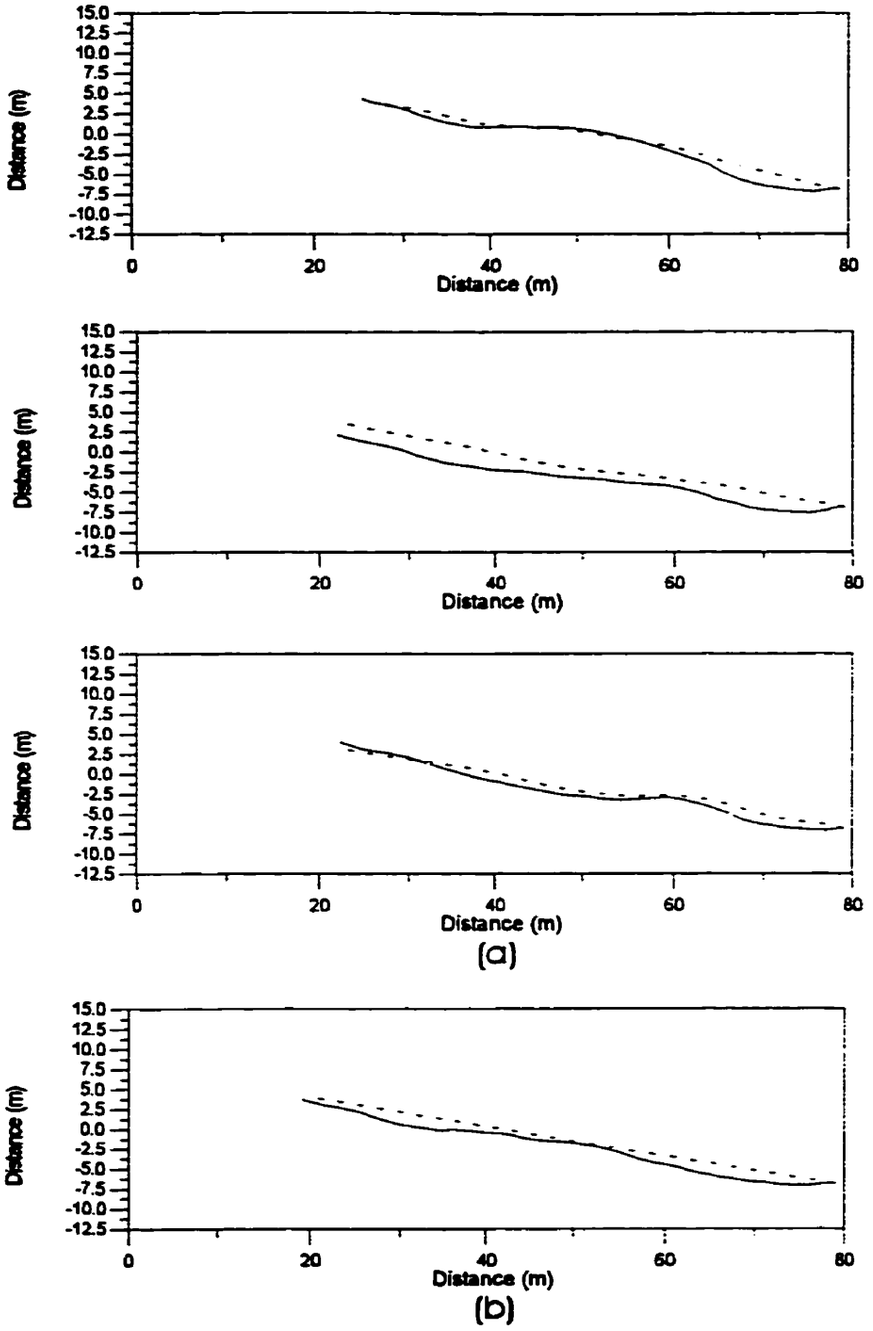

Figure 4.9: Comparison of the displacements observed under steady-state and transient flow conditions (a) selected heterogeneous realizations; (b) homogeneous medium. The dashed line represents the migration path of the centre of mass observed under steady-state conditions whereas the solid line represents the migration path of the centre of mass observed under transient flow conditions. Note that the plumes migrate from right to left (see Figure 4.2).

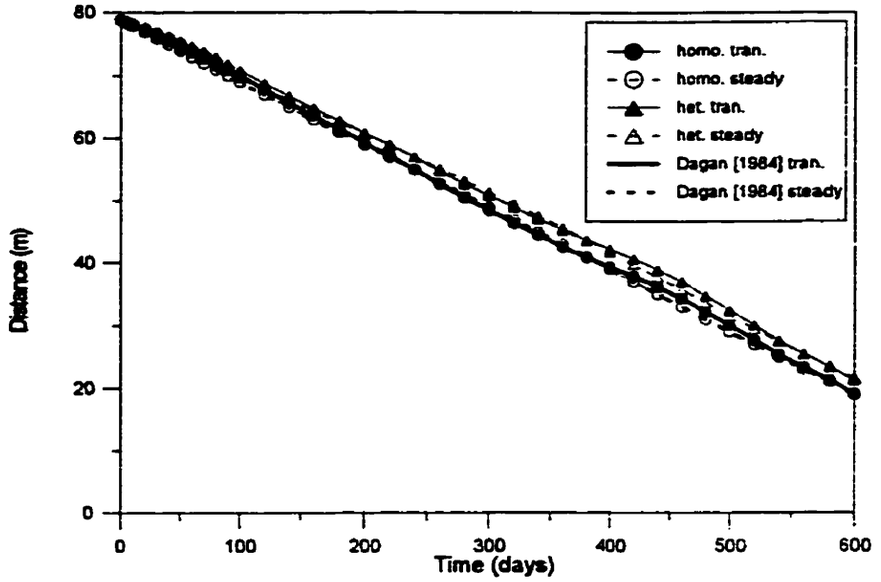

(a)

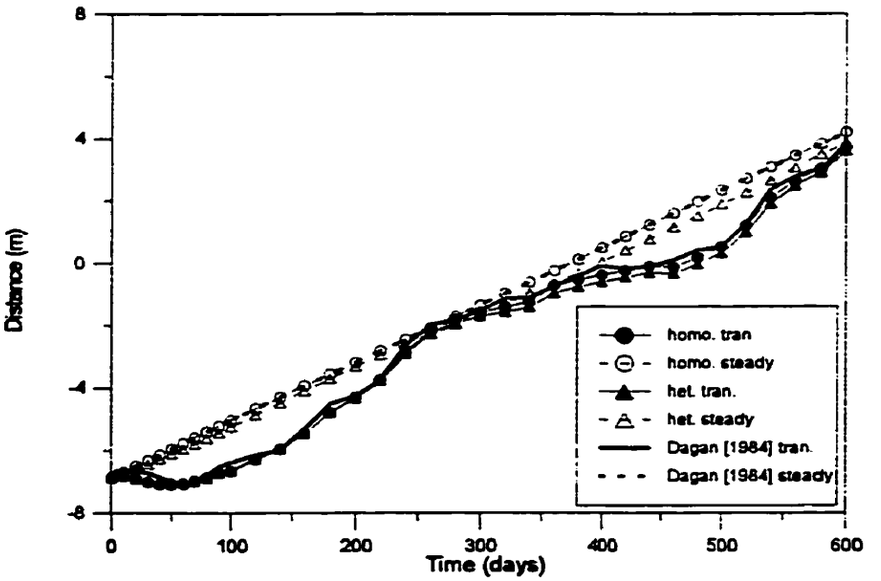

(b)

Figure 4.10: Comparison of ensemble centre of mass estimates with the analytical solution of Dagan [1984] (a) x-direction; (b) y-direction. Note that results for the simulations in the homogeneous medium are also plotted. (*"het."* represents heterogeneous, *"homo."* represents homogeneous, *"steady"* represents steady-state flow, and *"tran."* represents transient flow)

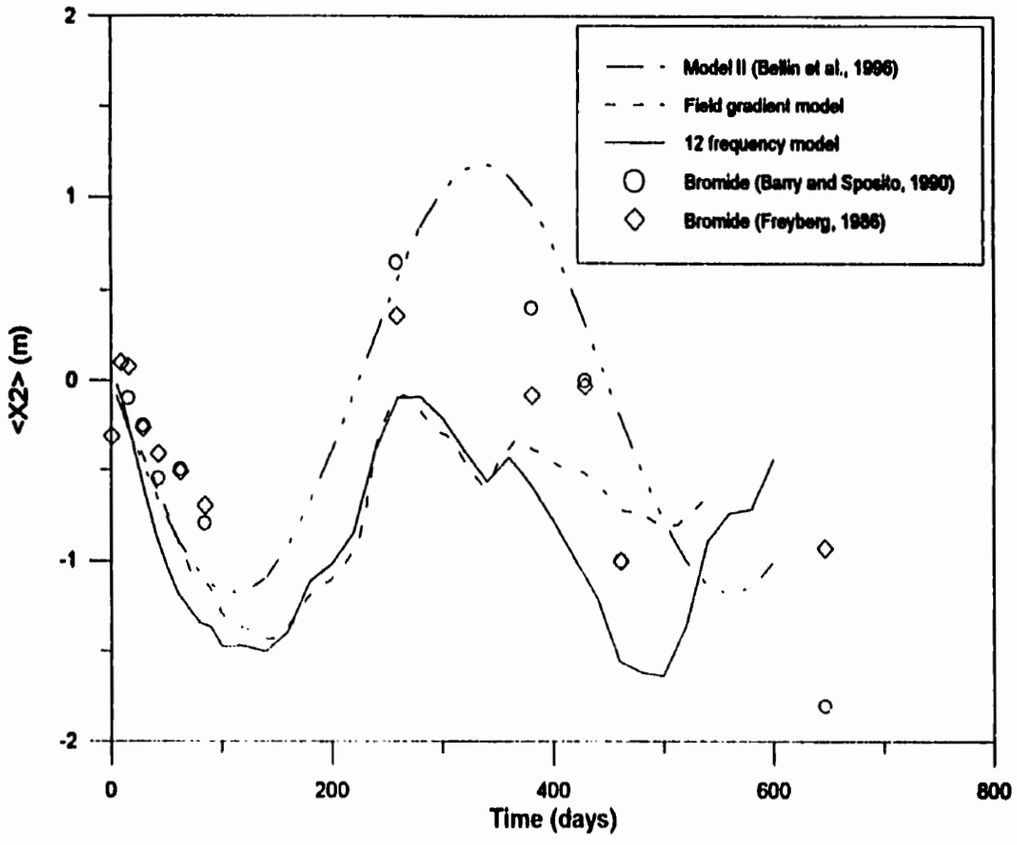

Figure 4.11: Comparison of centre of mass displacements computed using estimates of the a_2-component of the hydraulic gradient to the observed bromide centre of mass data reported by Freyberg [1986] and Barry and Sposito [1990] for the Stanford-Waterloo tracer experiment.

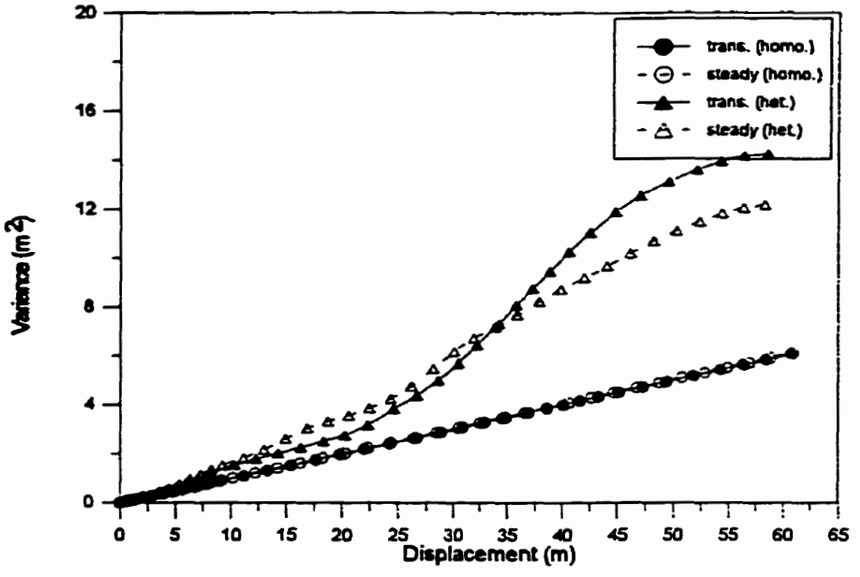

(a)

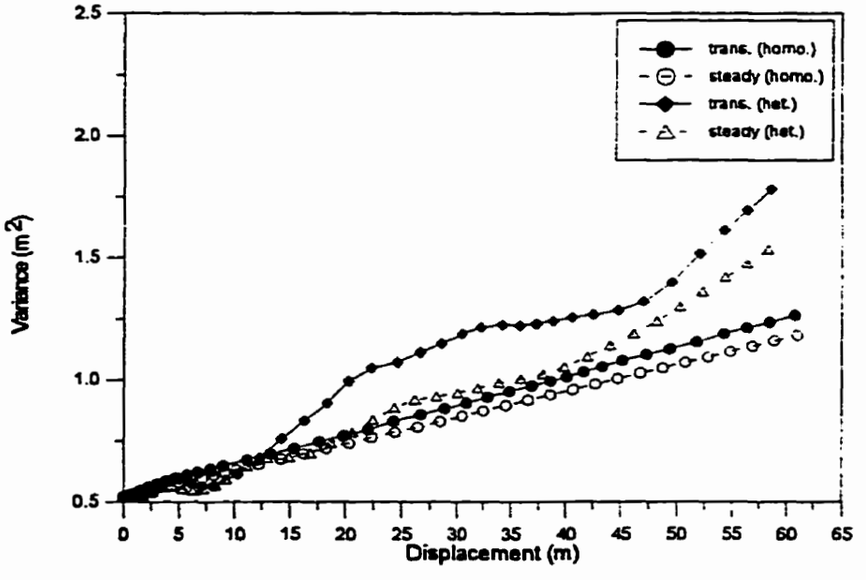

(b)

Figure 4.12: Spatial dependence of the covariances determined for the simulations in the homogeneous medium as well as ensemble average estimates for the steady-state and transient cases; (a) longitudinal direction; (b) transverse direction. (*"het."* represents heterogeneous and the abbreviation *"homo."* represents homogeneous)

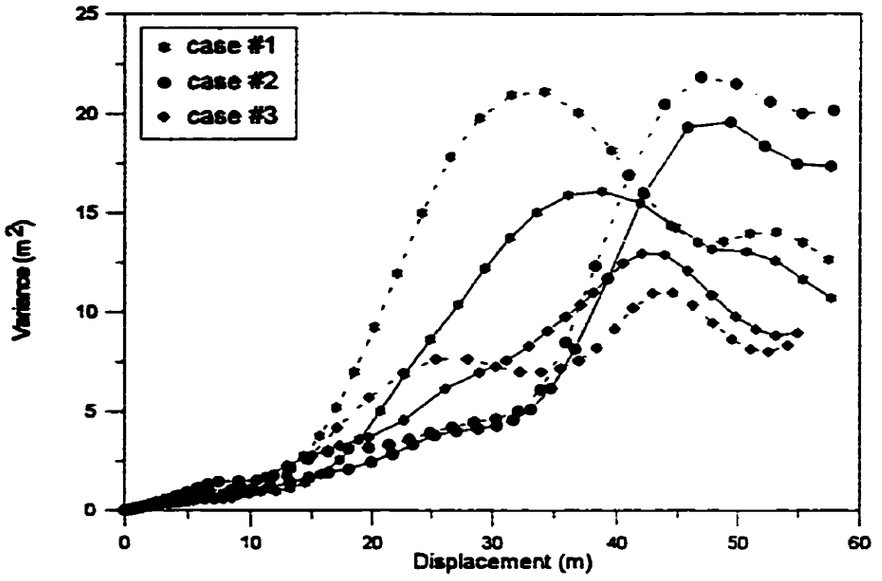

(a)

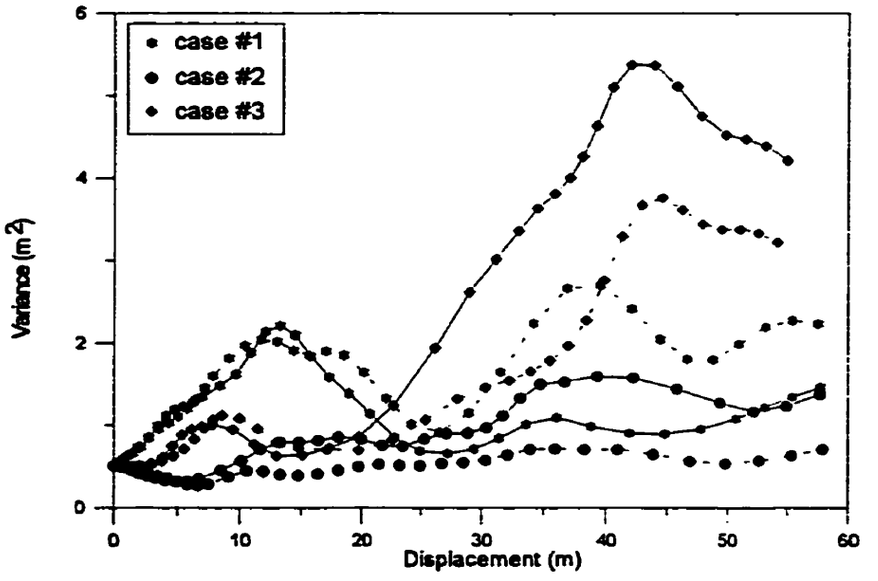

(b)

Figure 4.13: Covariances determined under transient and steady-state flow conditions for selected realizations; (a) longitudinal direction; (b) transient direction. The simulations in each realization of lnK are identified by similar symbols, with the transient cases represented by the solid lines and the steady-state cases by the dashed lines.

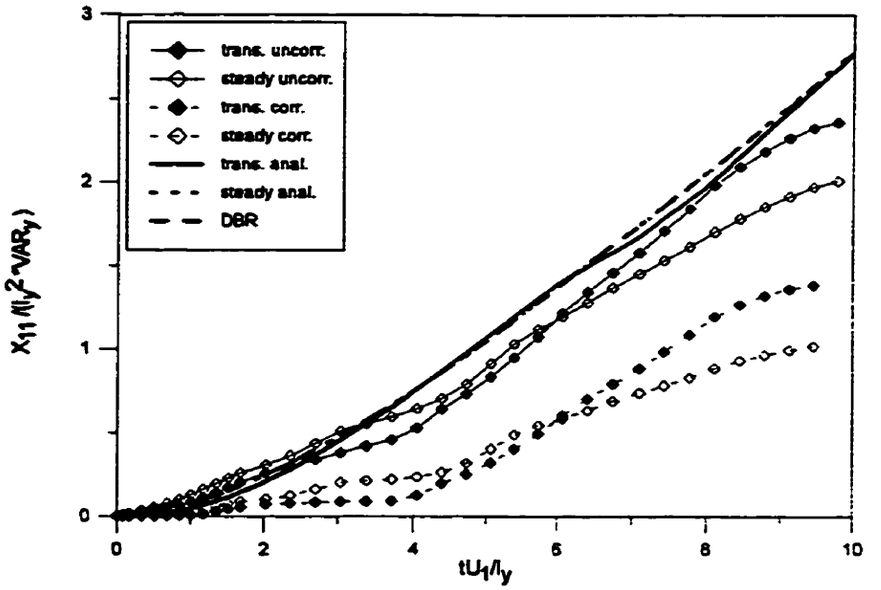

(a)

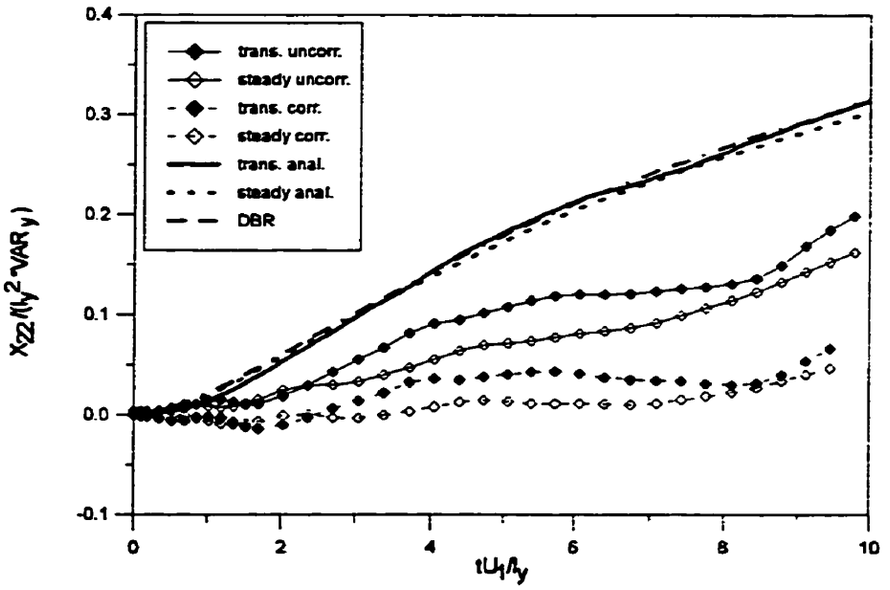

(b)

Figure 4.14: Non-dimensionalized covariance plots comparing the results of the DBR to the ensemble corrected and uncorrected variances determined from the simulations (a) longitudinal direction; (b) transverse direction.

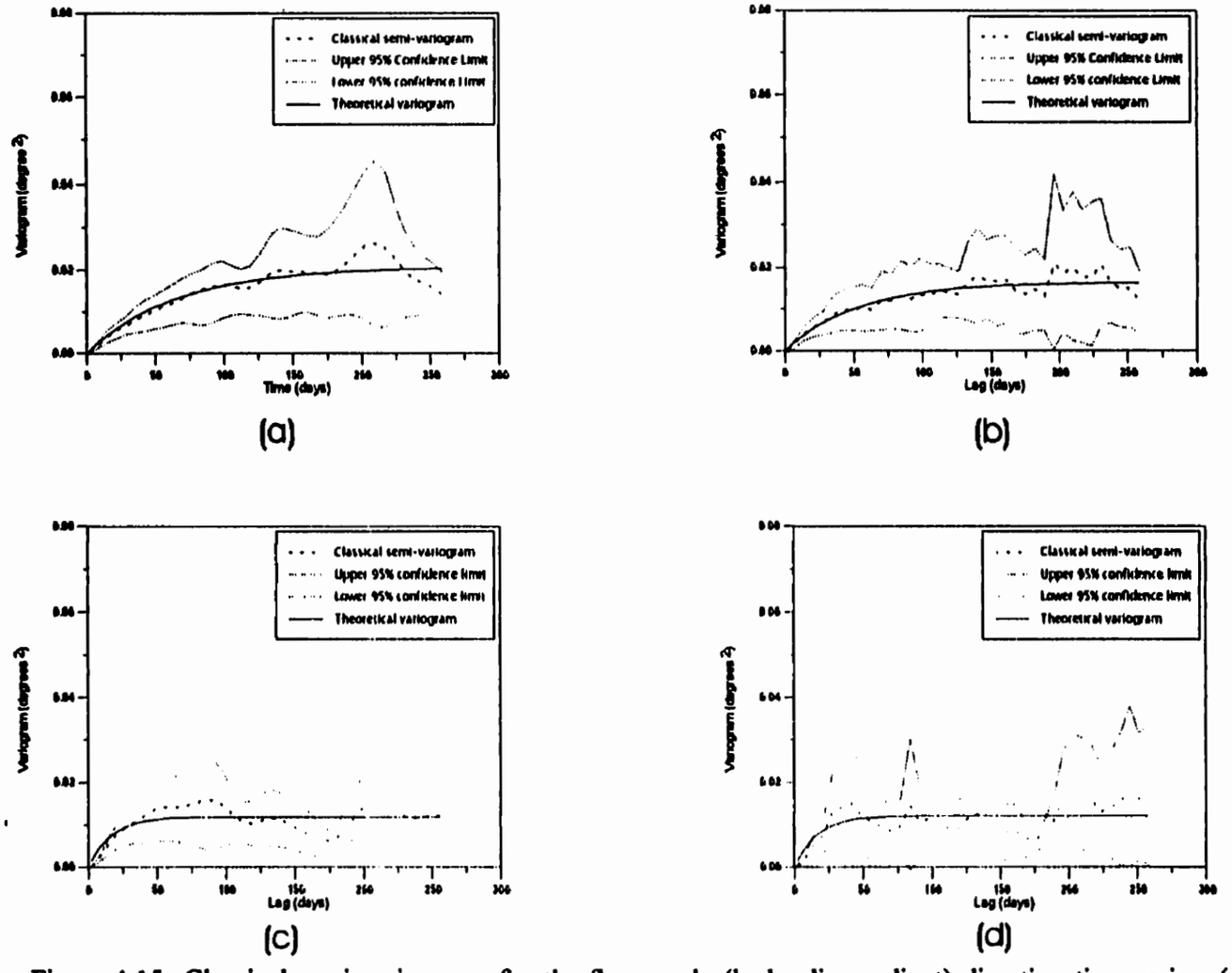

Figure 4.15: Classical semi-variograms for the flow angle (hydraulic gradient) direction time series; (a) Case #1 for the flow angle time series sampling proc. #1; (b) Case #1 for the flow angle time series sampling proc. #2; (c) Case #2 for flow angle time series sampling proc. #1; (d) Case #2 for flow angle time series sampling proc. #2.

Table 4.1
Velocity Estimates for the Steady-State and Transient Simulations

	Steady-state	Transient
v_x (max.) (m/day)	-0.125	-0.120
v_x (min.) (m/day)	-0.073	-0.076
v_y (max.) (m/day)	0.024	0.023
v_y (min.) (m/day)	0.013	0.012
$\bar{v}_x$ (m/day)	-0.096	-0.096
$\bar{v}_y$ (m/day)	0.018	0.018
σ_{Vx} (m/day)	0.013	0.012
σ_{Vy} (m/day)	0.003	0.003

Table 4.2
Apparent Longitudinal Dispersivity Estimates Based on the Ensemble Average Longitudinal Second Moments

Distance (m)	Apparent Longitudinal Dispersivity (m)	
	Steady-state	Transient
0 to 20	0.088 *0.039	0.074 *0.025
20 to 45	0.135 *0.086	0.215 *0.166
20 to 60	0.117 *0.068	0.167 *0.118

** indicates that the local dispersive component has been removed.*

Table 4.3
Apparent Transverse Dispersivity Estimates Based on the Ensemble Average Transverse Second Moments

Distance (m)	STEADY-STATE Apparent Transverse Dispersivity (m)	Distance (m)	TRANSIENT Apparent Transverse Dispersivity (m)
0 to 17	0.006 *-0.001	0 to 8	0.005 *-0.002
17 to 25	0.013 *0.006	8 to 20	0.017 *0.010
25 to 45	0.006 *-0.001	20 to 45	0.006 *-0.001
25 to 60	0.010 *0.003	20 to 60	0.009 *0.002

** indicates that the local dispersive component has been removed.*

Table 4.4a
Semi-Variogram Analyses of the Gradient Time Series:
Flow Angle Results
(Expected Value)

	Case #1		Case #2	
	Sampling Proc. #1	Sampling Proc. #2	Sampling Proc. #1	Sampling Proc. #2
Nugget (rad.^{2}) $\sigma_{\theta o}^2$	0.000 *0.000 †0.000	0.000 *0.000 †0.000	0.000 *0.000 †0.000	0.000 *0.000 †0.000
Variance (rad.^{2}) σ_θ^2	0.021 *0.033 †0.009	0.017 *0.029 †0.005	0.012 *0.019 †0.005	0.012 *0.022 †0.003
Integral Scale (days) λ_θ	65.18 *81.15 †39.90	53.41 *70.15 †20.35	16.37 *18.68 †10.91	16.21 *17.95 †8.07

* represents the upper 95 % confidence limit.
† represents the lower 95 % confidence limit.

Table 4.4b
Semi-Variogram Analyses of the Gradient Time Series:
Gradient Magnitude Results
(Expected Value)

	Case #1		Case #2	
	Sampling Proc. #1	Sampling Proc. #2	Sampling Proc. #1	Sampling Proc. #2
Nugget σ_{Jo}^2	0.000 *0.000 †0.000	0.000 *0.000 †0.000	0.000 *0.000 †0.000	0.000 *0.000 †0.000
Variance σ_J^2	7.27×10^{-7} $*9.92\times10^{-7}$ $†3.31\times10^{-7}$	7.37×10^{-7} $*11.55\times10^{-7}$ $†2.57\times10^{-7}$	4.05×10^{-7} $*7.28\times10^{-7}$ $†1.13\times10^{-7}$	3.77×10^{-7} $*5.28\times10^{-7}$ $†1.64\times10^{-7}$
Integral Scale (days) λ_J	63.45 *57.29 †63.79	80.42 *63.45 †69.47	26.86 *34.33 †17.63	17.38 *17.63 †24.26

* represents the upper 95 % confidence limit.
† represents the lower 95 % confidence limit.

Table 4.5
Enhancement of the Macrodispersivities Due to Transient Flow
Based on the Model of Rehfeldt and Gelhar (1992)

	Case #1		Case #2	
	Sampling Proc. #1	Sampling Proc. #2	Sampling Proc. #1	Sampling Proc. #2
$A_{22}^{(t)}$ (m)	0.133 *0.259 †0.035	0.088 *0.197 †0.010	0.019 *0.034 †0.005	0.019 *0.038 †0.002
$A_{11}^{(t)}$ (m)	0.186 *0.230 †0.085	0.239 *0.296 †0.072	0.043 *0.101 †0.008	0.026 *0.037 †0.016

* represents the upper 95 % confidence limit.
† represents the lower 95 % confidence limit.

Table 4.6a
Expected Macrodispersivities Due to Transient Flow: Transverse Component
(mid to late time expected values)

Distance (m)	Predicted Transverse Dispersivity (steady-state + RG) (m) Case #2	
	Sampling Proc. #1	Sampling Proc. #2
17 to 25	0.025	0.025
25 to 45	0.018	0.018
25 to 60	0.022	0.022

RG : Rehfeldt and Gelhar [1992] model.

Table 4.6b
Expected Macrodispersivities Due to Transient Flow: Longitudinal Component
(mid to late time expected values)

Distance (m)	Predicted Longitudinal Dispersivity (steady-state + RG) (m) Case #2	
	Sampling Proc. #1	Sampling Proc. #2
25 to 45	0.129	0.112
25 to 60	0.111	0.094

RG : Rehfeldt and Gelhar [1992] model.

Chapter 5

Discussion and Conclusions

5.1 Introduction

The format utilized in this work provided for in-depth discussions and conclusions at the end of each research chapter. In an attempt to avoid unnecessary repetition, brief summaries of these results are presented in this chapter. Part of this chapter deals with placing the major aspects of this entire work into a common perspective which ultimately reflects its contribution to the field of hydrogeology. This chapter concludes with a discussion of future research activities which have evolved as a consequence of the work presented in this thesis.

5.2 Summary

As mentioned above, the aim of this section is not to reproduce the in-depth discussions and conclusions contained in the previous chapters but to summarize the major issues addressed in those discussions. Such a summary is considered prudent due to the length of the work and the number of issues addressed. The following summary is presented on a chapter by chapter basis.

The primary aim of Chapter 2 was to show that the Arnoldi modal reduction method (AMRM) introduced into the hydrogeology literature by Woodbury et al. [1990] is an accurate and efficient approach for solving the system of equations which result from the finite element discretization of linear forms of the mass transport equation under steady-state

conditions. In an attempt to demonstrate these aspects, the performance of the AMRM was compared to that of the LTG method proposed earlier by Sudicky [1989] and utilized extensively in a number of high resolution three-dimensional simulation studies [cf. Chapter 4; Robin, 1991; Burr et al., 1994; Naff et al., 1996]. Note that Sudicky [1989] compared the LTG approach to the standard LU decomposition approach to demonstrate the greater efficiency and accuracy to be gained from the former, while Woodbury et al. [1990] used a similar comparison between the AMRM and the LU decomposition scheme to establish the improved efficiency of the former. The results contained in this work showed that for problems involving heterogeneous hydraulic conductivity fields and steady-state velocities such as those utilized in the high resolution simulation experiments described earlier, implementations of the AMRM were more efficient (direct solver version) or at least as efficient (iterative solver version) as the most efficient implementations of the LTG method for identical discretizations, while maintaining similar levels of accuracy. For most problems involving homogeneous hydraulic conductivities and steady-state velocities it was demonstrated that the LTG method was in most cases more accurate and as efficient as the AMRM. In the case of sharp front problems in homogeneous hydraulic conductivity fields the LTG was clearly the more superior of the two methods. It is also noteworthy to mention that the work in Chapter 2 demonstrated the modularity of the AMRM, in that it showed that the method easily allows both iterative and direct solvers to be implemented without significant modifications to the structure of the computer program.

Chapter 3 explored one aspect of improving the convergence rate associated with the AMRM . The method considered was a "shift" variant of the AMRM. The primary objective

of shifting is to improve the approximation of the eigenvalues of the sub-space system relative to those of the system in the original space. By improving the approximation of the eigenvalues of the system, the rate of convergence of the solution is improved. Shifting was found to be a "double edged sword", in that the choice of the shift could either improve or degrade the accuracy of the solution. The former generally occurred when the shift moved the eigenspectrum of the reduced system closer to the spectrum in the original problem space, whereas the latter occurred when the shift moved the eigenspectrum of the reduced system to the outer parts of the spectrum in the original problem space. These observations suggested the presence of an "optimal shift". This work showed that for the advection-dispersion equation (ADE) prediction and utilization of the optimal shift is a difficult task because the optimal shift cannot be predicted a priori. The analysis presented shows the optimal shift to be sensitive to changes in the number of Arnoldi vectors utilized, the material properties used and the degree of mesh discretization considered. Note that the last two indicate a sensitivity to the grid Peclet number. These sensitivities indicate that during the model calibration phase use of the optimal shift can present various challenges especially if several model parameters are altered simultaneously. For the practicing hydrogeologist wishing to calibrate a model, continuous estimation of the optimal shift is a distraction and thus a potential limitation of the shift AMRM.

The work in Chapter 4 is considered to be represent the major scientific achievement of this research since it marks the first time (based on available literature) that numerical simulation studies of non-reactive solute transport in high resolution hydraulic conductivity fields have been attempted under quasi steady-state (referred to in this work as "transient")

flow conditions. In order to make inferences about available field based observations the parameters used in the simulations were representative of those reported for the Borden site. Due to the domain size and the degree of discretization required to maintain a numerically stable and accurate system throughout the course of the simulations, the problem space was restricted to two-dimensions. Despite this limitation the study provides considerable insight with respect to plume dynamics. Since studies of this nature have not been previously reported, a means of implementing field observed gradients into the simulation methodology was devised based on the earlier arguments provided by Goode and Konikow [1990], and Rehfeldt and Gelhar [1992]. The devised approach which is based on a frequency spectrum analysis of waterlevel time series data is considered practical and relatively easy to implement. The results of the simulations show that under non-ergodic conditions, solute migration and dispersion in subsurface environments are strongly influenced not only by local variations in the hydraulic conductivity field as is commonly assumed but also by the temporal state of the flow field. In the various simulations the non-ergodic effects are demonstrated by the considerable variability present in the first and second moments, both within and across realizations. An important finding from an analysis of the simulations is that the transverse variance estimated under transient flow conditions is generally enhanced relative to that observed under steady-state conditions. Also, the longitudinal variances computed under transient conditions are in some cases found to be enhanced relative to those estimated under steady-state conditions; however this observation is not consistent across realizations and thus may be reflective of the nature of the hydraulic conductivity field. The enhancements observed under transient conditions are reinforced when ensemble averaging is performed on the

computed second moments. Comparisons of the ensemble moments estimated from the simulation analysis to those predicted by various stochastic theories yielded mixed results. These results were generally assumed to reflect possible shortcomings of the theories, the effects of finite source dimensions used in the simulations, as well as possible effects due to the limited number of simulations. Nevertheless it was concluded that the model of Dagan et al. [1996] reflected the trends in the ensemble data quantitatively better than that of Rehfeldt and Gelhar [1992].

5.3 Perspective

The discussion in this section is focused towards placing this work into perspective. This is necessitated due to the varied issues addressed in this work. An appropriate perspective from which to view this work is to focus on its primary objective: the effects of transient flow on the evolution of nonreactive solute plumes. As with previous studies of plume evolution in heterogeneous hydraulic conductivity fields, a numerical simulation methodology was adopted for this study. This approach allowed not only various scenarios to be considered but also allowed proposed analytical formulations describing dispersion in heterogeneous media to be evaluated.

Prior to developing the framework for the intended numerical simulator it was recognized that the transient nature of the groundwater flow field prevented the efficient implementation of data storage schemes and matrix solvers utilized in previous simulation attempts [Robin, 1991; and Burr et al., 1994]. In fact the computational effort required to solve the systems utilized by Robin [1991] and Burr et al. [1994] is generally considered to

be a major factor limiting the wide-spread use of high resolution simulation experiments. Thus in order to over-come potential computational limitations, part of the focus of this work involved identifying and developing alternate matrix solvers and data storage schemes for use in this work as well as in other simulation attempts. Work on the subspace Arnoldi modal reduction method (AMRM) by Woodbury et al. [1989] showed the method to be computationally efficient compared to the standard LU decomposition scheme (see Chapter 2). Although not fully exploited at that time due to software limitations (use of Fortran77 as opposed to Fortran90), the method does appear efficient in terms of data storage. Since the computational efficiency of the method was never evaluated relative to other efficient matrix solvers, it was considered prudent to first perform such an evaluation. Thus the work in Chapter 2. On the basis of the work performed in Chapter 2 accuracy and efficiency improvements to the AMRM were investigated in Chapter 3. The work performed in both Chapters 2 and 3 suggest that for high resolution simulations such as those reported by Robin [1991] and Burr et al. [1994] the AMRM is a highly efficient matrix solver, which if utilized can allow larger and more complex linear mass transport problems to be solved within realistic time frames.

Due to time constraints the applicability of the AMRM to mass transport in transient velocity fields was not investigated in this work. However, if the current implementation of the AMRM is examined several potential short comings become evident if it is applied to such problems. Of particular interest is the matrix $\boldsymbol{K}$ (Chapter 2, eqn. 2.5) which captures the effect of fluid velocity on the mass transport process. Changes in the fluid velocity field necessitate that $\boldsymbol{K}$ be updated. However, an update of $\boldsymbol{K}$ requires that a new subspace

reduction be performed and new Arnoldi vectors computed. In their works, Woodbury et al. [1990] and Farrell et al. [1997; cf. Chapter 2] showed the Arnoldi reduction process to be by far the most expensive aspect of the AMRM, thus the need to continously update and refactor the system of equations detracts from the efficiency of the AMRM. Hence for the transient simulations an alternate solver was utilized. It is important to note that the above should not be interpreted as a negative result. Instead it signifies that more in-depth research is needed to identify if and how the AMRM can be improved so that it can be efficiently applied to a larger class of problems.

5.4 Future Research

In this section, issues related to the various topics presented which warrant further investigation are summarized in point form.

- On the basis of the work performed in Chapter 4 it was postulated that from the center of mass data, aspects of the periodicity in the hydraulic gradient field may be recovered with any additional signal being interpreted as an "aquifer response function". This conjecture requires further study since it indicates that from a knowledge of the history of a plume's centre of mass properties of the hydraulic conductivity field through which it migrated can be determined. If this is indeed the case then the conditions under which it is possible need to be investigated since these conditions will affect the design of field tracer tests.

- In Chapter 4 possible dimensionality effects were recognized as potential

limitations to these results being representative of field-scale behaviours. To address this issue there is a need for an analysis similar to the one presented here to be performed in a three-dimensional domain. In order for such a simulation to be performed improved matrix solvers are required (especially for the finite element method) or alternate simulation methodologies such as particle tracking must be implemented.

- The enhanced dispersion of nonreactive plumes observed under transient flow conditions was demonstrated in Chapter 4. Whether similar enhancements are observed for all classes of reactive solutes as well as the possible ramifications (i.e., impact on reactive models) are unknown and requires investigation. Thus, data associated with known tracer experiments could be carefully re-evaluated (taking into account possible effects due to flow transients), especially if information is being sought in an effort to decide on or validate possible reactive models. In this vein it is also suggested that simulations under transient conditions be performed to examine the both reactive and nonreactive mass transport in domains containing spatially variable mobile and immobile porosity zones as well as spatially variable hydraulic conductivities to gage the effect of such combinations on the dispersion process. An analysis similar in principle was performed by Burr et al. [1994] for the case of steady-state flow and constant porosity. They concluded that small increases in the second moments were generally observed due to the high mass transfer rates.

- This study concluded that improvements in the AMRM are required if the method is to become more efficient and robust. Among the improvements which require further study are: a structuring of the computer code used in the solver to take advantage of new structures in Fortran90 which improve data storage efficiency; the implementation of fast iterative solvers in an attempt to better improve data storage efficiency; the implementation of fast and efficient approaches for estimating the optimal shift which do not negate the potential performance gains relative to the standard AMRM; and the possible development of variants of the AMRM which do not require a full reduction when single parameters are changed within a small percentage of their original value;

- Finally, this work suggest the need for "intelligent" systems which are capable of selecting the most accurate and efficient solver for particular aspects of a simulation problem. For example it was shown that the LTG method is more accurate and efficient than the AMRM for solving problems involving sharp fronts. Thus in a simulation environment this procedure could be utilized at early times when large concentration gradients are observed at the solute front. At later times when the concentration gradients at the front are reduced, other methods such as the AMRM can be implemented if they are judged to be more efficient at this stage of the problem.

References

Burr, D. T., E. A. Sudicky and R. L. Naff, Nonreactive and reactive transport in three-dimensional heterogeneous porous media: Mean displacement, plume spreading, and uncertainty, Water Resour. Res., 30(3), 791-815, 1994.

Dagan, G., A. Bellin, and Y. Rubin, Lagrangian analysis of transport in heterogeneous formations under transient flow conditions, Water Resour. Res., 32(4), 891-899, 1996.

Goode, D. J., and L. F. Konikow, Apparent dispersion in transient groundwater flow, Water Resour. Res., 26(10), 2339-2351, 1990.

Naff, R. L., D. F. Haley and E. A. Sudicky, High-resolution Monte-Carlo simulation of flow and conservative transport in heterogeneous porous media: 2, Transport results, [submitted to Water Resour. Res.]

Rehfeldt, K. R. and L. W. Gelhar, Stochastic analysis of dispersion in unsteady flow in heterogeneous aquifers, Water Resour. Res., 28(8), 2085-2099, 1992.

Robin, M. J. L., Migration of reactive solutes in three-dimensional heterogeneous porous media, Ph. D. thesis, 124 pp., Dept. of Earth Sci., Univ. of Waterloo, Waterloo, Ont., Canada, 1991.

Sudicky, E. A., The Laplace transform Galerkin technique: A time-continuous finite element theory and application to mass transport in groundwater, Water Resour. Res., 25(8), 1833-1846, 1989.

Woodbury, A. D., W. S. Dunbar, B. Nour-Omid, Application of the Arnoldi Algorithm to the solution of the advection-dispersion equation, Water Resour. Res., 26(10), 2579-2590, 1990.